



**UNIVERSITÀ DEGLI STUDI DI CAMERINO**  
**SCHOOL OF ADVANCED STUDIES**

**Doctoral course in:**  
**Chemical and Pharmaceutical Sciences and Biotechnology**  
**(Cycle XXXV)**

**DESIGN, SYNTHESIS AND BIOLOGICAL EVALUATION OF**  
**POTENT AND SELECTIVE DOPAMINE OR SIGMA RECEPTOR**  
**LIGANDS SHARING A COMMON PHARMACOPHORE**

**Ph.D. candidate:**

***Pegi Pavletić***

**Supervisors:**

***Prof. Fabio Del Bello***

***Prof. Wilma Quaglia***

---

**Academic Years 2020/21-2022/23**

*I would like to dedicate this work, firstly, to my parents, Iris and Denis, who have provided me with care and unconditional support in all my educational, personal efforts, as well as efforts related to students' representation. Even in cases in which they would not agree with my choices, they never doubted me, and they would go out of their way and possibilities to assure me the life I wanted to have. To my sisters, Beti and Megi who have shared their lives, ups and downs with me, and who have, and always will be, a part of myself. My grandparents Ana, Mirko and Josipa have always pushed me forward, and have helped me immensely through life, knowing that moving forward is moving away from them- thank you for the courage!*

*To the love of my life, Matej, the greatest thanks for supporting me even in the smallest things, visiting me, laughing with me, and building a life across the sea. You have been a silent but important contributor to my doctoral work, and my greatest source of inspiration and happiness. Marinela and Esat, I thank you for sustaining me and allowing me to steal away your son to come for many visits, as well as accepting and supporting me in my moves throughout Europe. I shall be forever grateful for the opportunities you have provided me with.*

*No less important are my co-mentors, prof. Fabio Del Bello and prof. Wilma Quaglia, who have recognized me and allowed me to come to the University of Camerino, and learn from them. I could not have wished for more research-driven, professional, and most importantly, emphatic and supportive mentors. Our journey together has not been easy- moving department laboratories, surviving COVID-19 and two mobilities scattered across 3 years of studies, but we have done it together! You will forever have a colleague and a friend in me. The same applies to the researchers from the Medicinal Chemistry Unit, prof. Alessandro Piergentili and prof. Gianfabio Giorgioni, who have always been a support mechanism in times I needed it.*

*I owe my thanks to prof. Giulio Vistoli, for allowing me to explore my interest in molecular modelling studies; to prof. Ivan Đikić, for believing in my potential and allowing me to explore innovative research topics in my field, pertaining to the development of PROTAC ligands, as well as the discovery of molecular glues; and to prof. Xinlai Cheng, for the support and teaching me how to synthesise, analyse and evaluate PROTAC molecules. Special thanks to their students who are too many to be mentioned, but they all contributed to my current research with their support.*

*Special thanks to my dearest friends who have, in a way, marked this era of my life: Ernestina Appiah, Oscar Moreno Araiza, Margareta Lugarov, Andrea Toić, Milan Petrović, Bobana Samardžija, Martina Mušković, Borna Nemet, Maciej Rewucki, Adam Gajek, Martin Hammerbauer, Stanimir Boyadzhiev, Kristel Jakobson, Damir Solak, Liv Teresa Muth, Irina Duma, and to those I have forgotten to mention here. A special place in my heart is reserved for Valeria Vinci, Benedetto Cardillo, Francesca Frizzo, Laura Montevioni, Sofia Coltrinari, Roberto Gaspari and Francesca Cipolletti, who have been my colleagues and friends, and they are mostly responsible for my knowledge of Italian.*

*Lastly, I want to thank all the other students, whom I have spent my days in the laboratory with, sharing knowledge, experiences, ideas about the future and love stories. I wish you all bright futures, and thank you for making my days brighter with your smiles (and lab coats). Hope our paths cross again in the future!*

# Table of Contents

1. INTRODUCTION .....	12
2. DOPAMINE RECEPTORS.....	15
3. DOPAMINE D4 RECEPTOR.....	18
3.1. Background.....	18
3.2. Introduction and objectives of the work .....	21
3.3. Results and discussion .....	30
3.3.1. Synthesis of DRD4 ligands .....	30
3.3.2. Radioligand binding assays .....	35
3.3.3. Bioluminescence resonance energy transfer (BRET) assays.....	40
3.3.4. Molecular modelling studies.....	42
3.3.5. In vitro studies on GBM cell lines .....	54
3.4. Conclusions .....	57
3.5. Experimental section.....	59
3.5.1. Synthesis of DRD4 ligands .....	59
3.5.2. Radioligand binding assays .....	77
3.5.3. Bioluminescence resonance energy transfer (BRET) assays.....	79
3.5.4. Molecular modelling studies.....	81
3.5.5. In vitro studies on GBM cell lines .....	83
3.6. Targeted protein degradation of the DRD4.....	85
3.6.1. Ubiquitination of DRD4 .....	85
3.6.2. Introduction to PROTAC molecules .....	86
3.6.3. Introduction and objectives of the work .....	89
3.6.4. Synthesis of DRD4 PROTACs and the analysis plan .....	91

3.6.5.	Experimental section.....	93
4.	DOPAMINE D3 RECEPTOR.....	100
4.1.	Background.....	100
4.2.	Introduction and objectives of the work .....	102
4.3.	Results and discussion .....	104
4.3.1.	Synthesis of DRD3 ligands .....	104
4.3.2.	Radioligand binding assays .....	108
4.3.3.	Functional assays.....	111
4.3.4.	Molecular modelling studies.....	113
4.4.	Conclusions .....	119
4.5.	Experimental section.....	120
4.5.1.	Synthesis of DRD3 ligands .....	120
4.5.2.	Radioligand binding assays .....	134
4.5.3.	Functional assays.....	137
4.5.4.	Molecular modelling studies.....	142
5.	SIGMA RECEPTOR .....	144
5.1.	Background.....	144
5.2.	Introduction and objectives of the work .....	149
5.3.	Results and discussion .....	152
5.3.1.	Synthesis of $\sigma_1$ ligands.....	152
5.3.2.	Radioligand binding assays .....	154
5.3.3.	Molecular modelling studies.....	156
5.3.4.	In vivo functional assays.....	158
5.4.	Conclusions .....	164
5.5.	Experimental section.....	165

5.5.1.	Synthesis of $\sigma_1$ ligands .....	165
5.5.2.	Radioligand binding assays .....	168
5.5.3.	In vivo functional assays .....	174
6.	REFERENCES .....	178
7.	LIST OF CO-AUTHORED PUBLICATIONS .....	208

## List of abbreviations

AD	Alzheimer's disease
AUC	Area under curve
BCS	Bovine calf serum
BRET	Bioluminescence resonance energy transfer
cAMP	Cyclic adenosine monophosphate
C <sub>max</sub>	Maximum mean concentration
CSA	10-Camphorsulfonic acid
CG	Control group
CNS	Central nervous system
DRD	Dopamine receptor
DA	Dopamine
DAST	Diethylamino-sulphur trifluoride
DAT	Dopamine transporter
DCM	Dichloromethane
DIPEA	Diisopropylethylamine
DMA	Dimethylacetamide
DME	Dimethoxyethane
DMEM	Dulbecco's Modified Eagle's Medium
DMF	Dimethylformamide
DMSO	Dimethylsulfoxide
DRIP	Dopamine receptor-interacting protein
EBP	Extended binding pocket
EBSS	Earle's balanced salt solution
EDTA	ethylenediaminetetraacetic acid
EG	Experimental group
EGF	Epidermal growth factor

FBS	Fetal bovine serum
FCS	Fetal calf serum
FST	Forced swimming test
Fu	Fraction unbound
GBM	Glioblastoma
GPCR	G protein-coupled receptor
GSC	Glioblastoma stem cells
HATU	Hexafluorophosphate Azabenzotriazole Tetramethyl Uronium
IL	Intracellular loop
mAChR	Muscarinic acetylcholine receptor
<i>m</i> -CPBA	<i>m</i> -Chloroperbenzoic acid
MD	Molecular dynamics
ND	Not determined
NMDA	N-methyl-D-aspartate
OBP	Orthosteric binding pocket
OF	Open-field
PBS	Phosphate-buffered saline
PCP	Phencyclidine
PD	Parkinson's disease
PDB	Protein Data Bank
PI	Ionic interaction
POI	Protein-of-interest
PP	Primary pharmacophore
PROTAC	Proteolysis targeting chimera
Rac-BINAP	(R)- and (S)-2,2'-bis(diphenylphosphino)-1,1'-binaphthyl
SAR	Structure-activity relationship
SERT	Serotonin transporter
SP	Secondary pharmacophore

STR	Short tandem repeat
TCA	Trichloroacetic acid
THF	Tetrahydrofuran
TLC	Thin-layer chromatography
TM	Transmembrane domain
UPS	Ubiquitin-proteasome system



## ABSTRACT

This Ph.D. thesis work has concerned the design and synthesis of new biologically active ligands directed to different receptor systems, including dopaminergic and sigma receptors, and sharing the features of a common pharmacophore, which consists of a lipophilic moiety linked by a spacer to a piperidine or piperazine basic function and an aromatic terminal. Highly selective or multitarget compounds, as well as ligands with a biased profile, were obtained and allowed to shed further light on the involvement of these receptors in investigated pathologies.

Specifically, the following research activities have been carried out:

(i) the brain penetrant and dopamine D4 receptor (DRD4)-selective compound 1-(3-(4-phenylpiperazin-1-yl)propyl)-3,4-dihydroquinolin-2(1*H*)-one has been selected as a lead compound for the discovery of new ligands endowed with high affinity and selectivity for DRD4. Structure-activity relationship (SAR) and molecular modelling studies, highlighted that the quinolinone nucleus of the lead compound can be replaced by an *N*-indole or an *N*-tetrahydroquinoline moiety and the propyl linker represents the optimal distance between the lipophilic portion and the basic function. The most DRD4 selective compounds were the ones with para-substituted aromatic terminals, which behaved as DRD4 antagonists. Instead, the 2-pyridyl derivative showed an interesting biased profile, being a partial agonist toward DRD4 G-protein activation and an antagonist toward  $\beta$ -arrestin recruitment. The para-chlorophenyl derivative and the 2-pyridyl compound have been evaluated for their potential in affecting the viability of glioblastoma (GBM) cell lines, and primary GBM stem cells. Both compounds decreased the viability of all the studied

cell lines, at 10  $\mu$ M concentration, eliciting an antiproliferative effect higher than that of **temozolomide**, the first-choice chemotherapeutic drug in GBM. Such an effect was contrasted by a DRD4 agonist, demonstrating the involvement of DRD4 in the antitumor activity of these compounds. The same lead compound has also been selected as protein-of-interest (POI) ligand in the design of new small-molecule proteolysis targeting chimeras (PROTACs) for DRD4, which will be evaluated as anticancer agents for the treatment of GBM.

-(ii) A scaffold hybridization strategy has been used for the discovery of potent dopamine DRD3-selective or multitarget ligands, potentially useful for central nervous system disorders. In particular, novel bitopic ligands bearing the *N*-(2,3-dichlorophenyl)piperazine nucleus as a primary pharmacophore linked by an unsubstituted or 3-F/3-OH substituted butyl chain to the 6,6- or 5,5-diphenyl-1,4-dioxane-2-carboxamide or the 1,4-benzodioxane-2-carboxamide scaffold as a secondary pharmacophore have been synthesised and studied. The biological results supported by molecular modelling studies highlighted that the ligands characterized by an unsubstituted butyl chain between the pharmacophores showed the highest DRD3 affinity. In particular, the 6,6-diphenyl-1,4-dioxane compound showed a DRD3-preferential profile, while an interesting multitarget profile was highlighted for the 5,5-diphenyl-1,4-dioxane and 1,4-benzodioxane derivatives, both behaving as potent DRD2 antagonists, 5-HT<sub>1A</sub>R and D4R agonists, as well as potent DRD3 partial agonists. They also behaved as low potency 5-HT<sub>2C</sub>R partial agonists and 5-HT<sub>2A</sub>R antagonists. This profile might be a promising starting point for the discovery of novel agents useful for the treatment of schizophrenia.

-(iii) A benzo-cracking approach was applied to a potent  $\sigma_1$  receptor antagonist bearing the conformationally constrained 1,3-benzodioxane for the preparation of more flexible 1,3-dioxane compounds. One of the synthesised compounds behaved as a potent  $\sigma_1$  receptor antagonist and showed unprecedented selectivity over  $\sigma_2$  receptor, opioid receptor subtypes, the PCP site of the NMDA receptor, as well as over dopamine transporter. In the *in vivo* studies, it demonstrated to counteract the overeating of highly palatable food in bingeing-rats, without affecting palatable food intake in the control group, as well as depression-related and anxiety-like behaviors. These findings strengthened the involvement of  $\sigma_1$  receptor in the compulsive-like eating behavior, suggesting  $\sigma_1$  receptor antagonists as promising candidates to treat binge episodes.

# 1. INTRODUCTION

The concept of pharmacophore has been used in medicinal chemistry for many years. It has been introduced by Paul Elrich in 1909 as “*A molecular framework that carries (phoros) the essential feature responsible for a drug’s (pharmacon) biological activity*”<sup>1</sup> and resumed by Peter Gund in 1977 as “*A set of structural features in a molecule that is recognized at a receptor site and is responsible for that molecule’s biological activity*”.<sup>2</sup> In 1998 IUPAC officially defines the pharmacophore as follows: “*A pharmacophore is the ensemble of steric and electronic features that is necessary to ensure the optimal supramolecular interactions with a specific biological target structure and to trigger (or to block) its biological response*”.<sup>3</sup> It does not represent a real molecule or a real association of functional groups (e.g. primary amines, thioamide, ...) or structural fragments (e.g. a pyrrolidine ring), but a purely abstract concept that accounts for the common molecular interaction capacities of a group of compounds towards their biological targets. Central to the pharmacophore concept is the notion that the molecular recognition of a biological target can be ascribed to a set of common features that interact with a set of complementary sites on the biological target. In pharmacophore research, quite general features such as hydrogen-bond acceptors, hydrogen-bond donors, positively/negatively charged groups, aromatic areas and hydrophobic regions are typically considered.

Some pharmacophore models are characterized by high versatility, representing a master key (*passe-partout*) in drug-receptor recognition. In fact, different ligands fitting the features of these versatile pharmacophores might interact with different biological systems, depending on their specific “*molecular decorations*”.

The research activity of my Ph.D. thesis has been focused on the design and synthesis of new compounds targeting different receptor systems, including dopamine and sigma receptors, and sharing the features of a common pharmacophore, consisting in a lipophilic moiety linked by a spacer to a piperidine or piperazine basic function and an aromatic terminal (Figure 1A).

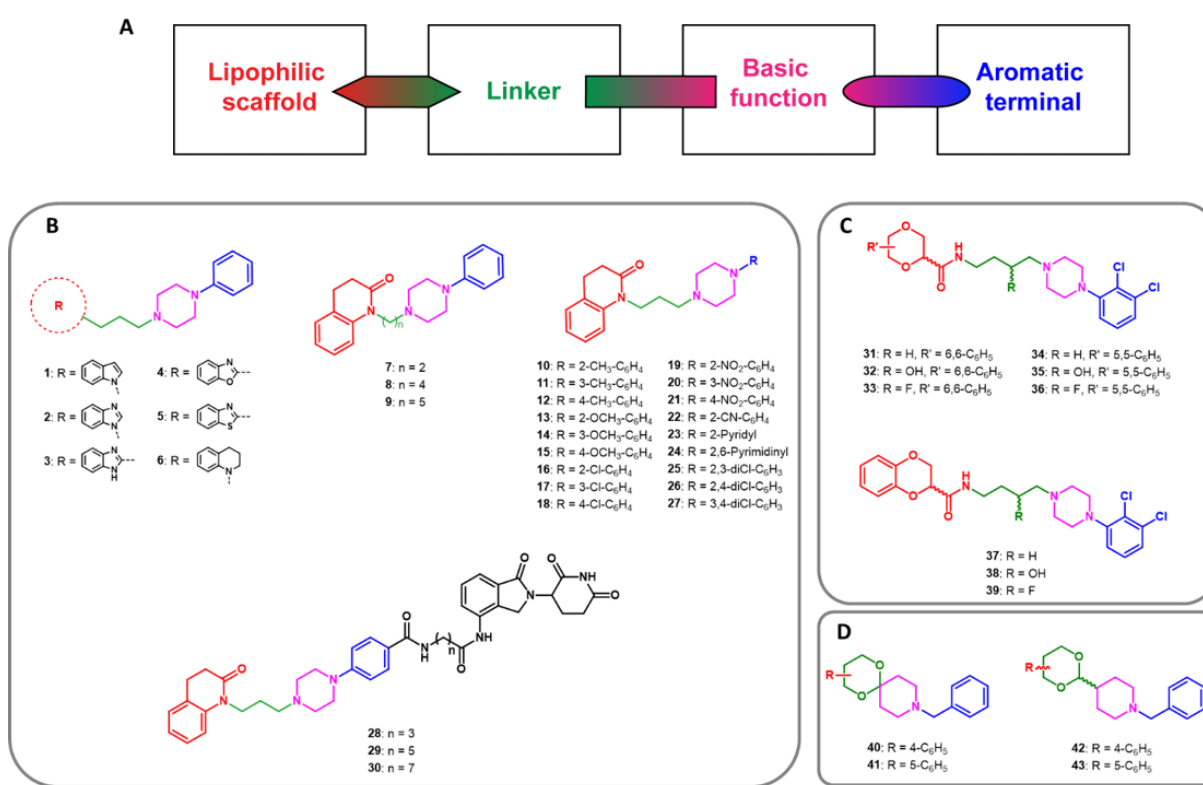


**Figure 1.** A) General pharmacophore model shared by: B) DRD4 ligands **1-30**, C) selective or multitarget DRD3 ligands **31-39** and D)  $\sigma_1$  receptor ligands **40-43**.

Specifically:

-(i) the brain penetrant and dopamine DRD4 selective lead compound 1-(3-(4-phenylpiperazin-1-yl)propyl)-3,4-dihydroquinolin-2(1*H*)-one (**54**) has been selected as a

model to perform an extensive structure-activity relationship study for the development of new potent and selective DRD4 ligands (compounds **1-27**, Figure 1B), potentially useful for the treatment of glioblastoma (GBM). During my mobility at the University of Milan, I performed molecular modelling studies on the synthesised DRD4 ligands. Moreover, during my mobility at the Goethe University of Frankfurt, I prepared new proteolysis targeting chimaeras (PROTACs) for DRD4 (compounds **28-30**, Figure 1B), to be tested as anticancer compounds for the treatment of GBM.

-(ii) a scaffold hybridization strategy has been used for the discovery of potent dopamine DRD3 selective or multitarget ligands (compounds **31-39**, Figure 1C), potentially useful for central nervous system disorders;

-(iii) a benzo-cracking approach was applied for the preparation of new potent and highly selective sigma1 receptor antagonists (compounds **40-43**, Figure 1D), which were evaluated in a preclinical model of binge eating disorders.

## 2. DOPAMINE RECEPTORS

Dopamine (DA) is a catecholamine neurotransmitter located in the central nervous system (CNS) of all mammals, where it is involved in working memory, locomotor activity, neuroendocrine secretion, emotion regulation and food intake. In the periphery, it also plays several physiological roles, including the control of cardiovascular, gastrointestinal and renal functions.<sup>4-6</sup>

All these physiological functions are mediated by five distinct dopamine receptors (DRDs) that are members of the class A G protein-coupled receptor (GPCR) superfamily, consisting of 7 domains, with the N-terminal being outside of the membrane, and the C-terminal inside it.<sup>6</sup> Based on their function, DRDs are divided into two main receptor groups namely the D1-like subfamily, which consists of D1 and D5 receptors (DRD1, DRD5), and the D2-like subfamily, comprising D2, D3 and D4 receptors (DRD2, DRD3, DRD4).<sup>4,5,7,8</sup> D1-like receptors couple to  $G_s$  proteins, which increase the level of intracellular cyclic adenosine monophosphate (cAMP) by activating adenylyl cyclase. Conversely, D2-like receptors decrease the production of cAMP through interactions with  $G_i/G_o$  protein.<sup>5-7</sup> Furthermore, both of these receptor subfamilies can regulate other G-protein dependent or independent pathways, involving phospholipases,  $\beta$ -arrestins, protein kinases, ion channels (calcium, potassium,  $Na^+/K^+$ -ATP-ase), and the  $Na^+/H^+$  antiporter.<sup>5,7</sup>

Structural homology between individual DRDs is high: DRD1 and DRD5 share 80% of amino acid residues of their transmembrane domains (TMs), while DRD2 and DRD3 share 75% and DRD2 and DRD4 53% of TMs' sequence.<sup>5</sup> The carboxylic terminal of D1-like receptors is 7 times longer than that of the D2-like receptors. The two cysteine

molecules found in IL2 and IL3 of both subfamilies of DRDs are considered relevant for the presumed formation of disulphide bridges contributing to the structural integrity of these receptors. Long IL3 is considered relevant for inhibiting adenylyl cyclase by binding to  $G_i$  and is characteristic only for the D2-like receptors, whereas it is short in D1-like subtypes. D2-like receptors differ amongst themselves by structural differences in the IL3. DRD2 (appearing as two spliced isomorphs) contains an insertion of 29 amino acids in IL3, contributing to different affinities of this receptor for adenylyl cyclase. There are two DRD3 splice variants, differentiating in the positions of spliced regions in IL3: one has a deletion in the transmembrane domain 3, while the other has a deletion between transmembrane domains 5 and 6. In the case of DRD4, insertions containing 2- to 11-fold repeats of the 16-amino acid sequence are present, with the 4-fold repeat being the most predominant (> 60% in the human population), followed by 7-fold and 2-fold repeats.<sup>5,7-9</sup> Despite the high structural homology, the binding affinity of DA differs significantly between DRDs belonging to the same subfamily (i.e. DA has 20 times higher affinity for DRD3 compared to DRD2 based on the differences between these receptors' IL3 structure). Similarly, DRD4 exhibits different binding affinity to several compounds, when compared to DRD2 and DRD3 (i.e. high affinity for clozapine and > 10 times lower affinity for chlorpromazine).<sup>5</sup>

DRDs are localized in different areas of the CNS, including the hippocampus (dentate gyrus) and the subventricular zone of the brain. Specifically, DRD1 and DRD5 are mostly present in the striatum, nucleus accumbens, olfactory bulb, putamen, hypothalamus, temporal and frontal cortex, caudate and substantia nigra pars reticulata, while DRD2, DRD3 and DRD4 are expressed in the pituitary gland, striatum, external globus pallidus,



basal ganglia and cortical parts of the nucleus accumbens and the brain, as well as hippocampus and amygdala. Moreover, all these receptors can be found in peripheral parts of the body, most notably in the vasculature and kidneys.<sup>6,9,10</sup>

Hypo- or hyperactivation of the dopaminergic system has been associated with several pathological conditions in CNS, including schizophrenia, Parkinson's disease (PD), Tourette's disorder, neuroleptic-induced akathisia, brain cancer, eating disorders, cognitive deficits, alcohol and substance use disorders, making the DRDs attractive therapeutic targets.<sup>11</sup>

Concerning the dopaminergic system, in the practical part of my Ph.D. thesis, I have focused on the development of ligands behaving as DRD3-selective or multitarget agents, as well as on the development of DRD4-selective ligands.

## 3. DOPAMINE D4 RECEPTOR

### 3.1. Background

Among the five DRD subtypes, DRD4 has the lowest expression levels and is predominantly localized in the CNS, especially in the frontal cortex, pituitary gland, hippocampus, medulla, hypothalamus, and amygdala.<sup>12</sup>

Since its identification and cloning in 1991,<sup>13</sup> DRD4 has gained great interest as a target for antipsychotic drugs.<sup>14</sup> **Clozapine** (Figure 2) was the first atypical antipsychotic agent to show high DRD4 antagonist activity and selectivity over the other D2-like receptor subtypes.<sup>13,15</sup> Pharmacological results obtained using clozapine prompted the researchers to discover other DRD4 antagonists potentially useful as antischizophrenic drugs.<sup>16</sup> Among them, the very selective and CNS penetrant DRD4 antagonist **L-745870** (Figure 2) was identified in Merck labs.<sup>17-19</sup> This compound showed a subnanomolar affinity for DRD4 and > 2000-fold selectivity over the other DRDs, which was significantly higher than that of **clozapine** and all the other DRD4 ligands at that time.<sup>18</sup> However, negative results from preclinical and clinical studies, in which **L-745870** failed to show the same efficacy as clozapine as an antipsychotic drug,<sup>17,19</sup> made researchers lose their interest in DRD4 as a therapeutic target for the treatment of schizophrenia.

Recent discoveries have renewed the interest in DRD4 as an emerging target for the management of pathologies different from neuropsychiatric disorders, such as eating disorders and alcohol or substance use disorders. This awareness continues to stimulate the search for novel potent and selective DRD4 ligands. Moreover, several neurobiological pieces of evidence suggest a possible relationship between DRD4 and

glioblastoma (GBM),<sup>20,21</sup> as it was shown that its inhibition leads to the disruption of the autophagy-lysosomal pathway of the GBM stem cells, propagating apoptosis. Based on the information stored in the Cancer Genome Atlas on GBM gene expression, the patients with increased DRD4 levels, in comparison to those with a lower one, have worse survival rates. Antagonists such as **L-745870**; **PNU-96415E**; **PD-168,568** and **L-741,742** (Figure 2) reduce the clonogenic potential of GBM stem cells, inhibit the autophagic flux, block the ERK/PDGFR $\beta$  pathway, act synergistically with **temozolomide** and stimulate apoptosis. However, at present, few data suggesting that the DRD4 is crucial for the survival of GBM cells are reported. Therefore, selective DRD4 antagonists might shed light on the role played by this subtype in GBM and, especially, become valuable alternatives to the standard treatments such as surgery and radiotherapy, which cannot always be applied, and pharmacological treatments, which are still very limited due to drug resistance.

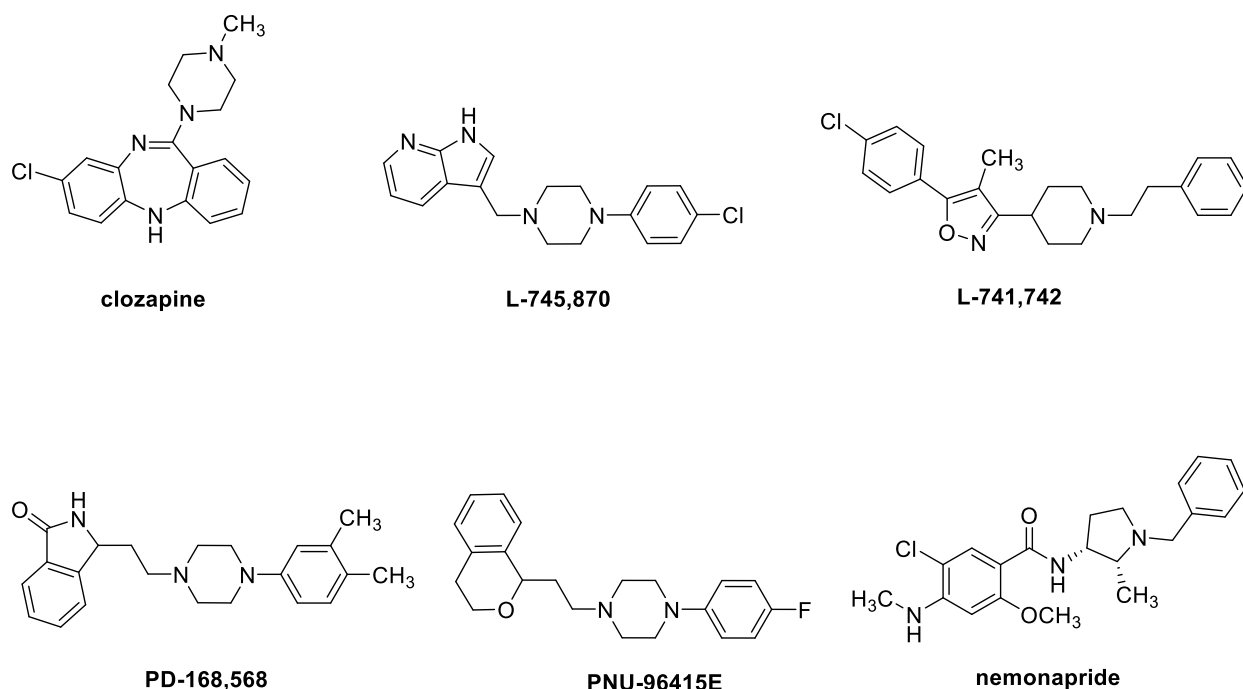


**Figure 2.** Chemical structures of potent DRD4 ligands.

The DRD4 ligands reported so far belong to different chemotypes, including piperazines, piperidines, dibenzodiazepines, morpholines and imidazolines.<sup>7</sup> Among them, the most studied ligands are characterized by arylpiperidine or arylpiperazine scaffolds and their structures can be described by a general pharmacophore consisting of a lipophilic scaffold linked by a spacer to a basic function and an aromatic terminal (Figure 3), which potentially affects the intrinsic activity of the compounds.<sup>22,23</sup> The linker may contain an amide function, which is also characteristic for many ligands targeting other DRDs. The length of the linker might potentially have a role in DRDs' subtype selectivity, so the modifications of this portion might prove useful for further understanding DRD4 subtype-selectivity.<sup>22,23</sup>

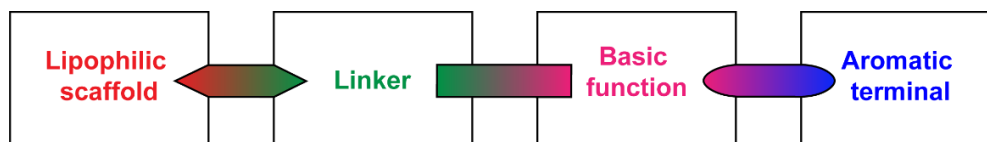


**Figure 3.** General pharmacophore model deduced from the structures of classic DRD4 piperazine- and piperidine-containing compounds.

Recently resolved crystal structures of the mouse DRD4 in complex with the potent antagonist **L-745870** (PDB code: 6IQL)<sup>24</sup> and the human DRD4 with the antipsychotic drug **nemonapride** (Figure 2) (PDB code: 5WIU)<sup>25</sup> have strongly improved the knowledge of the molecular requirement for the interaction with DRD4, further helping medicinal chemists in drug design.

### 3.2. Introduction and objectives of the work

In 2018, the medicinal chemistry team with whom I developed my Ph.D. thesis demonstrated that the known muscarinic acetylcholine receptor (mAChR) M1 bitopic agonist **77-LH-28-1** also showed high DRD4 affinity and selectivity over the other D2-like receptor subtypes ( $pK_i$  DRD2 = 6.17; DRD3 = 6.21; DRD4 = 9.01).<sup>26</sup> Curiously, the structure of **77-LH-28-1** (Figure 4B) fits the features of the pharmacophoric model reported in Figure 4A, except for the presence of a butyl chain instead of the aromatic terminal. Such a compound has been the first known example of DRD4 selective piperidines with a unique structural feature.

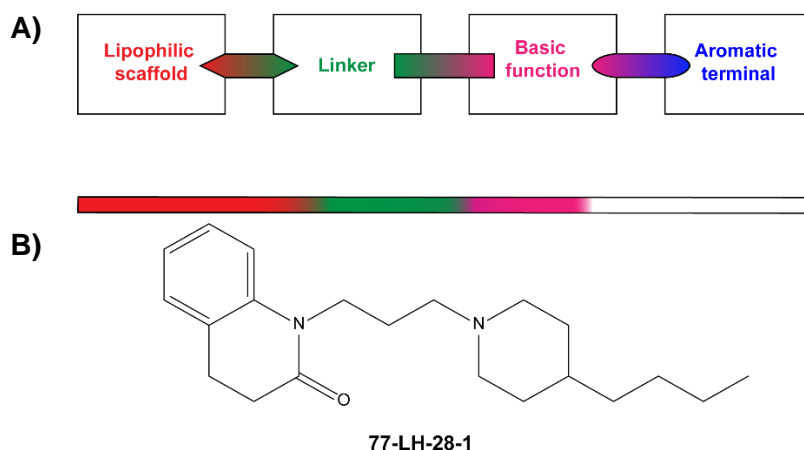


**Figure 4.** A) General pharmacophore of 1,4-disubstituted piperidines and piperazines deduced from the structures of classic DRD3 and DRD4 drugs. (B) Chemical structure of compound **77-LH-28-1**, composed of a lipophilic scaffold, a linker, a basic function and a butyl chain instead of an aromatic terminal.

Encouraged by its interesting affinity profile, an extensive SAR study has been undertaken to identify the structural features required for selective interaction with DRD4 and obtain compounds lacking mAChR activity. The preliminary approach was the modification of the aliphatic butyl chain of **77-LH-28-1**, which was replaced by alkyl, hydroxyalkyl, aryl and alkylaryl moieties, leading to the preparation of a novel series of piperidine and piperazine analogues (compounds **44-56**, Figure 5). These terminals were chosen specifically to assess the binding profiles of those compounds which did not possess strictly an aryl substituent (classic DRD4 pharmacophore terminal), but also contained an alkyl portion, to evaluate whether this could affect the affinity of newly-synthesised compounds for DRD4.

As expected, this study demonstrated that the aliphatic chain of **77-LH-28-1** can be successfully replaced by an aryl or alkylaryl chain without affecting the high DRD4 affinity and selectivity over DRD2 and DRD3 subtypes. In particular, the 4-benzylpiperidine **51**

and the 4-phenylpiperazine **54** showed high DRD4 affinity and selectivity not only over the other D2-like subtypes (Table 1), but also over M1-M5 mAChRs (Table 2). Compound **54** also displayed high selectivity over a series of selected off-targets, namely  $\alpha$ 1a-,  $\alpha$ 1b- and  $\alpha$ 1d-adrenoceptor ( $\alpha$ 1a-,  $\alpha$ 1b- and  $\alpha$ 1d-AR),  $\beta$ 1- and  $\beta$ 2-AR,  $\sigma$ 1 receptor, dopamine transporter (DAT) and serotonin transporter (SERT) (Table 2).<sup>26</sup>

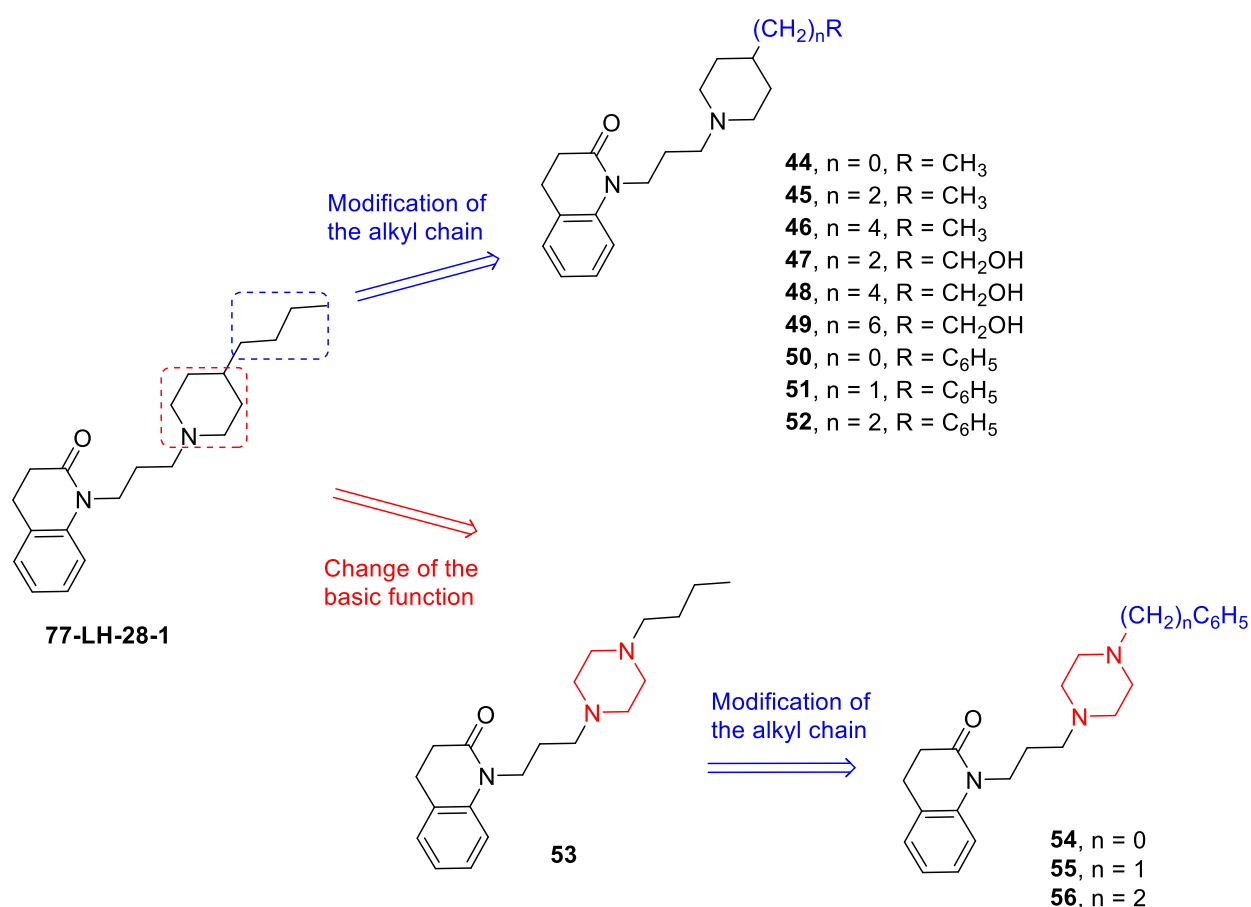


**Figure 5.** Chemical structures of **77-LH-28-1** and compounds **44-56**.

**Table 1.** Affinity constants, expressed as  $pK_i^a$  of compounds **77-LH-28-1**, **51** and **54** for human cloned DRD2, DRD3 and DRD4 expressed in HEK293T cells.

Compound	$pK_i^a$				
	hDRD2	hDRD3	hDRD4	D2/D4	D3/D4
<b>77-LH-28-1</b>	6.17 ± 0.16	6.21 ± 0.13	9.01 ± 0.04	691	631
<b>51</b>	6.04 ± 0.06	5.74 ± 0.28	8.90 ± 0.19	724	1445
<b>54</b>	5.96 ± 0.02	5.88 ± 0.10	8.54 ± 0.05	380	457

<sup>a</sup>The values represent the arithmetic mean ± S.E.M.; n represents the number of experiments.

**Table 2.** Affinity constants, expressed as  $pK_i^a$  of compounds **51** and **54** for selected off-targets.

Target	$pK_i^a$	
	<b>51</b>	<b>54</b>
<b>M1</b>	6.44 ± 0.21	5.37 ± 0.04
<b>M2</b>	6.10 ± 0.08	4.78 ± 0.05
<b>M3</b>	5.52 ± 0.14	4.75 ± 0.07
<b>M4</b>	6.14 ± 0.08	5.03 ± 0.23
<b>M5</b>	5.43 ± 0.25	4.56 ± 0.03
<b>α1a-AR</b>	6.59 ± 0.08	7.27 ± 0.12
<b>α1b-AR</b>	6.65 ± 0.07	7.13 ± 0.08
<b>α1d-AR</b>	6.52 ± 0.07	7.04 ± 0.19
<b>β1-AR</b>	4.99 ± 0.11	4.49 ± 0.26
<b>β2-AR</b>	5.02 ± 0.01	4.45 ± 0.03
<b>σ1</b>	8.00 ± 0.07	6.57 ± 0.09
<b>DAT</b>	6.35 ± 0.17	5.06 ± 0.09
<b>SERT</b>	7.33 ± 0.05	5.30 ± 0.08

<sup>a</sup>The values represent the arithmetic mean ± S.E.M.; n represents the number of experiments.



Bioluminescence resonance transfer (BRET)-based functional assays performed on compounds **77-LH-28-1**, **51** and **54** revealed that **77-LH-28-1** and **51** behaved as antagonists in both G<sub>i</sub> activation and β-arrestin2 recruitment assays, while, interestingly, **54** showed a biased behaviour, potently and partially activating G<sub>i</sub> protein and inhibiting β-arrestin2 recruitment (Table 3). Therefore, it was the first reported potent and selective piperazine DRD4 ligand showing functional selectivity.<sup>26</sup>

**Table 3.** Potency (expressed as pEC<sub>50</sub><sup>a</sup> or pIC<sub>50</sub><sup>a</sup>) and efficacy values (%<sup>a</sup>, normalized to dopamine E<sub>max</sub>) of dopamine and compounds **77-LH-28-1**, **51** and **54** for DRD4 expressed in HEK293T cells.<sup>a</sup>

Compound	DRD4							
	Gi protein activation				β-arrestin2 Recruitment			
	pEC <sub>50</sub>	E <sub>max</sub>	pIC <sub>50</sub>	I <sub>max</sub>	pEC <sub>50</sub>	E <sub>max</sub>	pIC <sub>50</sub>	I <sub>max</sub>
<b>Dopamine</b>	7.91±0.19	100			7.04±0.65	100		
<b>77-LH-28-1</b>	ND	ND	6.93±0.15	-98	ND	ND	8.22±0.31	-72
<b>51</b>	ND	ND	6.77±0.25	-68	ND	ND	6.24±0.19	-94
<b>54</b>	9.80±0.31	48	8.01±0.31	-41	ND	ND	9.14±0.38	-69

<sup>a</sup>The values represent the arithmetic mean ± S.E.M.; n represents the number of experiments. ND = cannot be determined.

The pharmacokinetic profile of **54** was determined in *in vitro* and *in vivo* assays. It exhibited high kinetic solubility at the physiological pH (pH = 7.4), moderate protein binding in the homogenate of mouse brain or mouse plasma, and had high permeability accompanied by low efflux ratios, when tested in MDCKII-Mdr1 cell lines, therefore not resulting a P-gp substrate (Table 4). Moreover, **54**'s brain penetration and systemic exposure (after subcutaneous administration at 3 mg/kg in male CD-1 mice) were

evaluated. After 0.25 h of treatment, the exposures reached maximal concentration in the mouse plasma or brain (Figure 6), with a relevant brain penetration ( $K_p = 4.35$ ) and no impact on the efflux transporters, but an influx potential. Measured exposure ( $AUC_{last}$ ) in plasma was 518.0 h·ng/mL while being 2384.0 h·ng/mL in the brain. Free concentration exposures ( $AUC_{ulast}$ ) were 50.5 in the plasma and 204.0 in the brain (Table 5).<sup>26</sup>

**Table 4.** ADME parameters of the compound **54**.

<b>54</b>		
Kinetic solubility (pH 7.4)	$\mu\text{M}$	520
	mg/mL	0.23
Protein binding <sup>a</sup>	Human plasma ( $f_u$ ) <sup>b</sup>	0.033
	Mouse plasma ( $f_u$ ) <sup>b</sup>	0.097
	Mouse brain ( $f_u$ ) <sup>b</sup>	0.086
Permeability <sup>c</sup>	Papp A-B (nm/sec)	162
	Papp B-A (nm/sec)	197
	Papp A-B inhibitor (nm/sec)	142
	Papp B-A inhibitor (nm/sec)	229
	Efflux Ratio (B-A/A-B)	1.22

<sup>a</sup>Experiment performed at 0.5 and 5  $\mu\text{M}$  in plasma and brain, respectively; <sup>b</sup> $f_u$  = fraction unbound; <sup>c</sup>the P-gp inhibitor used in permeability studies is Elacridar 10  $\mu\text{M}$ , Papp = passive membrane permeability, A-B = apical to basolateral, B-A = basolateral to apical.

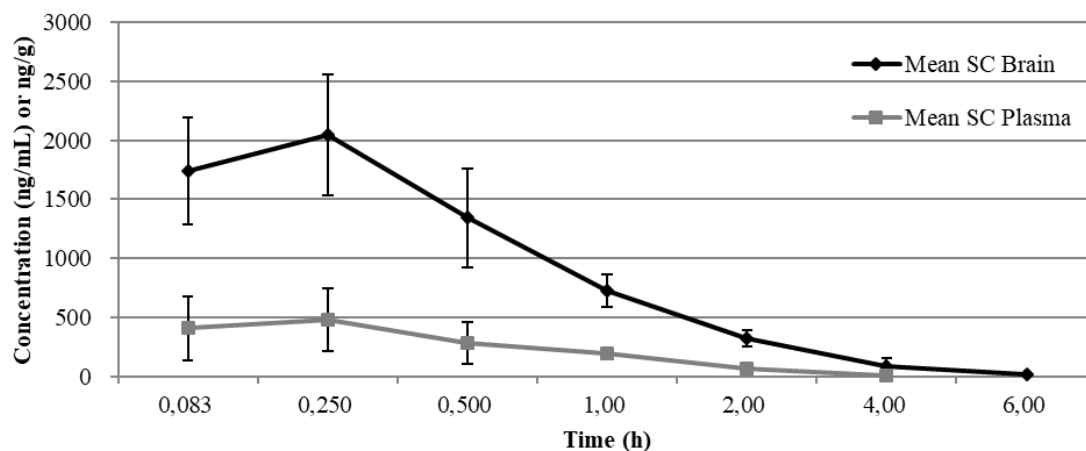


**Figure 6.** The plot of mean concentration with standard deviations of **54** in plasma and brain after subcutaneous administration (3 mg/kg).

**Table 5.** Pharmacokinetic profile of **54** after the subcutaneous administration in male CD1 mice.

	Brain	Plasma
$C_{max}$ (ng/mL) <sup>a</sup>	2046	481
$T_{max}$ (h) <sup>b</sup>	0.25	0.25
$AUC_{last}$ (h*ng/mL) <sup>c</sup>	2384	518
Half-life (h)	0.93	0.77
$K_p$ <sup>d</sup>	4.35	
$K_{puu,brain}$ <sup>e</sup>	4.05	

<sup>a</sup> $C_{max}$  = maximum mean concentration; <sup>b</sup> $T_{max}$  = time corresponding to maximum drug concentration; <sup>c</sup> $AUC$  = area under the curve; <sup>d</sup> $K_p$  =  $AUC_{brain}/AUC_{plasma}$ ; <sup>e</sup> $K_{puu,brain}$  =  $AUC_{brain}/AUC_{plasma}$ .

The promising profile of **54** prompted us to select it as a lead compound for the discovery of new potent and selective DRD4 ligands to be used as pharmacological tools to better understand the role of DRD4 in diseases for which the involvement of this receptor has been proposed. In particular, maintaining the *N*-arylpiperazine moiety, a well-known scaffold of potent DRD4 ligands,<sup>7,27</sup> the following modifications were designed (Figure 7):

- I) Replacement of the quinolinone moiety with different bioisosteric nuclei, whose choice was inspired by D4-selective ligands known in the literature<sup>7</sup> (compounds **1-6**);
- II) Replacement of the 3C linker with other spacers of different lengths to evaluate the role of the distance between the basic function and the lipophilic scaffold (compounds **7-9**);
- III) Insertion of substituents with different lipophilic and electronic contributions, in all possible combinations according to the Craig plot,<sup>28</sup> such as methyl group (+ $\pi$ , - $\sigma$ ), methoxy group (- $\pi$ , - $\sigma$ ), chlorine (+ $\pi$ , + $\sigma$ ) and nitro group (- $\pi$ , + $\sigma$ ), on all three positions (ortho-, meta- and para-) of the terminal phenyl ring (compounds **10-21**).

Additionally, compounds **22-24** (Figure 7), with substituted aromatic terminals being 2-cyanophenyl, 2-pyridyl and 2-pyrimidinyl, selected due to their presence in known DRD4 selective compounds, were synthesised.<sup>7</sup> Compounds **25-27** (Figure 7), containing double substitutions by chlorine on the phenyl ring, in all three combinations (ortho/meta; ortho/para; meta/para) were prepared as well.

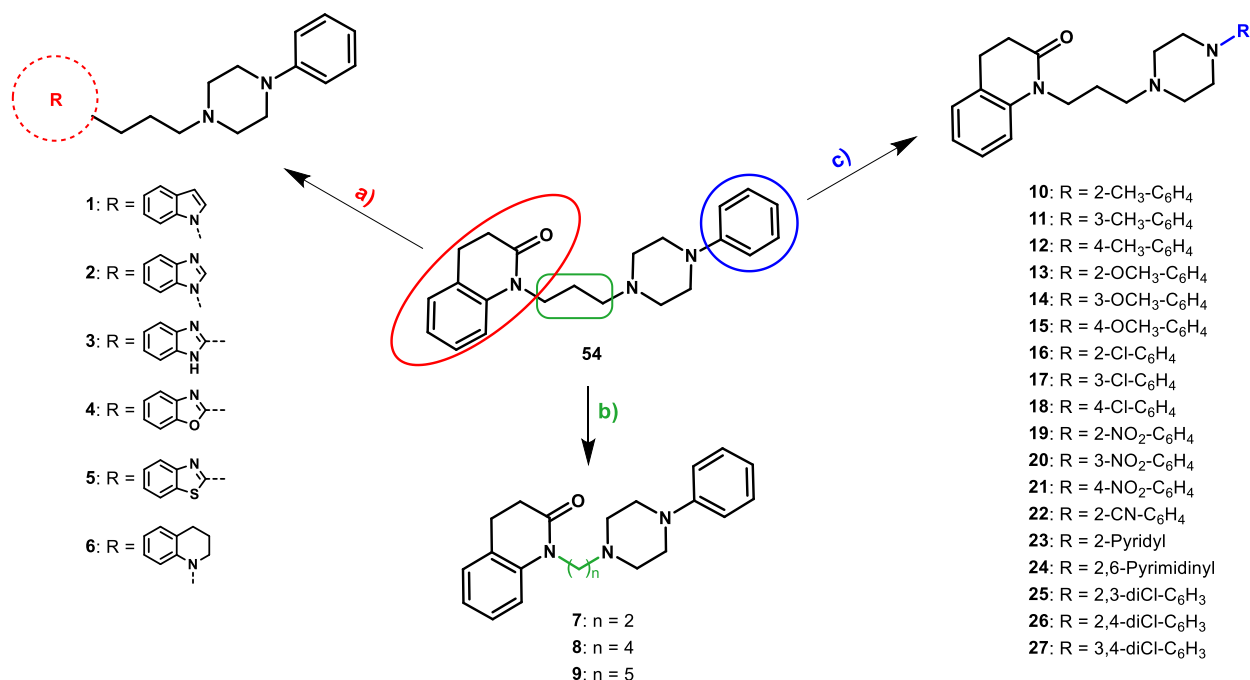


**Figure 7.** Modifications of the chemical structure of the lead compound **54** yielding derivatives **1-27**: a) modifications of the quinolinone moiety; b) modifications of the linker length; c) modifications of the N-phenyl terminal.

All the synthesised compounds were evaluated for their affinities at DRD2, DRD3 and DRD4 (via radioligand-binding assay), followed by testing the most DRD4 selective compounds for their functional activities in Gi protein activation and  $\beta$ -arrestin recruitment (via BRET assay). Molecular modelling studies were performed on all compounds, to rationalize the obtained results.

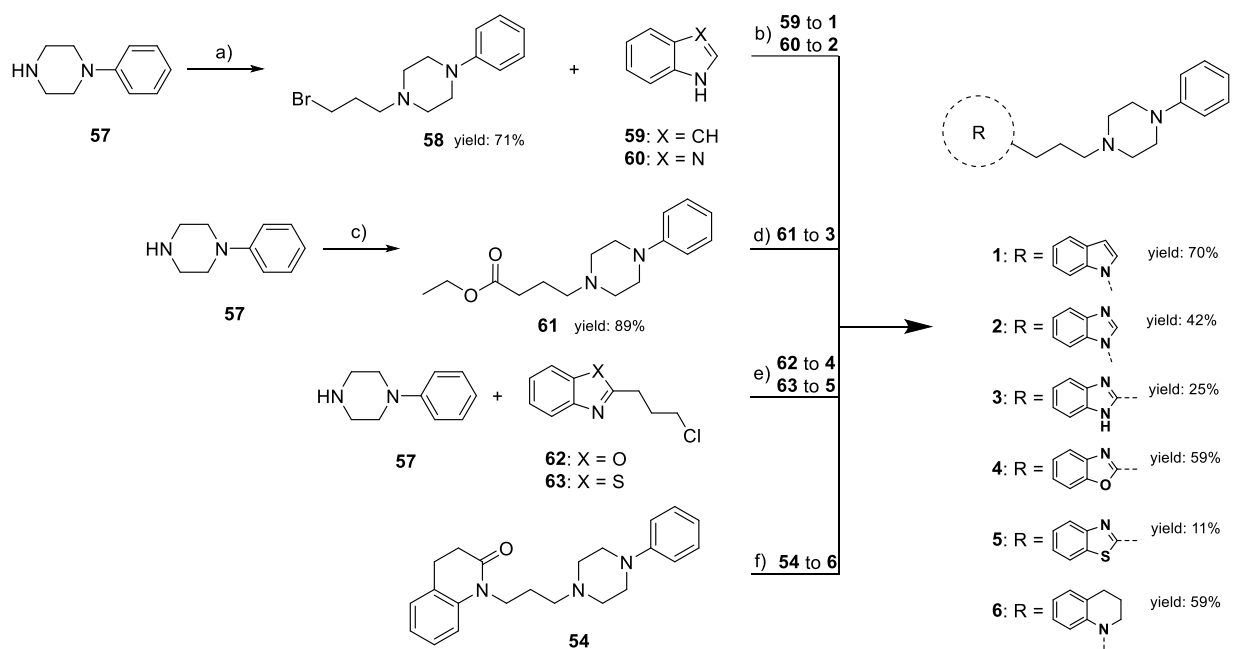
Only the most promising compounds were tested *in vitro* for their impact on GBM cells' viability. Compounds **1**,<sup>29</sup> **2**,<sup>30</sup> **8**,<sup>31</sup> **13**,<sup>32</sup> **15**,<sup>32</sup> **17**,<sup>33</sup> **23**,<sup>32</sup> **24**<sup>32</sup> and **25**<sup>32</sup> were known compounds, but they had never been previously tested on DRD4. Cell lines T98 and U251 were used, as well as GBM stem cell line GSC#83. Controls used for the experiment contained **temozolomide** for useful comparison. The goal of the *in vitro* investigation was

to evaluate the effectiveness of the most promising ligands emerging from this research, against the standard therapeutic approach.

### 3.3. Results and discussion

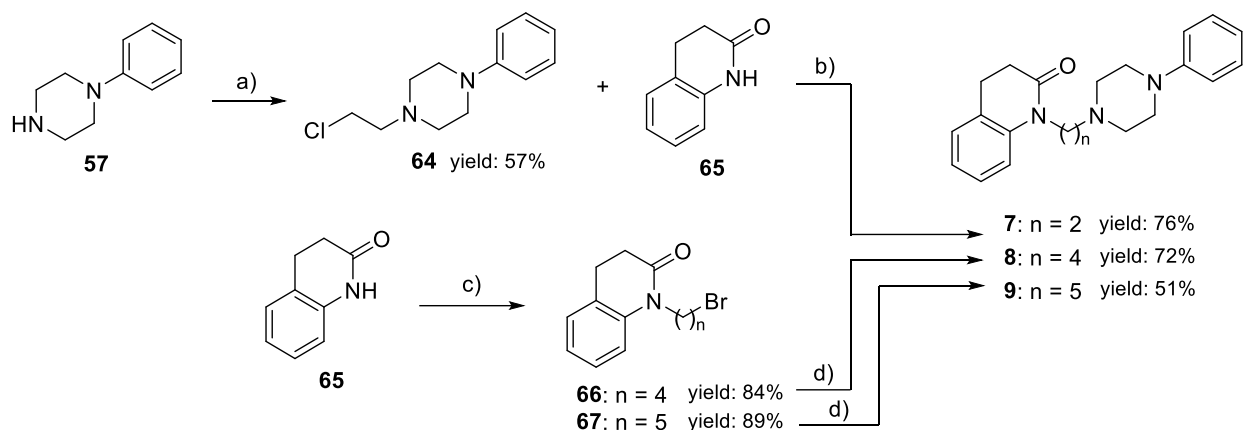
#### 3.3.1. Synthesis of DRD4 ligands

Compounds **1-6** were synthesised according to the procedures reported in Scheme 1. N-alkylation of the commercially available compound 1-phenylpiperazine (**57**) was performed using 1,3-dibromopropane in basic conditions (KOH) to produce the intermediate **58**,<sup>34</sup> which was then reacted with indole (**59**) or benzimidazole (**60**) in the presence of 60% NaH in mineral oil to obtain **1** (yield: 70%) and **2** (yield: 42%), respectively. The reaction of **57** with ethyl-4-bromobutanoate in the presence of NaHCO<sub>3</sub> resulted in the formation of the intermediate **61**,<sup>35</sup> whose treatment with benzene-1,2-diamine gave compound **3** (yield: 25%). Compound **57** was reacted with alkyl chlorides **62**<sup>36</sup> or **63**<sup>37</sup> in the presence of K<sub>2</sub>CO<sub>3</sub>, affording **4** (yield: 59%) or **5** (yield: 11%), respectively. Finally, amine **6** (yield: 59%) was obtained by reduction of the lead compound **54** with BH<sub>3</sub>·S(CH<sub>3</sub>)<sub>2</sub>.



**Scheme 1.** Synthesis of compounds **1-6**. Reagents and conditions: (a) 1,3-dibromopropane, KOH, dimethylsulfoxide (DMSO); (b) 60% NaH in mineral oil, DMF; (c) ethyl 4-bromobutanoate, NaHCO<sub>3</sub>, EtOH; (d) benzene-1,2-diamine, 4M HCl in dioxane; (e) K<sub>2</sub>CO<sub>3</sub>, KI, dimethoxyethane (DME); (f) BH<sub>3</sub>·S(CH<sub>3</sub>)<sub>2</sub>, tetrahydrofuran (THF).

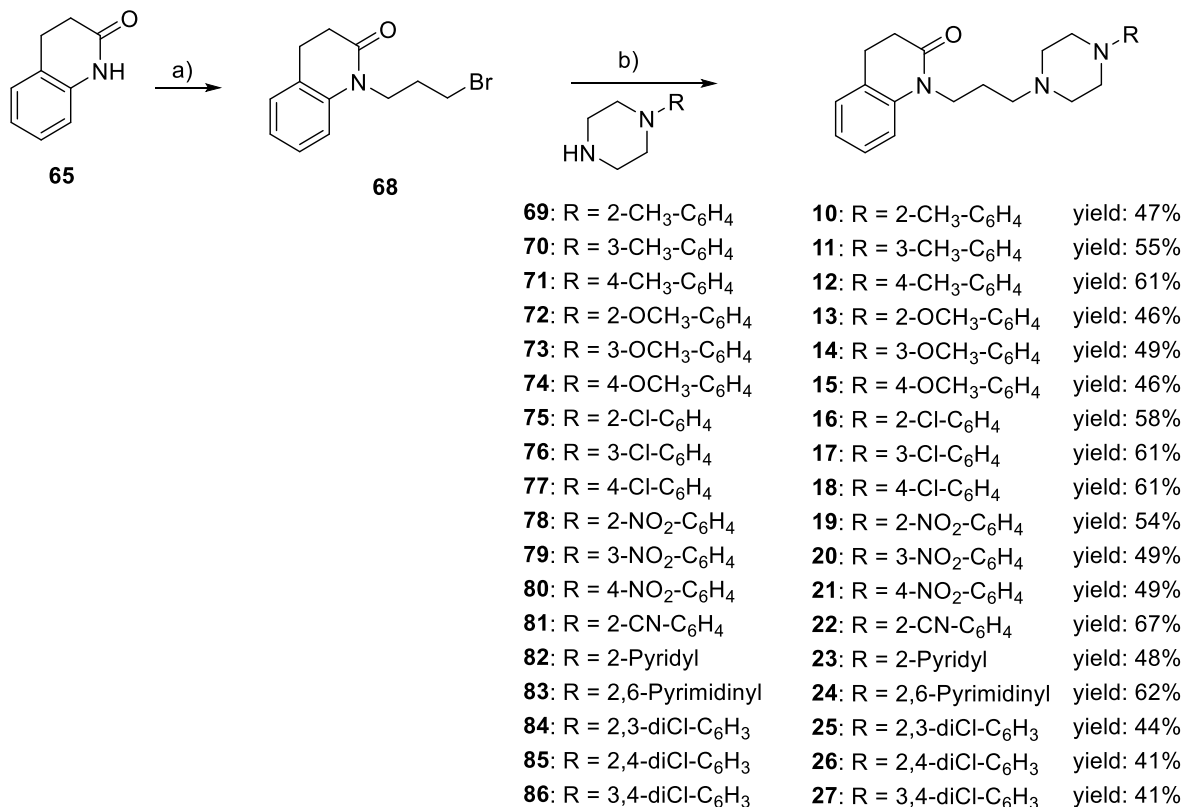
Compounds **7-9** were prepared as shown in Scheme 2. **7** (yield: 76%) was synthesised by reacting intermediate **64**,<sup>38</sup> obtained by N-alkylation reaction of **57** with 1-bromo-2-chloroethane in the presence of K<sub>2</sub>CO<sub>3</sub>, with the commercially available 3,4-dihydro-2(1H)-quinolinone (**65**), in the presence of 60% NaH in mineral oil. **65** was also reacted with 1,4-dibromobutane or 1,5-dibromopentane in the presence of 60% NaH in mineral oil to produce intermediates **66**<sup>39</sup> and **67**,<sup>40</sup> respectively, whose treatment with **57** in the presence of K<sub>2</sub>CO<sub>3</sub> afforded the corresponding final derivatives **8** (yield: 72%) and **9** (yield: 51%).



**Scheme 2.** Synthesis of compounds **7-9**. Reagents and conditions: (a) 1-bromo-2-chloroethane,  $\text{K}_2\text{CO}_3$ , acetone; (b) 60% NaH in mineral oil, xylene; (c) 1,4-dibromobutane (for **66**) or 1,5-dibromopentane (for **67**), 60% NaH in mineral oil, DMF; (d) **57**,  $\text{K}_2\text{CO}_3$ , DMF.

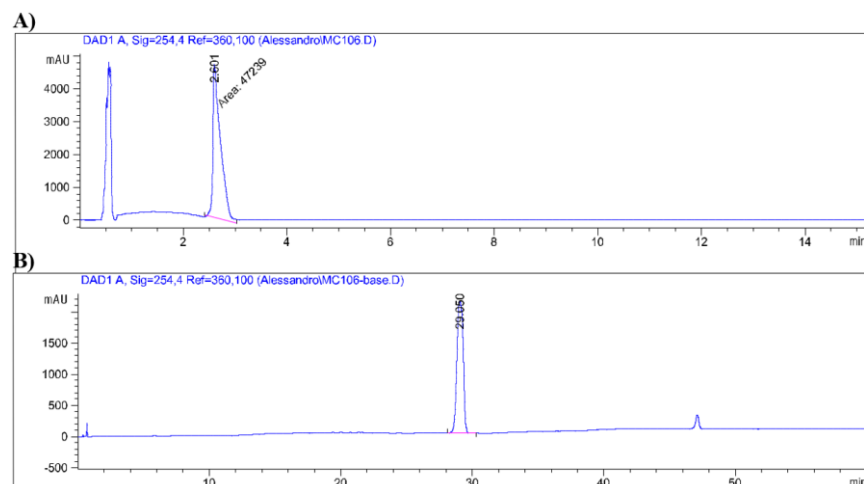
Compounds **10-27** were obtained following the procedure reported in Scheme 3. Intermediate **68** was synthesised by reacting **65** and 1,3-dibromopropane, in the presence of 60% NaH in mineral oil.<sup>41</sup> **68** was treated with the appropriate amines **69-86**, in the presence of  $\text{K}_2\text{CO}_3$  to afford **10-27** in moderate yields, from a minimum 41% in case of compounds **26** and **27** with double chlorine substitution on the aromatic terminal, to a maximum 67% in case of **22** (benzonitrile as the aromatic terminal).



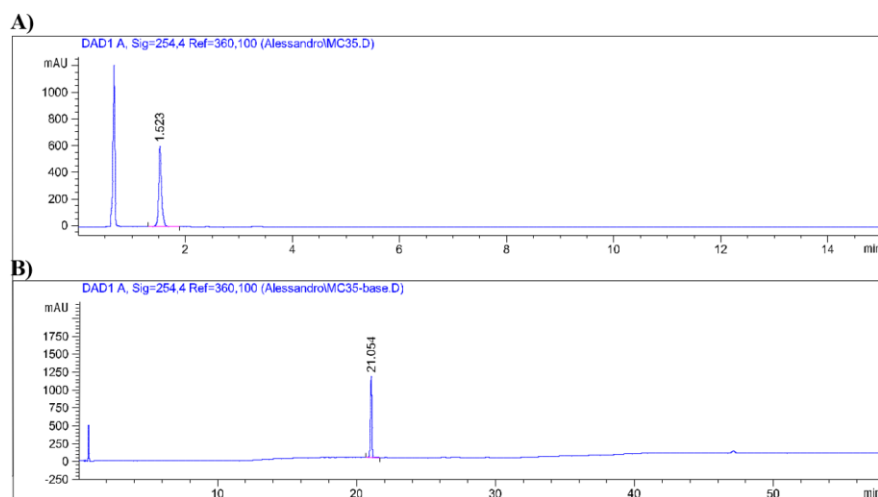


**Scheme 3.** Synthesis of compounds **10-27**. Reagents and conditions: (a) 1,3-dibromopropane, 60% NaH in mineral oil, DMF; (b) K<sub>2</sub>CO<sub>3</sub>, DMF.

The purity of all the novel compounds, determined by combustion analysis, was  $\geq 95\%$ . For the most interesting compounds **18** and **23**, it was confirmed by HPLC analysis as reported in Figures 8 and 9, respectively. The detection wavelength was set at a range of 210-280 nm, for the optimal detection of the expected peaks at  $\lambda$  254 nm, as previously described by Shaik et al. for the evaluation of eticlopride-based DRD2/DRD3 bitopic ligands.<sup>42</sup> This wavelength corresponds to the short wave (254 nm) UV light under which our ligands are visible, due to the presence of the aromatic groups.



**Figure 8.** HPLC chromatograms of **18**. HPLC-DAD analysis was performed using an Agilent Technologies 1260 Infinity system. For each HPLC run, multiple DAD absorbance signals were measured (range: 210-280 nm). Representative chromatograms were reported at 254 nm. Separation of the analyte was achieved using a Phenomenex Gemini C18 4.6x 50 mm. A 3 m column was used. A) Mobile phase: isocratic 30% ACN in water +0.1% TFA; 15-minute run; injection 20 L (0.5 mg/ mL); temperature 40 °C; purity > 95%; Method B) mobile phase: gradient 10%- 80% ACN in water +0.1% DEA; 60-minute run; injection 20 L (0.5 mg/ mL); temperature 40 °C; purity > 95%.

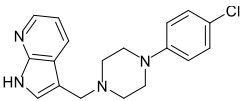
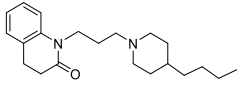
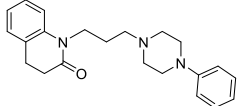
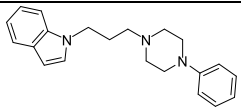
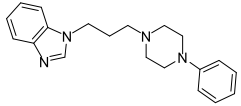
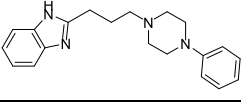
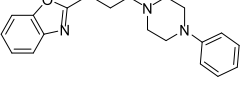


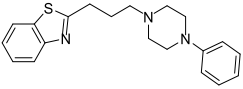
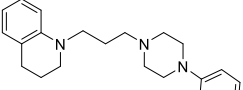
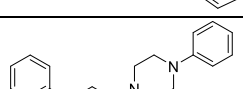
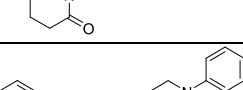
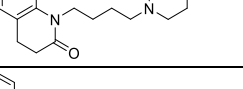
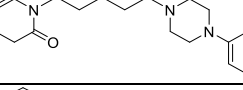
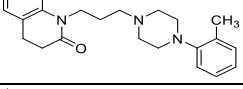
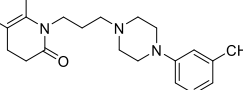
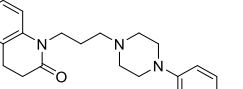
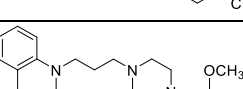
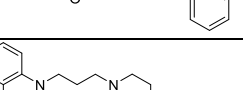
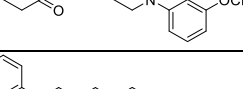
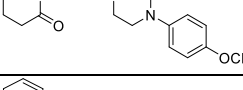
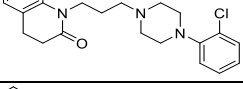
**Figure 9.** HPLC chromatograms of **23**. HPLC-DAD analysis was performed using an Agilent Technologies 1260 Infinity system. For each HPLC run, multiple DAD absorbance signals were measured (range: 210-280 nm). Representative chromatograms were reported at 254 nm. Separation of the analyte was achieved using a Phenomenex Gemini C18 4.6x 50 mm. A 3 m column was used. A) Mobile phase: isocratic 30% ACN in water +0.1% TFA; 15-minute run; injection 20 L (0.5 mg/ mL); temperature 40 °C; purity > 95%; Method B) mobile phase: gradient 10%- 80% ACN in water+ 0.1% DEA; 60-minute run; injection 20 L (0.5 mg/ mL); temperature 40 °C; purity > 95%.

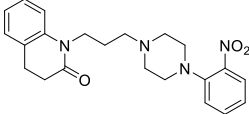
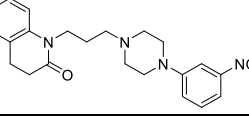
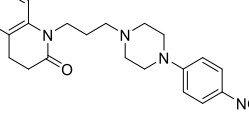
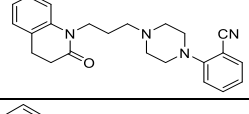
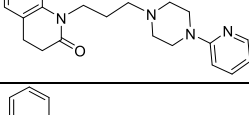
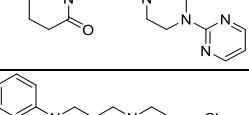
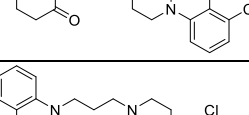
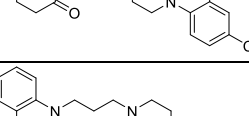
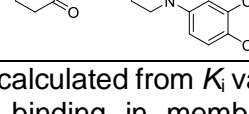
### 3.3.2. Radioligand binding assays

Ligands **1-27** were evaluated as oxalate salts by radioligand binding assay against all D2-like receptor subtypes expressed in HEK293T cells.<sup>9</sup> The high-affinity D2-like antagonist [<sup>3</sup>H]*N*-methylspiperone was used as a radioligand to label the receptors. All affinity values for D2-like receptors, determined according to the Cheng–Prusoff equation and expressed as pK<sub>i</sub>, are shown in Table 6 together with those of compounds **L-745870**, **77-LH-28-1** and **54**, included for useful comparison.

**Table 6.** Affinity constants, expressed as pK<sub>i</sub><sup>a</sup> values, of compounds **L-745870**, **77-LH-28-1**, **54** and **1-27** for DRD2, DRD3, and DRD4 expressed in HEK293T cells.

Compound	Structure	pK <sub>i</sub>			D2/D4 <sup>b</sup>	D3/D4 <sup>c</sup>
		DRD2	DRD3	DRD4		
<b>L-745870</b>		5.79 ± 0.09	6.42 ± 0.14	8.65 ± 0.14	724	170
<b>77-LH-28-1</b>		6.17 ± 0.16	6.21 ± 0.13	9.01 ± 0.04	691	631
<b>54</b>		5.96 ± 0.13	5.88 ± 0.09	8.54 ± 0.07	380	457
<b>1</b>		6.14 ± 0.10	6.31 ± 0.09	8.72 ± 0.05	380	257
<b>2</b>		4.92 ± 0.11	5.05 ± 0.13	7.91 ± 0.09	977	719
<b>3</b>		5.21 ± 0.08	6.08 ± 0.10	7.52 ± 0.06	204	28
<b>4</b>		5.77 ± 0.10	6.09 ± 0.11	7.43 ± 0.07	46	22

5		$5.75 \pm 0.07$	$6.16 \pm 0.07$	$7.99 \pm 0.08$	174	68
6		$6.15 \pm 0.12$	$6.25 \pm 0.15$	$8.58 \pm 0.10$	269	214
7		$4.89 \pm 0.11$	$5.97 \pm 0.13$	$7.20 \pm 0.08$	204	17
8		$5.95 \pm 0.13$	$7.09 \pm 0.13$	$8.37 \pm 0.11$	263	19
9		$6.55 \pm 0.05$	$6.71 \pm 0.06$	$7.63 \pm 0.09$	12	8
10		$6.40 \pm 0.14$	$6.56 \pm 0.14$	$8.87 \pm 0.07$	295	204
11		$5.84 \pm 0.12$	$6.10 \pm 0.10$	$8.75 \pm 0.08$	813	447
12		$5.29 \pm 0.09$	$5.77 \pm 0.13$	$9.01 \pm 0.09$	5248	1738
13		$7.09 \pm 0.16$	$7.00 \pm 0.11$	$9.21 \pm 0.07$	132	162
14		$5.51 \pm 0.15$	$5.81 \pm 0.11$	$8.38 \pm 0.10$	741	372
15		$4.68 \pm 0.10$	$5.08 \pm 0.13$	$8.16 \pm 0.10$	3020	1202
16		$6.86 \pm 0.08$	$7.22 \pm 0.09$	$9.22 \pm 0.04$	229	100
17		$6.12 \pm 0.12$	$6.55 \pm 0.15$	$8.98 \pm 0.13$	724	269
18		$5.26 \pm 0.07$	$5.61 \pm 0.11$	$9.18 \pm 0.06$	8318	3715

19		$6.88 \pm 0.18$	$6.89 \pm 0.15$	$9.39 \pm 0.10$	324	316
20		$5.60 \pm 0.11$	$5.90 \pm 0.14$	$8.45 \pm 0.11$	708	355
21		$4.62 \pm 0.09$	$4.96 \pm 0.19$	$8.18 \pm 0.12$	3631	1660
22		$6.45 \pm 0.10$	$6.47 \pm 0.08$	$8.97 \pm 0.11$	331	316
23		$5.56 \pm 0.09$	$5.59 \pm 0.16$	$8.65 \pm 0.09$	1230	1148
24		$5.40 \pm 0.16$	$5.64 \pm 0.16$	$8.35 \pm 0.16$	891	513
25		$7.26 \pm 0.07$	$7.67 \pm 0.17$	$9.16 \pm 0.08$	79	30
26		$6.26 \pm 0.15$	$6.30 \pm 0.13$	$9.17 \pm 0.03$	827	744
27		$6.02 \pm 0.16$	$6.20 \pm 0.17$	$9.06 \pm 0.11$	1098	725

<sup>a</sup>pK<sub>i</sub> values were calculated from K<sub>i</sub> values that were determined by competitive inhibition of [<sup>3</sup>H]N-methylspiperone binding in membranes harvested from HEK293T cells stably expressing hDRD2L, hDRD3, or hDRD4.4. All values are shown as an arithmetic mean value ± SEM. <sup>b</sup>Calculated as a ratio between K<sub>i</sub> values at DRD2 and DRD4. <sup>c</sup>Calculated as a ratio between K<sub>i</sub> values at DRD3 and DRD4.

From the analysis of the results, it emerged that ligands **2-5** exhibited lower affinities for DRD4, in comparison to **54**, while **1** and **6** retained the high DRD4 affinity and selectivity values of the lead. Even though **2** bound to DRD4 with lower affinity, it exhibited higher selectivity ratios (D2/D4 = 977; D3/D4 = 719) when compared to **54** (D2/D4 = 380; D3/D4 = 457).

The reduction of the linker length of **54**, obtaining **7**, caused a marked decrease in the binding affinity only at DRD4 ( $pK_i$  DRD4 = 8.54 for **54**;  $pK_i$  DRD4 = 7.20 for **7**) and DRD2 ( $pK_i$  DRD2 = 5.96 for **54**;  $pK_i$  DRD2 = 4.89 for **7**), with a consequent decrease in D3/D4 selectivity ratio (D3/D4 = 457 for **54**; D3/D4 = 17 for **7**). Differently, compound **8**, the higher homologue of **54** obtained by inserting a methylene unit in the linker, maintained similar DRD4 ( $pK_i$  DRD4 = 8.54 for **54**;  $pK_i$  DRD4 = 8.37 for **8**) and DRD2 ( $pK_i$  DRD2 = 5.96 for **54**;  $pK_i$  DRD2 = 5.95 for **8**) affinity values but showed an increase in the DRD3 affinity ( $pK_i$  DRD3 = 5.88 for **54**;  $pK_i$  DRD3 = 7.09 for **8**). Therefore, also in this case, the D3/D4 selectivity ratio was reduced. Although compounds **7** and **8** have shown different affinities for DRD2, DRD3 and DRD4 subtypes, the D2/D4 and D3/D4 selectivity ratios are similar (D2/D4 = 204, D3/D4 = 17, for **7**; D2/D4 = 263, D3/D4 = 19 for **8**). Further elongation of the linker, yielding **9**, resulted in lower DRD4 affinity, with a consequent decrease of D2/D4 and D3/D4 selectivity ratios (12 and 8, respectively). Taken together, these results highlight that the propyl chain represents the optimal distance between the quinolinone nucleus and the basic function.

The presence of a substituent on the terminal phenyl ring of **54** markedly affected the D2-like affinity and selectivity profiles of the ligands. All the ortho-, meta- and para-substituted derivatives showed high DRD4 affinities. However, the derivatives **10-12** and **16-18**, bearing substituents with  $+\pi$  values ( $\text{CH}_3$  and  $\text{Cl}$ ), displayed similar  $pK_i$  values at DRD4 regardless of their position on the phenyl ring, while substituents with  $-\pi$  values ( $\text{OCH}_3$  and  $\text{NO}_2$ ) conferred to the ligands the highest affinity when they are in the ortho-positions (**13** vs **14** and **15**; **19** vs **20** and **21**). Interestingly, whatever the nature of the substituent was, the most DRD4 selective compounds were the para-substituted ones (**12**, **15**, **18**,

and **21**) ( $D2/D4 = 5248$ ,  $D3/D4 = 1738$  for **12**;  $D2/D4 = 3020$ ,  $D3/D4 = 1202$  for **15**;  $D2/D4 = 8318$ ,  $D3/D4 = 3715$  for **18**;  $D2/D4 = 3631$ ,  $D3/D4 = 1660$  for **21**). The improved selectivity was due to the decrease in DRD2 and DRD3 affinity when the substituent was shifted from ortho- to meta- and especially to para-position.

Considering that, among the para-substituted compounds, the best selectivity profile was demonstrated by the 4-chloro derivative **18**, the influence of the dichlorophenyl disubstitution was probed by the synthesis and study of derivatives **25-27**. The results confirmed that the presence of a substituent in the para-position of the phenyl ring is detrimental to DRD2 and DRD3 binding affinity. Indeed, the ortho/para- and meta/para-disubstituted compounds **26** and **27** showed  $D2/D4$  and  $D3/D4$  selectivity ratios significantly higher than those of the ortho/meta-disubstituted compound **25**.

To extend the SARs concerning the aromatic terminal, the phenyl ring was replaced by other aromatic substituents, such as 2-cyanophenyl (**22**), 2-pyridyl (**23**), 2,6-pyrimidinyl (**24**) rings, which are also present in known potent and selective DRD4 ligands. Compounds **22-24** showed DRD4 affinity values similar to that of the lead compound **54**. Moreover, **23** and **24** exhibited a slight reduction in the affinity for DRD2 and DRD3 subtypes and, consequently, were more selective for DRD4 with respect to **54**. In particular, the 2-pyridyl derivative **23** showed the best selectivity profile ( $D2/D4 = 1230$ ,  $D3/D4 = 1148$ ).

It has been observed that ortho-, meta-, and para-regiosubstitutions on the terminal aryl ring might modulate the efficacy of arylpiperazines at DRD4.<sup>43,44</sup> However, previously reported DRD4 partial or highly efficacious agonists demonstrated to bind more readily when in competition against an agonist radioligand (i.e. [<sup>3</sup>H]-7-OH-DPAT) instead of the

classic antagonist [<sup>3</sup>H]N-methylspiperone. On the other hand, antagonists showed < 10-fold difference in binding  $K_i$ , or almost no difference at all, independently from the radioligand used.<sup>43</sup> Based on these observations, the DRD4 affinity of the ortho-, meta-, and para-chlorophenylpiperazines **16-18** has also been assessed using the agonist radioligand [<sup>3</sup>H]-7-OH-DPAT. None of the compounds showed any major shift in their pK<sub>i</sub> values when tested in the agonist-radioligand mode (**16**: pK<sub>i</sub> = 9.29±0.06; **17**: pK<sub>i</sub> = 9.11 ± 0.12; **18**: pK<sub>i</sub> = 8.83 ± 0.11) compared to the already reported affinity obtained with [<sup>3</sup>H]N-methylspiperone (**16**: pK<sub>i</sub> = 9.22±0.04; **17**: pK<sub>i</sub> = 8.98 ± 0.13; **18**: pK<sub>i</sub> = 9.18 ± 0.06), suggesting that they might behave as DRD4 antagonists.

### **3.3.3. Bioluminescence resonance energy transfer (BRET) assays**

Based on their remarkable DRD4 affinity/selectivity profiles, compounds **12**, **15**, **18**, **21** and **23** were selected to be evaluated for their functional activities in BRET-based assays at DRD4.<sup>9</sup> Unfortunately, **21** had an intrinsic light absorption property that interfered with BRET and, therefore, it was not possible to determine its functional profile.

The potencies and efficacies, expressed as pEC<sub>50</sub> (-log EC<sub>50</sub>) and E<sub>max</sub> (maximum efficacy), respectively, of **12**, **15**, **18** and **23** are reported in Table 7 along with those of DA (DRD4 full agonist) and **L745870** (DRD4 antagonist) as reference compounds. In parallel, the presence of antagonist effects of the tested compounds was studied using a fixed amount of dopamine (1 μM) at DRD4 (Table 7, pIC<sub>50</sub> and I<sub>max</sub>). Since functionally selective compounds, that exert preferential modulation on G protein or β-arrestin, are deemed to be therapeutically useful approaches, β-arrestin2 recruitment assays at DRD4



were also performed to characterize the functional properties of the ligands (Table 7,  $\beta$ -arrestin2 recruitment).

**Table 7.** Potency values, expressed as pEC<sub>50</sub><sup>a</sup> or pIC<sub>50</sub><sup>a</sup>; and efficacy values, expressed as %<sup>a</sup> (and normalized to DA E<sub>max</sub>) of DA and compounds **L-745870**, **12**, **15**, **18** and **23** expressed in HEK293T cells.

	G <sub>o</sub> activation (n≥ 5)		G <sub>i</sub> activation (n≥ 5)		$\beta$ -arrestin2 recruitment (n≥ 5)	
	pEC <sub>50</sub> (pIC <sub>50</sub> )	E <sub>max</sub> (I <sub>max</sub> )	pEC <sub>50</sub> (pIC <sub>50</sub> )	E <sub>max</sub> (I <sub>max</sub> )	pEC <sub>50</sub> (pIC <sub>50</sub> )	E <sub>max</sub> (I <sub>max</sub> )
<b>DA</b>	7.83 ± 0.09	100 ± 2.8	7.68 ± 0.15	100 ± 5.1	6.57 ± 0.24	100 ± 5.7
<b>L-745870</b>	(6.84 ± 0.18)	(-75.4 ± 4.7)	(5.71 ± 0.3)	(-83.9 ± 16.3)	(6.79 ± 0.30)	(-89.4 ± 9.3)
<b>12</b>	ND (6.48 ± 0.20)	0 (-91.6 ± 8.2)	ND (6.96 ± 0.66)	0 (-53.2 ± 14.5)	7.79 ± 1.39 (5.91 ± 0.26)	-30.2 ± 13.9 (-130 ± 15.1)
<b>15</b>	ND (6.97 ± 0.13)	0 (-97.2 ± 5.1)	ND (6.57 ± 0.32)	0 (-104.8 ± 7.3)	ND (6.41 ± 0.41)	0 (-64.6 ± 9.4)
<b>18</b>	ND (6.42 ± 0.35)	0 (-91.9 ± 15.0)	ND (6.60 ± 0.30)	0 (-88.2 ± 11.7)	7.29 ± 0.86 (4.98 ± 0.37)	-43.4 ± 13.8 (-144 ± 31.9)
<b>23</b>	8.07 ± 0.13 (ND)	46.2 ± 2.4 (0)	7.91 ± 0.50 (ND)	26.6 ± 5.4 (-20.2 ± 14.1)	ND (7.17 ± 0.27)	0 (-89.4 ± 7.8)

<sup>a</sup>The values represent the arithmetic mean ± SEM. ND = cannot be determined.

The results show that all the para-substituted compounds **12**, **15**, and **18** behaved as antagonists toward both G<sub>i</sub>/G<sub>o</sub>-protein activation and  $\beta$ -arrestin recruitment. On the contrary, the 2-pyridyl derivative **23** showed an interestingly biased profile, being a partial agonist with pEC<sub>50</sub> values similar to those of dopamine toward DRD4 G<sub>i</sub>/G<sub>o</sub>-protein activation and an antagonist toward  $\beta$ -arrestin recruitment with inhibitory potency and maximal inhibition (I<sub>max</sub>) similar to **L-745870**. These results confirm previous findings reporting that ligands with substituents in para-position behave as antagonists and those with substituents in ortho-position or bearing a 2-pyridine ring behave as partial agonists.<sup>7</sup>

The functional selectivity of **23** might be exploited to improve the knowledge of the biological functions associated with G-protein activation and  $\beta$ -arrestin recruitment pathways.

### **3.3.4. Molecular modelling studies**

Molecular docking studies were performed on all synthesised compounds (**1-27**) for all three D2-like receptors, and the results were compared with the binding profile of **54**.

The docking studies were performed in one or both of the following ways:

- I) Without any constraints applied (free docking);
- II) With the constraints applied according to the positions of the ligands complexed with the receptors (constrained docking).

#### *3.3.4.1. Free docking studies*

Free docking was performed first, to identify the unconditioned ability of the synthesised ligands to enter the binding site of DRD4 and establish interactions. We expected the lipophilic scaffold of our compounds to be positioned within the orthosteric binding pocket (OBP), with the basic function and the aromatic terminal extending into the extended binding pocket (EBP). The general overview of the DRD4 binding pockets, coloured by hydrophobicity, was given in Figure 10. These positions are in line with the described positioning of **L-745870** within the binding site of DRD4.<sup>24</sup> The benzamide ring of nemonapride binds within OBP, and it elicits an interaction with the conserved Asp115; while its benzyl group reacts with Leu90, Phe91 and Leu111 of the OBP.<sup>25</sup> This

conformational positioning of nemonapride further secured our expectations for the binding of **1-27** in the DRD4 binding site.

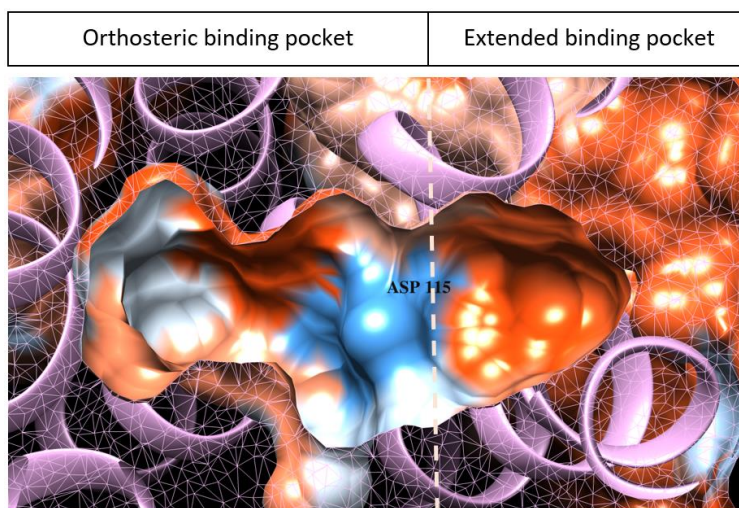


**Figure 10.** Side view of the DRD4 binding pocket with the surface coloured by hydrophobicity. The orthosteric binding pocket is shown left, it is deeper and it stretches until Asp115. The extended binding pocket is smaller, more hydrophobic and is shown on the right. The cut-off surface is shown as pink mesh.

Docking studies were performed first for **54** as the reference compound, to evaluate its binding and compare it to the binding profiles of other ligands. The orientation of the molecule was suboptimal for the first two best poses (Figure 11A), as the quinolinone portion did not enter deeper into the OBP, and the phenylpiperazine portion protruded toward the outer part of the binding pocket, moving away from the Asp115. Poses 3 and 4 (Figure 11A), on the other hand, bound with the quinolinone portion into the smaller EBP, with the terminal pointing downwards into the OBP, in case of pose 3, or away from the binding site, in case of pose 4. The relevant ion-pair interaction was present between the protonated piperazine of **54** and the conserved residue Asp115 within the OBP, for

the third most optimal pose (Figure 11B). The aromatic terminal established non-polar interactions with Val193.

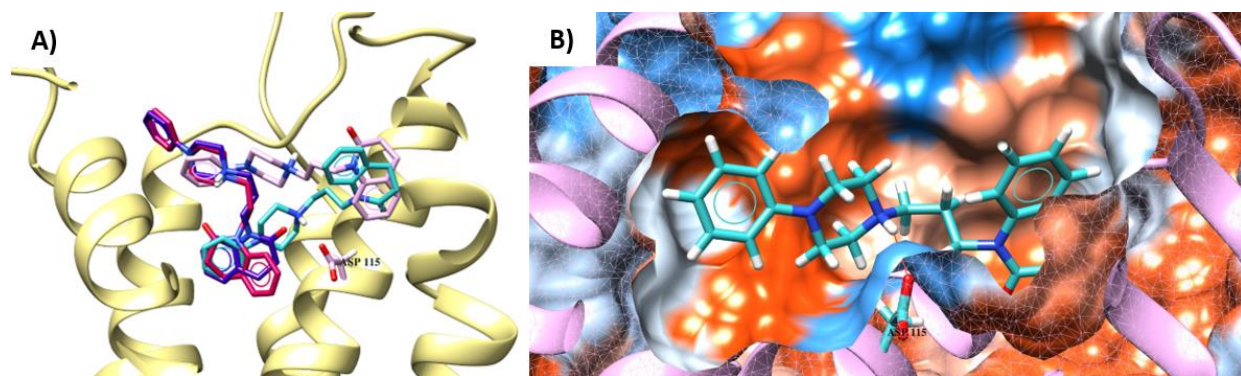


**Figure 11.** (A) PLANTS-calculated poses by docking of **54** in the pocket of DRD4 (PDB code: 5WIU): pose 1- light pink; pose 2- dark purple; pose 3- fluorescent blue; pose 4- dark pink. The position of the conserved residue Asp115 was given for reference. (B) The depiction of ion-pair interaction (orange line) between the protonated piperazine and Asp115 of the DRD4 orthosteric binding pocket. The cut-off surface is shown as pink mesh.

Ligands **7-9** were assuming theoretical positions within the binding site of the protein freely. The protonated amino groups on the piperazines of **7** and **8** were able to form ion pairs with Asp115, additionally supported by the interactions with Met112. The alkyl chain of **9** seemed to be too long for the molecule to extend into the limited space of EBP, forcing the tail (N-phenylpiperazine) to the external part of the binding site with limited interaction potential.

Other ligands were mostly able to form ion-pair with Asp115, but their binding profiles were hard to establish as the docking studies for most of them have found the most optimal position of those ligands to be inverted, with lipophilic scaffold within the EBP. In

terms of the lipophilic scaffolds of the ligands, as well as the aromatic terminal interactions, they differed based on the inversion state of the ligands' calculated poses. Most notable interactions of the lipophilic scaffolds of the properly-oriented ligands with the DRD4 amino acids involve a  $\pi$ - $\pi$  stacking interaction with His365. To further clarify,  $\pi$ - $\pi$  interactions are noncovalent interactions between unsaturated organic groups, such as aromatic compounds. These interactions, in the case of stacked systems, have a favourable electron correlation (dispersion) effect on the poly-unsaturated systems as proteins.<sup>45</sup> The aromatic side chains in proteins, including DRD4, are important for its folding, intermolecular stability and overall protein stability, regardless of the  $\pi$ - $\pi$  interaction type (parallel, parallel offset or T-shaped).<sup>46</sup>

Well-oriented compounds with the substituents in the meta-position (**14**, **17**, **20**) of their aromatic terminals were able to establish non-polar bonds between their quinolinone portion and Cys119 (Figure 12). The oxygen of the quinolinone group also exhibited weak hydrogen interactions with His365, in cases of **17** and **19**. The docking results of **21** and **26** have shown these ligands as exclusively inverted, probably indicating that the chlorine group, as well as the nitro group as big substituents in the para-position of the molecule, could hinder its DRD4 affinity.

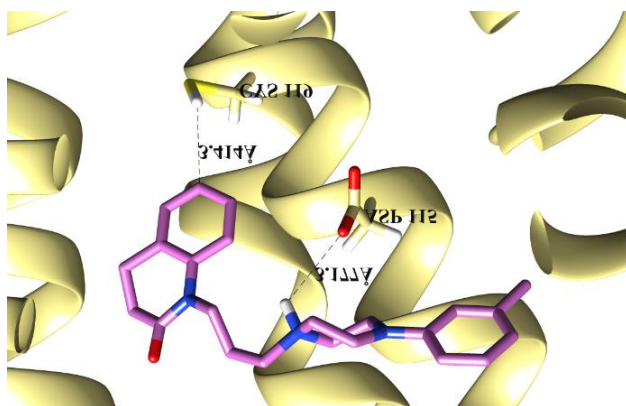


**Figure 12.** Side view of the interaction of the quinolinone portion of **14** and Cys119. The position of Asp115 is given for reference.

To understand the potential of our ligands for binding to DRD2 (PDB code: 6CM4), we have also performed docking studies on this receptor type. DRD2 was in complex with risperidone, an atypical antipsychotic drug. The structure had a lower resolution compared to 5WIU, obtained by X-ray diffraction, standing at 2.87 Å.<sup>47</sup> In the binding of **54** to the DRD2 binding site (Figure 15B), several differences were noticeable, compared to **54** binding in DRD4 binding site (Figure 15A). The quinolinone portion of the molecule was surrounded by the aromatic residues and, as previously noticed, the presence of the nearby alkyl chains had little to no impact on the binding of its lipophilic scaffold, with a singular  $\pi$ - $\pi$  interaction of the phenyl ring with the proximal Phe155. The phenyl ring of the aromatic terminal is situated within the EBP of the DRD2, which is much narrower than that of DRD4. Its size is limited by the residues of Trp100, Phe110 and Tyr408, which explains why having substituents on this aromatic terminal would be detrimental to the binding of the ligands, as well as why adding these substituents contributes to higher DRD4 selectivity of ligands. The limited size of DRD2 OBP, compared to that of DRD4, was confirmed using fPocket, a protein cavity detection tool<sup>48</sup> integrated into the Vega ZZ

suite.<sup>49</sup> The void volume of DRD4 equals 5694 Å<sup>3</sup>, and for the DRD2, it was 4275 Å<sup>3</sup>. If a substituent would be present, it should form H-bonds with Tyr408 or Thr412 (like in the case of **13**), which could stabilize the molecule within the pocket of DRD2. When it comes to the linker interactions within the pocket, it is noticeable that the increase in the chain length was followed by the drop in the DRD4 selectivity of ligands **7-9**. All compounds with para-substituents on their aromatic terminals (**12**, **15**, **18**, **21**) had difficulties entering the DRD2 binding site, which explains their higher DRD4 selectivity (Figure 13).

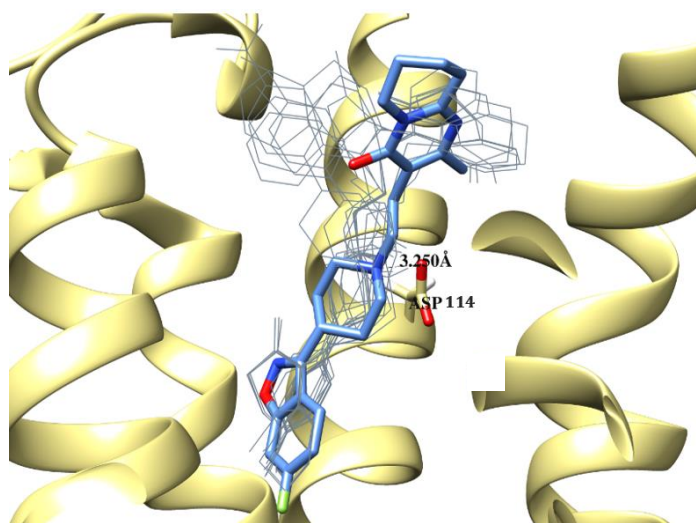


**Figure 13.** Side view of the best 3 PLANTS-computed poses for **12**, **15** and **21** (grey), as well as 4 best poses for **18** (grey); compared to the positioning of risperidone (blue) within the DRD2 binding pocket. Conserved residue Asp114 is given for reference.

The last part concerned our ligands' docking to DRD3 (PDB code: 3PBL), for which we have used an available DRD3 structure in a complex with eticlopride. In the binding site of DRD3, **54** was able to form the bond between the protonated amino group and Asp110. Laterally, the quinolinone ring of **54** engaged in T-shape  $\pi$ - $\pi$  interactions with Phe417

and Phe418, while its linker and aromatic terminal did not establish any significant interactions. **8** was able to bind within the DRD3 OBP, with its quinolinone portion forming a hydrophobic interaction with Val111 and a  $\pi$ - $\pi$  interaction with Phe417. **10-27** mostly had no interactions in the linker portion, and either none (**10-13**, **17-21**) or limited interactions on their aromatic terminals. For **10-21**, with changes of the substituents on the aromatic terminal from ortho- to meta- and para-positions, the number of steric hindrances between the piperazine portion and the surrounding amino acid residues increased as follows: ortho < meta < para. Compounds with double-substituted aromatic terminals (**25-27**) established many halogen bonds, as well as  $\pi$ - $\pi$  interactions with Phe106 and Tyr446. The most optimal binding is evident for **25**, but for both **26** and **27** with chlorine in para-positions, clashes against the atoms of the aminoacid backbone were apparent, with more clashes evident for the compound with chlorine in positions 3 and 4 (**27**; Figure 14). These findings were in line with the results of the affinity assays, in which **27** had the highest individual DRD4 selectivity with respect to **25** and **26**.

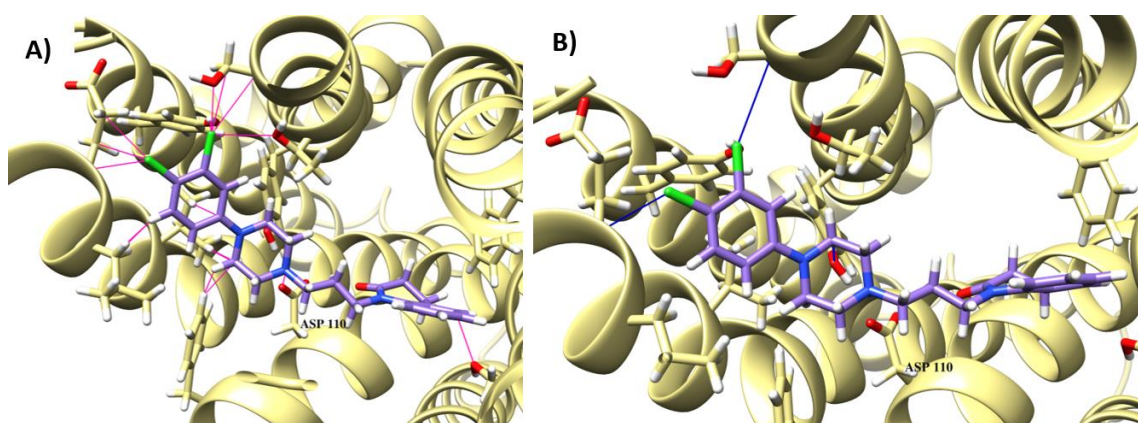


**Figure 14.** Side view of **27** establishing (A) contacts (pink) characterised by steric hindrances around the aromatic terminal; or (B) clashes (dark blue) against the atoms of the DRD3 backbone atoms. Asp110 is shown for reference.



The results of the free docking did not give us satisfactory results regarding binding to DRD4, as many of the ligands did not assume positions either within the OBP or the EBP, and were inverted. Therefore, we have decided to repeat the calculations with the constraints applied, to see whether we can eliminate inversion for these two receptors, as similar orientation is not expected under physiological conditions.

We have also searched the literature for the evidence of inversion of molecules within the binding site of D2-like receptors to gain an understanding of the appearance and significance of such results. One article denotes the possibility of clozapine binding to DRD3 and DRD2 binding sites in two different poses, rotated by 180°- a behaviour described in this thesis as inversion.<sup>50</sup> Aside from the rotation of the molecule, the depth to which the ligands travel within the binding site is different based on the inversion, and by obtaining affinity binding studies' results, they have discovered that the ligands with deeper binding-site penetration have higher affinities. The authors mention that the ligands while travelling into the OBP of DRD2 and DRD3, which are deeper in respect to the EBP, can interact for a prolonged period with so-called "metastable binding sites", which can correspond to the allosteric sites.<sup>50</sup>

Molecular dynamic (MD) needs to be used as a tool to better understand the binding of ligands to DRDs, as docking studies can be misleading. MD results provided input on the ligands binding extracellularly, or partially within the OBP/EBP. Overall, to rationalise our affinity studies, docking studies have proven useful, but we were not able to obtain docking poses for ligands only in a non-inverted state, which could contribute to the bias of the results. However, those conclusions which indicated a correlation with our experimental data were presented.

#### 3.3.4.2. *Constrained docking studies*

Constraints applied to the binding site of DRD4 measured a maximum 10 Å distance from the position of nemonapride. The docking studies for **54** were performed first, as past considerations for said molecule were done on an altered structure of DRD3 (PDB code: 3PBL).<sup>26</sup> The key interaction was the ion-pair between the protonated piperazine of **54** and the Asp115 of the DRD4 (Figure 15A), additionally supported by the interaction of the same protonated piperazine nitrogen to Tyr389. The quinolinone moiety of our ligands engaged in  $\pi$ - $\pi$  interactions with the aromatic groups in the proximity of it, i.e. Trp358, Phe361, Phe362, and His365, and these could also involve the lactam group.

We have noted a particular role of  $\pi$ - $\pi$  interactions in compounds **1-5**, where the lipophilic scaffold of the **54** structure was modified by introducing different bioisosteric heteroaromatic nuclei. These bioisosteres' affinity aligns with the calculated  $\pi$ - $\pi$  interactions between different heterocycles and the aromatic residues in the following order: pyrrole > imidazole > thiazole > oxazole.<sup>51</sup> In the case of **6**, quinolinone established hydrophobic interactions with Leu187 and Val116, which explained its good binding profile for DRD4. The propyl linkers of **1-6** and **10-27** created non-polar interactions with Met112 and Val193, while the aromatic terminals containing phenyl rings interacted through  $\pi$ - $\pi$  interactions with Phe91 and Trp101. Different substituents on phenyl rings of **10-27** exerted diverse roles of these compounds when bound to DRD4. Substituents which are small and hydrophobic (such as methyl and chlorine) exerted positive contributions regardless of their conformation, as they interacted with non-polar residues rid of steric hindrances. For example, **18** contained chlorine in the para position on the phenyl ring of the aromatic terminal, which interacted with Val87, Leu90 and Leu111, and

could engage in a halogen bond with Ser94 (Figure 15C). Such interactions were also characteristic for the other two chlorine-containing compounds, **16** and **17**, establishing similar interactions. Contrary to the described substituents, large and polar substituents like the methoxy group or the nitro group assumed the most optimal conformation in the ortho-position, where their interaction with Ser94 did not cause steric hindrances, as in compound **19** (Figure 15D).

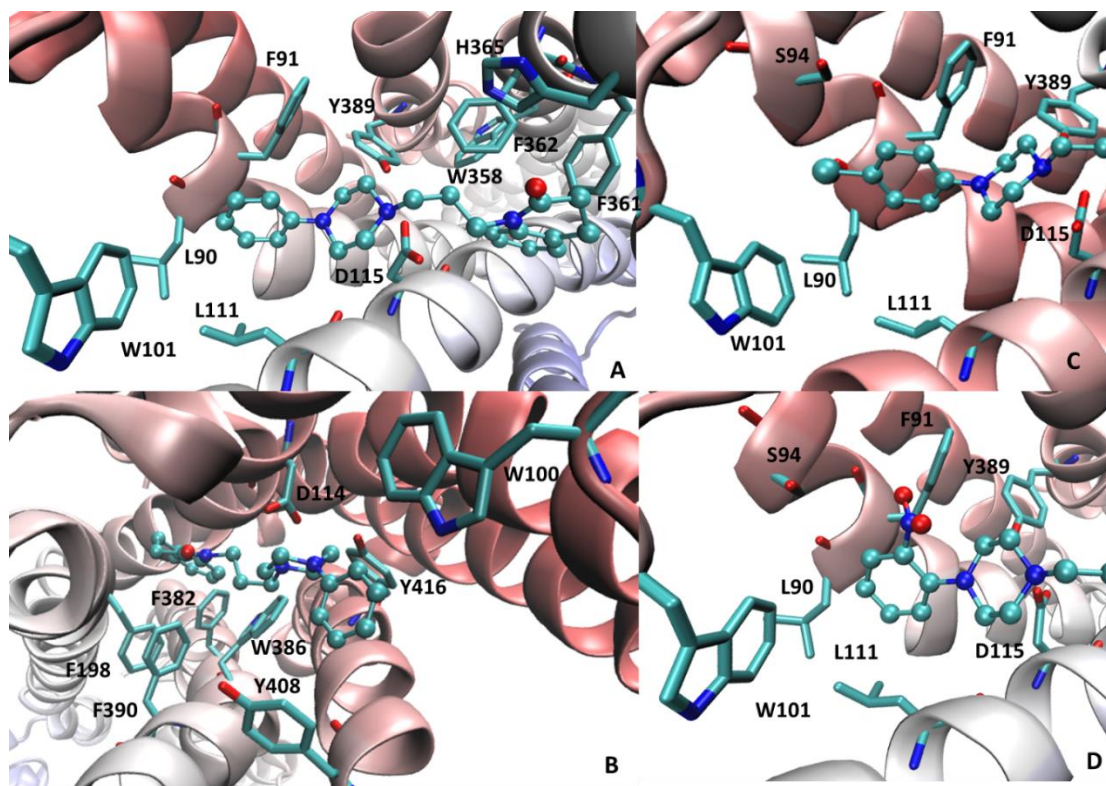


**Figure 15.** Main interactions stabilizing the putative complexes of **54** in the binding sites of DRD4 (PDB code: 5WIU; picture A) and DRD2 (PDB code: 6CM4; picture B). Focus on the interactions of the substituted phenyl ring of **18** (picture C) and **19** (picture D) in the DRD4.

In cases in which such groups were in the meta- or para-positions, they clashed against the Trp111 residue and against the atoms of the backbone (involved in peptide bond) of Leu90 and Phe91 in the vicinity of the group.

An overlap of the general positioning of DRD4 ligands within the DRD4 binding site without the constraints applied is shown in Figure 16A; while the overlap of the general positioning of DRD4 ligands within the DRD4 binding site with the constraints applied is shown in Figure 16B. The ligands were compared with the general positioning of nemonapride in the binding site.

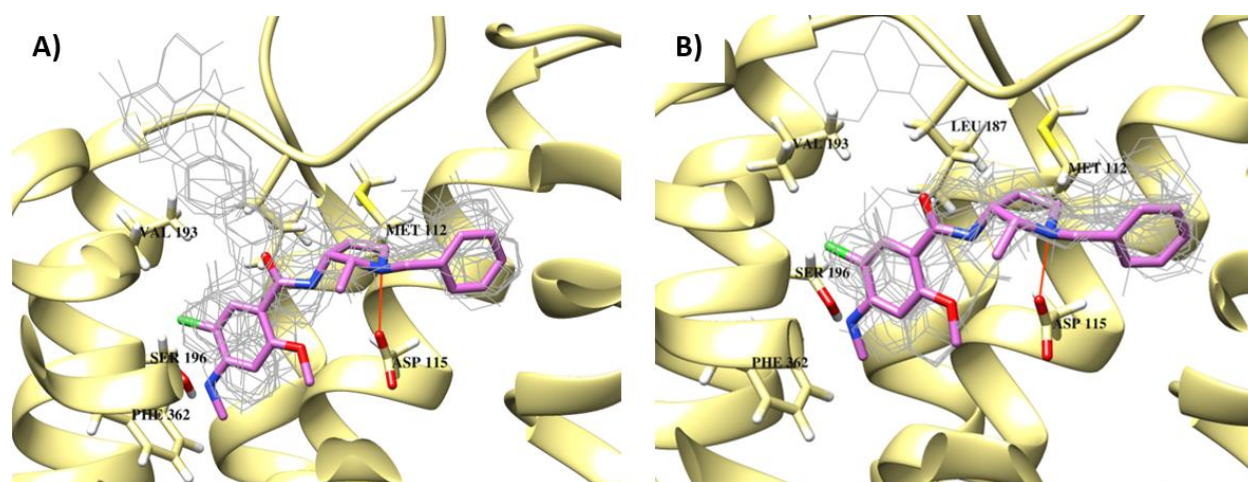


**Figure 16.** Ion-pair elicited between nemonapride and Asp115 is shown in orange. (A) Side-view overlap of the best computed poses (grey) using PLANTS software of compounds 1-27 within the DRD4 binding site, without any constraints applied. The computed pose of nemonapride is shown in purple. (B) Side-view overlap of the best computed poses (grey) using PLANTS software of compounds 1-27 within the DRD4 binding site, with constraints applied based on the general position of nemonapride (shown in purple).

We have also decided to check whether applying constraints to the DRD3 would have any impact on the quality of results. The binding pocket was defined as a 10 Å radius from the position of the original eticlopride pose within the complex (PDB code: 3PBL). **54** had a suboptimal binding profile, only establishing several interactions of the quinolinone portion with the C, S and H atoms of Cys122, and its protonated amino group formed a salt bridge with Asp110. These interactions, as well as many of the other ligands, were also considered improbable since it was visible that there were many steric hindrances pertaining to the binding profiles of **1-27**. Compounds with large polar groups exhibited many clashes with the backbone atoms of the amino acid residues, regardless of the position of their substituents on the aromatic terminal.

Computational analyses were also employed to characterize the ADME/Tox profile of the studied compounds. Thus, Table 8 compiles some relevant physico-chemical descriptors for all considered compounds. In detail, Table 8 reveals that all compounds show satisfactory physico-chemical profiles (e.g., MW < 500; logP < 5; HBA < 10; HBD < 5; PSA < 140 Å<sup>2</sup>; rotors < 10).<sup>52</sup> The in silico ADME profile of compounds **18** and **13** was further investigated by interrogating the swissADME webserver.<sup>53</sup> Compound **18** was predicted to be orally bioavailable, brain-blood barrier (BBB) permeant, P-gp substrate with no CYP inhibition apart from CYP2D6. The compound does not violate the most common drug-likeness sets of rules (e.g. Lipinski, Ghose, Veber) without PAINS and Brenk alerts. Its metabolic profile as predicted by the MetaClass method<sup>54</sup> indicates that **18** can undergo redox reactions on nitrogen and Csp<sup>2</sup> aromatic atoms. Compound **23** has an ADME profile almost superimposable to that of **18** except for being predicted BBB non-permeant, reasonably due to its lower lipophilicity.

**Table 8.** Physico-chemical properties of compounds **1-27**.

Compound	Rotors	HbAcc	HbDon	PSA	LogP	MW
<b>1</b>	5	1	0	11.4	4.11	319.4
<b>2</b>	5	2	0	22.6	3.24	320.4
<b>3</b>	5	2	1	34.7	4.44	320.4
<b>4</b>	5	3	0	30.5	4.83	321.4
<b>5</b>	5	2	0	42	4.37	337.5
<b>6</b>	5	1	0	11.7	4.91	335.5
<b>7</b>	4	2	0	27.7	2.77	335.4
<b>8</b>	6	2	0	27.5	3.61	363.5
<b>9</b>	7	2	0	28.6	3.84	377.5
<b>10</b>	5	2	0	27.5	3.45	363.5
<b>11</b>	5	2	0	27.7	3.58	363.5
<b>12</b>	5	2	0	28.2	3.6	363.5
<b>13</b>	6	3	0	39	3.34	379.5
<b>14</b>	6	3	0	40.6	3.25	379.5
<b>15</b>	6	3	0	39	3.28	379.5
<b>16</b>	5	2	0	28.2	3.77	383.9
<b>17</b>	5	2	0	28	3.76	383.9
<b>18</b>	5	2	0	27.6	3.71	383.9
<b>19</b>	5	4	0	66.9	3.67	394.5
<b>20</b>	5	4	0	68.3	3.71	394.5
<b>21</b>	5	4	0	69.2	3.58	394.5
<b>22</b>	5	2	0	47	2.47	374.5
<b>23</b>	5	3	0	37.4	2.21	350.5
<b>24</b>	5	4	0	48	1.58	351.5
<b>25</b>	5	2	0	27.6	4.32	418.4
<b>26</b>	5	2	0	28.6	4.28	418.4
<b>27</b>	5	2	0	28	4.33	418.4

### ***3.3.5. In vitro studies on GBM cell lines***

Considering the abovementioned involvement of DRD4 in brain cancers and the therapeutic potential of DRD4 ligands in the treatment of GBM, the highly potent and selective DRD4 antagonist **18** and the biased ligand **23** were selected to be evaluated for

their potential in affecting the viability of the **temozolomide**-resistant T98 and **temozolomide**-sensitive U251 GBM cell lines,<sup>55</sup> and the primary GBM stem cells GSC#83 as well.<sup>9</sup> Specifically, GSC and GBM cell lines were treated with the compounds **18** and **23** (from 5  $\mu$ M to 50  $\mu$ M) for 24h (experimental groups). Parallel cultures (control groups) were incubated for 24 h with **temozolomide**, which is the first-choice chemotherapeutic drug in GBM approved by the FDA in 2005,<sup>56,57</sup> the known DRD4 receptor antagonist **PNU-96145E** (Tocris), the DRD4 agonist **A412997** (Tocris) (all used at the concentrations ranging from 5  $\mu$ M to 50  $\mu$ M), or the vehicle only.

Dose-response studies showed decreased GBM cell lines and GSC#83's viability in cultures treated with compounds **18** and **23**, as well as with controls **temozolomide** and **PNU-96145E**, with respect to the solely vehicle incubated cultures. Conversely, the selective DRD4 agonist **A412997** did not significantly modulate cell viability (Figure 17). The maximal efficiency of the compounds, both in the experimental and in the control groups, was reached at the concentration of 10  $\mu$ M and, more importantly, the treatment with both compounds **18** and **23** induced an increased effect in reducing the T98, U251 cell lines and GSC#83 viability with respect to the control drugs **temozolomide** and **PNU-96145E** (Figure 17). Moreover, the results confirm the higher sensitivity of T98 cells vs U251 cells to **temozolomide** treatment. On the contrary, both the GBM cell lines were equally sensitive in vitro to treatment with DRD4 compounds **18** and **23**.

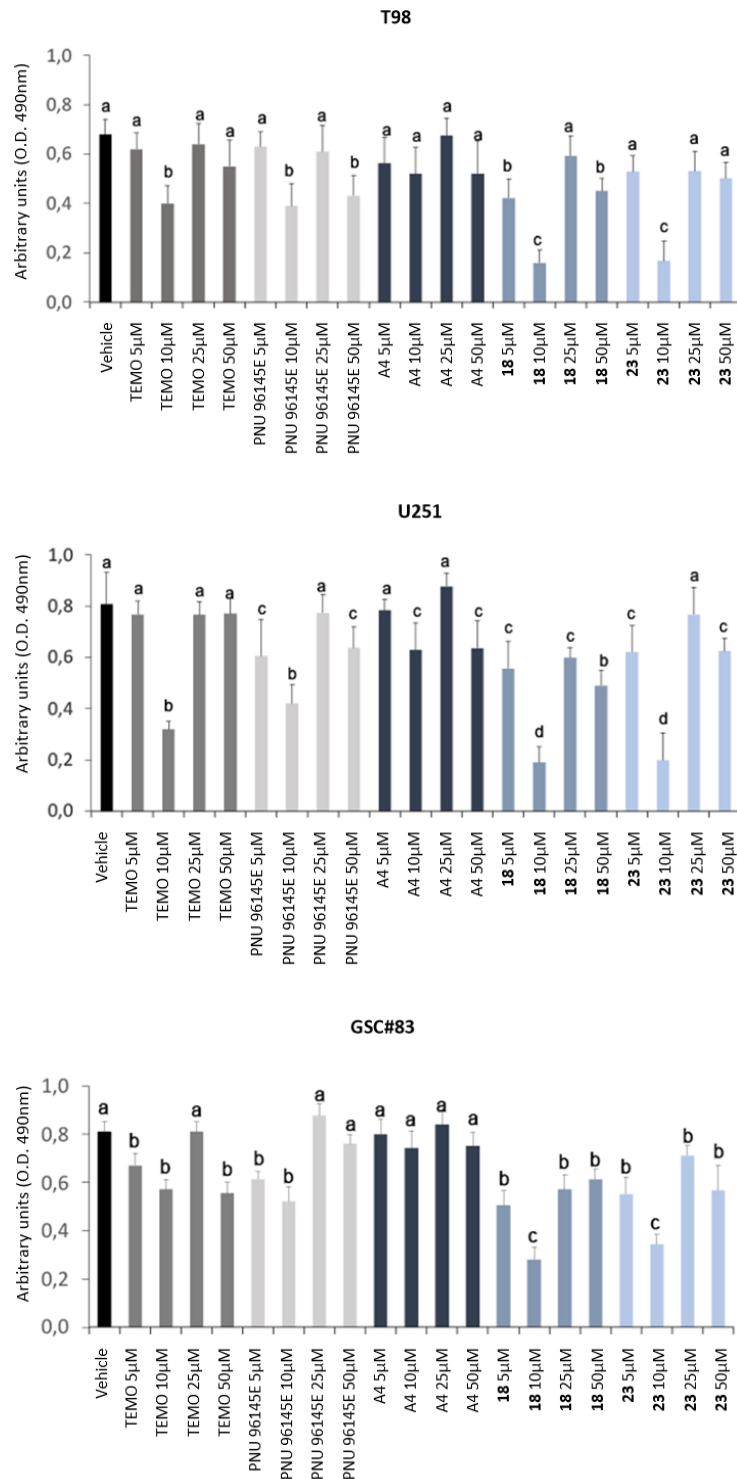


**Figure 17.** Cell viability assay was performed in GBM cell lines T98 and U251, as well as in GSC#83. The data was analysed using a two-way analysis of variance. Lowercase letters denote homogeneous subsets ( $n = 6$ , data is shown as mean values  $\pm$  standard error,  $p < 0.05$ ). Vehicle = DMSO. TEMO = **temozolomide**. A4 = **A412997**.



Since the maximal antiproliferative activity of ligands was detected at the dose of 10  $\mu\text{M}$ , it was considered of interest to evaluate their activity also in the narrower range of concentration from 10  $\mu\text{M}$  to 20  $\mu\text{M}$ . Moreover, since all the compounds showed similar activity against the three considered cell lines, the experiment was performed only on the T98 cell line. Figure 18 shows that the maximal activity of all the tested compounds is further confirmed at the dose of 10  $\mu\text{M}$ .

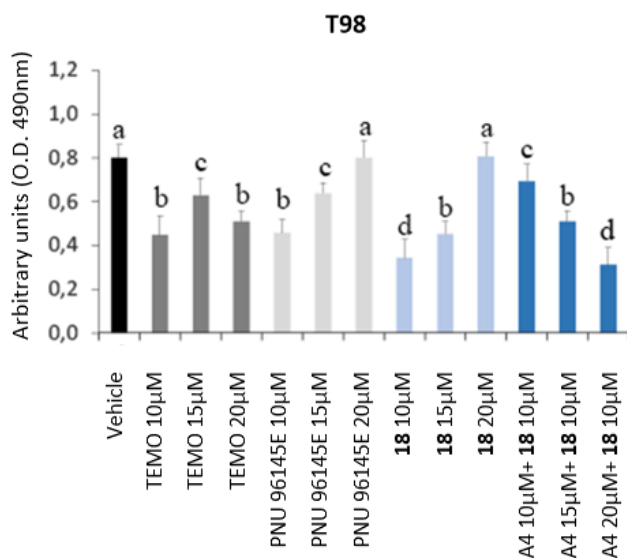


**Figure 18.** Cell viability assay performed in T98 cell line. Data were analysed using a two-way analysis of variance. Lowercase letters denote homogeneous subsets ( $n = 6$ , data is shown as mean values  $\pm$  standard error,  $p < 0.05$ ). Vehicle = DMSO. TEMO = temozolomide. A4 = A412997.

### 3.4. Conclusions

In this study, starting from the brain penetrant and DRD4 selective lead compound **54**, new ligands endowed with high affinity and selectivity for DRD4 were discovered.

Specifically, maintaining the *N*-arylpiperazine moiety, the following modifications were performed:

- the quinolinone portion was replaced by bioisosteric nuclei;
- the propyl linker was replaced by chains of different lengths;
- substituents with different electronic and lipophilic contributions were inserted in the ortho-, meta- and para-position of the *N*-aryl terminal.

SAR studies, supported by molecular modelling simulations, highlighted that the tetrahydroquinolinone nucleus of **54** can be replaced by an *N*-indole or an *N*-tetrahydroquinoline moiety, with no negative effects on the DRD4 activity or selectivity of the ligands. Among the compounds with linker modifications, those containing a propyl linker have shown the best DRD4 selectivity, meaning that this spacer represents an optimal distance between the lipophilic portion and the basic function. Interestingly, concerning the substitution in the aromatic terminal, the most DRD4 selective compounds were the para-substituted ones, due to the decrease in DRD2 and DRD3 affinity when the substituent was shifted from ortho- to meta- and especially to para-position. From the functional studies, while the para-substituted compounds **12**, **15**, and **18** behaved as DRD4 antagonists, the 2-pyridyl derivative **23** showed an interestingly biased profile, being a partial agonist toward DRD4 G<sub>i</sub>/G<sub>o</sub>-protein activation and an antagonist toward  $\beta$ -arrestin recruitment. The functional selectivity of **23** could further help to evaluate the involvement of G-proteins and  $\beta$ -arrestins in associated physiological functions, but this was outside of the scope of this research.

As the inhibition of the DRD4 function leads to the disruption of the autophagy-lysosomal pathway of the GBM stem cells, causing tumour cell apoptosis, and the patients with

increased DRD4 levels have worse GBM survival rates, the potent and highly selective DRD4 antagonist **18** and the biased ligand **23** were evaluated for their GBM antitumor activity. Both compounds decreased the viability of GBM cell lines and GSC#83, showing the maximal efficacy at the concentration of 10  $\mu$ M. Interestingly, the treatment with compounds **18** and **23** resulted in a more potent reduction of cell viability with respect to the first-choice chemotherapeutic drug in GBM **temozolomide**. The observation that the effect of **18** was contrasted by the DRD4 agonist **A412997** (10  $\mu$ M) supports that DRD4 is involved in the antitumor activity of this compound.

Therefore, these new selective DRD4 ligands might further shed light on the role played by this subtype in GBM and, especially, become lead compounds for the discovery of new alternatives to the standard treatments such as surgery and radiotherapy, that cannot always be applied, and pharmacological treatments, that are still very limited because of drug resistance.

### **3.5. Experimental section**

#### ***3.5.1. Synthesis of DRD4 ligands***

Melting points were taken in glass capillary tubes on a Büchi SMP-20 apparatus and are uncorrected. <sup>1</sup>H-NMR spectra were recorded either with a Bruker 500 Ascend (Bruker BioSpin Corporation, Billerica, MA, USA) and Varian Mercury AS400 instruments, and chemical shifts (ppm) are reported relative to tetramethylsilane. Spin multiplicities are given as s (singlet), d (doublet), dd (double doublet), t (triplet), or m (multiplet). IR spectra were recorded on PerkinElmer 297 instrument and spectral data (not shown because of

the lack of unusual features) were obtained for all compounds reported and are consistent with the assigned structures. The microanalyses were recorded on FLASH 2000 instrument (ThermoFisher Scientific). The elemental composition of the compounds agreed to within  $\pm 0.4\%$  of the calculated value. All reactions were monitored by thin-layer chromatography using silica gel plates (60 F254; Merck), visualizing with ultraviolet light. Chromatographic separations were performed on silica gel columns (Kieselgel 40, 0.040-0.063 mm, Merck) by flash chromatography. Compounds were named following IUPAC rules as applied by ChemBioDraw Ultra (version 12.0) software for systematically naming organic chemicals. The purity of the novel compounds was determined by combustion analysis and was  $\geq 95\%$ .

#### 3.5.1.1. *Synthesis of 1-(3-(4-phenylpiperazin-1-yl)propyl)-1H-indole (1).*

A solution of **59** (1 mmol) in dimethyl formamide (5 mL) was added dropwise to a suspension of sodium hydride (0.04 g, 60% in mineral oil) and dimethyl formamide (5 mL). The resulting mixture was stirred at room temperature for 10 min, followed by the addition of a solution of **58** (1 mmol) in dimethyl formamide (5 mL). The resulting mixture was stirred at 60 °C for 20 h. Then, it was poured onto ice, and the aqueous phase was extracted with EtOAc (2 x 30 mL). The combined organic phases were washed with brine (5 x 30 mL) and dried over anhydrous Na<sub>2</sub>SO<sub>4</sub>. The organic phase was washed with brine (20 mL) and dried over anhydrous Na<sub>2</sub>SO<sub>4</sub>. The evaporation of the solvent under reduced pressure afforded a residue, which was purified by flash chromatography, eluting with cyclohexane/EtOAc (75:25). An oil was obtained (70% yield). <sup>1</sup>H NMR (CDCl<sub>3</sub>, 500 MHz):  $\delta$  7.62 (d, 1H,  $J = 7.9$  Hz), 7.39 (d, 1H,  $J = 8.2$  Hz), 7.24-6.87 (m, 8H), 6.50 (d, 1H,  $J =$

3.1 Hz), 4.26 (t, 2H,  $J = 6.6$  Hz), 3.33-3.20 (m, 4H), 2.74-2.34 (m, 6H), 2.17-2.05 (m, 2H). The free base was transformed into the oxalate salt, which was crystallized from EtOH to give a white solid: m.p. 99-100 °C, ESI/MS  $m/z$  320 [M + H]<sup>+</sup>, 342 [M + Na]<sup>+</sup>. Anal. Calcd (C<sub>21</sub>H<sub>25</sub>N<sub>3</sub>·C<sub>2</sub>H<sub>2</sub>O<sub>4</sub>): C, 67.46%; H, 6.65%; N, 10.26%. Found: C, 67.21%; H, 6.78%; N, 10.11%.

#### 3.5.1.2. Synthesis of 1-(3-(4-phenylpiperazin-1-yl)propyl)-1H-benzo[d]imidazole (**2**).

This compound was prepared starting from **60** and **58** following the procedure described for **7**: an oil was obtained (42% yield). <sup>1</sup>H NMR (CDCl<sub>3</sub>, 500 MHz): δ 8.98 (s, 1H), 7.86 (d, 1H,  $J = 7.9$  Hz), 7.64 (d, 1H,  $J = 8.0$  Hz), 7.47-7.27 (m, 4H), 6.95 (t, 1H,  $J = 7.3$  Hz), 6.89 (d, 2H,  $J = 8.1$  Hz), 4.64 (t, 2H,  $J = 6.8$  Hz), 3.60-3.07 (m, 8H), 2.73-2.64 (m, 2H), 2.25-2.06 (m, 2H). The free base was transformed into the oxalate salt, which was crystallized from EtOH to give a white solid: m.p. 195-196 °C, ESI/MS  $m/z$  321 [M + H]<sup>+</sup>, 343 [M + Na]<sup>+</sup>. Anal. Calcd (C<sub>20</sub>H<sub>24</sub>N<sub>4</sub>·C<sub>2</sub>H<sub>2</sub>O<sub>4</sub>): C, 64.37%; H, 6.38%; N, 13.65%. Found: C, 64.66%; H, 6.17%; N, 13.82%.

#### 3.5.1.3. Synthesis of 2-(3-(4-phenylpiperazin-1-yl)propyl)-1H-benzo[d]imidazole (**3**).

Benzene-1,2-diamine (1 mmol) was added to a solution of **61** (1.2 mmol) in 4N HCl in dioxane (10 mL) and the mixture was stirred at reflux for 24 hours. The reaction mixture was cooled to room temperature, poured over ice-cold H<sub>2</sub>O (20 mL), neutralised to pH = 7 with NaOH and extracted with CHCl<sub>3</sub> (3x 20 mL). The organic phase was dried over anhydrous Na<sub>2</sub>SO<sub>4</sub>. The evaporation of the solvent under reduced pressure afforded a

residue, which was purified by flash chromatography, eluting with EtOAc/MeOH (8:2). A yellow solid was obtained (25% yield).  $^1\text{H}$  NMR ( $\text{CDCl}_3$ , 500 MHz):  $\delta$  7.59-7.15 (m, 6H), 6.99 (d, 2H,  $J = 7.8$  Hz), 6.93 (m, 1H), 3.38-3.32 (m, 4H), 3.17-3.12 (m, 2H), 2.82-2.67 (m, 6H), 2.09-2.04 (m, 3H). The free base was transformed into the oxalate salt, which was crystallized from EtOH to give a white solid: m.p. 216-219 °C, ESI/MS  $m/z$  321  $[\text{M} + \text{H}]^+$ , 343  $[\text{M} + \text{Na}]^+$ . Anal. Calcd ( $\text{C}_{20}\text{H}_{24}\text{N}_4 \cdot \text{C}_2\text{H}_2\text{O}_4$ ): C, 64.37%; H, 6.38%; N, 13.65%. Found: C, 64.12%; H, 6.29%; N, 13.43%.

#### 3.5.1.4. Synthesis of 2-(3-(4-phenylpiperazin-1-yl)propyl)benzo[d]oxazole (**4**).

$\text{K}_2\text{CO}_3$  (5 mmol) and KI (0.2 mmol) were added to a solution of **57** (1 mmol) in DME (10 mL) and the mixture was stirred at room temperature for 10 minutes, followed by the addition of a solution of **62** (5 mmol) in DME (5 mL). The resulting mixture was stirred at reflux for 15 hours. Then, after cooling, EtOAc (20 mL) was added, and the mixture was extracted with brine (3 x 20 mL). The organic phase was dried over anhydrous  $\text{Na}_2\text{SO}_4$ . The evaporation of the solvent under reduced pressure afforded a residue, which was purified by flash chromatography, eluting with cyclohexane/EtOAc (7:3). A white solid was obtained (59% yield).  $^1\text{H}$  NMR ( $\text{CDCl}_3$ , 500 MHz):  $\delta$  7.72-7.26 (m, 6H), 6.96-6.85 (m, 3H), 3.21-3.15 (m, 4H), 3.04 (t, 2H,  $J = 7.5$  Hz), 2.66-2.63 (m, 4H), 2.56 (t, 2H,  $J = 7.1$  Hz), 2.18-2.12 (m, 2H). The free base was transformed into the oxalate salt, which was crystallized from MeOH to give a white solid: m.p. 215-216 °C, ESI/MS  $m/z$  322  $[\text{M} + \text{H}]^+$ , 344  $[\text{M} + \text{Na}]^+$ . Anal. Calcd ( $\text{C}_{20}\text{H}_{23}\text{N}_3\text{O} \cdot \text{C}_2\text{H}_2\text{O}_4$ ): C, 64.22%; H, 6.12%; N, 10.21%. Found: C, 63.99%; H, 6.36%; N, 10.34%.

#### 3.5.1.5. Synthesis of 2-(3-(4-phenylpiperazin-1-yl)propyl)benzo[d]thiazole (**5**).

This compound was prepared starting from **57** and **63** following the procedure described for **4**: an oil was obtained (11% yield).  $^1\text{H}$  NMR ( $\text{CDCl}_3$ , 500 MHz):  $\delta$  7.97 (d, 1H,  $J = 8.1$  Hz), 7.86-7.24 (m, 4H), 6.95-6.85 (m, 4H), 3.28-3.18 (m, 6H), 2.75-2.59 (m, 8H). The free base was transformed into the oxalate salt, which was crystallized from EtOH to give a white solid: m.p. 184-186 °C, ESI/MS  $m/z$  338  $[\text{M} + \text{H}]^+$ , 360  $[\text{M} + \text{Na}]^+$ . Anal. Calcd ( $\text{C}_{20}\text{H}_{23}\text{N}_3\text{S}\cdot\text{C}_2\text{H}_2\text{O}_4$ ): C, 61.81%; H, 5.89%; N, 9.83%; S, 7.50%. Found: C, 62.11%; H, 7.30%; N, 6.10%; S, 7.27%.

#### 3.5.1.6. Synthesis of 1-(3-(4-phenylpiperazin-1-yl)propyl)-1,2,3,4-tetrahydroquinoline (**6**).

$\text{BH}_3\cdot\text{S}(\text{CH}_3)_2$  (0.34 ml) was added to an ice-cooled solution of **54** (1 mmol) in THF (10 mL) at 0 °C under nitrogen and the mixture was stirred at reflux for 3 hours. Then, after cooling to 0 °C, MeOH (10 mL) was added. The mixture was acidified with 2N HCl (5 mL) and stirred at reflux for 1 hour. Then it was cooled to room temperature, basified with 2N NaOH and extracted with dichloromethane (DCM) (3 x 20 mL). The combined organic phases were dried over anhydrous  $\text{Na}_2\text{SO}_4$ . The evaporation of the solvent under reduced pressure afforded a residue, which was purified by flash chromatography, eluting with cyclohexane/EtOAc (7:3). A yellow oil was obtained (59% yield).  $^1\text{H}$  NMR ( $\text{CDCl}_3$ , 500 MHz):  $\delta$  7.29-6.92 (m, 6H), 6.87 (t, 1H,  $J = 7.3$  Hz), 6.62 (d, 1H,  $J = 8.2$  Hz), 6.56 (t, 1H,  $J = 7.3$  Hz), 3.36-3.22 (m, 8H), 2.79-2.47 (m, 8H), 1.98-1.84 (m, 4H). The free base was transformed into the oxalate salt, which was crystallized from EtOH to give a white solid: m.p. 292-294 °C, ESI/MS  $m/z$  336  $[\text{M} + \text{H}]^+$ , 358  $[\text{M} + \text{Na}]^+$ . Anal. Calcd

(C<sub>22</sub>H<sub>29</sub>N<sub>3</sub>·C<sub>2</sub>H<sub>2</sub>O<sub>4</sub>): C, 67.74%; H, 7.34%; N, 9.88%. Found: C, 67.44%; H, 7.19%; N, 9.99%.

3.5.1.7. *Synthesis of 1-(2-(4-phenylpiperazin-1-yl)ethyl)-3,4-dihydroquinolin-2(1H)-one (7).*

Sodium hydride (0.12 g, 60% in mineral oil) was added to a solution of **65** (10 mmol) in xylene (5 mL) and the mixture was stirred at room temperature for 20 min, followed by the addition of a solution of **64** (5 mmol) in xylene (5 mL). The resulting mixture was stirred at reflux for 4 h. Then, after cooling, it was poured onto ice, and the organic phase was extracted with 5% HCl (3 x 20 mL). The aqueous phase was basified with 2N NaOH and extracted with DCM (3 x 20 mL). The combined organic phases were washed with brine (2 x 20 mL) and dried over anhydrous Na<sub>2</sub>SO<sub>4</sub>. The evaporation of the solvent under reduced pressure afforded a residue, which was purified by flash chromatography, eluting with EtOAc/MeOH (99:1). An oil was obtained (76% yield). <sup>1</sup>H NMR (CDCl<sub>3</sub>, 400 MHz): δ 7.60-6.95 (m, 9H), 4.04 (m, 2H), 3.74-3.62 (m, 6H), 3.32-3.10 (m, 4H), 2.96 (m, 2H), 2.68 (m, 2H). The free base was transformed into the oxalate salt, which was crystallized from 2-PrOH to give a white solid: m.p. 210-211 °C, ESI/MS m/z 336 [M + H]<sup>+</sup>, 358 [M + Na]<sup>+</sup>. Anal. Calcd (C<sub>21</sub>H<sub>25</sub>N<sub>3</sub>O·C<sub>2</sub>H<sub>2</sub>O<sub>4</sub>): C, 62.99%; H, 7.93%; N, 10.02%. Found: C, 63.25%; H, 7.90%; N, 10.19%.



3.5.1.8. *Synthesis of 1-(4-(4-phenylpiperazin-1-yl)butyl)-3,4-dihydroquinolin-2(1H)-one (8).*

A solution of **66** (1 mmol) in DMF (5 mL) was added dropwise to a solution of **57** (1 mmol) and  $K_2CO_3$  (1.2 mmol) in DMF (10 mL). The reaction mixture was stirred at 70 °C for 4h, then it was diluted with water (20 mL) and extracted with EtOAc (2 x 30 mL). The organic layer was washed with brine (5 x 20 mL) and dried over anhydrous  $Na_2SO_4$ . The evaporation of the solvent under reduced pressure afforded a residue, which was purified by flash chromatography, eluting with EtOAc/MeOH (99:1). An oil was obtained (72% yield).  $^1H$  NMR ( $CDCl_3$ , 400 MHz):  $\delta$  7.39-6.88 (m, 9H), 4.03 (m, 2H), 3.30 (m, 4H), 2.97-2.42 (m, 10H), 1.90-1.55 (m, 4H). The free base was transformed into the oxalate salt, which was crystallized from 2-PrOH to give a white solid: m.p. 164-165 °C, ESI/MS  $m/z$  364  $[M + H]^+$ , 386  $[M + Na]^+$ . Anal. Calcd ( $C_{23}H_{29}N_3O \cdot C_2H_2O_4$ ): C, 66.21%; H, 6.89%; N, 9.27%. Found: C, 65.27%; H, 6.54%; N, 9.36%.

3.5.1.9. *Synthesis of 1-(5-(4-phenylpiperazin-1-yl)pentyl)-3,4-dihydroquinolin-2(1H)-one (9).*

This compound was prepared starting from **67** and **57** following the procedure described for **8**: an oil was obtained (51% yield).  $^1H$  NMR ( $CDCl_3$ , 400 MHz):  $\delta$  7.35-6.82 (m, 9H), 3.95 (m, 2H), 3.30 (m, 4H), 2.95 (m, 2H), 2.81-2.45 (m, 8H), 1.85-1.41 (m, 6H). The free base was transformed into the oxalate salt, which was crystallized from 2-PrOH to give a white solid: m.p. 156-158 °C, ESI/MS  $m/z$  378  $[M + H]^+$ , 400  $[M + Na]^+$ . Anal. calcd ( $C_{24}H_{31}N_3O \cdot C_2H_2O_4$ ): C, 66.79%; H, 7.11%; N, 8.99%. Found: C, 66.41%; H, 7.02%; N, 9.09%.

3.5.1.10. *Synthesis of 1-(3-(4-(o-tolyl)piperazin-1-yl)propyl)-3,4-dihydroquinolin-2(1H)-one (10).*

This compound was prepared starting from **68** and **69** following the procedure described for **8**: an oil was obtained (47% yield). <sup>1</sup>H NMR (CDCl<sub>3</sub>): δ 7.31-6.92 (m, 8H), 4.05 (m, 2H), 3.14 (m, 4H), 2.92 (m, 2H), 2.71-2.49 (m, 8H), 2.38 (s, 3H), 1.95 (m, 2H). The free base was transformed into the oxalate salt, which was crystallized from 2-PrOH to give a white solid: m.p. 149-150 °C, ESI/MS m/z 364 [M + H]<sup>+</sup>. Anal. Calcd (C<sub>23</sub>H<sub>29</sub>N<sub>3</sub>O·C<sub>2</sub>H<sub>2</sub>O<sub>4</sub>): C, 66.21%; H, 6.89%; N, 9.27%. Found: C, 65.88%; H, 6.83%; N, 9.08%.

3.5.1.11. *Synthesis of 1-(3-(4-(m-tolyl)piperazin-1-yl)propyl)-3,4-dihydroquinolin-2(1H)-one (11).*

This compound was prepared starting from **68** and **70** following the procedure described for **8**: an oil was obtained (55% yield). <sup>1</sup>H NMR (CDCl<sub>3</sub>, 500 MHz): δ 7.27-6.89 (m, 8H), 4.04 (m, 2H), 3.23 (m, 4H), 2.92 (m, 2H), 2.67 (m, 6H), 2.49 (m, 2H), 2.33 (s, 3H), 1.92 (m, 2H). The free base was transformed into the oxalate salt, which was crystallized from 2-PrOH to give a white solid: m.p. 185-186 °C, ESI/MS m/z 364 [M + H]<sup>+</sup>. Anal. Calcd (C<sub>22</sub>H<sub>26</sub>N<sub>4</sub>O<sub>3</sub>·C<sub>2</sub>H<sub>2</sub>O<sub>4</sub>): C, 66.21%; H, 6.89%; N, 9.27%. Found: C, 66.10%; H, 6.81%; N, 9.33%.

3.5.1.12. *Synthesis of 1-(3-(4-(p-tolyl)piperazin-1-yl)propyl)-3,4-dihydroquinolin-2(1H)-one (12).*

This compound was prepared starting from **68** and **71** following the procedure described for **8**: an oil was obtained (61% yield). <sup>1</sup>H NMR (CDCl<sub>3</sub>, 500 MHz): δ 7.29-6.85 (m, 8H), 4.04 (m, 2H), 3.18 (m, 4H), 2.93 (dd, 2H, *J* = 18.4 and 11.5 Hz), 2.67 (m, 6H), 2.56 (t, 2H, *J* = 7.1 Hz), 2.29 (s, 3H), 1.92 (m, 2H). The free base was transformed into the oxalate salt, which was crystallized from 2-PrOH to give a white solid: m.p. 198-199 °C, ESI/MS *m/z* 364 [M + H]<sup>+</sup>. Anal. Calcd (C<sub>23</sub>H<sub>29</sub>N<sub>3</sub>O·C<sub>2</sub>H<sub>2</sub>O<sub>4</sub>): C, 66.21%; H, 6.89%; N, 9.27%. Found: C, 66.34%; H, 6.96%; N, 9.34%.

3.5.1.13. *Synthesis of 1-(3-(4-(2-methoxyphenyl)piperazin-1-yl)propyl)-3,4-dihydroquinolin-2(1H)-one (13).*

This compound was prepared starting from **68** and **72** following the procedure described for **8**: an oil was obtained (46% yield). <sup>1</sup>H NMR (CDCl<sub>3</sub>, 500 MHz): δ 7.31-6.88 (m, 8H), 4.07 (m, 2H), 3.79 (s, 3H), 3.22 (m, 4H), 2.94 (m, 2H), 2.76-2.35 (m, 8H), 1.95 (m, 2H). The free base was transformed into the oxalate salt, which was crystallized from 2-PrOH to give a white solid: m.p. 164-166 °C, ESI/MS *m/z* 380 [M + H]<sup>+</sup>. Anal. Calcd (C<sub>23</sub>H<sub>29</sub>N<sub>3</sub>O<sub>2</sub>·C<sub>2</sub>H<sub>2</sub>O<sub>4</sub>): C, 63.95%; H, 6.66%; N, 8.95%. Found: C, 64.11%; H, 6.47%; N, 9.12%.

3.5.1.14. Synthesis of 1-(3-(4-(3-methoxyphenyl)piperazin-1-yl)propyl)-3,4-dihydroquinolin-2(1H)-one (**14**).

This compound was prepared starting from **68** and **73** following the procedure described for **8**: an oil was obtained (49% yield). <sup>1</sup>H NMR (CDCl<sub>3</sub>, 500 MHz): δ 7.26-6.42 (m, 8H), 4.04 (m, 2H), 3.81 (s, 3H), 3.23 (m, 4H), 2.92 (m, 2H), 2.71–2.61 (m, 6H), 2.50 (m, 2H), 1.91 (m, 2H). The free base was transformed into the oxalate salt, which was crystallized from 2-PrOH to give a white solid: m.p. 153-154 °C, ESI/MS m/z 380 [M + H]<sup>+</sup>. Anal. Calcd (C<sub>23</sub>H<sub>29</sub>N<sub>3</sub>O<sub>2</sub>·C<sub>2</sub>H<sub>2</sub>O<sub>4</sub>): C, 63.95%; H, 6.66%; N, 8.95%. Found: C, 63.74%; H, 6.80%; N, 8.92%.

3.5.1.15. Synthesis of 1-(3-(4-(4-methoxyphenyl)piperazin-1-yl)propyl)-3,4-dihydroquinolin-2(1H)-one (**15**).

This compound was prepared starting from **68** and **74** following the procedure described for **8**: a white solid was obtained (46% yield): m.p. 98-99 °C. <sup>1</sup>H NMR (CDCl<sub>3</sub>, 500 MHz): δ 7.25-6.81 (m, 8H), 4.01 (m, 2H), 3.77 (s, 3H), 3.10 (m, 4H), 2.92–2.58 (m, 8H), 2.49 (t, 2H, *J* = 7.2 Hz), 1.90 (m, 2H). The free base was transformed into the oxalate salt, which was crystallized from 2-PrOH to give a white solid: m.p. 175-177 °C, ESI/MS m/z 380 [M + H]<sup>+</sup>. Anal. Calcd. (C<sub>23</sub>H<sub>29</sub>N<sub>3</sub>O<sub>2</sub>·C<sub>2</sub>H<sub>2</sub>O<sub>4</sub>): C, 63.95%; H, 6.66%; N, 8.95%. Found: C, 63.90%; H, 6.41%; N, 8.76%.

3.5.1.16. Synthesis of 1-(3-(4-(2-chlorophenyl)piperazin-1-yl)propyl)-3,4-dihydroquinolin-2(1H)-one (**16**).

This compound was prepared starting from **68** and **75** following the procedure described for **8**: an oil was obtained (58% yield). <sup>1</sup>H NMR (CDCl<sub>3</sub>, 500 MHz): δ 7.41-6.92 (m, 8H), 4.07 (m, 2H), 3.19 (m, 4H), 2.94 (m, 2H), 2.73-2.55 (m, 8H), 1.94 (m, 2H). The free base was transformed into the oxalate salt, which was crystallized from EtOH to give a white solid: m.p. 176-178 °C, ESI/MS m/z 384 [M + H]<sup>+</sup>, 406 [M + Na]<sup>+</sup>. Anal. Calcd (C<sub>22</sub>H<sub>26</sub>ClN<sub>3</sub>O·C<sub>2</sub>H<sub>2</sub>O<sub>4</sub>): C, 60.82%; H, 5.96%; N, 7.48%. Found: C, 60.74%; H, 5.83%; N, 7.60%.

3.5.1.17. Synthesis of 1-(3-(4-(3-chlorophenyl)piperazin-1-yl)propyl)-3,4-dihydroquinolin-2(1H)-one (**17**).

This compound was prepared starting from **68** and **76** following the procedure described for **8**: an oil was obtained (61% yield). <sup>1</sup>H NMR (CDCl<sub>3</sub>, 500 MHz): δ 7.40-6.96 (m, 8H), 4.05 (m, 2H), 3.11 (m, 4H), 2.92 (m, 2H), 2.67 (m, 6H), 2.53 (t, 2H, *J* = 7.1 Hz), 1.91 (m, 2H). The free base was transformed into the oxalate salt, which was crystallized from EtOH to give a white solid: m.p. 172-173 °C, ESI/MS m/z 384 [M + H]<sup>+</sup>, 406 [M + Na]<sup>+</sup>. Anal. Calcd (C<sub>22</sub>H<sub>26</sub>ClN<sub>3</sub>O·C<sub>2</sub>H<sub>2</sub>O<sub>4</sub>): C, 60.82%; H, 5.96%; N, 7.48%. Found: C, 60.52%; H, 6.01%; N, 7.61%.

3.5.1.18. Synthesis of 1-(3-(4-(4-chlorophenyl)piperazin-1-yl)propyl)-3,4-dihydroquinolin-2(1H)-one (**18**).

This compound was prepared starting from **68** and **77** following the procedure described for **8**: an oil was obtained (61% yield). <sup>1</sup>H NMR (CDCl<sub>3</sub>, 500 MHz): δ 7.31-6.83 (m, 8H), 4.04 (m, 2H), 3.19 (m, 4H), 2.93 (dd, 2H, *J* = 19.1 and 12.3 Hz), 2.67 (m, 6H), 2.50 (t, 2H, *J* = 7.0 Hz), 1.90 (m, 2H). The free base was transformed into the oxalate salt, which was crystallized from EtOH to give a white solid: m.p. 212-214 °C, ESI/MS *m/z* 384 [M + H]<sup>+</sup>, 406 [M + Na]<sup>+</sup>. Anal. Calcd (C<sub>22</sub>H<sub>26</sub>ClN<sub>3</sub>O·C<sub>2</sub>H<sub>2</sub>O<sub>4</sub>): C, 60.82%; H, 5.96%; N, 7.48%. Found: C, 61.02%; H, 6.06%; N, 7.50%.

3.5.1.19. Synthesis of 1-(3-(4-(2-nitrophenyl)piperazin-1-yl)propyl)-3,4-dihydroquinolin-2(1H)-one (**19**).

This compound was prepared starting from **68** and **78** following the procedure described for **8**: an oil was obtained (54% yield). <sup>1</sup>H NMR (CDCl<sub>3</sub>, 500 MHz): δ 7.84-7.00 (m, 8H), 4.07 (m, 2H), 3.12 (m, 4H), 2.94 (m, 2H), 2.63 (m, 6H), 2.52 (m, 2H), 1.97 (m, 2H). The free base was transformed into the oxalate salt, which was crystallized from 2-PrOH to give a yellow solid: m.p. 172-173 °C, ESI/MS *m/z* 395 [M + H]<sup>+</sup>, 417 [M + Na]<sup>+</sup>. Anal. Calcd (C<sub>22</sub>H<sub>26</sub>N<sub>4</sub>O<sub>3</sub>·C<sub>2</sub>H<sub>2</sub>O<sub>4</sub>): C, 59.50%; H, 5.83%; N, 11.56%. Found: C, 59.59%; H, 5.70%; N, 11.80%.

3.5.1.20. Synthesis of 1-(3-(4-(3-nitrophenyl)piperazin-1-yl)propyl)-3,4-dihydroquinolin-2(1H)-one (**20**).

This compound was prepared starting from **68** and **79** following the procedure described for **8**: an oil was obtained (49% yield). <sup>1</sup>H NMR (CDCl<sub>3</sub>, 500 MHz): δ 7.84-7.00 (m, 8H), 4.10 (t, 2H, *J* = 7.0 Hz), 3.73 (m, 6H), 3.21 (m, 2H), 2.94 (m, 2H), 2.69 (m, 2H), 2.40 (m, 2H), 1.97 (m, 2H). The free base was transformed into the oxalate salt, which was crystallized from 2-PrOH to give a yellow solid: m.p. 192-193 °C, ESI/MS *m/z* 395 [M + H]<sup>+</sup>, 417 [M + Na]<sup>+</sup>. Anal. Calcd (C<sub>22</sub>H<sub>26</sub>N<sub>4</sub>O<sub>3</sub>·C<sub>2</sub>H<sub>2</sub>O<sub>4</sub>): C, 59.50%; H, 5.83%; N, 11.56%. Found: C, 59.38%; H, 5.83%; N, 11.34%.

3.5.1.21. Synthesis of 1-(3-(4-(4-nitrophenyl)piperazin-1-yl)propyl)-3,4-dihydroquinolin-2(1H)-one (**21**).

This compound was prepared starting from **68** and **80** following the procedure described for **8**: an oil was obtained (49% yield). <sup>1</sup>H NMR (CDCl<sub>3</sub>, 500 MHz): δ 8.15 (d, 2H, *J* = 9.5 Hz), 7.28-6.99 (m, 4H), 6.84 (d, 2H, *J* = 9.5 Hz), 4.05 (m, 2H), 3.46 (m, 4H), 2.92 (m, 2H), 2.70-2.62 (m, 6H), 2.51 (t, 2H, *J* = 7.0 Hz), 1.92 (m, 2H). The free base was transformed into the oxalate salt, which was crystallized from 2-PrOH to give a yellow solid: m.p. 206-207 °C, ESI/MS *m/z* 395 [M + H]<sup>+</sup>, 417 [M + Na]<sup>+</sup>. Anal. Calcd (C<sub>22</sub>H<sub>26</sub>N<sub>4</sub>O<sub>3</sub>·C<sub>2</sub>H<sub>2</sub>O<sub>4</sub>): C, 59.50%; H, 5.83%; N, 11.56%. Found: C, 59.29%; H, 5.98%; N, 11.40%.

3.5.1.22. *Synthesis of 2-(4-(3-(2-oxo-3,4-dihydroquinolin-1(2H)-yl)propyl)piperazin-1-yl)benzotrile (22).*

This compound was prepared starting from **68** and **81** following the procedure described for **8**: an oil was obtained (67% yield). <sup>1</sup>H NMR (CDCl<sub>3</sub>, 500 MHz): δ 7.58-7.00 (m, 8H), 4.04 (m, 2H), 3.26 (m, 4H), 2.92 (m, 2H), 2.67 (m, 6H), 2.53 (t, 2H, *J* = 7.1 Hz), 1.90 (m, 2H). The free base was transformed into the oxalate salt, which was crystallized from EtOH to give a pale yellow solid: m.p. 173-174 °C, ESI/MS *m/z* 375 [M + H]<sup>+</sup>, 397 [M + Na]<sup>+</sup>. Anal. Calcd (C<sub>23</sub>H<sub>26</sub>N<sub>4</sub>O·C<sub>2</sub>H<sub>2</sub>O<sub>4</sub>): C, 64.64%; H, 7.00%; N, 14.96%. Found: C, 64.78%; H, 7.01%; N, 15.20%.

3.5.1.23. *Synthesis of 1-(3-(4-(pyridin-2-yl)piperazin-1-yl)propyl)-3,4-dihydroquinolin-2(1H)-one (23).*

This compound was prepared starting from **68** and **82** following the procedure described for **8**: an oil was obtained (48% yield). <sup>1</sup>H NMR (CDCl<sub>3</sub>, 500 MHz): δ 8.15 (dd, 1H, *J* = 5.0 and 1.5 Hz), 7.46-6.96 (m, 5H), 6.62-6.55 (m, 2H) 3.98 (m, 2H), 3.50-2.90 (m, 6H), 2.65-2.48 (m, 8H), 1.90 (m, 2H). The free base was transformed into the oxalate salt, which was crystallized from 2-PrOH to give a white solid: m.p. 180-182 °C, ESI/MS *m/z* 351 [M + H]<sup>+</sup>, 373 [M + Na]<sup>+</sup>. Anal. Calcd (C<sub>21</sub>H<sub>26</sub>N<sub>4</sub>O·C<sub>2</sub>H<sub>2</sub>O<sub>4</sub>): C, 62.71%; H, 6.08%; N, 12.06%. Found: C, 62.99%; H, 6.31%; N, 12.31%.



3.5.1.24. Synthesis of 1-(3-(4-(pyrimidin-2-yl)piperazin-1-yl)propyl)-3,4-dihydroquinolin-2(1H)-one (**24**).

This compound was prepared starting from **68** and **83** following the procedure described for **8**: an oil was obtained (62% yield). <sup>1</sup>H NMR (CDCl<sub>3</sub>, 500 MHz): δ 8.32 (d, 2H, *J* = 4.7 Hz), 7.27-6.99 (m, 4H), 6.50 (t, 1H, *J* = 4.7 Hz), 4.04 (m, 2H), 3.84 (m, 4H), 2.94 (m, 2H), 2.67 (m, 2H), 2.50 (m, 6H), 1.90 (m, 2H). The free base was transformed into the oxalate salt, which was crystallized from 2-PrOH to give a white solid: m.p. 181-182 °C, ESI/MS *m/z* 352 [M + H]<sup>+</sup>, 374 [M + Na]<sup>+</sup>. Anal. Calcd (C<sub>20</sub>H<sub>25</sub>N<sub>5</sub>O·C<sub>2</sub>H<sub>2</sub>O<sub>4</sub>): C, 59.85%; H, 6.16%; N, 15.86%. Found: C, 59.98%; H, 6.00%; N, 16.03%.

3.5.1.25. Synthesis of 1-(3-(4-(2,3-dichlorophenyl)piperazin-1-yl)propyl)-3,4-dihydroquinolin-2(1H)-one (**25**).

This compound was prepared starting from **68** and **84** following the procedure described for **8**: an oil was obtained (44% yield). <sup>1</sup>H NMR (CDCl<sub>3</sub>, 500 MHz): δ 7.28-6.93 (m, 7H), 4.02 (m, 2H), 3.09 (m, 4H), 2.89 (dd, 2H, *J* = 16.4 and 9.6 Hz), 2.66 (m, 6H), 2.52 (t, 2H, *J* = 7.2 Hz), 1.90 (m, 2H). The free base was transformed into the oxalate salt, which was crystallized from 2-PrOH to give a white solid: m.p. 190-191 °C, ESI/MS *m/z* 419 [M + H]<sup>+</sup>. Anal. Calcd (C<sub>22</sub>H<sub>25</sub>Cl<sub>2</sub>N<sub>3</sub>O·C<sub>2</sub>H<sub>2</sub>O<sub>4</sub>): C, 56.70%; H, 5.35%; N, 8.27%. Found: C, 56.60%; H, 5.24%; N, 8.38%.

3.5.1.26. *Synthesis of 1-(3-(4-(2,4-dichlorophenyl)piperazin-1-yl)propyl)-3,4-dihydroquinolin-2(1H)-one (26).*

This compound was prepared starting from **68** and **85** following the procedure described for **8**: an oil was obtained (41% yield). <sup>1</sup>H NMR (CDCl<sub>3</sub>, 500 MHz): δ 7.39-6.96 (m, 7H), 4.05 (m, 2H), 3.13 (m, 4H), 2.83-2.54 (m, 10H), 1.94 (m, 2H). The free base was transformed into the oxalate salt, which was crystallized from 2-PrOH to give a white solid: m.p. 209-209 °C, ESI/MS m/z 419 [M + H]<sup>+</sup>. Anal. Calcd (C<sub>22</sub>H<sub>25</sub>Cl<sub>2</sub>N<sub>3</sub>O·C<sub>2</sub>H<sub>2</sub>O<sub>4</sub>): C, 56.70%; H, 5.35%; N, 8.27%. Found: C, 56.51%; H, 5.31%; N, 8.12%.

3.5.1.27. *Synthesis of 1-(3-(4-(3,4-dichlorophenyl)piperazin-1-yl)propyl)-3,4-dihydroquinolin-2(1H)-one (27).*

This compound was prepared starting from **68** and **86** following the procedure described for **8**: an oil was obtained (41% yield). <sup>1</sup>H NMR (CDCl<sub>3</sub>, 500 MHz): δ 7.32-6.73 (m, 7H), 4.04 (m, 2H), 3.22 (m, 4H), 2.92 (m, 2H), 2.70-2.44 (m, 8H), 1.91 (m, 2H). The free base was transformed into the oxalate salt, which was crystallized from 2-PrOH to give a white solid: m.p. 187-189 °C, ESI/MS m/z 419 [M + H]<sup>+</sup>. Anal. Calcd (C<sub>22</sub>H<sub>25</sub>Cl<sub>2</sub>N<sub>3</sub>O·C<sub>2</sub>H<sub>2</sub>O<sub>4</sub>): C, 56.70%; H, 5.35%; N, 8.27%. Found: C, 56.62%; H, 5.20%; N, 8.38%.

3.5.1.28. *Synthesis of 1-(3-bromopropyl)-4-phenylpiperazine (58).*

A solution of **57** (10 mmol) in DMSO (10 mL) was added dropwise to a solution of 1,3-dibromopropane (22 mmol) and KOH (0.6 g) in DMSO (30 mL) and the mixture was stirred for 4 h at 70 °C. Then, it was poured into absolute ethanol to precipitate a solid, which was

filtered and rinsed with absolute ethanol 3 times. Evaporation of the solvent gave **58** as a pale yellow hygroscopic solid (71% yield).  $^1\text{H}$  NMR ( $\text{CDCl}_3$ , 500 MHz):  $\delta$  7.26 (t, 2H,  $J = 8.7$  Hz), 6.93 (d, 2H,  $J = 8.1$  Hz), 6.85 (t, 1H,  $J = 6.9$  Hz), 3.50 (t, 2H,  $J = 6.6$  Hz), 3.20 (m, 4H), 2.62 (m, 4H), 2.55 (t, 2H,  $J = 7.5$  Hz), 2.08 (m, 2H).

#### 3.5.1.29. *Synthesis of ethyl 4-(4-phenylpiperazin-1-yl)butanoate (61).*

Ethyl 4-bromobutanoate (5.0 mmol) was added to the solution of **57** (5.0 mmol) in ethanol (20 mL) at room temperature and the resulting solution was stirred at reflux for 6 h. After the completion of reaction, the mixture was cooled to room temperature. Sat.  $\text{NaHCO}_3$  (50 mL) was added, and the resulting solution was extracted with DCM (3 x 50 mL). The organic layer was dried over anhydrous  $\text{Na}_2\text{SO}_4$ . The evaporation of the solvent under reduced pressure afforded a residue, which was purified by flash chromatography, eluting with DCM/MeOH (95:5). An oil was obtained (89% yield).  $^1\text{H}$  NMR ( $\text{CDCl}_3$ , 500 MHz):  $\delta$  7.30-7.26 (m, 2H), 6.97-6.93 (m, 2H), 6.88 (t, 1H,  $J = 7.3$  Hz), 4.18-4.13 (m, 2H), 3.26-3.21 (m, 4H), 2.69-2.63 (m, 4H), 2.49-2.39 (m, 4H), 1.93-1.86 (m, 2H), 1.31-1.26 (m, 3H).

#### 3.5.1.30. *Synthesis of 1-(2-chloroethyl)-4-phenylpiperazine (64).*

1-Bromo-2-chloroethane (7.2 mmol) was added dropwise to a solution of **57** (6.15 mmol) and  $\text{K}_2\text{CO}_3$  (9.25 mmol) in acetone (10 mL). The reaction mixture was stirred under nitrogen atmosphere for 15 h. Then it was filtered, and the filtrate was concentrated under reduced pressure. The residue was diluted with water and extracted with EtOAc (3 x 50 mL). The organic layer was dried over anhydrous  $\text{Na}_2\text{SO}_4$ . The evaporation of the solvent

under reduced pressure afforded a residue, which was purified by flash chromatography, eluting with cyclohexane/EtOAc (7:3). An oil was obtained (57% yield). <sup>1</sup>H NMR (CDCl<sub>3</sub>, 400 MHz): δ 7.30-6.80 (m, 5H), 3.63 (t, 2H, *J* = 8.0 Hz), 3.21 (t, 4H), 2.79 (t, 2H, *J* = 8.0 Hz), 2.68 (m, 4H).

#### 3.5.1.31. Synthesis of 1-(4-bromobutyl)-3,4-dihydroquinolin-2(1H)-one (**66**).

A solution of **65** (13.6 mmol) in DMF (10 mL) was added dropwise to a suspension of sodium hydride (0.54 g, 60% in mineral oil) and DMF (20 mL). The resulting mixture was stirred at room temperature for 20 min, followed by the addition of a solution of 1,4-dibromobutane (13.7 mmol) in DMF (10 mL). The resulting mixture was stirred at room temperature for 20 min. Then, it was poured onto ice, and the aqueous phase was extracted with EtOAc (2 x 30 mL). The combined organic phases were washed with brine (5 x 30 mL) and dried over anhydrous Na<sub>2</sub>SO<sub>4</sub>. The evaporation of the solvent under reduced pressure afforded a residue, which was purified by flash chromatography, eluting with cyclohexane/EtOAc (7:3). An oil was obtained (84% yield). <sup>1</sup>H NMR (CDCl<sub>3</sub>, 400 MHz): 7.23-6.96 (m, 4H), 3.93 (m, 2H), 3.40 (m, 2H), 2.85 (t, 2H, *J* = 8 Hz), 2.60 (t, 2H, *J* = 8 Hz), 1.97 (m, 2H), 1.77 (m, 2H).

#### 3.5.1.32. Synthesis of 1-(5-bromopentyl)-3,4-dihydroquinolin-2(1H)-one (**67**).

This compound was prepared starting from **65** and 1,5-dibromopentane following the procedure described for **66**: an oil was obtained (89% yield). <sup>1</sup>H NMR (CDCl<sub>3</sub>, 400 MHz):

$\delta$   $^1\text{H}$  NMR ( $\text{CDCl}_3$ ): 6.96-7.23 (m, 4H), 3.95 (m, 2H), 3.40 (m, 2H), 2.91 (t, 2H,  $J = 7.8$  Hz), 2.63 (t, 2H,  $J = 7.8$  Hz), 1.94 (m, 2H), 1.68 (m, 2H), 1.52 (m, 2H).

#### 3.5.1.33. *Synthesis of 1-(3-bromopropyl)-3,4-dihydroquinolin-2(1H)-one (68).*

This compound was prepared starting from **65** and 1,3-dibromopropane following the procedure described for **66**: an oil was obtained (56% yield).  $^1\text{H}$  NMR ( $\text{CDCl}_3$ , 400 MHz):  $\delta$  7.30-6.99 (m, 4H), 4.11 (m, 2H), 3.50 (t, 2H,  $J = 6.5$  Hz), 2.93 (m, 2H), 2.67 (dd, 2H,  $J = 8.5$  and 6.6 Hz), 2.26 (m, 2H).

#### 3.5.2. **Radioligand binding assays**

The cells were grown in Dulbecco's Modified Eagle's Medium (DMEM): Ham's F12 culture media = 1:1. The media was supplemented with 20 mM HEPES, 2mM L-glutamine, 0.1 mM nonessential amino acids, 200  $\mu\text{g}/\text{mL}$  hygromycin, 10% heat activated Fetal Bovine Serum (FBS) and 1% antibiotic/antimycotic. Cells were kept in an incubator at 37°C, with 5%  $\text{CO}_2$ . After the cells have reached 80-90% confluence, they were harvested using Earle's balanced salt solution (EBSS) with 5 mM ethylenediaminetetraacetic acid (EDTA), centrifuged (3000 rpm) for 10 minutes at 21°C and the supernatant was carefully removed by vacuum suction to afford cell pellet. The pellet was resuspended in 10 mL of hypotonic lysis buffer containing 5 mM  $\text{MgCl}_2$  and 5 mM Tris (pH = 7.4 at 4°C) and centrifuged for 30 minutes at 20 000 rpm, at 4°C. The supernatant was once again removed by vacuum suction, carefully, and the remaining pellet was resuspended in binding buffers containing 8.7 g/L Earle's Balanced Salts without phenol red, 2.2 g/L  $\text{NaHCO}_3$ , and the pH was set

to 7.4 for the test with [<sup>3</sup>H]N-methylspiperone as a radioligand. For [<sup>3</sup>H]-(R)-(+)-7-OH-DPAT assay, 50 mM Tris, 10 mM MgCl<sub>2</sub> and 1 mM EDTA were added and the pH was set to 7.4.

To define the protein concentration, Bradford protein assay was used, and the membranes were either used freshly prepared, in case of [<sup>3</sup>H]-(R)-(+)-7-OH-DPAT assay (500-600 µg/mL), or were stored at -80°C, in case of [<sup>3</sup>H]N-methylspiperone assay (500 µg/ml). If frozen, the cell suspension was thawed and later diluted with fresh EBSS until the density was 200 µg/mL (in case of DRD2 and DRD3) or 300 µg/mL (in case of DRD4) stock for binding. To prepare the solution for the well plates, we first needed to prepare the membranes by adding [<sup>3</sup>H]N-methylspiperone in the amount of 20 µg/well total protein for DRD2 or DRD3 (depending on the assay), or 30 µg/well total protein for DRD4. In the case of the [<sup>3</sup>H]-(R)-(+)-7-OH-DPAT assay, we have used approximately 50–60 µg/well total protein concentration of DRD4.

As the tests were performed on 96-well plates, the cell solutions were prepared as follows: in 300 mL of a new binding buffer, we added 100 mL of membranes (prepared as described before), 50 mL of the diluted solution of ligands and 50 mL dilutions of either [<sup>3</sup>H]N-methylspiperone (0.4 nM) or [<sup>3</sup>H]-(R)-(+)-7-OH-DPAT (3 nM) in their binding buffers. For each ligand, total and nonspecific binding were determined. For the total binding, 30% DMSO solution was used, and it took up 3% of the final concentration in wells. For nonspecific binding, we have used 10 µM (+)-butaclamol. Dilutions were prepared in triplicates for each ligand for the validation of the obtained results. Such prepared plates were kept for 60 minutes at room temperature, in the case of [<sup>3</sup>H]N-methylspiperone, or 90 minutes in the case of [<sup>3</sup>H]-(R)-(+)-7-OH-DPAT.

Termination of the reaction was performed by filtering the solutions through PerkinElmer Uni-Filter-96 GF/B or GF/C (the filter is presoaked in 0.5% polyethyleneimine for the duration of incubation), using a Brandel 96-well plates Harvester manifold. The filters were then washed thrice using 3 mL of the binding buffer cooled to 0°C, and 65 µL of PerkinElmer MicroScint 20 scintillation cocktail was added to each individual well. The filters were then counted via PerkinElmer MicroBeta microplate counter. The efficiency of the counter had to be experimentally defined for separate radioligands, and the aliquots of their dilutions were measured to determine the quantity of [<sup>3</sup>H] ligand added in each of the experiments. The IC<sub>50</sub> was determined via dose-response curves, based on the obtained results. K<sub>i</sub> values were determined by using the Cheng-Prusoff equation.<sup>58</sup> If the complete inhibition was not obtained even for the highest prepared concentrations of ligands, the values of K<sub>i</sub> were calculated through extrapolation by the constraint of the bottom of the dose-response curves in nonlinear regression analysis, where the value of residual specific binding amounts to 0%. K<sub>d</sub> values for [<sup>3</sup>H]Nmethylspiperone and [<sup>3</sup>H]-(R)-(+)-7-OH-DPAT were obtained by homologous competitive binding experiments and the analysis of the results via software GraphPad Prism version 9.00 for Macintosh. K<sub>i</sub> values were determined for triplicates and the results are shown as mean values ± SEM.

### **3.5.3. Bioluminescence resonance energy transfer (BRET) assays**

BRET functional assays were performed on the same cell lines as the radioligand-binding assay: HEK293T. The cells were transfected with constructs containing renilla luciferase variant RLuc8 and mVenus as the acceptor protein with yellow fluorescence properties. The luciferase and the protein formed a BRET pair fused to the proteins within this

research. Firstly, the G-protein activation assays were performed, and the Gai1 or GaoA subunit was fused to RLuc8 and Gy2 to the mVenus protein. For the  $\beta$ -arrestin recruitment assays,  $\beta$ -arrestin was fused to mVenus protein, while the DRD4 was fused to RLuc8.

HEK293T cells were grown in DMEM with 10% FBS, 1% penicillin-streptomycin and 2mM glutamine, on dishes with a diameter of 10 cm. Cells were transfected with 15  $\mu$ g total plasmid cDNA with 30  $\mu$ g polyethyleneimine as a transfection agent. The dishes were left in the incubator for 6 h at 37 °C (5% CO<sub>2</sub>), after which the incubation was terminated by changing the medium. 48 hours later, the transfected cells were washed with phosphate-buffered saline (PBS), then harvested and resuspended in PBS with 200  $\mu$ M NaHSO<sub>3</sub> and 0.1% glucose. Cells were transferred onto 96-well plates (in the following quantity: 2x10<sup>5</sup> cells/well) and 5  $\mu$ M of the luciferase substrate, coelenterazine H, was added to individual wells. Antagonists were added to the cells, then the plates were left to incubate for 10 minutes, and were taken out to room temperature and left to rest for 2 min. Subsequently, the ligands were transferred to each well, and the luminescence was measured after 2.5 min (using a PherastarFSX plate reader) at 485 nm, which corresponds to the RLuc8 wavelength and the fluorescence wavelength window of the mVenus (530 nm).

BRET ratio was determined as the ratio of the detected fluorescence and luminescence against the background determined in cells expressing only RLuc8. The background was subtracted from the obtained emission values. Software Prism 9 was used for the generation of dose-response curves representing BRET ratios, as well as for the statistical analysis.



### **3.5.4. Molecular modelling studies**

The detailed crystal structure of DRD4 in complex with **nemonapride** (a selective DRD4 antagonist) was described for the first time in 2017 by Wang et al., even though the existence of DRD4 was known before.<sup>25</sup> By 2017, only the low-resolution structure (2.89 Å) of DRD3 complexed with eticlopride, a DRD2/DRD3 specific antagonist was described, and DRD4 *in silico* studies were done by modifying that particular structure.<sup>59</sup> The DRD4 structure complexed with **nemonapride** involved a replacement of residues 228-336 of the IL3 with thermostabilized apocytochrome b562RIL.<sup>25</sup> This complex had a Protein Data Bank (PDB) code: 5WIU and its resolution was 1.962 Å, obtained by X-ray diffraction. To understand better the binding positions of ligands, we needed to describe the structural uniqueness of the DRD4 binding pocket. DRD4 binding site is elongated and is divided into two pockets: an orthosteric binding pocket (OBP) and the extended binding pocket (EBP), and its particular structure was described by Zhou et al. in which DRD4 (PDB code: 5WIU) was complexed with **L-745,870**.<sup>24</sup> Not all TMs have a role in forming the pockets, only TM2, TM3, TM5, TM6 and TM7 do. OBP is mostly hydrophobic, with Val113, Phe330 and Phe331 on the sides of the pocket, and Cys116 and Trp327 on the lower side. In this pocket can be found Ser191, Ser192 and Ser195, responsible for the DRD4 activation by DA.<sup>60</sup> On the other hand, the EBP elongates from the OBP, and it is closed by the residues of TM2 and TM3. In the case of DRD2 and DRD3, this pocket is formed by TM2 and TM7. Leu83, Phe88, Ser91, Trp98 (on the top of the pocket), Leu108 and Met109 surround the DRD4 EBP, as well as the disulfide bond between Cys105 and Cys180. An H-bond between Glu92 and Ser351 limits the pocket extension.<sup>24</sup>

DRD2 (PDB code: 6CM4) binding site is also constituted of an OBP and the EBP. Compared to DRD3 and DRD4, the OBP of DRD2 is deeper and more hydrophobic, and it is situated between TM3, TM5 and TM6. Cys118, Thr119, Ser197, Phe198, Phe382, Phe390 and Trp386 form a smaller sub-pocket beneath the OBP, while another hydrophobic sub-pocket forms above the OBP, in which we find a conserved residue Asp114 that forms a salt bridge with the tertiary amine of risperidone. TM7 moves outwards in DRD2, creating a much bigger EBP compared to that of DRD4.<sup>47</sup>

The nature of the DRD3 (PDB code: 3PBL) binding site is similar to that of the  $\beta_2$  adrenergic receptor ( $\beta_2$ AR), aside from the fact that the  $\beta_2$ AR has a more open crevice to the extracellular part of the protein, while TM5 and TM6 of DRD3 face inward, limiting the access of molecules to its binding site.<sup>59</sup> The OBP is formed between TM1, TM2, TM3, TM7 and the ECL2, with its EBP being positioned extracellularly, at the junction of TM1, TM2 and TM7. Ligands extend from the pocket and are additionally stabilized by ECL1/ECL2 residues.

The primary sequence of the human DRD4 was taken from the UniProt database (Id: P21917, DRD4\_HUMAN). The homology model used in the research was built by using Modeller 9.12,<sup>61</sup> based on the known and resolved structure of the human DRD3 complexed with eticlopride as baseline (PDB code: 3PBL). 10 structures were generated and the best models were chosen according to the scores of Modeller9.12 (GA341 and DOPE scores, for example), and the percentage of residues in the allowed regions according to the Ramachandran plot. The selected model was minimized (protein backbone fixed) to keep the appropriate DRD4 predicted folded structure. Structural checks were performed to evade having any incorrect configurations, unpredicted gaps,

cis-peptide bonds or clashing residues. 98.8% (90.3% within the core regions) of residues fell in the allowed regions of the Ramachandran plot, and 95.1% fell into the allowed regions of the chi space. Hydrogen atoms were added to DRD4 using the H++ software, at a physiological pH value (7.4).<sup>62</sup> All the Lys residues were positively charged at pH 7.4 and were not later modified. The simulation of ligands was done in their protonated states and their conformational space was evaluated through MonteCarlo simulations (1000 minimized conformers for each ligand were calculated). The structure of the lowest energy was subsequently optimized by PM7 semiempirical calculations<sup>63</sup> and underwent docking simulations. Docking was performed using PLANTS, integrated into VEGA ZZ molecular modelling suite.<sup>49</sup> For the free docking, the search for best conformation was limited to a 13 Å radius sphere around Asp115. For each simulated molecule, 10 poses were generated and ranked by the ChemPLP scoring function (speed = 1). All computed results were minimized and rescored by using ReScore+, as described by Pedretti et al.<sup>64</sup>

### **3.5.5. *In vitro* studies on GBM cell lines**

Cell lines T98 and U251 (grade IV) were obtained from the European Collection of Cell Cultures (ECACC, Salisbury, UK), and were maintained and grown in Eagle's Minimum Essential Medium.<sup>65</sup> The medium was supplemented with 10% heat-inactivated FBS, 2mmol/L of L-glutamine, 100 U/mL of penicillin and 50 µg/mL streptomycin. Cells were kept in an incubator at 37°C, with 5% CO<sub>2</sub>. GSC#83 was isolated from a surgical sample of human adult patients with a primitive brain tumour, at the Institute of Neurosurgery, under the Catholic University School of Medicine in Rome, Italy.<sup>66</sup> GSC culture was formed from the tumoural specimen by mechanical dissociation and culturing cells in

DMEM/F12 serum-free medium. The medium was supplemented with the epidermal growth factor (EGF) and basic fibroblast growth factor, and it contained 9.6 g/mL putrescine, 0.1 mg/mL transferrin sodium salt, 2 mM glutamine, 0.025 mg/mL insulin, 0.6% glucose, 6.3 ng/mL progesterone, and 5.2 ng/mL sodium selenite. GSC line was grown in medium without serum, in a form of floating spheres and in an undifferentiated state (rounded morphology type, high ratio of nucleus: cytoplasm). GSC#83 of human origin was verified by profiling of its short tandem repeat (STR), based on the standard ASN-0002-2011.12 of the American National Standards Institute.

MTS assay was performed as well to determine GBM cells' viability. All three cell lines (T98, U251 and GSC#83) were cultured in 96-well plates with a density of 5000 cells per well. The growing process was the same as for the biological studies described earlier. At 80% of confluence, the cells were treated by **18** and **23** in gradually increasing concentrations from 5  $\mu$ M to 50  $\mu$ M (DMSO dilutions), for 24 hours. Controls were prepared by treating the cells with **temozolomide** in the same dilutions as the two ligands, or in the vehicle only (DMSO). So prepared cultures were incubated with CellTiter 96 Aqueous One Solution Reagent in a quantity of 200  $\mu$ L/well for 2 hours, at 37 °C, in an atmosphere containing 5% of CO<sub>2</sub>, as mentioned in the previous research.<sup>67</sup> The coloured formazan product absorbance was measured at the wavelength of 490 nm, on the Tecan infinite multiplate reader intended for 96-well plates.

GBM and GSC lines were treated for 24 hours with ligands **18** and **23**, in different concentrations ranging from 5 to 50  $\mu$ M. These preparations were named the experimental group (EG). Control group (CG) was prepared by incubating GBM and GSC lines for 24 hours with vehicle solely, with **temozolomide**, with **PNU 96145E** (known

DRD4 antagonist) or **A412997** (known DRD4 agonist), in concentrations ranging from 5 to 50  $\mu\text{M}$ .

### **3.6. Targeted protein degradation of the DRD4**

#### ***3.6.1. Ubiquitination of DRD4***

DRDs can activate different effectors through G protein, but they can also signal through interactions with dopamine receptor-interacting proteins (DRIPs).<sup>68,69</sup> In 2016, researchers from Ghent decided to ubiquitinate DRD4 to try and identify novel DRD4-interacting proteins via a yeast two-hybrid screening.<sup>70</sup> The DRD4 IL3, containing 4 tandem repeats, was used as bait. A BTB-Kelch protein named KLHL12 was identified as a positive candidate, which acts as an adaptor in Cullin3-based E3 ubiquitin ligases.<sup>71</sup> More specifically, Cullin3 is a scaffold protein that recruits the POI and facilitates the onset of the ubiquitination process via POI-specific BTB adaptor proteins. After the ubiquitination (monoubiquitination or polyubiquitination), the remaining ubiquitin could be removed via deubiquitinating enzymes.<sup>70</sup> They have proven that DRD4 is capable of undergoing polyubiquitination via one of the 7 ubiquitin lysins, with Lys48 being promoted by KLHL12.<sup>70,72</sup>

By mutating one of the lysins, no changes were noticed in the ubiquitination pattern, and generally, limited evidence mentioned non-lysine ubiquitination of a GPCR by cysteines, serines, threonines, and the N-terminus of the polypeptide backbone.<sup>72-77</sup> Additionally, it was shown that the levels of basal ubiquitination and the KLHL12-mediated ubiquitination decrease with the increasing number of repeats in the IL3 of DRD4.<sup>70</sup>

DRD4 could be ubiquitinated for several reasons, such as targeting the receptors for degradation in cases in which pathologies occur due to changes in signalling pathways. In the case of DRD4 polyubiquitination via Lys48, no DRD4 degradation was noted, no difference in cAMP was noticed and the ubiquitination or recruitment of  $\beta$ -arrestin did not occur.<sup>70</sup>

In 2017, researchers discovered that both isopeptide and ester bond ubiquitination regulate proteasomal degradation of DRD4, in the absence of an exogenous agonist.<sup>78</sup> In HEK293T cells and in primary mouse cortical neurons, ubiquitinated DRD4s were also detected at the plasma membrane, probably because they were not undergoing lysosomal degradation. However, the role of DRD4 in cell signalling remained unclear.<sup>78</sup>

### **3.6.2. Introduction to PROTAC molecules**

PROTACs are heterobifunctional molecules consisting of three consecutively linked portions of a larger molecule (Figure 19): an E3 ubiquitin ligase ligand, a linker and a ligand of the targeted protein (in this case, DRD4).<sup>79–85</sup> Protein degradation is achieved by hijacking the intracellular ubiquitin-proteasome system (UPS) while maintaining its catalytic properties, making the drug more effective than small molecule inhibitors, as smaller doses can be administered.<sup>79</sup> Additionally, PROTACs can target the “undruggable” targets, due to their specific structure.

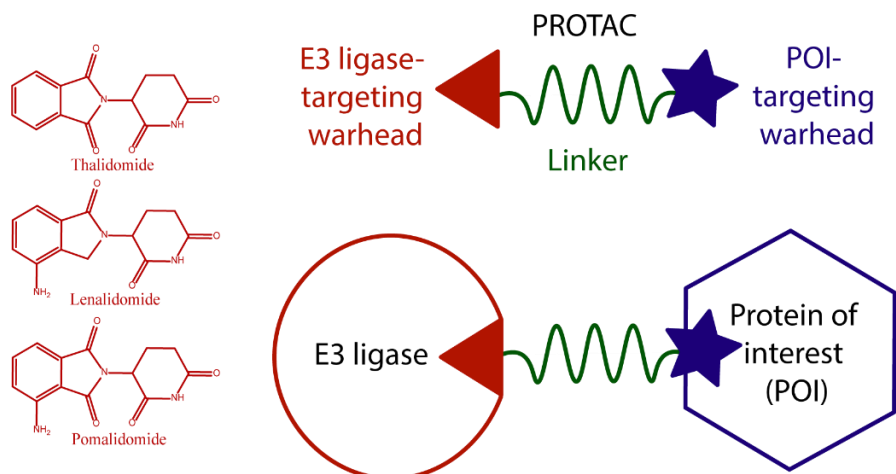


**Figure 19.** General PROTAC pharmacophore composed of an E3 ligase-targeting warhead (red), a linker (green) and a protein of interest (POI)-targeting warhead (blue). Common E3 ligases-thalidomide, lenalidomide and pomalidomide are shown on the left.

UPS is a pathway responsible for cell homeostasis by degrading more than 80 cellular proteins.<sup>86</sup> It includes ubiquitin (small, conserved protein in eukaryotes that labels proteins for degradation), proteasome, enzymes and targeted cellular proteins. UPS protein degradation consists of three steps. The first step is the interaction between ubiquitin and the targeted protein, in which the energy is consumed (ATP is degraded) to activate ubiquitin and generate an E1 ligase-ubiquitin complex (E1 ubiquitin-activating enzyme has to be present). The second step is the transfer of the activated ubiquitin to the E2 ubiquitin-conjugating enzyme and the formation of the E2 ubiquitin complex. The third and final step involves the transfer of ubiquitin to the E3 ubiquitin ligase that recognizes the targeted protein and binds ubiquitin by an amide bond to the  $\epsilon$ -amino group of Lys on the targeted protein, therefore marking it for degradation by the proteasome (Figure 20).<sup>79</sup>

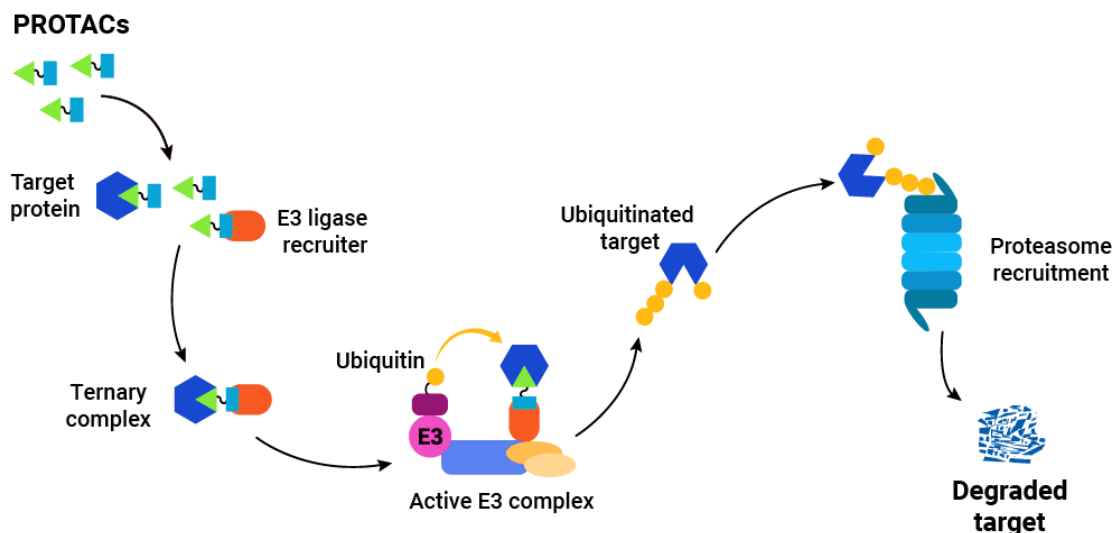


**Figure 20.** Mechanism of protein ubiquitination by proteasome. Image copyright: Promega Connections.

There are three generations of PROTACs so far. The first generation of PROTACs were peptide-based molecules developed in 2001 and reported by Sakamoto *et al.*<sup>87</sup> These molecules consisted of one of the potent angiogenesis inhibitors, namely fumagillin or ovalicin, linked to the I $\kappa$ B $\alpha$  phosphopeptide (recognized by  $\beta$ -TCRP as an E3 ligase). Later, in 2004, to improve the cell permeability of the initial PROTAC molecules, 8 arginines were added at the end of the VHL E3 ligase, and the first cell-permeable PROTACs were discovered.<sup>88</sup> In this case, FKBP12 or DHT were used as protein-of-interest-targeting molecules, otherwise known as protein-of-interest (POI) warheads. All first-generation PROTAC molecules had low cell permeability and chemical stability.<sup>82</sup>

For the development of the second generation of PROTACs, an analysis was conducted on E3 ligases<sup>81,82</sup> (IAP, CRBN, VHL and MDM2) to try and discover the small molecules that could have higher efficacy and permeability. However, the issue of high molecular weight of PROTACs, toxicity and off-target specificity persisted.<sup>82,89,90</sup>



In the third generation of PROTACs, molecules could be controlled better, and there have been developments of phosphate-dependent (phospho-PROTACs) and light-controlled PROTACs (opto-PROTACs and PHOTACS/ photo-PROTACs).<sup>79</sup> In particular, phospho-PROTACs would bind to VHL E3 ligase to specifically degrade targets with an activated kinase-signalling clue. However, they still rely on traditional, rather than tumour-specific clues.<sup>82</sup> Light-controlled PROTACs consist of pomalidomide as an E3-ligase-targeting molecule, which activates in the presence of UVA light. However, UVA might damage DNA, and cannot penetrate tissues well, so the research in terms of cancer therapy remains limited.<sup>82</sup>

### **3.6.3. Introduction and objectives of the work**

In the last years, several “POI ligands” have been used for the preparation of PROTACs.<sup>91</sup> They span from non-covalent, irreversible and reversible covalent ligands to allosteric ones. They are directed to more than 100 targets, including chromatin readers such as BRD4, cytoplasmic hormone receptors scaffolding and regulatory proteins, aggregation-prone misfolding proteins (e.g., Tau), fusion proteins (e.g., BCR-ABL), and receptor tyrosine kinases (e.g., EGFR, HER3, FLT3).

Recently, Li et al. reported the first small-molecule PROTACs able to induce the  $\alpha$ 1-AR degradation, inhibiting the proliferation of PC-3 prostate cancer cells and suppressing tumour growth *in vivo*. To our knowledge, these compounds represent the first PROTACs for GPCRs.<sup>92</sup>

Based on these observations, in my research work, this approach has been used in the design and synthesis of new small molecule PROTACs potentially able to induce DRD4 degradation, to be evaluated for the treatment of GBM. Specifically, we selected the lead compound **54** as a POI ligand to be linked to lenalidomide as an E3 ubiquitin ligase warhead by spacers of different lengths (compounds **28-30**, Figure 21). These molecules could potentially help in understanding the role of DRD4 in brain cancers.

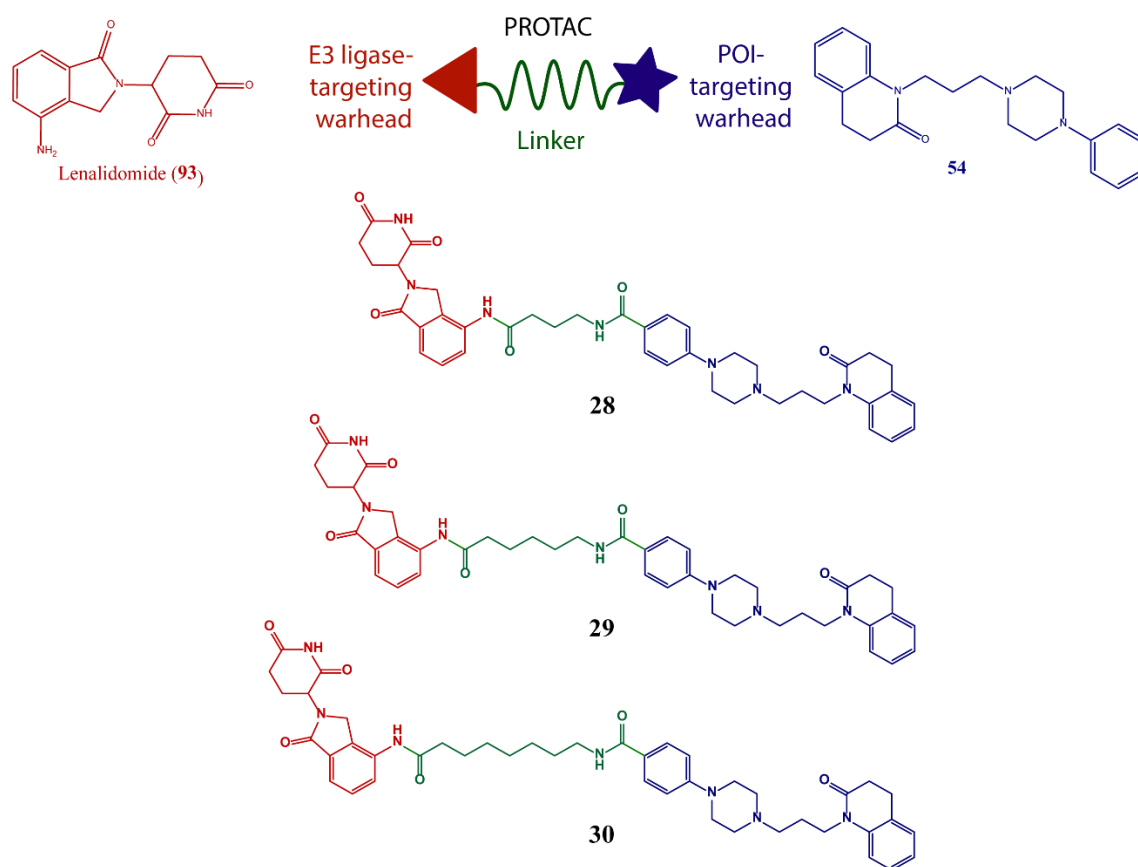
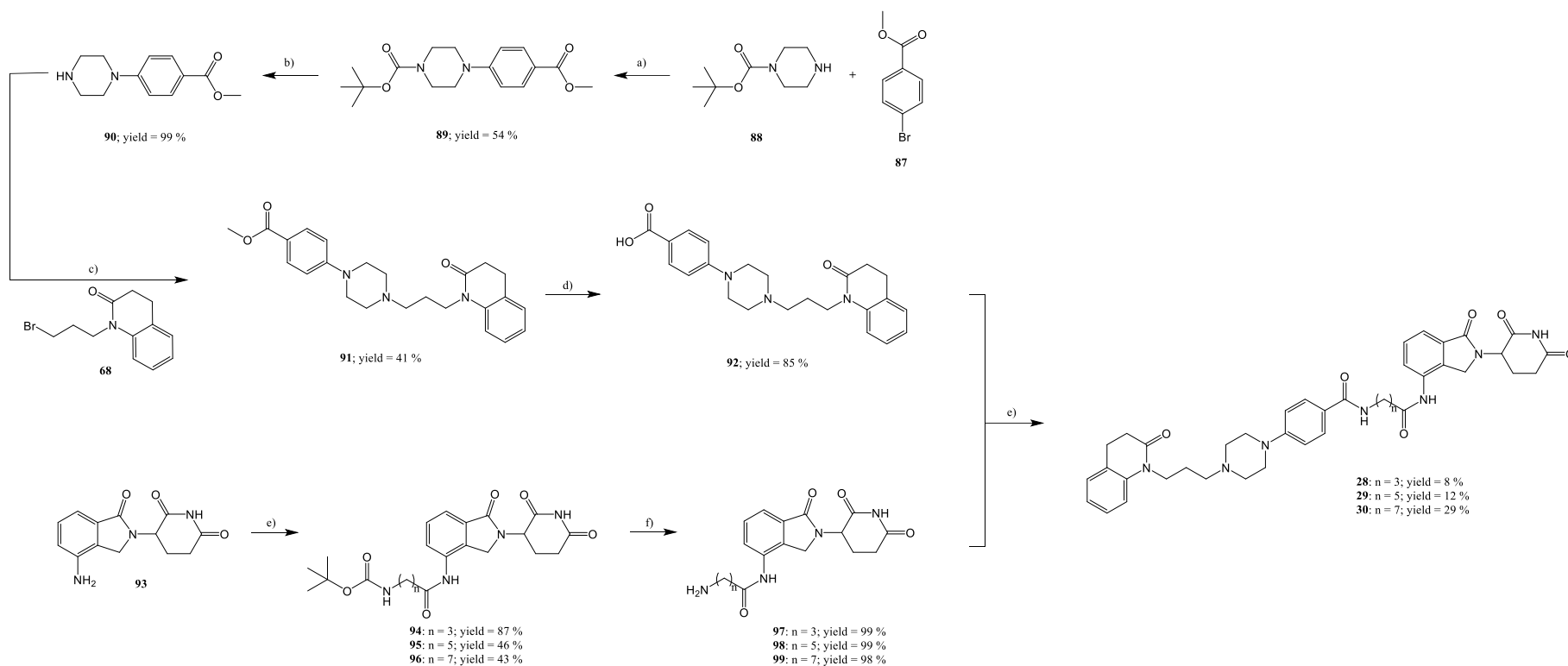


**Figure 21.** PROTACs **28-30**, composed of the E3 ligase ligand lenalidomide (**93**, red), a linker (green) and the DRD4 lead compound **54** (blue) as a POI ligand.

### **3.6.4. Synthesis of DRD4 PROTACs and the analysis plan**

DRD4 PROTACs **28-30** were prepared following the procedure shown in Scheme 4. The N-alkylation of **65** to afford intermediate **68** was performed as described in Scheme 3. Methyl 4-bromobenzoate (**87**) and 1-Boc-piperazine (**88**) were reacted to afford intermediate **89**, in the presence of Pd(OAc)<sub>2</sub>, Cs<sub>2</sub>CO<sub>3</sub> and rac-BINAP in toluene. The Boc protection of **89** was removed using a 3M solution of HCl in MeOH to obtain **90**, which was coupled with **68** to afford **91**. The saponification reaction performed on **91**, using an aqueous solution of KOH, afforded **92**. Separately, **93** was coupled with 4-(Boc-amino)butanoic acid, 6-(Boc-amino)hexanoic acid and 8-(Boc-amino)octanoic acid in the presence of hexafluorophosphate azabenzotriazole tetramethyl uronium (HATU) in DMF and diisopropylethylamine (DIPEA), to afford intermediates **94**, **95** and **96**, respectively. The deprotection of the Boc group for **94**, **95** and **96** was performed using CF<sub>3</sub>COOH in DCM, to afford the corresponding primary amines **97**, **98** and **99**, which were coupled with **92** under the same conditions as for the intermediates **94**, **95** and **96**, yielding the final PROTACs **28**, **29** and **30**, respectively.

The PROTACs **28-30** will be evaluated for their binding affinity for CRBN E3 ligase and for the DRD4. Molecular modelling studies will be performed to evaluate the binding mode of **28-30** to CRBN, as well as to DRD4. Lastly, *in vitro* studies will be performed to assess the ability of the compounds to affect the viability of GBM cell lines.



**Scheme 4.** Synthesis of PROTACs **28-30**. Reagents and conditions: (a) Pd(OAc)<sub>2</sub>, Cs<sub>2</sub>CO<sub>3</sub>, rac-BINAP, toluene; (b) 3M HCl in MeOH; (c) K<sub>2</sub>CO<sub>3</sub>, DMF; (d) KOH, H<sub>2</sub>O; (e) 4-(Boc-amino)butanoic acid (for **69**)/ 6-(Boc-amino)hexanoic acid (for **70**)/ 8-(Boc-amino)octanoic acid (for **71**), HATU, DIPEA, DMF; (f) CF<sub>3</sub>COOH, DC.

### 3.6.5. Experimental section

#### 3.6.5.1. Synthesis of *N*-(4-((2-(2,6-dioxopiperidin-3-yl)-1-oxoisoindolin-4-yl)amino)-4-oxobutyl)-4-(4-(3-(2-oxo-3,4-dihydroquinolin-1(2H)-yl)propyl)piperazin-1-yl)benzamide (**28**).

A mixture of **92** (1 mmol), **97** (1 mmol) and HATU (1.1 mmol) was stirred under N<sub>2</sub> for 10 minutes at room temperature. Anhydrous DMF (3 mL) was added, followed by DIPEA (4 mmol), and the reaction mixture was left stirring overnight, at room temperature, under N<sub>2</sub>. EtOAc (10 mL) was added to the flask, and the solution was washed with H<sub>2</sub>O (3 x 10 mL). The aqueous phase was extracted with EtOAc (20 mL) and the combined organic phases were dried over anhydrous Na<sub>2</sub>SO<sub>4</sub>, filtered and evaporated under vacuum to give a residue which was purified by flash chromatography, using CHCl<sub>3</sub>/MeOH (9:1). **28** was obtained as a white solid (8% yield); m.p. 51-53 °C). <sup>1</sup>H NMR (DMSO, 500 MHz): δ 11.02 (s, 1H), 9.82 (s, 1H), 8.23 (m, 1H), 7.81 (d, *J* = 7.2 Hz, 1H), 7.72 (d, *J* = 8.8 Hz, 2H), 7.48 (m, *J* = 7.6 Hz, 2H), 7.28-7.18 (m, 3H), 6.99 (t, *J* = 7.3 Hz, 1H), 6.93 (d, *J* = 8.8 Hz, 2H), 5.14 (m, 1H), 4.37 (m, 2H), 3.96-3.90 (m, 2H), 3.66-3.58 (m, 2H), 3.38 (m, 4H), 3.23 (s, 4H), 3.14 (m, 2H), 2.97-2.81 (m, 4H), 2.63 (m, 1H), 2.39 (m, 4H), 2.05-1.97 (m, 1H), 1.85 (m, 2H), 1.73 (m, 2H). ESI/MS *m/z* 720 [M + H]<sup>+</sup>, 742 [M + Na]<sup>+</sup>. Anal. Calcd (C<sub>40</sub>H<sub>45</sub>N<sub>7</sub>O<sub>6</sub>): C, 66.74%; H, 6.30%; N, 13.62%. Found: C, 66.55%; H, 6.20%; N, 13.48%.

3.6.5.2. *Synthesis of N-(6-((2-(2,6-dioxopiperidin-3-yl)-1-oxoisindolin-4-yl)amino)-6-oxohexyl)-4-(4-(3-(2-oxo-3,4-dihydroquinolin-1(2H)-yl)propyl)piperazin-1-yl)benzamide (29).*

This compound was prepared starting from **98** following the procedure described for **28**: a white solid was obtained (12% yield); m.p. 59-61 °C. <sup>1</sup>H NMR (DMSO, 500 MHz): δ 11.02 (s, 1H), 9.80 (s, 1H), 8.18 (t, *J* = 5.5 Hz, 1H), 7.81 (d, *J* = 7.0 Hz, 1H), 7.71 (d, *J* = 8.8 Hz, 2H), 7.51-7.45 (m, 2H), 7.27-7.18 (m, 3H), 6.99 (m, 1H), 6.93 (d, *J* = 8.9 Hz, 2H), 5.14 (m, 1H), 4.36 (m, 2H), 3.93 (t, *J* = 7.2 Hz, 2H), 3.65-3.55 (m, 2H), 3.23 (m, 6H), 3.12 (m, 2H), 2.87-2.83 (m, 2H), 2.59 (m, 4H), 2.36 (m, 4H), 2.05-1.96 (m, 2H), 1.77 (m, 2H), 1.63 (m, 2H), 1.54 (m, 2H), 1.35 (m, 2H). ESI/MS *m/z* 748 [M + H]<sup>+</sup>, 770 [M + Na]<sup>+</sup>. Anal. Calcd (C<sub>42</sub>H<sub>49</sub>N<sub>7</sub>O<sub>6</sub>): C, 67.45%; H, 6.60%; N, 13.11%. Found: C, 67.16%; H, 6.74%; N, 13.01%.

3.6.5.3. *Synthesis of N-(8-((2-(2,6-dioxopiperidin-3-yl)-1-oxoisindolin-4-yl)amino)-8-oxooctyl)-4-(4-(3-(2-oxo-3,4-dihydroquinolin-1(2H)-yl)propyl)piperazin-1-yl)benzamide (30).*

This compound was prepared starting from **99** following the procedure described for **28**: a white solid was obtained (29% yield); m.p. 66-68 °C. <sup>1</sup>H NMR (DMSO, 500 MHz): δ 11.02 (s, 1H), 9.76 (s, 1H), 8.74 (s, 1H), 8.06 (d, *J* = 9.1 Hz, 1H), 7.87-7.64 (m, 4H), 7.29-7.13 (m, 6H), 5.16 (m, 1H), 4.42-4.30 (m, 2H), 3.94 (m, 2H), 3.61 (m, 2H), 3.49 (m, 2H), 3.20 (m, 4H), 2.95-2.83 (m, 8H), 2.73 (m, 2H), 2.61 (m, 2H), 2.37 (m, 7H), 1.28-1.23 (m, 10H). ESI/MS *m/z* 776 [M + H]<sup>+</sup>, 798 [M + Na]<sup>+</sup>. Anal. Calcd (C<sub>44</sub>H<sub>53</sub>N<sub>7</sub>O<sub>6</sub>): C, 68.11%; H, 6.88%; N, 12.64%. Found: C, 67.98%; H, 6.99%; N, 12.44%.

3.6.5.4. *Synthesis of tert-butyl 4-(4-(methoxycarbonyl)phenyl)piperazine-1-carboxylate (89).*

A mixture of **87** (1 mmol), **88** (1.1 mmol), Pd(OAc)<sub>2</sub> (0.1 mmol), Cs<sub>2</sub>CO<sub>3</sub> (2 mmol) and rac-BINAP (0.1 mmol) in toluene (10 mL) was stirred under N<sub>2</sub>, for 12 hours under reflux. Toluene was evaporated and the residue was washed with DCM (5 mL) and filtered. The solvent was evaporated and the remaining crude was purified by flash chromatography, using cyclohexane/EtOAc (8:2), to obtain **89** in a 54% yield (m.p. 217-218 °C). <sup>1</sup>H NMR (DMSO, 500 MHz): δ 7.97 (m, 2H), 7.09-6.93 (m, 2H), 3.90-3.86 (m, 3H), 3.72-3.60 (m, 4H), 3.34 (t, *J* = 16.8 Hz, 4H), 1.47 (d, *J* = 10.2 Hz, 9H). ESI/MS *m/z* 321 [M + H]<sup>+</sup>, 343 [M + Na]<sup>+</sup>.

3.6.5.5. *Synthesis of methyl 4-(piperazin-1-yl)benzoate (90).*

Compound **89** (1 mmol) was dissolved in MeOH (0.5 mL), and a freshly prepared 3M solution of HCl in MeOH was added until the reaction completion was confirmed by thin-layer chromatography (TLC). Subsequently, the solvent was evaporated, H<sub>2</sub>O (20 mL) was added, and the mixture was washed with diethyl ether (2 x 20 mL). The aqueous layer was basified to pH = 11, using a 2M solution of NaOH, and the solution was extracted with CHCl<sub>3</sub> (3 x 20 mL). The combined organic phases were dried over anhydrous Na<sub>2</sub>SO<sub>4</sub>, filtered and evaporated under reduced pressure to obtain **90** (99% yield; m.p. 184-185 °C). <sup>1</sup>H NMR (DMSO, 500 MHz): δ 7.96 (m, 2H), 7.11-6.94 (m, 2H), 3.92-3.85 (m, 3H), 3.74-3.61 (m, 4H), 3.30 (m, 4H), 1.08 (m, 1H). ESI/MS *m/z* 221 [M + H]<sup>+</sup>, 243 [M + Na]<sup>+</sup>.

3.6.5.6. *Synthesis of methyl 4-(4-(3-(2-oxo-3,4-dihydroquinolin-1(2H)-yl)propyl)piperazin-1-yl)benzoate (91).*

Compound **90** (1 mmol) and  $K_2CO_3$  (1.2 mmol) were added to a solution of **68** (1 mmol) in DMF (10 mL) and the reaction mixture was left stirring for 4 hours, at 70 °C. After cooling to room temperature, the mixture was washed with brine (20 mL) and extracted with EtOAc (2 x 20 mL). The organic layer was washed with  $H_2O$  (5 x 30 mL), dried over anhydrous  $Na_2SO_4$ , filtered and evaporated under reduced pressure to obtain a residue which was purified by flash chromatography, using EtOAc/cyclohexane (6:4). A yellow solid was obtained (41% yield, m.p. 93-95 °C).  $^1H$  NMR (DMSO, 500 MHz):  $\delta$  7.92 (d, J = 9.0 Hz, 2H), 7.24 (t, J = 8.5 Hz, 1H), 7.17 (d, J = 7.0 Hz, 1H), 7.09 (d, J = 8.1 Hz, 1H), 7.00 (t, J = 7.4 Hz, 1H), 6.86 (d, J = 9.0 Hz, 2H), 4.05-4.00 (m, 2H), 3.86 (s, 3H), 3.36 (s, 4H), 2.92-2.87 (m, 2H), 2.65 (dd, J = 8.5, 6.3 Hz, 6H), 2.51 (s, 2H), 1.91 (s, 2H). ESI/MS  $m/z$  408  $[M + H]^+$ , 430  $[M + Na]^+$ .

3.6.5.7. *Synthesis of 4-(4-(3-(2-oxo-3,4-dihydroquinolin-1(2H)-yl)propyl)piperazin-1-yl)benzoic acid (92).*

A solution of KOH (13.9 mmol) in  $H_2O$  (0.4 mL) was added dropwise to a solution of **91** (0.42 mmol) in MeOH (7 mL) and the reaction mixture was left stirring for 5 hours, at 75 °C. The solvent was evaporated under reduced pressure and the residue was washed with  $CHCl_3$  (5 x 10 mL) and filtered. The filtrate was evaporated under reduced pressure to obtain **92** (85% yield; m.p.: 146-148 °C).  $^1H$  NMR (DMSO, 500 MHz):  $\delta$  12.42 (s, 1H), 7.80 (s, 2H), 7.25 (d, J = 7.2 Hz, 2H), 7.19 (d, J = 8.1 Hz, 1H), 7.03 (s, 3H), 4.06-3.93 (m,



4H), 3.55 (s, 2H), 3.15 (dd,  $J = 26.2, 14.1$  Hz, 8H), 2.88 (s, 2H), 2.00 (s, 2H). ESI/MS  $m/z$  394 [M + H]<sup>+</sup>, 416 [M + Na]<sup>+</sup>.

3.6.5.8. *Synthesis of tert-butyl (4-((2-(2,6-dioxopiperidin-3-yl)-1-oxoisindolin-4-yl)amino)-4-oxobutyl)carbamate (94).*

This compound was prepared starting from **93** and 4-(Boc-amino)butanoic acid following the procedure described for **28**: a white solid was obtained (87% yield; m.p.: 112-114 °C). <sup>1</sup>H NMR (DMSO, 500 MHz):  $\delta$  11.02 (s, 1H), 9.79 (s, 1H), 7.80 (s, 1H), 7.50 (s, 2H), 6.85 (s, 1H), 5.15 (dd,  $J = 8.9, 4.0$  Hz, 1H), 4.49-4.29 (m, 2H), 2.97 (s, 2H), 2.34 (s, 2H), 2.17-1.95 (m, 6H), 1.37 (s, 9H). ESI/MS  $m/z$  445 [M + H]<sup>+</sup>, 467 [M + Na]<sup>+</sup>. Anal. Calcd (C<sub>22</sub>H<sub>28</sub>N<sub>4</sub>O<sub>6</sub>): C, 59.45%; H, 6.35%; N, 12.61%; O, 21.60%.

3.6.5.9. *Synthesis of tert-butyl (6-((2-(2,6-dioxopiperidin-3-yl)-1-oxoisindolin-4-yl)amino)-6-oxohexyl)carbamate (95).*

This compound was prepared starting from **93** and 6-(Boc-amino)hexanoic acid following the procedure described for **28**: a light-yellow solid was obtained (46% yield; m.p.: 206-207 °C). <sup>1</sup>H NMR (DMSO, 500 MHz):  $\delta$  11.02 (s, 1H), 9.76 (s, 1H), 7.81 (dd,  $J = 7.2, 1.3$  Hz, 1H), 7.53-7.46 (m, 2H), 6.78 (t,  $J = 5.4$  Hz, 1H), 5.14 (s, 1H), 4.36 (q,  $J = 17.5$  Hz, 2H), 2.96-2.87 (m, 3H), 2.61 (d,  $J = 16.9$  Hz, 1H), 2.44-2.28 (m, 3H), 2.02 (m, 1H), 1.64-1.55 (m, 2H), 1.40 (dd,  $J = 14.6, 7.3$  Hz, 2H), 1.36 (s, 9H), 1.27 (dt,  $J = 17.8, 9.4$  Hz, 2H). ESI/MS  $m/z$  473 [M + H]<sup>+</sup>, 495 [M + Na]<sup>+</sup>. Anal. Calcd (C<sub>24</sub>H<sub>32</sub>N<sub>4</sub>O<sub>6</sub>): C, 61.00%; H, 6.83%; N, 11.86%; O, 20.31%.

3.6.5.10. *Synthesis of tert-butyl (8-((2-(2,6-dioxopiperidin-3-yl)-1-oxoisoindolin-4-yl)amino)-8-oxooctyl)carbamate (96).*

This compound was prepared starting from **93** and 8-(Boc-amino)octanoic acid following the procedure described for **28**: a hygroscopic solid was obtained (43% yield). <sup>1</sup>H NMR (DMSO, 500 MHz): δ 11.04 (s, 1H), 9.46 (s, 1H), 7.68 (m, 1H), 7.59-7.50 (m, 2H), 6.78 (t, *J* = 5.0 Hz, 1H), 4.51 (m, 1H), 4.31 (m, 2H), 3.24 (m, 2H), 2.37-2.20 (m, 3H), 2.20-1.91 (m, 3H), 1.67 (m, 2H), 1.51 (m, 2H), 1.44 (s, 9H), 1.28 (m, 6H). ESI/MS *m/z* 501 [M + H]<sup>+</sup>, 523 [M + Na]<sup>+</sup>. Anal. Calcd (C<sub>26</sub>H<sub>36</sub>N<sub>4</sub>O<sub>6</sub>): C, 62.38%; H, 7.25%; N, 11.19%; O, 19.18%.

3.6.5.11. *Synthesis of 4-amino-N-(2-(2,6-dioxopiperidin-3-yl)-1-oxoisoindolin-4-yl)butanamide (97).*

CF<sub>3</sub>COOH (13 mL) was added dropwise to a solution of **94** (1 mmol) in DCM (1.5 mL), and the mixture was left stirring for 2 hours at room temperature. After evaporation of the solvent diethyl ether (10 mL) was added to the residue, and the mixture was filtered to obtain a hygroscopic solid (99% yield). <sup>1</sup>H NMR (DMSO, 500 MHz): δ 11.01 (s, 1H), 9.91 (s, 1H), 7.82 (d, *J* = 7.3 Hz, 1H), 7.74 (s, 2H), 7.54-7.47 (m, 2H), 5.16 (t, *J* = 13.3, 5.1 Hz, 1H), 4.36 (q, *J* = 17.4 Hz, 2H), 2.98-2.62 (m, 4H), 2.42 (d, *J* = 15.5 Hz, 1H), 2.36-2.26 (m, 1H), 2.05-1.93 (m, 2H), 1.87 (dt, *J* = 14.8, 7.3 Hz, 2H). ESI/MS *m/z* 345 [M + H]<sup>+</sup>, 367 [M + Na]<sup>+</sup>. Anal. Calcd (C<sub>17</sub>H<sub>20</sub>N<sub>4</sub>O<sub>4</sub>): C, 59.29%; H, 5.85%; N, 16.27%; O, 18.58%.

3.6.5.12. *Synthesis of 6-amino-N-(2-(2,6-dioxopiperidin-3-yl)-1-oxoisindolin-4-yl)hexanamide (98).*

This compound was prepared starting from **95** following the procedure described for **97**: a white solid was obtained (99% yield; m.p.: 175-177 °C). <sup>1</sup>H NMR (DMSO, 500 MHz): δ 11.04 (s, 1H), 9.81 (s, 1H), 7.83 (d, *J* = 7.2 Hz, 1H), 7.66 (s, 2H), 7.55-7.45 (m, 2H), 5.16 (dd, *J* = 13.3, 5.1 Hz, 1H), 4.37 (q, *J* = 17.4 Hz, 2H), 3.39 (q, *J* = 7.0 Hz, 2H), 2.80 (dd, *J* = 13.7, 6.8 Hz, 2H), 2.45-2.28 (m, 4H), 1.67-1.52 (m, 4H), 1.36 (m, 2H). ESI/MS *m/z* 373 [M + H]<sup>+</sup>, 395 [M + Na]<sup>+</sup>. Anal. Calcd (C<sub>19</sub>H<sub>24</sub>N<sub>4</sub>O<sub>4</sub>): C, 61.28%; H, 6.50%; N, 15.04%; O, 17.18%.

3.6.5.13. *Synthesis of 8-amino-N-(2-(2,6-dioxopiperidin-3-yl)-1-oxoisindolin-4-yl)octanamide (99).*

This compound was prepared starting from **96** following the procedure described for **97**: a hygroscopic solid was obtained (98% yield). <sup>1</sup>H NMR (DMSO, 500 MHz): δ 11.03 (s, 1H), 9.78 (s, 1H), 7.81 (d, *J* = 7.3 Hz, 1H), 7.63 (s, 2H), 7.52-7.45 (m, 2H), 5.15 (dd, *J* = 13.3, 5.1 Hz, 1H), 4.42 – 4.32 (m, 2H), 2.96-2.88 (m, 2H), 2.77 (dd, *J* = 14.1, 6.4 Hz, 2H), 2.39-2.28 (m, 4H), 1.60 (d, *J* = 6.8 Hz, 2H), 1.52 (s, 2H), 1.31 (s, 6H). ESI/MS *m/z* 401 [M + H]<sup>+</sup>, 423 [M + Na]<sup>+</sup>. Anal. Calcd (C<sub>21</sub>H<sub>28</sub>N<sub>4</sub>O<sub>4</sub>): C, 62.98%; H, 7.05%; N, 13.99%; O, 15.98%.

## 4. DOPAMINE D3 RECEPTOR

### 4.1. Background

DRD3 is predominantly expressed in the CNS circuits responsible for emotional and cognitive functions.<sup>93</sup> Since its discovery in 1990,<sup>94</sup> this receptor has been investigated as a potential target for antipsychotics,<sup>93,95</sup> as well as for the treatment of substance use disorder, Parkinson's disease (PD), depression, and restless leg syndrome.<sup>95-98</sup>

For some of these conditions, including substance use disorders, selective DRD3 ligands might represent important pharmacological tools that provide further information towards the DRD3 pathophysiological role and that lack motor side effects associated with DRD2 blockade. In other disorders, such as PD and schizophrenia, D2-like multitarget ligands have demonstrated a therapeutic potential greater than selective agents. Specifically, combining D2-like receptor and serotonin 5-HT<sub>1A</sub>R activation might be favourable in the treatment of PD, in which the 5-HT<sub>1A</sub>R stimulation might attenuate the dyskinetic side effects induced by the activation of D2-like receptors. Instead, the combination of DRD2 and DRD3 antagonism, 5-HT<sub>1A</sub>R agonism, and 5-HT<sub>2A</sub>R antagonism proved to be advantageous in schizophrenia therapy.

A possible route for the improvement of DRD3 affinity could be the development of bitopic ligands, composed of an arylpiperazine as the primary pharmacophore (PP), an alkyl linker and an arylcarboxamide moiety as the secondary pharmacophore (SP), as shown in Figure 22.<sup>99-102</sup>

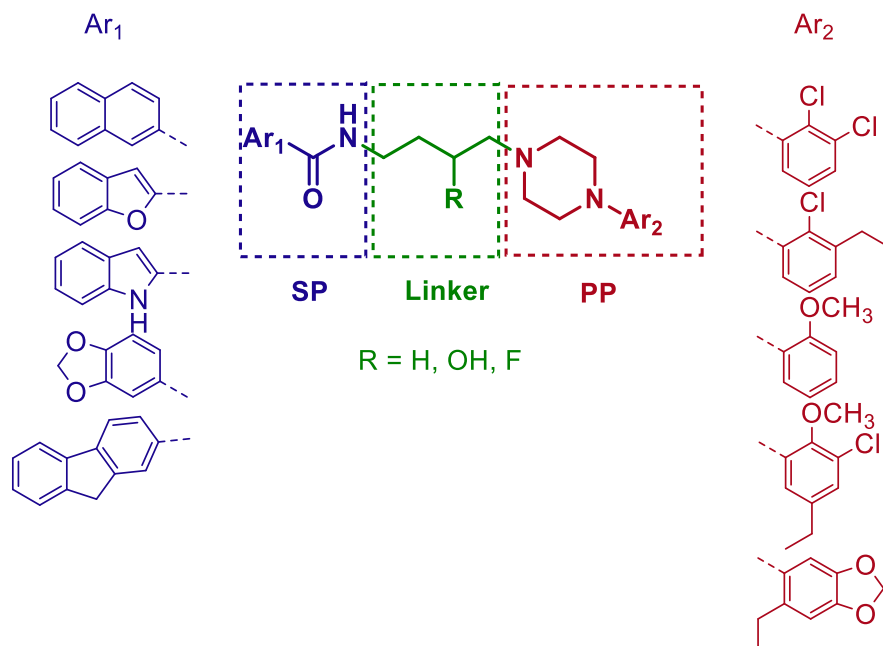


**Figure 22.** The general structure of DRD3 selective bitopic ligands and selected representative primary pharmacophores (PPs; Ar<sub>2</sub>, red) and secondary pharmacophores (SPs; Ar<sub>1</sub>, blue), with linkers (green).

The resolved crystal structure of DRD3 in complex with the DRD2/DRD3-specific antagonist eticlopride has greatly improved the knowledge on the molecular basis of ligand-receptor interactions, providing useful information for the design of novel DRD3 ligands.<sup>59,103</sup> Molecular modelling studies based on this crystal structure demonstrated that the PP recognizes the OBP, and the SP binds into the EBP of DRD3. The substitution/s on the linker portion can affect the binding of the ligands within the pockets.<sup>102</sup>

## 4.2. Introduction and objectives of the work

The medicinal chemistry team with whom I developed my Ph.D. thesis demonstrated that the 1,4-dioxane nucleus could act as a bioversatile carrier of ligands that interact with different receptors, including the D2-like subtypes.<sup>104–114</sup> Specifically, two substituted 1,4-dioxane nucleus-containing compounds have been discovered as promising multitarget agents, one of which was a 5-HT<sub>1A</sub>R/DRD4 agonist and DRD2/DRD3/5-HT<sub>2A</sub>R antagonist (**100**; Figure 23) and the other was a DRD2/DRD3/5-HT<sub>2A</sub>R agonist (**101**; Figure 23). **100** and **101** represented good starting points for the development of novel pharmacological tools in the treatment of schizophrenia and PD, respectively.<sup>104</sup>

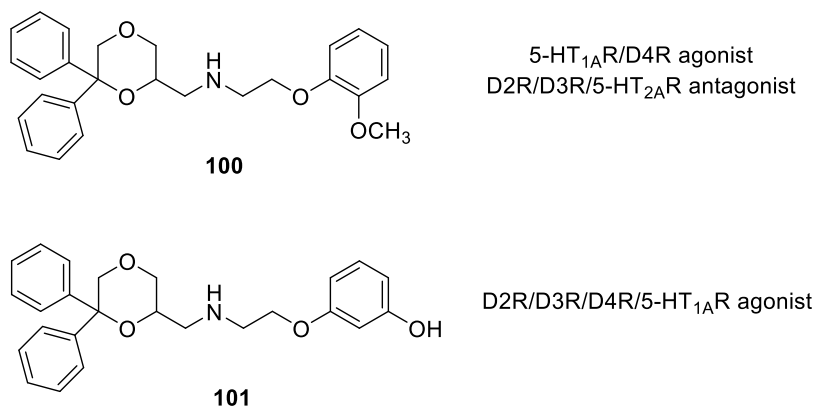


**Figure 23.** Chemical structures of derivatives **100** and **101**, with the description of their multitarget behaviour.

Based on these observations, our objective was to evaluate the role of the substituted 1,4-dioxane as an SP in bitopic DRD3-selective or multitarget compounds for potential use in therapy. Specifically, the compounds were designed with the following pharmacophoric modifications: (i) the *N*-(2,3-dichlorophenyl)piperazine nucleus, which is

common in molecules acting as partial DRD3 agonists and antagonists, as a PP;<sup>102</sup> (ii) an unsubstituted or 3-F/3-OH substituted butyl chain as a linker and (iii) a 5,5-diphenyl-1,4-dioxane-2-carboxamide or a 6,6-diphenyl-1,4-dioxane-2-carboxamide, in case of compounds **31-36**; or a 1,4-benzodioxane-2-carboxamide, in case of compounds **37-39**, as a SP (Figure 24).

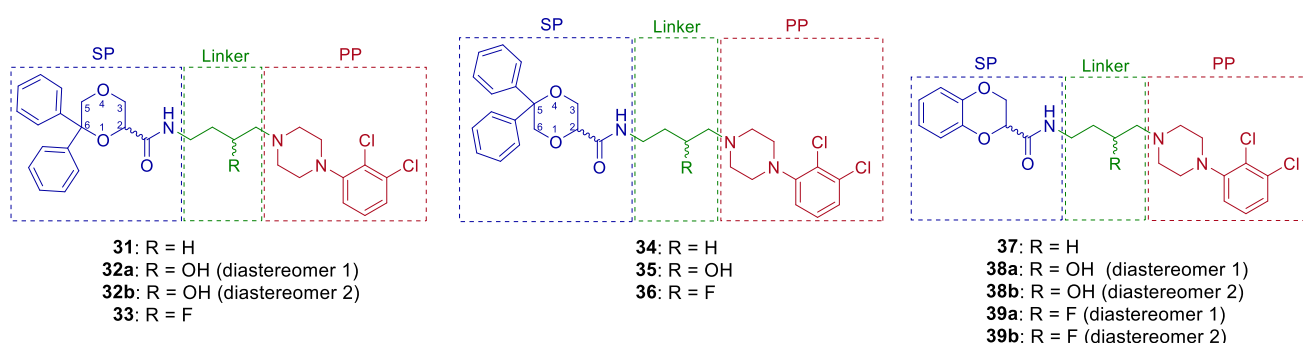


**Figure 24.** Chemical structures of the designed and synthesised compounds **31-39** (SP = secondary pharmacophore, PP = primary pharmacophore).

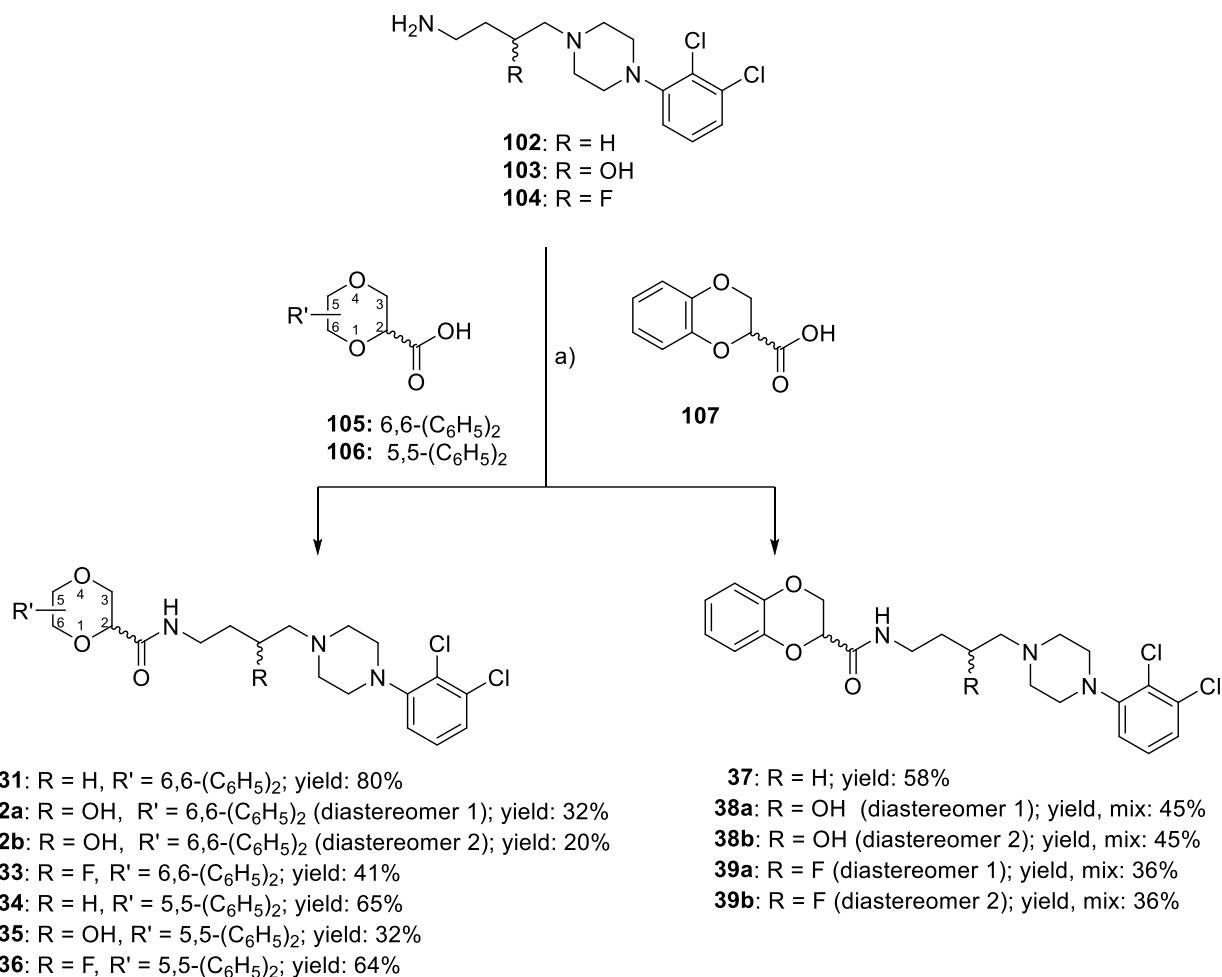
All the synthesised compounds were evaluated for their affinity at human DRD2, DRD3 and DRD4, and the most promising ones were further evaluated in binding assays at other selected targets, such as DRD1, 5-HT<sub>1A</sub>R, 5-HT<sub>2A</sub>R and 5-HT<sub>2C</sub>R as well as in functional assays on those receptors for which they have shown the highest affinity. Most promising compounds underwent molecular modelling studies too, to rationalise their binding profiles.

## 4.3. Results and discussion

### 4.3.1. Synthesis of DRD3 ligands

Compounds **31-39** were synthesised by amidation of either **105**, **106** or the commercially available **107** with the amines **102-104** in the presence of 1,1'-carbonyldiimidazole in THF (Scheme 5). Diastereomers **32**, **38**, and **39** were separated employing different methods. In the case of **32a** and **32b**, separation was performed via flash column chromatography. **38a** and **38b** were separated by fractional crystallization while **39a** and **39b** were separated by preparative TLC, as described in the experimental section. However, all diastereomers showed poor results in biological studies (Table 6), so their relative configuration was not assigned. In the case of **33**, **35** and **36** only one of the two possible diastereomers was obtained.

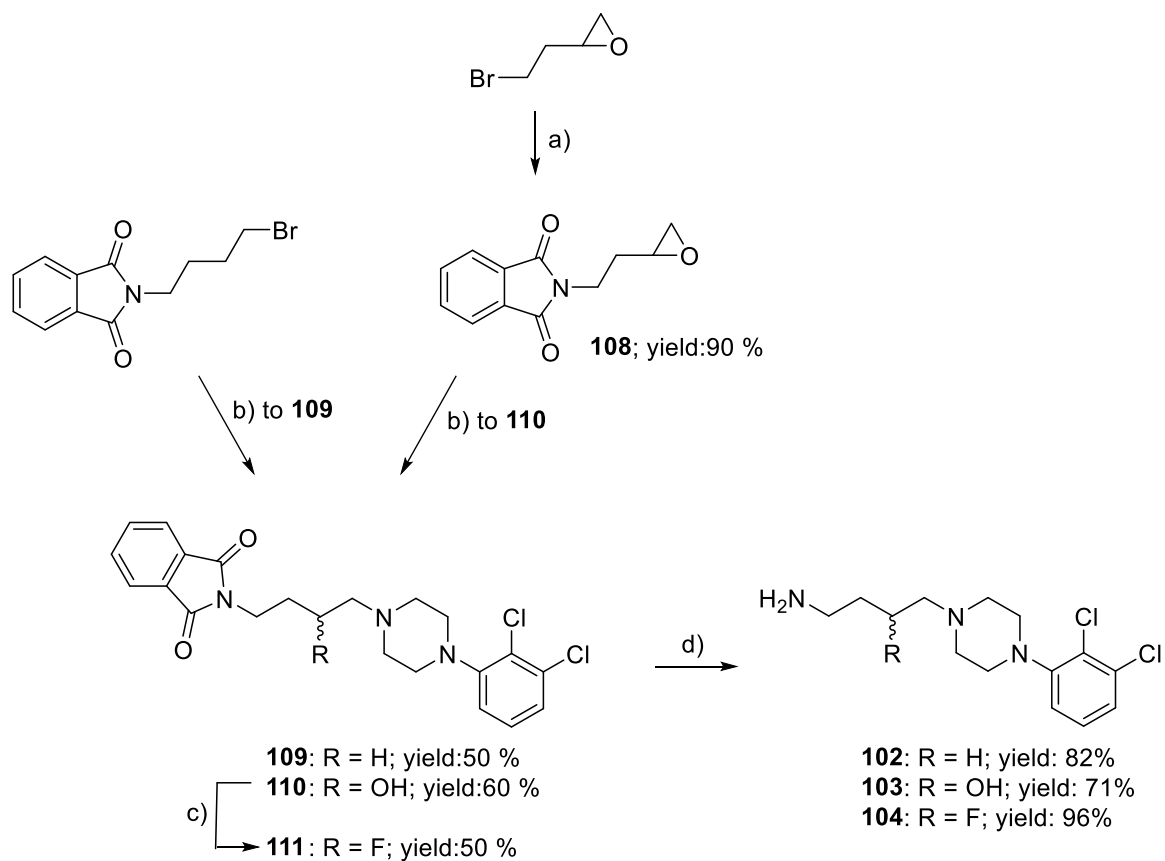




**Scheme 5.** Synthetic routes for compounds **31-39**. Reagents: a) 1,1'-carbonyldiimidazole, THF.

The intermediate amines **102-104** were prepared according to the procedures reported in the literature (Scheme 6).<sup>106,115-117</sup> The commercially available 2-(4-bromobutyl)isoindoline-1,3-dione and compound **108**, obtained by reaction between 2-(2-bromoethyl)oxirane and potassium phthalimide, were treated with the commercially available 1-(2,3-dichlorophenyl)piperazine in K<sub>2</sub>CO<sub>3</sub> to afford the intermediates **109** and **110**, respectively. Treatment of **110** with *N,N*-diethylamino-sulphur trifluoride (DAST) led

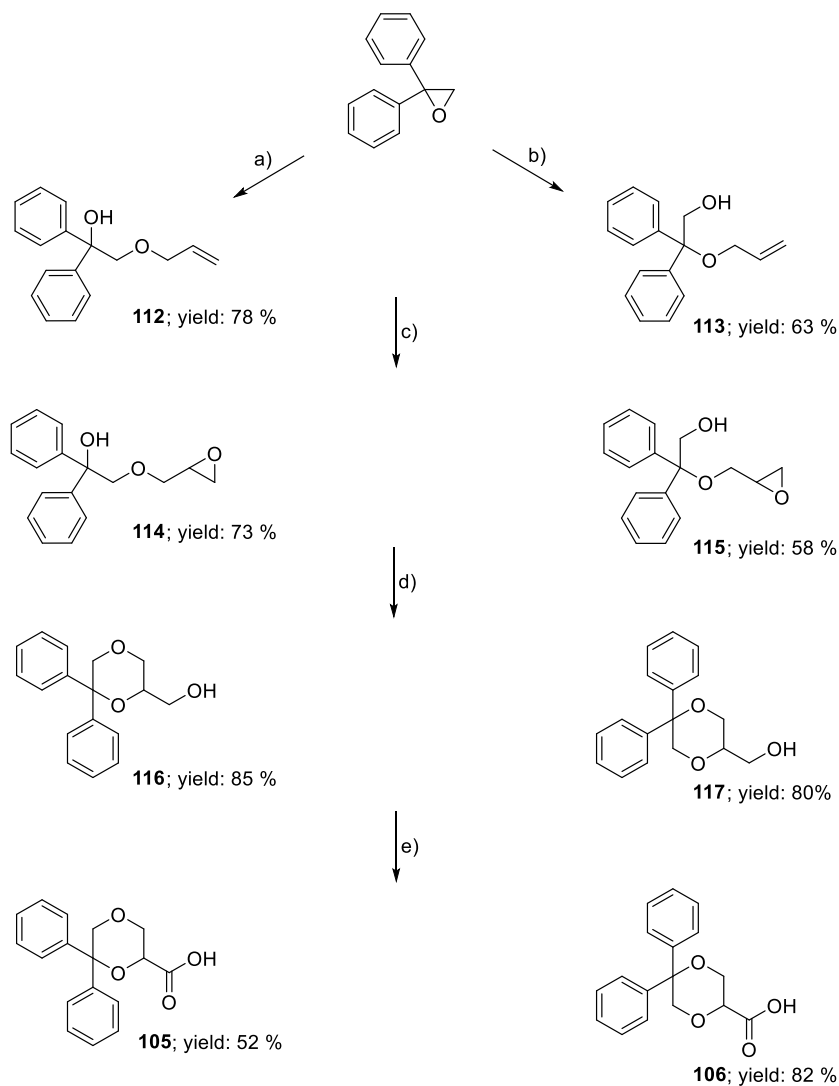
to **111**. Finally, compounds **109-111** were subjected to phthalimide deprotection using hydrazine to give the primary amines **102-104**.



**Scheme 6.** Synthesis of compounds **102-104**. Reagents: a) potassium phthalimide, DMF; b) 1-(2,3-dichlorophenyl)piperazine,  $K_2CO_3$ , DMF; c) DAST, DCM; d) hydrazine, EtOH.

The intermediate carboxylic acids **105** and **106** were prepared as shown in Scheme 7. Epoxidation of the olefines **112** and **113**, obtained by opening the commercially available 2,2-diphenyloxirane with allyl alcohol in basic or acidic conditions, afforded compounds **114** and **115**, respectively. Treatment with (1*S*)-(+)-10-camphorsulfonic acid [(1*S*)-(+)-10-

CSA] in DCM led to alcohols **116** and **117**, which were subjected to oxidation with  $\text{KMnO}_4$  to give the desired carboxylic acids **105** and **106**, respectively.



**Scheme 7.** Synthesis of compounds **105** and **106**. Reagents: a) Na, allyl alcohol; b)  $\text{HClO}_4$ , allyl alcohol; c) *m*-chloroperbenzoic acid (*m*-CPBA), DCM; d) (1*S*)-(+)-10-CSA, DCM; e)  $\text{KMnO}_4$ , 1M KOH.

#### **4.3.2. Radioligand binding assays**

The novel hybrids **31-39** were tested at human DRD2, DRD3, or DRD4 stably expressed in HEK293 cells by competition binding assays, using [<sup>3</sup>H]*N*-methylspiperone as a radioligand.<sup>118</sup>

The  $K_i$  values are shown in Table 9 along with those of the previously reported compounds **100** and **101**.

**Table 9.** Affinity values ( $K_i$ )<sup>a</sup> of compounds **31–39**, **100** and **101** at human D2-like receptor subtypes and of **31**, **34**, **37**, **100**, **101** at human DRD1, 5-HT<sub>1A</sub>R, 5-HT<sub>2A</sub>R and 5-HT<sub>2C</sub>R.

Compound	$K_i \pm \text{SEM}$ (nM), human cloned receptors								
	DRD1	DRD2	DRD3	DRD4	D2/D3	D4/D3	5-HT <sub>1A</sub> R	5-HT <sub>2A</sub> R	5-HT <sub>2C</sub> R
<b>100</b>	22.9 ± 3.1 <sup>b</sup>	12.2 ± 1.5 <sup>b</sup>	13.1 ± 1.7 <sup>b</sup>	8.34 ± 0.6 <sup>b</sup>	0.9	0.6	0.66 ± 0.02 <sup>b</sup>	52.5 ± 4.4 <sup>b</sup>	1819 ± 165 <sup>b</sup>
<b>101</b>	123 ± 11 <sup>b</sup>	3.16 ± 1.0 <sup>b</sup>	1.38 ± 0.07 <sup>b</sup>	10.5 ± 0.1 <sup>b</sup>	2	8	1.15 ± 0.03 <sup>b</sup>	1412 ± 224 <sup>b</sup>	9772 ± 501 <sup>b</sup>
<b>31</b>	442 ± 52	342 ± 105	2.39 ± 0.69	1352 ± 449	143	566	288 ± 15	257 ± 38	642 ± 80
<b>32a</b>	ND <sup>d</sup>	39.5% <sup>c</sup>	164 ± 52	39.2% <sup>c</sup>	ND <sup>d</sup>	ND <sup>d</sup>	ND <sup>d</sup>	ND <sup>d</sup>	ND <sup>d</sup>
<b>32b</b>	ND <sup>d</sup>	41% <sup>c</sup>	77.1 ± 25.5	54.4% <sup>c</sup>	ND <sup>d</sup>	ND <sup>d</sup>	ND <sup>d</sup>	ND <sup>d</sup>	ND <sup>d</sup>
<b>33</b>	ND <sup>d</sup>	21.2% <sup>c</sup>	716 ± 178	19.1% <sup>c</sup>	ND <sup>d</sup>	ND <sup>d</sup>	ND <sup>d</sup>	ND <sup>d</sup>	ND <sup>d</sup>
<b>34</b>	700 ± 150	28.7 ± 5.4	1.58 ± 0.24	54.6 ± 7.3	18	35	9.1 ± 0.97	28 ± 6.0	90 ± 16
<b>35</b>	ND <sup>d</sup>	526 ± 28.2	23.4 ± 3.1	390 ± 46	23	17	ND <sup>d</sup>	ND <sup>d</sup>	ND <sup>d</sup>
<b>36</b>	ND <sup>d</sup>	1200 ± 210	295 ± 100	43.6% <sup>c</sup>	4	ND <sup>d</sup>	ND <sup>d</sup>	ND <sup>d</sup>	ND <sup>d</sup>
<b>37</b>	680 ± 160	46.4 ± 5.9	2.16 ± 0.63	74.7 ± 24.5	22	35	23.8 ± 5.2	62 ± 15	97 ± 25
<b>38a</b>	ND <sup>d</sup>	1097 ± 125	44.1 ± 8.2	282 ± 76	25	6	ND <sup>d</sup>	ND <sup>d</sup>	ND <sup>d</sup>
<b>38b</b>	ND <sup>d</sup>	783 ± 19	23.4 ± 2.4	244 ± 54	35	10	ND <sup>d</sup>	ND <sup>d</sup>	ND <sup>d</sup>
<b>39a</b>	ND <sup>d</sup>	10.6% <sup>c</sup>	54.8% <sup>c</sup>	29.4% <sup>c</sup>	ND <sup>d</sup>	ND <sup>d</sup>	ND <sup>d</sup>	ND <sup>d</sup>	ND <sup>d</sup>
<b>39b</b>	ND <sup>d</sup>	8.7% <sup>c</sup>	65.4% <sup>c</sup>	26.6% <sup>c</sup>	ND <sup>d</sup>	ND <sup>d</sup>	ND <sup>d</sup>	ND <sup>d</sup>	ND <sup>d</sup>

<sup>a</sup> $K_i$  values were determined by competitive inhibition of [<sup>3</sup>H]SCH23390 binding in mouse fibroblast cells stably expressing hDRD1; [<sup>3</sup>H]N-methylspiperone binding in HEK 293 cells stably expressing human DRD2, DRD3, or DRD4; [<sup>3</sup>H]8-OH-DPAT binding in HeLa cells stably expressing human 5-HT<sub>1A</sub>R; and [<sup>125</sup>I]DOI binding in HEK cells stably expressing 5-HT<sub>2A</sub>R or 5-HT<sub>2C</sub>R. <sup>b</sup>Taken from reference <sup>104</sup>. <sup>c</sup>For low-affinity compounds, only the inhibition percentage of the radioligand binding at a test compound concentration of 10 μM is given. DRD1, 5-HT<sub>1A</sub>R, 5-HT<sub>2A</sub>R and 5-HT<sub>2C</sub>R-related data was obtained through the NIDA Addiction Treatment Discovery Program contract with Oregon Health & Science University. <sup>d</sup>ND = Not Determined.

The results revealed that all compounds showed higher DRD3 affinities with respect to DRD2 and DRD4. The nature of the linker plays an important role in D2-like receptor binding and selectivity. Specifically, compounds bearing an unsubstituted butyl chain as a linker (**31**, **34** and **37**) possessed the highest D2-like receptor affinities. The insertion of a hydroxyl group (**32**, **35** and **38**) and even more of a fluorine atom (**33**, **36** and **39**) in position 3 of the linker proved to be detrimental for the binding of the compounds to DRD2, DRD3 and DRD4. The differences between the  $K_i$  values of diastereomers **32a** and **32b**; **38a** and **38b**; as well as **39a** and **39b** were not significant, suggesting that the relative configuration between the stereocenters in the butyl chain and in position 2 of the 1,4-dioxane nucleus doesn't play a crucial role in receptor interaction.

The nature of the SP also affects the DRD3 selectivity profiles of the ligands. Compound **31**, containing the 6,6-diphenyl-1,4-dioxane scaffold, showed the best DRD3 selectivity profile over DRD2 and DRD4 ( $D2/D3 = 143$ ;  $D4/D3 = 566$ ) compared to the 5,5-diphenyl-1,4-dioxane and the 1,4-benzodioxane derivatives **32** ( $D2/D3 = 18$  and  $D4/D3 = 35$ ) and **33** ( $D2/D3 = 22$  and  $D4/D3 = 35$ ), respectively. Compared to the already published 6,6-diphenyl-1,4-dioxane multitarget compounds **100** and **101**, the hybrid derivative **31** maintained high affinity only for DRD3, gaining in DRD3 subtype selectivity.

The most promising hybrids **31**, **34** and **37** were additionally evaluated for their binding affinity to DRD1, on mouse fibroblast cells, using [ $^3H$ ]SCH23390 as a radioligand, to 5-HT $_{1A}$ R and 5-HT $_{2A}$ R on HeLa cells, using [ $^3H$ ]8-OH-DPAT as a radioligand; as well as to 5-HT $_{2C}$ R receptor on HEK cells, using [ $^{125}I$ ]DOI as a radioligand (Table 9).

Interestingly, **31** displayed high DRD3 selectivity over DRD1 ( $D1/D3 = 185$ ), DRD2 ( $D2/D3 = 143$ ), DRD4 ( $D4/D3 = 566$ ), 5-HT $_{1A}$ R ( $5-HT_{1A}/D3 = 121$ ), 5-HT $_{2A}$ R ( $5-HT_{2A}/D3 =$

108) and 5-HT<sub>2C</sub>R (5-HT<sub>2C</sub>/D3 = 269). Conversely, **34** and **37** showed very low DRD1 affinities, but their K<sub>i</sub> values at all serotonergic receptors were significantly lower, indicating a favourable multitarget profile between serotonergic and dopaminergic receptors.

#### **4.3.3. Functional assays**

*In vitro* functional assays were performed for compounds **31**, **34** and **37** at all receptors at which they showed K<sub>i</sub> values < 500 nM.<sup>118</sup> The results, obtained through the NIDA Addiction Treatment Discovery Program contract with Oregon Health & Science University, are reported in Table 10 and confirm the DRD3-preferential profile of **31**, which behaves as a partial agonist (EC<sub>50</sub> = 9.8 nM), with 36% efficacy in agonist mode. When tested as an antagonist, **31** showed an IC<sub>50</sub> value of 38 nM with 82.7 % inhibition rate. Additionally, it acted as a 5-HT<sub>1A</sub>R full agonist and showed low potency at DRD1 and 5-HT<sub>2A</sub>R.

The results also highlighted the interesting multitarget behaviour of **34** and **37**, which were characterized by similar functional profiles at all the studied receptors: they both were efficacious DRD2 and 5-HT<sub>2A</sub>R antagonists with high and low potency, respectively, efficacious 5-HT<sub>1A</sub>R and DRD4 agonists with high potency, as well as DRD3 and 5-HT<sub>2C</sub>R partial agonists with high and low potency, respectively. Moreover, when tested as DRD3 antagonists, **34** and **37** showed IC<sub>50</sub> values of 6.6 nM with 64.0% efficacy and 40.4 nM with 64.2% efficacy, respectively.

**Table 10.** Potency expressed as EC<sub>50</sub> or IC<sub>50</sub><sup>a</sup> and efficacy (% of stimulation or inhibition)<sup>b</sup> values of **31**, **34**, and **37** at DRD1-DRD4, 5-HT<sub>1A</sub>R, 5-HT<sub>2A</sub>R and 5-HT<sub>2C</sub>R.

Receptor	Functional profile of 31		Functional profile of 34		Functional profile of 37	
	EC <sub>50</sub> , nM (IC <sub>50</sub> , nM)	% stim. (% inhib.)	EC <sub>50</sub> , nM (IC <sub>50</sub> , nM)	% stim. (% inhib.)	EC <sub>50</sub> , nM (IC <sub>50</sub> , nM)	% stim. (% inhib.)
<b>DRD1 cAMP assay</b>	(> 10.000)	ND <sup>c</sup>	ND <sup>c</sup>	ND <sup>c</sup>	ND <sup>c</sup>	ND <sup>c</sup>
<b>DRD2 mitogenesis assay</b>	(139.2 ± 5.9)	(93.5)	(8.5 ± 1.3)	(95.2)	(40.0 ± 7.2)	(94.4)
<b>DRD3 mitogenesis assay</b>	9.8 ± 1.6	36.0	2.72	25.7	5.0 ± 1.7	34.0
<b>DRD4 adenylate cyclase</b>	ND <sup>c</sup>	ND <sup>c</sup>	21.7 ± 8.4	76.7	15.3 ± 1.9	73.1
<b>5-HT<sub>1A</sub>R [<sup>35</sup>S]GTPγS binding</b>	232 ± 19	82.7	23.9 ± 8.8	90.8	22.7 ± 0.82	96.3
<b>5-HT<sub>2A</sub>R IP-1 formation</b>	(7900 ± 9.8)	(45.4)	(650 ± 100)	(88.6)	(612 ± 58)	(86.8)
<b>5-HT<sub>2C</sub>R IP-1 formation</b>	ND <sup>c</sup>	ND <sup>c</sup>	380 ± 130	33	750 ± 280	37

<sup>a</sup>EC<sub>50</sub> or IC<sub>50</sub> values were from three experiments and data are presented as means ± SEM. <sup>b</sup>The standard agonists SKF-38393 (DRD1), quinpirole (D2-like subtypes), and serotonin (5-HT<sub>1A</sub>R, 5-HT<sub>2A</sub>R, and 5-HT<sub>2C</sub>R) were used to determine the % of stimulation; the standard antagonists SCH23390 (DRD1), (+)-butaclamol (DRD2), NGB 2904 (DRD3), haloperidol (DRD4), WAY 100,635 (5-HT<sub>1A</sub>R), ketanserin (5-HT<sub>2A</sub>R), and SB242084 (5-HT<sub>2C</sub>R) were used to determine the % of inhibition. <sup>c</sup>ND = not determined.

This multitarget behaviour is interesting because it was earlier demonstrated that the DRD2/DRD3 partial agonism or antagonism, in combination with 5-HT<sub>1A</sub>R agonism and 5-HT<sub>2A</sub>R antagonism, could reduce schizophrenia-induced cognitive impairment.<sup>119,120</sup> Additionally, the activation of DRD4 could contribute to the improvement of schizophrenia-



induced cognitive impairment;<sup>121</sup> and the partial activation of 5-HT<sub>2c</sub>R could also contribute to the antipsychotic activity of **34** and **37**.<sup>122</sup>

#### **4.3.4. Molecular modelling studies**

Docking simulations were conducted on the resolved DRD3 structure in complex with eticlopride (PDB code: 3PBL) to evaluate the main interactions stabilizing the computed complexes and to rationalize the observed differences in ligand affinity.<sup>118</sup> The computed complexes of compounds **31** and **37** also underwent 200 ns MD simulations to assess their stability and to investigate the resulting behaviour of the human DRD3 structure. Figures 25 and 26 display the overall putative complexes and the main stabilizing interactions for **31** (Figures 25A and 26A) and **37** (Figures 25B and 26B) as derived by the most representative cluster from MD runs. The reported complexes reveal that the dichlorophenylpiperazine moiety of **31** and **37** assumes comparable poses stabilized by similar key interactions. In detail, the ligand ammonium head elicits an ion-pair with D.3.32 (Asp110) further stabilized by the H-bond with Y7.43 (Tyr373). The 2,3-dichlorophenyl ring is engaged in  $\pi$ - $\pi$  stacking interactions with F6.51 (Phe345) and F.6.52 (Phe346), while the chlorine atoms can be involved in halogen bonds with S5.42 (Ser192), S5.42 (Ser193) and H6.55 (His349). C3.36 (Cys114) can also participate in this set of contacts through a  $\pi$ -S interaction. While showing a greater variability, the diphenyl-dioxane moiety in **31**, as well as the benzodioxane ring in **37**, are harboured within the same subpocket where they mostly stabilize hydrophobic contacts. In detail, they elicit similar  $\pi$ - $\pi$  stacking interactions with Y7.35 (Tyr365) plus hydrophobic contacts with surrounding

apolar side chains. The dioxane oxygen and the amide linker are engaged in weak H-bonds with Y7.35 (Tyr365), S7.36 (Ser366) and S7.39 (Thr369).

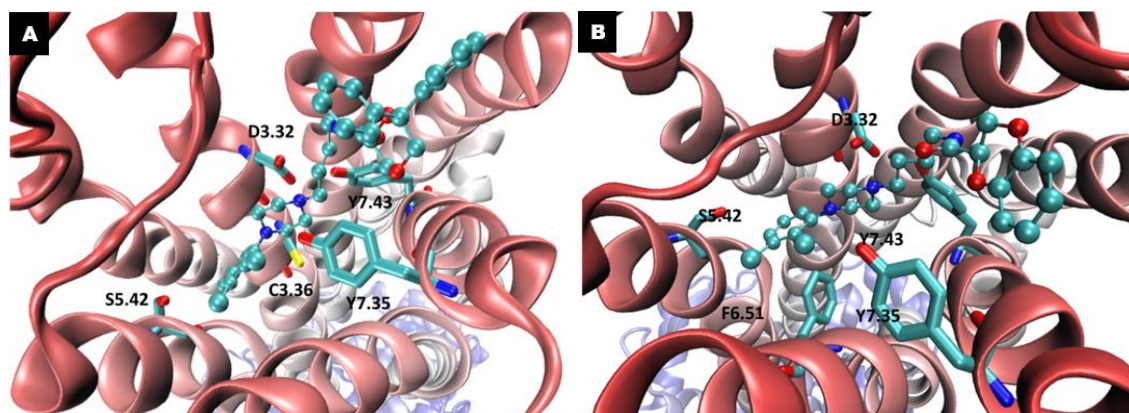


**Figure 25.** Key interactions stabilizing the putative complexes of DRD3 and (A) **31** or (B) **37**, within the DRD3 binding site. (A) D3.32 = Asp110; C3.36 = Cys114; S5.42 = Ser192; Y7.35 = Tyr365; Y7.43 = Tyr373. (B) D3.32 = Asp110; S5.42 = Ser192; F6.51 = Phe345; Y7.35 = Tyr365; Y7.43 = Tyr373.

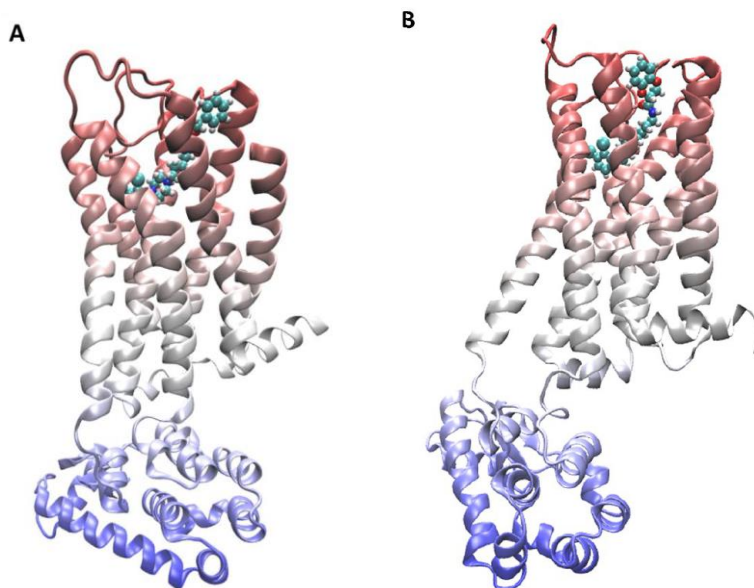


**Figure 26.** Cartoon depiction of the computed DRD3 complexed with **31** (A) and **37** (B). The backbone is coloured by the Y axis (red = extracellular part of the protein; blue = intracellular part of the protein; white = portion of the protein within the membrane). The ligand is coloured by heteroatoms.

Figure 27A analyses the stability of these poses as assessed by the RMSD values computed for the ligand's atoms only. The obtained rmsd profile suggests the occurrence of two possible binding modes which differ by about 2.0 Å. A visual analysis of the two corresponding complexes reveals that the differences between the two poses are focused on the arrangement of the diphenyldioxane moiety in **31** and benzodioxane ring in **37**, while the dichlorophenylpiperazine moiety of both ligands retains significant stability during the MD simulations. Such a behaviour is explainable by considering that these mobile moieties are engaged by weak interactions and thus are free to move to optimize the H-bonds stabilized by the amide linker and dioxane ring. Figure 27B shows that **31** assumes almost exclusively a binding mode which is that displayed in Figure 25 and is slightly shifted compared to that derived from docking simulations, while **37** exhibits an up-and-down profile with the starting pose being largely predominant.

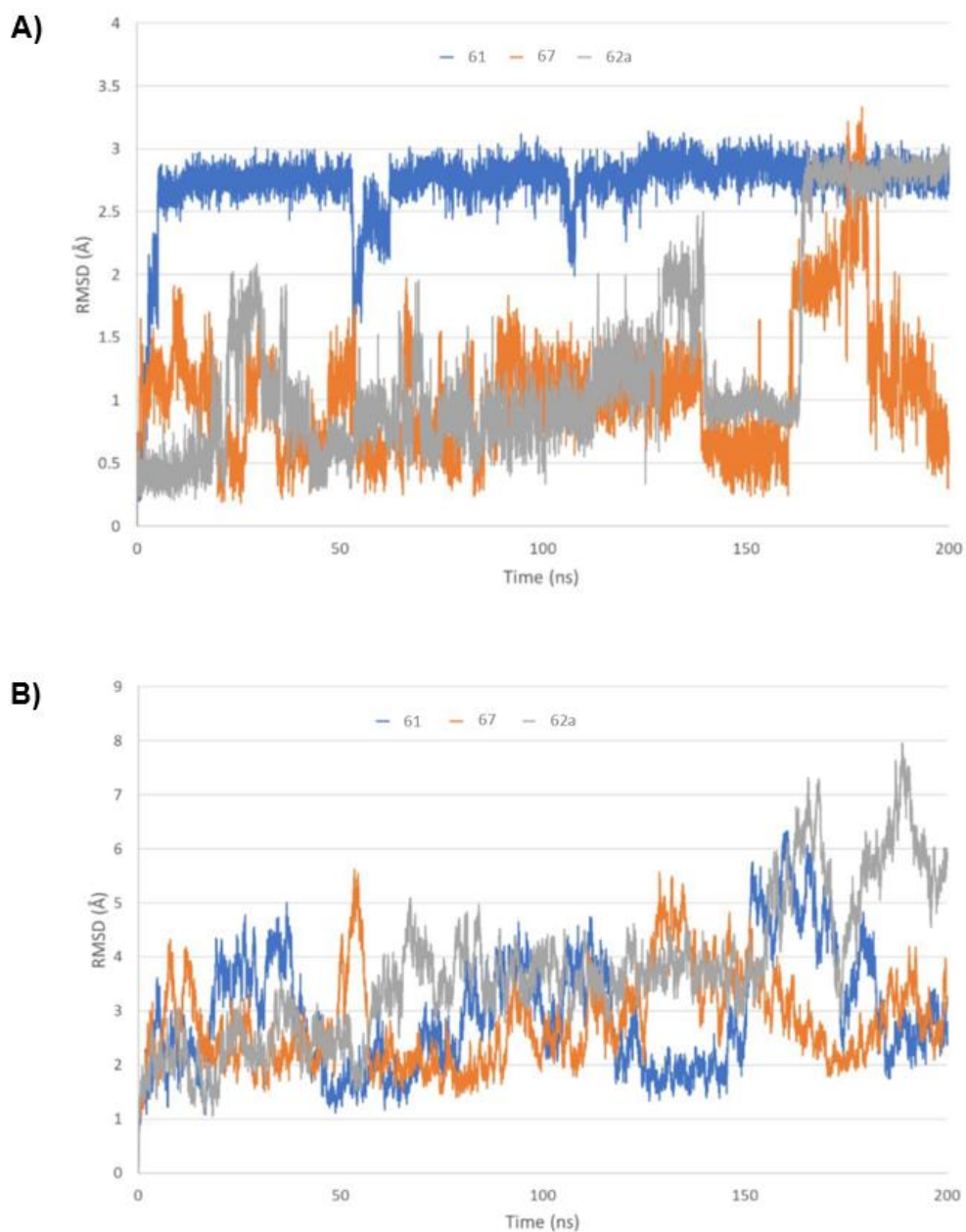


**Figure 27.** RMSD profiles shown as derived from the molecular dynamics runs for complexes of DRD3 and **31** (blue), **37** (orange) or **32a** (grey), computed for only the atoms of the ligand (A) or DRD3 backbone atoms (B).

Figure 27B focuses on the RMSD profiles as computed for the backbone atoms of the human DRD3 and evidences substantial stability with RMSD values almost always lower than 6.0 Å. The complex with **31** reveals a slightly greater mobility than that with **37** which can be ascribed to its greater steric hindrance. Collectively, the overall stability of both ligands and the receptor offers an encouraging confirmation of the reliability of the complexes shown in Figure 25.

Taken together, the reported computational results can explain why diphenyl-dioxane and benzodioxane analogues show similar affinity profiles. Indeed, these ligands stabilize an almost identical pattern of interactions with marginal differences involving the variable portion that however seems to be not so crucial for affinity, while having a key role in determining the observed selectivity profile. The DRD3 selectivity of these ligands can be explained by considering the different wideness of the more external sub-pocket that accommodates the diphenyl-dioxane moiety. To verify this hypothesis, docking simulations were repeated for **31** on the resolved structure of the DRD4 in complex with nemonapride (PDB Id: 5WIV) by applying the same computational procedure based on the PLANTS program. In this case, the ligand is unable to assume acceptable poses in which the ammonium head contacts with D3.32 (Asp115). To further confirm the role of the pocket size in determining the selectivity of the simulated ligands, the void volume of the two binding sites was computed by using FPocket as implemented by the VEGA suite of programs and DRD3 shows a larger pocket than DRD4 (5043 vs. 4494 Å<sup>3</sup>).

Docking results indicate that fluorine and hydroxyl derivatives can stabilize comparable sets of contacts. This finding is highly expected for the fluorine substitution since a marginal structural modification cannot have such a detrimental effect on the interaction

capability of the resulting ligands. Similar considerations can be drawn for the hydroxyl analogues since the putative complexes do not reveal any detrimental roles of the hydroxyl function that can take part in the contacts stabilized by the ammonium head. Hence, docking results suggest that the negative effect played by these linker substitutions should not be ascribed to their interfering role on the interaction patterns with the DRD3.

A possible explanation for the observed detrimental impact of these substitutions can be found in their effect on the basicity of the piperazine ring. An estimation of the effect of the fluorine atom on the basicity can be derived by combining the available experimental  $pK_a$  value for aripiprazole which is equal to 7.6 in 20% aqueous ethanol<sup>123</sup> with the average effect of the H/F exchange in  $\beta$  position to an amino group which decreases its basicity of around 2.0  $pK_a$  unit.<sup>124</sup>

A similar (albeit less pronounced) effect is also exerted by the hydroxyl function, which decreases the basicity of the vicinal amino groups due to the residual electronic delocalization from N to O atoms through the linking methylene groups.<sup>125</sup> For  $\beta$  hydroxyl functions, this effect is estimated to be equal to -1.0 in the corresponding  $pK_a$  values. Hence, fluorine and hydroxyl groups have a similar effect in decreasing the basicity of the ammonium head. In both cases, the resulting  $pK_a$  value should be less than 7.0 and this means that for these derivatives the protonated form (which is involved in receptor recognition) is no longer the most probable state at physiological pH. As detailed above, such an effect is more marked for fluorine derivatives for which the predicted  $pK_a$  value should range around 5.5, thus indicating that the protonated state is virtually absent at physiological pH. The predicted value for the hydroxyl derivatives should be around 6.5,

thus suggesting that the protonated state should represent about 10-15%. Notably, the different abundances of the protonated forms for the fluorine and hydroxyl analogues are in agreement with the measured affinity values.

To further confirm this hypothesis, the computed complex for **32a** underwent MD run with the same characteristics as described for **31** and **37**. Figure 27 also reports the RMSD profiles for the hydroxyl derivative (**32a**) and reveals remarkable stability of the corresponding complex. As described for the previous ligands, **32a** also shows two possible binding modes even though the starting pose appears here as the more frequent one, probably due to the stabilizing effect exerted by the hydroxyl group. Altogether, the performed simulations are not indicative of detrimental effects played by the hydroxyl function and a similar consideration can be also extended to the fluorine atom and indirectly suggests that the drop in affinity of these derivatives should be explained by considering factors that go beyond their interacting capacity with the human DRD3.

#### 4.4. Conclusions

Under this research, our goal was to evaluate the therapeutic potential of the ligands containing 1,4-dioxane nucleus as an SP in bitopic DRD3-selective or multitarget compounds. This nucleus has been chosen due to its ability to act as a bioversatile carrier of D2-like receptor ligands.

DRD3 ligands, containing the *N*-(2,3-dichlorophenyl)piperazine nucleus as a PP; an unsubstituted or 3-F/3-OH substituted butyl chain as a linker and a 5,5-diphenyl-1,4-

dioxane-2-carboxamide or a 6,6-diphenyl-1,4-dioxane-2-carboxamide as an SP, were synthesised and studied.

The biological assays highlighted that derivatives **31**, **34** and **37**, characterized by an unsubstituted butyl chain between the pharmacophores, showed the highest overall DRD3 affinity. In particular, the 6,6-diphenyl-1,4-dioxane compound **31** showed a DRD3-preferential profile, behaving as a partial agonist with 36% efficacy. An interesting multitarget behaviour was highlighted for compounds **34** and **37**, both displaying potent DRD2 antagonism, 5-HT<sub>1A</sub>R and DRD4 agonism, as well as potent DRD3 partial agonism. They also behaved as low-potency 5-HT<sub>2C</sub>R partial agonists and 5-HT<sub>2A</sub>R antagonists. According to the literature, this profile might be a promising starting point for the discovery of novel agents useful for the treatment of schizophrenia. Molecular modelling results rationalized the biological results, highlighting that the drop in the affinity of 3-OH and especially 3-F derivatives should be explained by considering factors that go beyond their interacting capacity with the human DRD3. The detrimental impact of these substitutions can be found in their effect on the basicity of the piperazine ring.

## 4.5. Experimental section

### 4.5.1. Synthesis of DRD3 ligands

#### 4.5.1.1. *Synthesis of N-(4-(4-(2,3-dichlorophenyl)piperazin-1-yl)butyl)-6,6-diphenyl-1,4-dioxane-2-carboxamide (31).*

1,1'-Carbonyldiimidazole (0.18 g; 1.10 mmol) was added to a solution of **105** (0.30 g; 1.10 mmol) in THF (10 mL). The reaction was stirred at room temperature for 2 hours. Amine



**102** (0.33 g; 1.10 mmol) was added dropwise to the cooled solution (0 °C). The reaction was allowed to warm to room temperature and, then, was stirred for 3 hours. The solvent was removed under vacuum and the residue was diluted in CHCl<sub>3</sub> and washed with NaHCO<sub>3</sub>-saturated aqueous solution. The organic phase was dried over anhydrous Na<sub>2</sub>SO<sub>4</sub>, filtered and concentrated under vacuum. The crude compound was purified by column chromatography eluting with EtOAc/CHCl<sub>3</sub> (5:5) to afford compound **31** as an oil in 80% yield. <sup>1</sup>H NMR (400 MHz, CDCl<sub>3</sub>): δ 7.66-6.85 (m, 13H), 4.63 (d, *J*=32.49 Hz, 1H), 4.18 (dd, *J*=9.74, 9.75 Hz, 1H), 3.79 (d, *J*=12.07 Hz, 1H), 3.62-3.43 (m, 2H), 3.04 (m, 5H), 2.65-2.39 (m, 8H), 1.63 (m, 2H), 1.51 (m, 2H). <sup>13</sup>C NMR (100 MHz, CDCl<sub>3</sub>): δ 172.71, 150.11, 139.62, 133.34, 128.18, 127.18, 126.26, 123.98, 117.64, 90.21, 85.10, 84.23, 74.91, 51.83, 51.33, 40.90, 39.25, 27.73, 25.40. The free base was transformed into the corresponding oxalate salt, which was crystallized from 2-PrOH (m.p. 107-108 °C). Anal. calcd for C<sub>31</sub>H<sub>35</sub>Cl<sub>2</sub>N<sub>3</sub>O<sub>3</sub>·C<sub>2</sub>H<sub>2</sub>O<sub>4</sub>: C, 60.19%, H, 5.66%, N, 6.38%. Found: C, 60.34%, H, 5.51%, N, 6.52%.

4.5.1.2. *Synthesis of N-(4-(4-(2,3-dichlorophenyl)piperazin-1-yl)-3-hydroxybutyl)-6,6-diphenyl-1,4-dioxane-2-carboxamide (32a, 32b).*

These compounds were prepared following the procedure described for compound **31**, starting from **103** and **105**. The crude mixture of diastereomers was purified by column chromatography eluting with EtOAc/MeOH (99:1). The diastereomer **32a** eluted first as an oil in a 32% yield. <sup>1</sup>H NMR (400 MHz, CDCl<sub>3</sub>): δ 7.71-6.95 (m, 13H), 4.61 (d, *J*=12.50 Hz, 1H), 4.20 (m, 1H), 3.95-3.25 (m, 4H), 3.10 (m, 7H), 2.85 (m, 2H), 2.62 (m, 3H), 2.48 (m, 2H), 1.79-1.60 (m, 2H). The free base was transformed into the corresponding oxalate

salt, which was crystallized from 2-PrOH (m.p. 146-147 °C).  $^{13}\text{C}$  NMR (100 MHz, DMSO):  $\delta$  162.71, 150.01, 140.62, 133.34, 129.22, 128.18, 127.18, 126.22, 121.98, 117.64, 93.12, 86.62, 83.23, 71.91, 69.13, 61.68, 56.06, 51.15, 45.48, 36.43. Anal. calcd for  $\text{C}_{31}\text{H}_{35}\text{Cl}_2\text{N}_3\text{O}_4 \cdot \text{C}_2\text{H}_2\text{O}_4$ : C, 58.76%, H, 5.53%, N, 6.23%. Found: C, 58.49%, H, 5.59%, N, 6.11%.

The second fraction was the diastereomer **32b** as an oil in a 20% yield.  $^1\text{H}$  NMR (400 MHz,  $\text{CDCl}_3$ ):  $\delta$  7.49-6.95 (m, 13H), 4.66 (d,  $J = 12.12$  Hz, 1H), 4.24 (m, 1H), 4.09 (dd,  $J = 2.74, 3.51$  Hz), 3.79 (d,  $J = 12.50$  Hz, 1H), 3.48 (m, 2H), 3.08 (m, 8H), 2.81 (m, 2H), 2.58 (m, 2H), 2.39 (m, 2H), 1.63-1.51 (m, 2H). The free base was transformed into the corresponding oxalate salt, which was crystallized from 2-PrOH (m.p. 122-123 °C).  $^{13}\text{C}$  NMR (100 MHz, DMSO):  $\delta$  172.71, 150.11, 139.62, 133.34, 129.25, 128.18, 127.18, 126.22, 123.98, 117.64, 93.12, 86.62, 83.23, 75.91, 69.13, 61.48, 56.08, 51.12, 45.58, 36.38. Anal. calcd for  $\text{C}_{31}\text{H}_{35}\text{Cl}_2\text{N}_3\text{O}_4 \cdot \text{C}_2\text{H}_2\text{O}_4$ : C, 58.76%, H, 5.53%, N, 6.23%. Found: C, 58.55%, H, 5.63%, N, 6.04%.

#### 4.5.1.3. Synthesis of *N*-(4-(4-(2,3-dichlorophenyl)piperazin-1-yl)-3-fluorobutyl)-6,6-diphenyl-1,4-dioxane-2-carboxamide (**33**).

This compound was prepared following the procedure described for compound **31**, starting from **104** and **105**. The crude compound was purified by column chromatography eluting with  $\text{CHCl}_3$ /acetone (8:2) to afford diastereomer **33** as an oil in a 41% yield.  $^1\text{H}$  NMR (400 MHz,  $\text{CDCl}_3$ ):  $\delta$  7.49-6.95 (m, 13H), 4.80 (m, 1H), 4.66 (d,  $J = 12.50$  Hz), 4.23 (dd,  $J = 3.52, 3.52$  Hz), 4.10 (dd,  $J = 3.12, 3.52$  Hz), 3.79 (d,  $J = 12.50$  Hz, 1H), 3.41 (m, 3H), 3.10 (m, 5H), 2.75 (m, 6H), 1.60-1.29 (m, 2H,  $\text{CH}_2$ ).  $^{19}\text{F}$  NMR (376 MHz,

CDCl<sub>3</sub>/CFCl<sub>3</sub>): δ -183.98 to -183.42 (m, 1F). The free base was transformed into the corresponding oxalate salt, which was crystallized from EtOH (m.p. 100-101 °C). <sup>13</sup>C NMR (100 MHz, DMSO): δ 162.71, 150.01, 140.62, 133.34, 129.22, 128.18, 127.18, 126.22, 121.98, 117.64, 90.20, 89.81, 85.00, 84.23, 74.90, 61.10, 51.88, 51.31, 34.80, 33.51. Anal. calcd for C<sub>31</sub>H<sub>34</sub>Cl<sub>2</sub>FN<sub>3</sub>O<sub>3</sub>·C<sub>2</sub>H<sub>2</sub>O<sub>4</sub>: C, 58.58%, H, 5.36%, N, 6.21%. Found: C, 58.28%, H, 5.44%, N, 6.10%.

4.5.1.4. *Synthesis of N-(4-(4-(2,3-dichlorophenyl)piperazin-1-yl)butyl)-5,5-diphenyl-1,4-dioxane-2-carboxamide (34).*

This compound was prepared following the procedure described for compound **31**, starting from **102** and **106** to afford **34** as an oil in a 65% yield. <sup>1</sup>H NMR (400 MHz, CDCl<sub>3</sub>): δ 7.66-6.85 (m, 13H), 1.56 (m, 2H), 4.87 (d, *J* =29.31 Hz, 1H), 3.64-3.24 (m, 4H), 3.11 (m, 5H), 2.69-2.35 (m, 8H), 1.72 (m, 2H). <sup>13</sup>C NMR (100 MHz, CDCl<sub>3</sub>): δ 25.40, 27.73, 39.25, 40.90, 51.33, 51.85, 69.13, 82.21, 90.04, 92.96, 117.64, 123.98, 126.22, 127.18, 128.26, 129.29, 133.34, 139.68, 150.11, 172.71. The free base was transformed into the corresponding oxalate salt, which was crystallized from EtOH (m.p. 94-95 °C). Anal. calcd for C<sub>31</sub>H<sub>35</sub>Cl<sub>2</sub>N<sub>3</sub>O<sub>3</sub>·C<sub>2</sub>H<sub>2</sub>O<sub>4</sub>: C, 60.19%, H, 5.66%, N, 6.38%. Found: C, 59.99%, H, 5.48%, N, 6.60%.

4.5.1.5. *Synthesis of N-(4-(4-(2,3-dichlorophenyl)piperazin-1-yl)-3-hydroxybutyl)-5,5-diphenyl-1,4-dioxane-2-carboxamide (35).*

This compound was prepared following the procedure described for compound **31**, starting from **103** and **106**. The crude compound was purified by column chromatography eluting with EtOAc/CHCl<sub>3</sub>/MeOH (5:5:1) to afford diastereomer **35** as an oil in a 32% yield. <sup>1</sup>H NMR (400 MHz, CDCl<sub>3</sub>): δ 7.66-6.85 (m, 13H), 4.89 (m, 1H), 3.93-3.59 (m, 4H), 3.31 (m, 1H), 3.08 (m, 6H), 2.92-2.31 (m, 8H), 1.65-1.46 (m, 2H). <sup>13</sup>C NMR (100 MHz, CDCl<sub>3</sub>): δ 172.71, 150.11, 139.68, 133.34, 129.22, 128.26, 127.18, 126.22, 123.98, 117.64, 93.12, 86.62, 83.23, 75.91, 69.13, 61.48, 56.08, 51.82, 45.68, 36.33. The free base was transformed into the corresponding oxalate salt, which was crystallized from MeOH (m.p. 132-133 °C). Anal. calcd for C<sub>31</sub>H<sub>35</sub>Cl<sub>2</sub>N<sub>3</sub>O<sub>4</sub>·C<sub>2</sub>H<sub>2</sub>O<sub>4</sub>: C, 58.76%, H, 5.53%, N, 6.23%. Found: C, 59.01%, H, 5.40%, N, 6.35%.

4.5.1.6. *Synthesis of N-(4-(4-(2,3-dichlorophenyl)piperazin-1-yl)-3-fluorobutyl)-5,5-diphenyl-1,4-dioxane-2-carboxamide (36).*

This compound was prepared following the procedure described for compound **31**, starting from **104** and **106**. The crude compound was purified by column chromatography eluting with CHCl<sub>3</sub>/acetone (8:2) to afford diastereomer **36** as an oil in a 64% yield. <sup>1</sup>H NMR (400 MHz, CDCl<sub>3</sub>): δ 7.49-6.95 (m, 13H), 4.85 (m, 2H), 4.30 (m, 3H), 3.78 (m, 1H), 3.58 (m, 2H), 3.01 (m, 4H), 2.68 (m, 3H), 2.48 (m, 2H), 2.29 (m, 2H), 1.63-1.45 (m, 2H). The free base was transformed into the corresponding oxalate salt, which was crystallized from 2-PrOH (m.p. 126-127 °C). <sup>13</sup>C NMR (100 MHz, DMSO): δ 162.71, 150.51, 140.62, 133.34, 129.33, 128.18, 127.18, 126.22, 121.98, 117.64, 93.10, 90.08, 89.84, 82.23,

69.13, 61.10, 51.88, 51.29, 34.78, 33.43.  $^{19}\text{F}$  NMR (376 MHz, DMSO):  $\delta$  ppm -181.58 to -181.12 (m, 1F). Anal. calcd for  $\text{C}_{31}\text{H}_{34}\text{Cl}_2\text{FN}_3\text{O}_3 \cdot \text{C}_2\text{H}_2\text{O}_4$ : C, 58.58%, H, 5.36%, N, 6.21%. Found: C, 58.33%, H, 5.53%, N, 6.06%.

4.5.1.7. *Synthesis of N-(4-(4-(2,3-dichlorophenyl)piperazin-1-yl)butyl)-2,3-dihydrobenzo[b][1,4]dioxine-2-carboxamide (37).*

This compound was prepared following the procedure described for compound **31**, starting from **102** and **107**. The crude compound was purified by column chromatography eluting with EtOAc/ $\text{CHCl}_3$  (5:5) to afford compound **37** as an oil in a 58% yield.  $^1\text{H}$  NMR (400 MHz,  $\text{CDCl}_3$ ):  $\delta$  7.18-6.90 (m, 7H), 4.68 (dd,  $J = 7.43, 7.03$  Hz, 1H), 4.54 (dd,  $J = 2.73, 2.73$  Hz, 1H), 4.19 (dd,  $J = 7.03, 7.43$  Hz, 1H), 3.39 (m, 2H), 3.11 (m, 3H), 2.63 (m, 4H), 2.42 (m, 4H), 1.60 (m, 4H). The free base was transformed into the corresponding oxalate salt, which was crystallized from 2-PrOH (m.p. 167-168 °C).  $^{13}\text{C}$  NMR (100 MHz, DMSO):  $\delta$  167.22, 164.73, 150.28, 143.48, 142.61, 133.14, 129.03, 126.51, 125.55, 122.01, 121.92, 120.22, 117.79, 117.44, 73.03, 65.29, 55.86, 51.73, 48.72, 38.24, 26.63, 21.29. Anal. calcd for  $\text{C}_{23}\text{H}_{27}\text{Cl}_2\text{N}_3\text{O}_3 \cdot \text{C}_2\text{H}_2\text{O}_4$ : C, 54.16%, H, 5.27%, N, 7.58%. Found: C, 54.01%, H, 5.34%, N, 7.32%.

4.5.1.8. *Synthesis of N-(4-(4-(2,3-dichlorophenyl)piperazin-1-yl)-3-hydroxybutyl)-2,3-dihydrobenzo[b][1,4]dioxine-2-carboxamide (38a, 38b).*

These compounds were prepared following the procedure described for compound **31**, starting from **103** and **107**. The crude compound was purified by column chromatography

eluting with CHCl<sub>3</sub>/MeOH (95:5) to afford the diastereomeric mixture **38a/38b** as an oil in a 45% yield. <sup>1</sup>H NMR (400 MHz, CDCl<sub>3</sub>): δ ppm 6.90-7.12 (m, 7H), 4.67 (dd, *J* = 6.64, 7.03, 1H), 4.49 (m, 1H), 4.22 (m, 1H), 3.80 (m, 1H), 3.63 (m, 2H), 3.37 (m, 2H), 3.04 (m, 4H), 2.78 (m, 2H), 2.56 (m, 2H), 2.39 (m, 2H), 1.51-1.70 (m, 2H). The free bases were transformed into the corresponding oxalate salts and the diastereomers were separated by crystallization from 2-PrOH.

Diastereomer **38a** (m.p. 88-89 °C): <sup>1</sup>H NMR (400 MHz, DMSO): δ 8.20 (m, 1H), 7.31 (m, 2H), 7.16 (m, 1H), 6.95 (m, 1H), 6.81 (m, 2H), 4.77 (dd, *J* = 5.85, 5.86 Hz, 1H), 4.31 (dd, *J* = 3.10, 2.25 Hz, 1H), 4.20 (dd, *J* = 6.30, 5.86 Hz, 1H), 3.82 (m, 1H), 2.43 (m, 2H), 3.19 (m, 10H), 3.01 (m, 1H), 2.90 (m, 1H), 1.45-1.55 (m, 2H). <sup>13</sup>C NMR (100 MHz, DMSO): δ 167.34, 163.82, 150.37, 143.48, 142.60, 133.49, 129.05, 126.52, 125.14, 122.06, 121.99, 120.22, 117.74, 105.00, 90.79, 73.04, 67.76, 61.79, 54.19, 52.46, 48.64, 35.72, 35.13, 25.92. Anal. calcd for C<sub>23</sub>H<sub>27</sub>Cl<sub>2</sub>N<sub>3</sub>O<sub>4</sub>·C<sub>2</sub>H<sub>2</sub>O<sub>4</sub>: C, 52.64%, H, 5.12%, N, 7.37%. Found: C, 52.37%, H, 5.30%, N, 7.51%.

Diastereomer **38b** (m.p. 99-100 °C). <sup>1</sup>H NMR (400 MHz, DMSO): δ 8.20 (m, 1H), 7.37 (m, 2H), 7.20 (m, 1H), 6.95 (m, 1H), 6.81 (m, 2H), 4.80 (dd, *J* = 5.85, 5.86 Hz, 1H), 4.31 (d, *J* = 11.26 Hz, 1H), 4.22 (dd, *J* = 5.41, 5.86 Hz, 1H), 3.84 (m, 1H), 3.10 (m, 11H), 2.95 (m, 1H), 2.43 (m, 2H), 1.53 (m, 2H). <sup>13</sup>C NMR (100 MHz, DMSO): δ 167.35, 163.10, 150.17, 143.48, 142.60, 133.14, 129.05, 126.48, 125.63, 122.03, 120.22, 117.75, 117.45, 106.67, 102.34, 73.01, 65.32, 63.10, 61.35, 52.56, 48.28, 35.62, 35.08, 15.57. Anal. calcd for C<sub>23</sub>H<sub>27</sub>Cl<sub>2</sub>N<sub>3</sub>O<sub>4</sub>·C<sub>2</sub>H<sub>2</sub>O<sub>4</sub>: C, 52.64%, H, 5.12%, N, 7.37%. Found: C, 52.45%, H, 5.28%, N, 7.56%.

4.5.1.9. *Synthesis of N-(4-(4-(2,3-dichlorophenyl)piperazin-1-yl)-3-fluorobutyl)-2,3-dihydrobenzo[b][1,4]dioxine-2-carboxamide (39a, 39b)*

These compounds were prepared following the procedure described for compound **31**, starting from **104** and **107** to afford the diastereomeric mixture **39a/39b** as an oil in a 36% yield. <sup>1</sup>H NMR (400 MHz, CDCl<sub>3</sub>): δ 7.18 (m, 2H), 6.78-6.99 (m, 5H), 4.92 (m, 1H), 4.70 (m, 1H), 4.49 (m, 1H), 4.21 (m, 1H, diastereomeric ratio 50:50), 3.49 (m, 2H), 3.04 (m, 4H), 2.63-2.88 (m, 6H), 2.18 (m, 1H), 1.90 (m, 2H). The diastereomers **39a** and **39b** were separated by preparative TLC eluting with CHCl<sub>3</sub>/MeOH (95:5). <sup>19</sup>F NMR (376 MHz, CDCl<sub>3</sub>/CFCl<sub>3</sub>): δ ppm -182.43 to -182.18 (m, 1F, diastereomer **39a**), -182.98 to -182.60 (m, 1F, diastereomer **39b**). The free bases were transformed into the corresponding oxalate salts, which were crystallized from 2-PrOH. Diastereomer **39a** (m.p. 200-201 °C). Anal. calcd for C<sub>23</sub>H<sub>26</sub>Cl<sub>2</sub>FN<sub>3</sub>O<sub>3</sub>·C<sub>2</sub>H<sub>2</sub>O<sub>4</sub>: C, 52.46%, H, 4.93%, N, 7.34%. Found: C, 52.67%, H, 5.08%, N, 7.25%. C, H, N. Diastereomer **39b** (m.p. 180-182 °C). Anal. calcd for C<sub>23</sub>H<sub>26</sub>Cl<sub>2</sub>FN<sub>3</sub>O<sub>3</sub>·C<sub>2</sub>H<sub>2</sub>O<sub>4</sub>: C, 52.46%, H, 4.93%, N, 7.34%. Found: C, 52.22%, H, 5.03%, N, 7.22%.

4.5.1.10. *Synthesis of 4-[4-(2,3-dichlorophenyl)piperazin-1-yl]butylamine (102)*

Anhydrous hydrazine (0.14 mL, 4.4 mmol) was added to a solution of **109** (2.1 mmol) in EtOH (20 mL). The mixture was heated to reflux for 2 h and then allowed to cool to room temperature. The solvent was removed in vacuo, and the solid residue was dissolved in 40% KOH (w/v, 50 mL). The product was extracted with ether (4 × 50 mL) and dried over anhydrous Na<sub>2</sub>SO<sub>4</sub>. Evaporation of the solvent gave 0.52 g (yield 82%) of **102** as an oil that was used in the next reaction without further purification. <sup>1</sup>H NMR (CDCl<sub>3</sub>): δ 7.18-

7.09 (m, 2H), 6.95 (dd,  $J = 6.5, 3.1$  Hz, 1H), 3.16-2.98 (m, 4H), 2.72 (t,  $J = 6.8$  Hz, 2H), 2.63 (d,  $J = 7.0$  Hz, 4H), 2.48-2.36 (m, 2H), 1.62-1.42 (m, 4H), 1.37 (s, 2H).

*4.5.1.11. Synthesis of 4-amino-1-(4-(2,3-dichlorophenyl)piperazin-1-yl)butan-2-ol (103).*

This compound was prepared following the procedure described for **102** starting from **110**: 71% yield.  $^1\text{H NMR}$  ( $\text{CDCl}_3$ ):  $\delta$  7.09-7.14 (m, 2H), 6.92 (dd,  $J = 6.3, 3.1$ , 1H), 3.89 (m, 1H), 2.97-3.05 (m, 9H), 2.80 (s, 2H), 2.61 (s, 2H), 2.40 (m, 2H), 1.56 (m, 2H).

*4.5.1.12. Synthesis of 4-(4-(2,3-dichlorophenyl)piperazin-1-yl)-3-fluorobutan-1-amine (104).*

This compound was prepared following the procedure described for **102** starting from **111**: 96% yield.  $^1\text{H NMR}$  ( $\text{CDCl}_3$ ):  $\delta$  ppm 7.72 (dd,  $J = 5.6, 3.2$  Hz, 2H), 7.13-7.15 (m, 2H), 7.11-7.16 (m, 2H), 6.95 (dd,  $J = 6.4, 2.8$  Hz, 1H), 4.75-4.94 (m, 1H), 3.07 (brs, 4H), 1.62-1.91 (m, 2H), 1.49-1.94 (m, 7H).

*4.5.1.13. Synthesis of 6,6-diphenyl-1,4-dioxane-2-carboxylic acid (105).*

A solution of  $\text{KMnO}_4$  (20.6 mmol) in  $\text{H}_2\text{O}$  (15 mL) was added dropwise to a stirred mixture of **116** (11.1 mmol) in 1N  $\text{KOH}$  (15 mL) such that the temperature was maintained below 10 °C. After 18 h at room temperature, the mixture was filtered over Celite,  $\text{MeOH}$  was added, and the solvent was concentrated under vacuum. The resulting aqueous solution was acidified with 6N  $\text{H}_2\text{SO}_4$  and extracted with  $\text{CHCl}_3$ . After evaporation of the dried



solvent, the residue was crystallized from EtOAc/petroleum ether: 52% yield; mp 197-199 °C. <sup>1</sup>H NMR (CDCl<sub>3</sub>): δ 7.27-7.54 (m, 10H, ArH), 7.08 (br s, 1H, exchangeable with D<sub>2</sub>O), 4.35 (dd, 1H), 4.61 (d, 1H), 4.21 (dd, 1H), 3.68 (dd, 1H), 3.62 (d, 1H).

#### 4.5.1.14. *Synthesis of 5,5-diphenyl-1,4-dioxane-2-carboxylic acid (106).*

This compound was prepared following the procedure described for **105** starting from **117**: 82% yield; mp 188-190 °C. <sup>1</sup>H NMR (CDCl<sub>3</sub>): δ 7.20-7.54 (m, 10H), 6.87 (br s, 1H, exchangeable with D<sub>2</sub>O), 4.66 (d, 1H), 4.41 (dd, 1H), 4.15 (dd, 1H), 3.95 (d, 1H), 3.72 (dd, 1H).

#### 4.5.1.15. *Synthesis of 2-(oxiran-2-yl)ethylisoindoline-1,3-dione (108).*

A suspension of phthalimide potassium salt (10.0 mmol) in DMF (20 mL) was treated with 2-(2-bromoethyl)oxirane (15.0 mmol) and the reaction was stirred at 100 °C for 12 h. The cooled reaction mixture was filtered, diluted with EtOAc (20 mL), and washed with H<sub>2</sub>O (2 × 10 mL). The organic phase was dried over anhydrous Na<sub>2</sub>SO<sub>4</sub> and the solvent was removed in vacuo to give **108** as a foam (78% yield), which was used without further purification. <sup>1</sup>H NMR (CDCl<sub>3</sub>): δ 7.83-7.87 (m, 2H), 7.70- 7.74 (m, 2H), 3.89 (m, 2H), 3.00 (m, 1H), 2.73 (t, J 3.9, 1H), 2.46 (m, 1H), 2.00 (m, 1H), 1.86 (m, 1H). <sup>13</sup>C NMR (CDCl<sub>3</sub>): δ 168.4, 134.1, 132.2, 123.4, 50.4, 46.5, 35.2, 31.7.

4.5.1.16. *Synthesis of 2-{4-[4-(2,3-dichlorophenyl)piperazin-1-yl]butyl}isoindoline-1,3-dione (109).*

The commercially available 1-(2,3-dichlorophenyl)piperazine (1.0 mmol), 2-(4-bromobutyl)isoindoline-1,3-dione the alkyl bromide (1.1 mmol), and K<sub>2</sub>CO<sub>3</sub> (2.0 mmol) were heated to 80 °C in DMF (3 mL) for 5 h, under an atmosphere of nitrogen. The mixture was cooled to room temperature and H<sub>2</sub>O was added. After extraction with ethyl acetate (3 × 20 mL), the combined organic phases were washed with H<sub>2</sub>O (2 × 20 mL) and brine (20 mL). The organic extract was dried over anhydrous Na<sub>2</sub>SO<sub>4</sub> and filtered and the solvent evaporated in vacuo to give the product as a clear oil (63% yield). <sup>1</sup>H NMR (CDCl<sub>3</sub>): δ 7.80-7.85 (m, 2H), 7.68-7.73 (m, 2H), 7.09-7.15 (m, 2H), 6.92- 6.95 (m, 1H), 3.72 (t, J = 6.9 Hz, 2H), 3.04 (m, 4H), 2.61 (m, 4H), 2.44 (t, J = 7.4 Hz, 2H), 1.69-1.76 (m, 2H), 1.52-1.62 (m, 2H). <sup>13</sup>C NMR (CDCl<sub>3</sub>): δ 168.4, 151.3, 134.0, 133.9, 132.1, 127.4, 124.5, 123.2, 118.6, 57.9, 53.3, 51.3, 37.8, 26.6, 24.2.

4.5.1.17. *Synthesis of 2-(4-(4-(2,3-dichlorophenyl)piperazin-1-yl)-3-hydroxybutyl)isoindoline-1,3-dione (110).*

This compound was prepared following the procedure described for **109** starting from **108** to afford an oil: 73% yield. <sup>1</sup>H NMR (CDCl<sub>3</sub>): δ 7.81 (m, 2H), 7.67 (m, 2H), 7.06-7.11 (m, 2H), 6.90 (m, 1H), 3.74-3.83 (m, 3H), 3.60 (s, 1H), 3.02 (s, 4H), 2.79 (m, 2H), 2.56 (s, 2H), 2.42 (m, 2H), 1.79 (m, 2H). <sup>13</sup>C NMR (CDCl<sub>3</sub>): δ 167.7, 150.4, 133.4, 133.4, 131.6, 127.0, 124.1, 122.7, 118.2, 64.5, 63.8, 53.4, 51.4, 35.3, 33.9.

4.5.1.18. *Synthesis of 2-(3-fluoro-4-(4-(2,3-dichlorophenyl)piperazin-1-yl)butyl)-isoindoline-1,3-dione (111).*

To a solution of compound **110** (5.5 mmol) in dry DCM (50 mL) cooled at -78 °C was added a solution of DAST (5.5 mmol) in dry DCM (25 mL) over a period of 30 min. This reaction mixture was continuously stirred for 12 h at room temperature. The reaction mixture was diluted with DCM and washed with water and 5% NaHCO<sub>3</sub> solution, and the organic layer was dried over anhydrous Na<sub>2</sub>SO<sub>4</sub>. The solvent was removed under vacuum to afford the crude product in 58% yield. Mp 97-99 °C; <sup>1</sup>H NMR (CDCl<sub>3</sub>): δ 7.85 (dd, J = 5.6, 2.8 Hz), 7.71 (dd, J = 5.6, 3.2 Hz), 6.83-7.01 (m, 4H), 4.70-4.88 (m, 1H), 3.86-3.90 (m, 1H), 3.85 (m, 3H), 3.07 (br s, 4H), 2.50-2.78 (m, 7H), 1.95-2.13 (m, 2H). <sup>13</sup>C NMR (CDCl<sub>3</sub>): δ 168.40, 152.37, 141.38, 134.11, 132.23, 123.41, 123.03, 121.08, 118.31, 111.23, 90.68 (d, 1C), 62.27 (d, 1C), 55.45, 54.16, 50.69, 34.64 (d, 1C), 32.41 (d, 1C); <sup>19</sup>F NMR (CDCl<sub>3</sub>): δ -183.30 to -182.85 (m, 1F).

4.5.1.19. *Synthesis of 2-(allyloxy)-1,1-diphenylethanol (112).*

2,2-Diphenyloxirane (32.1 mmol) was added dropwise to a stirred solution of freshly cut sodium (9.56 mmol) in allyl alcohol (22 mL) at room temperature. After 1 h at room temperature, the reaction mixture was refluxed for 20 h. Most of the unreacted allyl alcohol was then separated by distillation at atmospheric pressure. After cooling to room temperature, 6N H<sub>2</sub>SO<sub>4</sub> (0.6 mL) was added to the residual solution to neutralize the sodium alloxide, and solvent removal was continued to afford a residual oil, which was purified by column chromatography, eluting with cyclohexane/EtOAc (10: 0.05) to give a

solid: 85% yield; mp 29-31 °C. <sup>1</sup>H NMR (CDCl<sub>3</sub>): δ 7.21-7.53 (m, 10H), 5.94 (m, 1H), 5.28 (m, 2H), 4.15 (d, 2H), 4.02 (s, 2H), 3.54 (br s, 1H, exchangeable with D<sub>2</sub>O).

*4.5.1.20. Synthesis of 2-(allyloxy)-2,2-diphenylethanol (113).*

Perchloric acid (70%, 0.75 mL) was added to a stirred solution of 2,2-diphenyloxirane (3.0 g, 15.3 mmol) in allyl alcohol (7.5 mL) at 0 °C. After 0.5 h at room temperature, the reaction mixture was poured into H<sub>2</sub>O (75 mL) and extracted with Et<sub>2</sub>O. The organic phase was washed with H<sub>2</sub>O and dried over anhydrous Na<sub>2</sub>SO<sub>4</sub>. Removal of dried solvents gave a residue, which was purified by column chromatography, eluting with cyclohexane to afford an oil: 380% yield. <sup>1</sup>H NMR (CDCl<sub>3</sub>): δ 7.15-7.52 (m, 10H), 5.98 (m, 1H), 5.13-5.47 (m, 2H), 4.35 (s, 2H), 3.82 (d, 2H), 1.85 (br s, 1H, exchangeable with D<sub>2</sub>O).

*4.5.1.21. Synthesis of 2-(oxiran-2-ylmethoxy)-1,1-diphenylethanol (114).*

*m*-CPBA (50%) (11.6 g, 33.6 mmol) was added to a solution of **112** (16.8 mmol) in DCM (120 mL). After 20 h at room temperature under stirring the reaction mixture was washed with 10% Na<sub>2</sub>SO<sub>3</sub>, 5% Na<sub>2</sub>CO<sub>3</sub>, and H<sub>2</sub>O. Evaporation of the dry solvent gave an oil: mp 83-84 °C; 90% yield. <sup>1</sup>H NMR (CDCl<sub>3</sub>): δ 7.18-7.52 (m, 10H), 4.10 (dd, 2H), 3.52-3.90 (m, 2H), 3.16 (m, 1H), 2.55-2.80 (m, 2H), 1.60 (br s, 1H, exchangeable with D<sub>2</sub>O).

4.5.1.22. *Synthesis of 2-(oxiran-2-ylmethoxy)-2,2-diphenylethanol (115).*

This compound was prepared following the procedure described for **114** starting from **113** to afford an oil: 50% yield. <sup>1</sup>H NMR (CDCl<sub>3</sub>): δ 7.17-7.50 (m, 10H), 4.30 (dd, 2H), 3.43-3.64 (m, 2H), 3.24 (m, 1H), 2.90 (m, 2H), 1.62 (br s, 1H, exchangeable with D<sub>2</sub>O).

4.5.1.23. *Synthesis of (6,6-diphenyl-1,4-dioxan-2-yl)methanol (116).*

A solution of **114** (151.4 mmol) and [(1S)-(+)-10-CSA] (142.1 mmol) in DCM (1340 mL) was refluxed for 8 h. The reaction mixture was then washed with NaHCO<sub>3</sub> saturated solution and dried over anhydrous Na<sub>2</sub>SO<sub>4</sub>. Removal of the solvent afforded a residue, which was purified by column chromatography, eluting with cyclohexane/EtOAc (9:1) to afford a solid: 60% yield; mp 114-115 °C. <sup>1</sup>H NMR (CDCl<sub>3</sub>): δ 7.20-7.58 (m, 10H), 3.64 and 4.61 (two d, 2H), 3.53-3.83 (m, 5H), 1.84 (br s, 1H, exchangeable with D<sub>2</sub>O).

4.5.1.24. *Synthesis of (5,5-diphenyl-1,4-dioxan-2-yl)methanol (117).*

This compound was prepared following the procedure described for **116** starting from **115**. The residue was purified by column chromatography, eluting with cyclohexane/EtOAc (8:2) to afford a solid: 50% yield; mp 95-97 °C. <sup>1</sup>H NMR (CDCl<sub>3</sub>): δ 7.11-7.56 (m, 10H), 3.79 and 4.69 (dd, 2H), 3.88 (m, 1H), 3.40-3.75 (m, 4H), 1.82 (br s, 1H, exchangeable with D<sub>2</sub>O).

## **4.5.2. Radioligand binding assays**

### *4.5.2.1. DRD2, DRD3 and DRD4*

The membranes were prepared from HEK293 cells in which there was a stable expression of DRD2, DRD3 and DRD4 of human origin. The cells were prepared according to the procedure reported under section 3.5.2. Previously frozen membranes were diluted in freshly-prepared EBSS to the concentration of 100 µg/mL, in case of DRD2 and DRD3 tests, or 200 µg/mL, in case of DRD4 tests. Radioligand competition experiments were performed in glass tubes, for 60 minutes, as described under section 3.5.2. for [<sup>3</sup>H]Nmethylspiperone as a radioligand. The reaction was stopped by filtration through Whatman GF/B filters, presoaked in 0.5% polyethylenimine for 60 min, using a Brandel R48 filtering manifold. The filters were washed thrice using 3mL of EBSS buffer, cooled to 0 °C, and subsequently transferred to scintillation vials. To these vials, CytoScint liquid scintillation cocktail (3 mL) was added, and the counting was performed using a PerkinElmer Tri-Carb 2910 TR liquid scintillation counter.

### *4.5.2.2. DRD1.*

Human DRD1-overexpressing mouse fibroblast cells (LhD1) were grown until confluence in DMEM, supplemented by 10% FetalClone1 serum (FCS), 0.05% penicillin-streptomycin (pen-strep) and 400 µg/mL of Geneticin (G418). Three assay plates were seeded with ~10-15 µg of protein per well. Cells grown on three 150 mm plates were scraped and centrifuged at 500×g for a total of 5 minutes. The remaining pellet was overlaid with 2 mL of assay buffer constituted of 50 mM Tris-HCl containing 120 mM NaCl, 5 mM KCl, 2 mM CaCl<sub>2</sub>, and 1 mM MgCl<sub>2</sub>. So prepared mixture was frozen at -70 °C.

Before the start of the experiment, the pellet was homogenized with a polytron in 30 mL of the freshly prepared assay buffer. To the wells containing 800  $\mu$ L of the test drug or buffer, a 100  $\mu$ L of cell homogenate was added and the plates were pre-incubated for 10 minutes. Then, 100  $\mu$ L of the radioligand [ $^3$ H]SCH-23390 was added (final concentration = 0.18 nM). The plates were incubated for 60 minutes, at 25  $^{\circ}$ C, after which the reaction was terminated by filtration, using a Tomtec 96 well harvester. The radioactivity on the filters was determined using a PerkinElmer microbeta scintillation counter. Nonspecific binding was determined using 1  $\mu$ M SCH-23390.

#### 4.5.2.3. 5-HT<sub>1A</sub>R.

5-HT<sub>1A</sub>R was expressed in the human HeLa cell line transfected with genomic clone G-21 coding for the human 5-HT<sub>1A</sub>R. Cells were grown as monolayers in DMEM supplemented with 10% FCS and 100  $\mu$ g/ mL gentamycin and were incubated at 37  $^{\circ}$ C with 5% CO<sub>2</sub>. At 95% confluency, the plates were scraped and the content was lysed using 5 mM Tris, cooled to 0  $^{\circ}$ C, and 5 mM EDTA buffer, until pH = 7.4. So prepared homogenates were centrifuged at 40 000g, for 20 minutes, after which the supernatant was removed and the pellet was resuspended in a small volume of the same lysing solution (5 mM Tris, cooled to 0  $^{\circ}$ C, and 5 mM EDTA buffer). So prepared samples were frozen and kept at -70  $^{\circ}$ C. Before the start of the experiment, the pellet was resuspended in the binding buffer (pH = 7.4) containing 50 mM Tris, 10 mM pargyline and 2.5 mM MgCl<sub>2</sub>. The membranes were incubated in a final volume of 320  $\mu$ L, for 30 minutes, at 30  $^{\circ}$ C, with the added radioligand [ $^3$ H]8-OHDPAT (1 nM), with or without the addition of

competing drugs (1  $\mu$ M-1 pM dilutions, in triplicates). Non-specific binding was performed in the presence of 10  $\mu$ M 5-HT.

#### 4.5.2.4. *5-HT<sub>2A</sub>R and 5-HT<sub>2C</sub>R.*

For the expression of human 5-HT<sub>2A</sub>R and 5-HT<sub>2C</sub>R, human embryonic kidney cells were used, and marked correspondingly: HEK-h5-HT<sub>2A</sub> (for 5-HT<sub>2A</sub>R) and HEK-h5-HT<sub>2C</sub> (for 5-HT<sub>2C</sub>R). The cells were grown until confluence. The medium was removed and the plates were washed with PBS, then scraped into 2 mL PBS; frozen and stored at -20 °C. Before the start of the experiment, the cell suspension was thawed, and 10 mL of the assay buffer was added per cell plate. The assay buffer contained 50 mM Tris, with pH 7.4 at 37 °C with the addition of 0.1% of ascorbic acid and 5 mM CaCl<sub>2</sub>. So prepared samples were polytronned for 5 seconds, at setting 6. The homogenate was centrifuged at 15,500 rpm for 20 min. For the minimization of the residual 5-HT concentration, the pellet was resuspended, polytronned and centrifuged as described, once more. The pellet was then resuspended in 2 mL of buffer per plate. The binding assay sample included 50  $\mu$ L of the test compound, 5-HT or buffer, 50  $\mu$ L of the cell homogenate, 50  $\mu$ L of the radioligand [<sup>125</sup>I]DOI (~0.1 nM), and buffer in a final volume of 250  $\mu$ L. Specific binding was defined as the difference between the total binding and the binding in the presence of 5-HT (10  $\mu$ M). The reaction was left incubating for 60 minutes, at 37 °C, and was terminated by filtration through the Wallac A filter mats (presoaked in 0.05% polyethylenimine) using a Tomtec 96-well harvester. The radioactivity that remained on the filters was detected via Wallac betaplate reader.



### **4.5.3. Functional assays**

#### *4.5.3.1. Adenylate Cyclase/cAMP Functional Assay.*

Mouse glioma cells which were expressing monkey DRD1 at low density (C6D1 low-D1-density cells) were used. All the cells were grown on 48-well plates containing DMEM supplemented by 10% FCS, 0.05% of penicillin/ streptomycin and 2 g/mL of puromycin. The cells were grown until 80-90% of confluence, after which the DMEM was removed, and the wells were individually rinsed with 0.5 mL of freshly-prepared EBSS containing: 116.4 mM NaCl, 15 mM HEPES, 10 mM glucose, 5.4 mM KCl, 1.3 mM CaCl<sub>2</sub>, 1.2 mM Na<sub>2</sub>HPO<sub>4</sub>, 1.2 mM MgSO<sub>4</sub>, at pH 7.4; room temperature; and supplemented with 0.1% ascorbic acid, 2% bovine calf serum (BCS), 0.11% 3-isobutyl-1-methyl-xanthine (IBMX), an inhibitor of cAMP phosphodiesterase. Cells were counted on a 48-well plate. 200 000 cells per well were grown for the use of the cAMP EIA kit. The 48-well plates were preincubated for 20 minutes, at 37 °C, with pure EBSS, then 20 minutes with EBSS-compound dilutions until reaching a final volume of 1 mL (triplicates were prepared). EBSS was subsequently removed, 50 µL of 3% trichloroacetic acid (TCA) was added to each individual well, and the plate was left for 1 hour. Then, the supernatant was diluted in a ratio of 1:50, and 50 µL of it was added to the cAMP EIA test plate, with a final assay volume being 200 µL per well. The plate was put in an incubator, for 18 hours, at the temperature of 4 °C, after which the supernatant was removed and the wells were rinsed five times using 300 µL of the EIA buffer. 200 µL of Ellman's developing reagent was added to each individual well and the plate was incubated for 2 hours at room temperature while rotating gently. The plate reader (BioRad Benchmark Plus spectrometer) was set

at 405 nm for detection, and the linearity of the signal was observed at approximately 100 pg of cAMP.

#### 4.5.3.2. *Mitogenesis Functional Assay.*

Chinese hamster ovary (CHO) cells expressing DRD2 (CHOp-DRD2) and DRD3 (CHOp-DRD3) were kept in  $\alpha$ -MEM medium supplemented by 10% FBS, 0.05% penicillin-streptomycin, and 400  $\mu$ g/mL of G418. The agonist assay refers to the DRD2 or DRD3 stimulation of mitogenesis, while the antagonist assay refers to the inhibition of quinpirole mitogenesis stimulation. CHOp-DRD2 or CHOp-DRD3 cells were, for both the agonist and the antagonist assays, seeded in 96-well plates in a concentration of 5000 cells per well. The cells were incubated at 37°C in the  $\alpha$ -MEM medium supplemented with 10% FBS for 48-72 h. After the incubation, the cells were rinsed twice with pure  $\alpha$ -MEM (without FBS) and were further incubated for 24h at 37 °C. Serial dilutions of the test compounds were prepared in pure  $\alpha$ -MEM. For the agonist assay, the medium was removed and replaced with 100  $\mu$ L of a test compound in pure  $\alpha$ -MEM. For the antagonist assay, 90  $\mu$ L of the serial dilution of the antagonist test compound was added (1.1x of the final concentration), as well as 10  $\mu$ L of 300 nM quinpirole (30 nM final); and the samples were left incubating for 24 hours (in case of DRD2) or 26 hours (in case of DRD3), at 37 °C. Subsequently, 0.25  $\mu$ Ci of the radioligand [<sup>3</sup>H]thymidine in  $\alpha$ -MEM supplemented with 10% FBS was added to individual wells, and the plates were left to incubate for 2 hours at 37 °C. Cells were lysed using 10x trypsin solution (1% of trypsin added to the Ca-Mg-free PBS), and the plates were filtered and counted using a standard procedure.

Quinpirole was run each day as an internal control, and dopamine was used as a reference compound.

#### 4.5.3.3. *Adenylate Cyclase/cAMP Functional Assay.*

HEK-D4.4-AC1 cells were grown on 15 cm plates until confluent. The cells were plated in 48-well plates, at a density of 375 000 cells per well. DMEM supplemented by 10% FCS, 0.05% of penicillin/ streptomycin and 2 g/mL of puromycin. The cells were grown until 80-90% of confluence, after which the DMEM was removed DMEM supplemented with 5% FetalClone, 5% BCS and penicillin-streptomycin was used as medium, and the cells were left incubating for approximately 36 hours. Then, the old medium was removed and changed to DMEM supplemented by 10% charcoal-stripped FetalClone and penicillin-streptomycin, and the cells were incubated for additional 18 hours.

For the agonist assays, 0.8 mL of EBSS was added and the cells were left incubating for 20 minutes, after which the agonists were added and the plates were additionally incubated for 20 minutes. Then, 10  $\mu$ M forskolin was added in a final volume of 1 mL. For the antagonist assay, 0.7 mL of EBSS was added and the cells were incubated for 10 minutes. Then, the antagonists were added, the cells were incubated for 10 minutes, 2 nM quinpirole was added and after the additional 20 minutes of incubation, 10  $\mu$ M forskolin was added in a final volume of 1 mL. For both assays, after the addition of forskolin, the reaction was incubated for 20 minutes, after which the reaction was terminated by removing the buffer by aspiration, and the addition of 0.1 mL of TCA. The plates were incubated for 2 hours, at room temperature, under gentle rotation. Adenylate cyclase activity was measured via cAMP EIA kit. 9  $\mu$ L aliquots of individual wells were

diluted to 200  $\mu\text{L}$  using the EIA buffer of the kit, and the tracer, as well as the monoclonal body, were added. The plates were incubated at  $4^{\circ}\text{C}$  for a total of 18 hours, after which the media was removed and the plates were washed five times with 300  $\mu\text{L}$  of the wash buffer and Ellman's reagent was added. The plates were left incubating for 2 hours at room temperature, in the dark, while gently rotating, and were later read at 410 nm. DRD4 agonists inhibited forskolin-stimulated cAMP formation, and the maximal inhibition was defined using 1  $\mu\text{M}$  quinpirole. For the antagonists, the maximal reversal of inhibition of cAMP formation was defined using 10  $\mu\text{M}$  haloperidol.

#### 4.5.3.4. $[^{35}\text{S}]\text{GTP}\gamma\text{S}$ Binding Assay.

The modified Stanton and Beer method<sup>104</sup> was used for the determination of  $[^{35}\text{S}]\text{GTP}\gamma\text{S}$  binding in HeLa cells stably expressing 5-HT<sub>1A</sub>R. The simulation experiments were performed as described further: cell membranes containing 50-70  $\mu\text{g}$  of protein were resuspended in a buffer with 20 mM HEPES, 3 mM MgSO<sub>4</sub> and 120 mM NaCl (pH = 7.4), and were incubated for 20 minutes, at  $30^{\circ}\text{C}$ , with 30  $\mu\text{M}$  GDP and various concentrations of either 8-OH-DPAT or test compounds (in serial dilutions from 10  $\mu\text{M}$  to 0.1 nM) in a final volume of 500  $\mu\text{L}$ . The samples were then transferred to ice,  $[^{35}\text{S}]\text{GTP}\gamma\text{S}$  in 200 pM concentration was added, and the samples were further incubated for 30 minutes, at  $30^{\circ}\text{C}$ . The preincubation with the agonist and the antagonist was a step necessary to ensure that the agonist and the antagonist are at equilibrium. Nonspecific binding was measured with 10 mM GTP $\gamma\text{S}$  present. The incubation was interrupted by the addition of HEPES buffer cooled to  $0^{\circ}\text{C}$  and rapid filtration through Unifilter B filters, using Filtermate cell harvester. The filters were washed using HEPES buffer cooled to  $0^{\circ}\text{C}$ , and the

radioactivity retained on the filters was measured via TopCount, PerkinElmer liquid scintillation counter (90% efficiency).

#### 4.5.3.5. *Inositol-1-phosphate (IP-1) formation assay.*

As a tissue source for this experiment, HEK-h5-HT<sub>2A</sub> or HEK-h5-HT<sub>2C</sub> were used. The cells were seeded in 24-well plates, at a density of 400 000 cells per well, and DMEM supplemented by charcoal-stripped FetalClone was used as a media. The cells were left to incubate for 24 hours. Test compounds were made up of a stimulation buffer obtained from a kit. After the cell-incubation period was completed, the medium was aspirated, and one of the following was added to the wells: test compounds, antagonist, buffer or serotonin. Following this addition, the cells were left to incubate for additional 60 minutes. Then the cells were lysed over 30 minutes, and 50 µL of the cell lysate was added to IP-1 plates. Specific antibodies were added, the plates were left incubating for 3 hours, and they were washed six times. Then, the substrate was added and the incubation proceeded for 20 minutes, after which the reaction was terminated and the plate was read at 450 nm wavelength (correction was applied at 620 nm). Agonists were normalized to the maximum stimulation by serotonin, while the antagonists were tested in the presence of 0.1 µM serotonin, and were normalized to the 10 µM ketanserin( in case of 5-HT<sub>2A</sub>R) or 1 µM SB 242084 (in case of 5-HT<sub>2C</sub>R) inhibition.

#### **4.5.4. Molecular modelling studies**

The docking simulations were based on the resolved structure of the DRD3 in complex with eticlopride (PDB Id: 3PBL). The protein structure was checked and prepared as reported elsewhere.<sup>113</sup> The ligands were generated in their protonated state and their structure was optimized by PM7 semi-empirical calculations as implemented by MOPAC2016 (keywords = PM7 CHARGE = 1.00 PRECISE GEO-OK).<sup>63</sup> The docking simulations were carried out using PLANTS focusing the search within a 10 Å radius sphere around the bound eticlopride. For each ligand, 10 poses were generated, as mentioned under section 3.5.4. The same procedure was applied to perform docking simulations on the resolved structure of the DRD4 in a complex with nemonapride (PDB Id: 5WIV). For the performed MD runs, the membrane was added to the computed complexes using the CHARMM-GUI server.<sup>126</sup> The protein was oriented using the PPM server,<sup>127</sup> the bilayer was made by phosphatidylcholine (POPC, 70%) and cholesterol (30%). TIP3P water molecules were added to both sides of the membrane, as well as Na<sup>+</sup> and Cl<sup>-</sup> ions to reach an ionic concentration of 0.15 M. Amber force fields ff14SB, GAFF and Lipid17 were used for the protein, the ligands and the lipids, respectively. The systems underwent three steps of minimization: first, the hydrogen atoms were minimized, then the solvent molecules and finally the whole system, applying restraints (5 kcal/mol-Å) in the alpha carbons. Then systems underwent to a heating where the temperature was brought to 300 K using the Langevin thermostat, followed by an equilibration phase first using the NPT ensemble with the Berendsen barostat (1 atm), and finally an NVT ensemble. The 200 ns production runs were performed with the NVT

ensemble, with a time step of 0.02 fs and the -SHAKE algorithm. PME and PBC were applied.

## 5. SIGMA RECEPTOR

### 5.1. Background

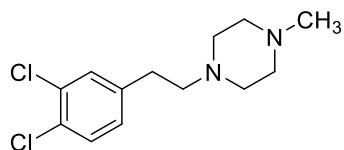
Sigma ( $\sigma$ ) receptors are transmembrane proteins which employ a specific role in different cellular functions. In 1976, the  $\sigma$  receptors were described for the first time by Martin et al.<sup>128</sup> and, since then, the understanding of this receptor and its role has further developed. Initially, these receptors were thought to belong to the opioid receptor family, and subsequently to correspond to the phencyclidine (PCP) binding site of the ionotropic N-methyl-D-aspartate (NMDA) receptor.<sup>129</sup> However, today they are considered a separate receptor family, consisting of two subtypes, namely  $\sigma_1$  and  $\sigma_2$  receptors, depending on their biological actions, distribution, sizes, and other factors.<sup>130</sup>

Concerning this system, in my Ph.D. thesis work, I focused on the development of ligands selectively targeting  $\sigma_1$  receptors, potentially useful for the treatment of binge eating disorders.

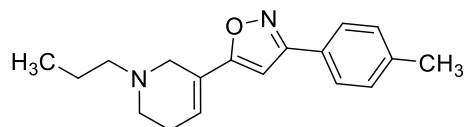
$\sigma_1$  Receptors behave as molecular chaperones in the mitochondria-associated endoplasmic reticulum, and they are involved in the cellular response to stress, as well as in cellular homeostasis.<sup>131,132</sup> More specifically, the  $\sigma_1$  receptor can alter proper  $\text{Ca}^{2+}$  signalling patterns, as it aids the inositol triphosphate receptor, similarly to a chaperone, in the endoplasmic reticulum membrane. Additionally, it has a role in the regulation of cholinergic, dopaminergic and glutamatergic neurotransmission, as well as in the regulation of the opening of some ion channels ( $\text{K}^+$ ,  $\text{Na}^+$ ,  $\text{Ca}^{2+}$ ).<sup>133</sup> They are widely distributed across the nervous system, and in some peripheral tissues. They are also expressed in cells and organs of the endocrine and immune systems and are



overexpressed in several tumour cell lines.<sup>134</sup> Their involvement in several physiological and pathological conditions makes them very promising targets for the management of several disorders. Particularly, central  $\sigma_1$  receptor agonists have demonstrated efficacy in different neuropsychiatric (such as cognition, depression, delirium, etc) and neurodegenerative diseases, such as Alzheimer's and Parkinson's diseases.<sup>135–137</sup> Conversely,  $\sigma_1$  Receptor antagonists can be used in neuropathic pain, as well as in other types of pain including inflammatory, orofacial, and visceral pain.<sup>138</sup> Moreover, they have a potential in the treatment of psychostimulant-related addiction<sup>139,140</sup> and alcoholism.<sup>141,142</sup> Despite the involvement of  $\sigma_1$  receptor in addiction being proven, limited information is available on its role in binge-eating disorder.<sup>143,144</sup> In a study conducted by Cottone et al. in 2012, the  $\sigma_1$  antagonist **BD-1063**<sup>145</sup> (Figure 28) was proven to reduce binge-eating episodes and prevented compulsive eating in palatable rats.<sup>143</sup> This indicated the possible involvement of the  $\sigma_1$  receptor in neurobiological adaptations pertaining to binge-like eating. More recently, Tapia et al. have demonstrated the ability of the highly selective  $\sigma_1$  antagonist **PD-144,418**<sup>146</sup> (Figure 28) to impact the motivational effort in food-reinforced behaviour in rats. They have discovered that **PD-144,418** at 10  $\mu\text{mol/kg}$  altered active lever response for sucrose pellets in sated animals. However, in a state of energy deficit (24-hour long food deprivation), the administration of **PD-144,418** did not alter the motivational pattern for sucrose pellet consumption in rats.<sup>144</sup>



**BD-1063**



**PD-144,418**

**Figure 28.** Chemical structures of the  $\sigma_1$  antagonists BD-1063 and PD-144,418.

$\sigma_1$  Receptor has been cloned from various tissues,<sup>133,147,148</sup> and its crystal structures complexed with known agonists and antagonists (i.e., **(+)-pentazocine**, **haloperidol**, **NE-100**, **4-IBP**, and **PD-144,418**; Figure 29) have recently been reported.<sup>149,150</sup>

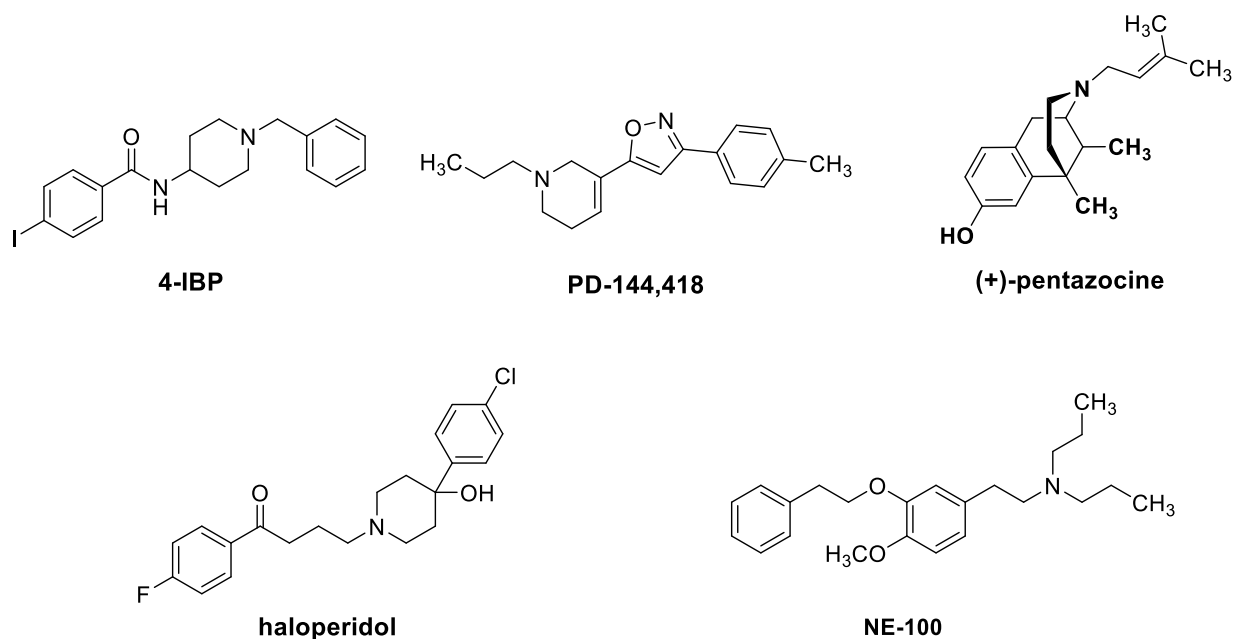


**Figure 29.** Chemical structures of  $\sigma_1$  agonists and antagonists **4-IBP**, and **PD-144,418**, **(+)-pentazocine**, **haloperidol**, **NE-100**, analyzed in complex with  $\sigma_1$  receptor.

The reported structures showed a trimeric architecture with a single transmembrane domain in each protomer. The ligand-binding site is deeply located inside the large  $\beta$ -

barrel region where ligands are accommodated in a very hydrophobic pocket entirely occluded from solvent molecules. In Figure 30A, the positioning of **PD-144,418** within the  $\sigma_1$  receptor internalized binding pocket, coloured by the polar surfaces within the pocket, is shown. The main H-bond interaction (Figure 30B) was established between the basic nitrogen and the highly conserved residue Glu172 (located within the PHP), as previously reported in the literature.<sup>149,151</sup>

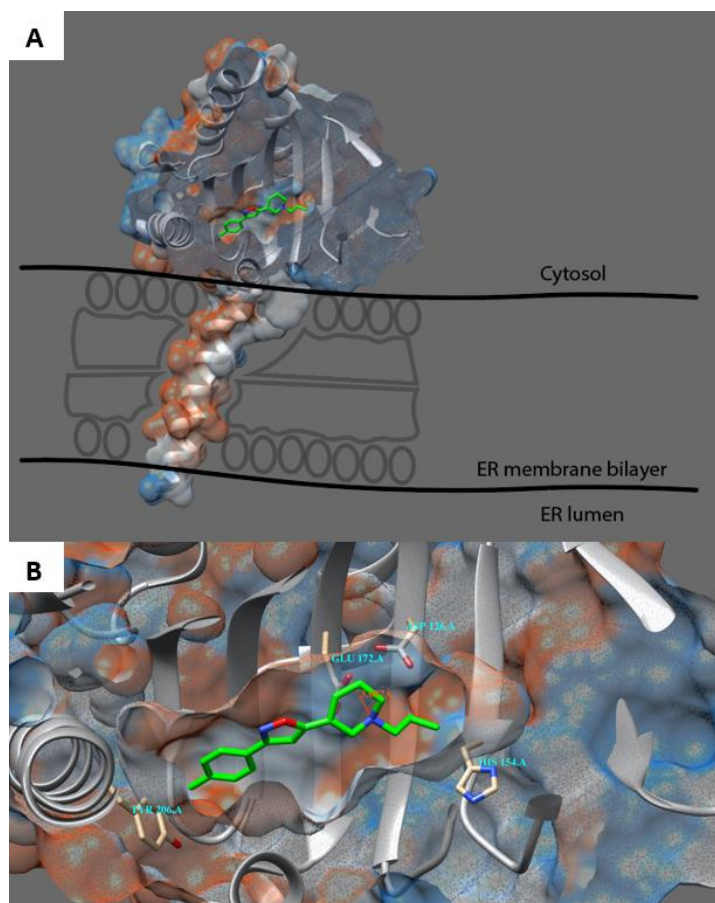


**Figure 30.** (A) Side view of the positioning of **PD-144,418** (coloured green) within the human  $\sigma_1$  receptor (PDB code: 5HK1) binding pocket, as present within the endoplasmic reticulum (ER) membrane. (B) The main interactions of **PD-144,418** within the binding site of the human  $\sigma_1$  receptor are shown in green. The hydrogen bond is shown in orange (length: 3.097 Å). Surface coloured by hydrophobicity. The cut-off surface is shown as grey mesh.

There is no straightforward pharmacophoric model of  $\sigma_1$  receptor ligands, but the general model was deduced in 1994 by Glennon, based on the structure of a highly conserved binding site of  $\sigma_1$  receptor.<sup>152</sup> In this model, a basic amine moiety (proton donor site) is flanked on two sides by hydrophobic pockets of the  $\sigma_1$  receptor binding site (Figure 31B). An optimal binding distance for the  $\sigma_1$  ligands is considered to be between 6 and 10 Å between the amine and the primary hydrophobic pocket (PHP; bigger, accommodates aromatic groups), and 2.5 to 3.9 Å between the amine and the secondary hydrophobic pocket (SHP; smaller, accommodates less lipophilic groups like THF or 1,3-dioxane). Newer pharmacophoric models exist as well, and they share structural similarities with the pharmacophores of  $\sigma_2$  receptors.<sup>153–156</sup>

In 2019, two new pharmacophoric models for  $\sigma_1$  receptors were proposed by Pascual et al., based on the interactions between **PD-144,418** and  $\sigma_1$  receptor crystal structure (PDB code: 5HK1), compared to 4 other available models at that time (Langer, Gund, Zampieri, Banister).<sup>157</sup> One model was based on an algorithm that identified the most important interactions between the ligand and the receptor (5HK1–Ph.A), while the other was based on the manual fusion of two hydrophobic features (5HK1–Ph.B). All 5 pharmacophoric models analysed indicated the importance of an ionic interaction of  $\sigma_1$  ligands with Glu172. Additionally, a hydrophobic feature or a hydrophobic aromatic site was found in a pocket surrounded by Tyr103, Leu105, Leu95, Tyr206, Leu182, and Ala185 and delimited by the  $\alpha$ -helices  $\alpha_4$  and  $\alpha_5$  of the  $\sigma_1$  receptor. All models mention the presence of another hydrophobic region, but only in the Langer, 5HK1–Ph.A and 5HK1–Ph.B models, this region is found near Asp126, at the bottom of the  $\beta$ -barrel.<sup>157</sup> The proposed

Langer (Figure 31A) and Glennon (Figure 31B) pharmacophores, as well as an overlap between the Langer and 5HK1–Ph. The pharmacophore models are shown in Figure 31.

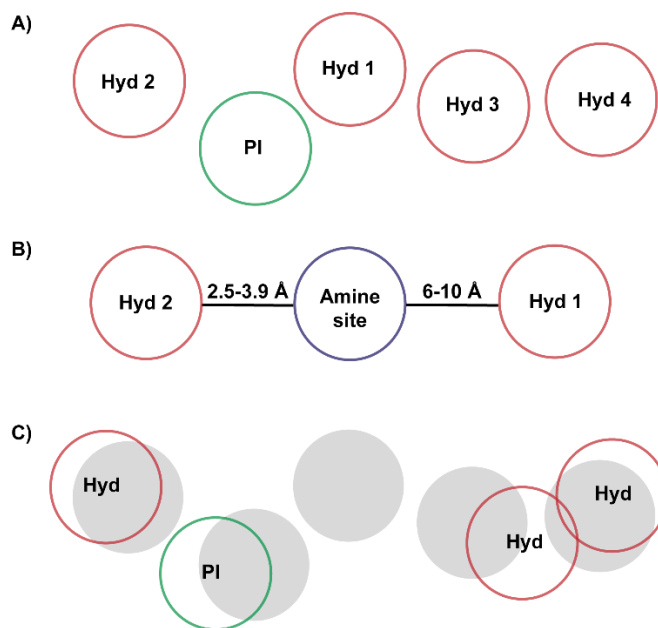


**Figure 31.** (A) Langer pharmacophore. (B) Glennon pharmacophore. (C) An overlap between the proposed model of a Langer pharmacophore (grey) and a 5HK1–Ph.A pharmacophore, without exclusion spheres. PI = ionic interaction (green). Hyd = hydrophobic feature/ hydrophobic region.

## 5.2. Introduction and objectives of the work

The medicinal chemistry team with whom I developed my Ph.D. thesis has reported the synthesis and biological evaluation of a series of analogues of the potent and selective  $\sigma_1$  receptor ligand **spipethiane** (Figure 32).<sup>158</sup> Among them, the potent  $\sigma_1$  receptor antagonist 2-(1-benzylpiperidin-4-yl)thiochroman-4-one (**118**) (Figure 32), proved to decrease binge-eating episodes in female rats, therefore supporting  $\sigma_1$  receptor's involvement in the pathology of binge-eating disorder.<sup>159</sup>

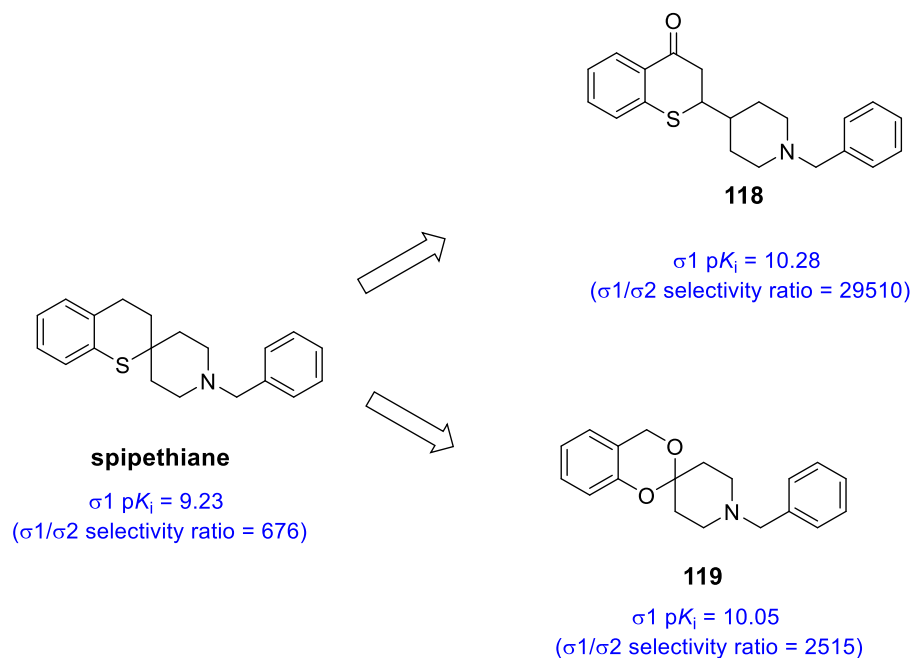


**Figure 32.** Chemical structures of lead compound **spipethiane** and its analogues **118** and **119**.

Another analogue showing  $\sigma_1$  receptor affinity ( $pK_i = 10.05$ ) and selectivity ( $\sigma_1/\sigma_2 = 2515$ ) higher than **spipethiane** was the 1,3-benzodioxane derivative **119**. Functional assays performed on MCF-7 and MCF-7/ADR highlighted the  $\sigma_1$  antagonist profile of this compound.<sup>158</sup>

To further improve the  $\sigma_1$  receptor affinity and selectivity over the  $\sigma_2$  subtype, in this research work, the conformationally constrained 1,3-benzodioxane moiety of the lead compound **119** was replaced by a more flexible 1,3-dioxane nucleus, obtaining compounds **40-43** via benzo-cracking approach.<sup>160</sup> Specifically, derivatives **40** and **41**, in which the phenyl substituent is linked to the positions 4 or 5 of the 1,3-dioxane ring, respectively, were prepared and studied (Figure 33). Moreover, to assess the role of the distance between the two hydrophobic portions that flank the basic function of **40** and **41**,

compounds **42** and **43** were also prepared and their diastereomers were separated. These newly synthesised derivatives have the *N*-benzyl piperidine spaced from the 1,3-dioxane nucleus (Figure 33), contributing to the overall higher flexibility of the structure of the final products. The separation of the diastereomers of **42** and **43** allowed us to probe the role played by the relative configuration on the  $\sigma_1$  receptor affinity and selectivity.

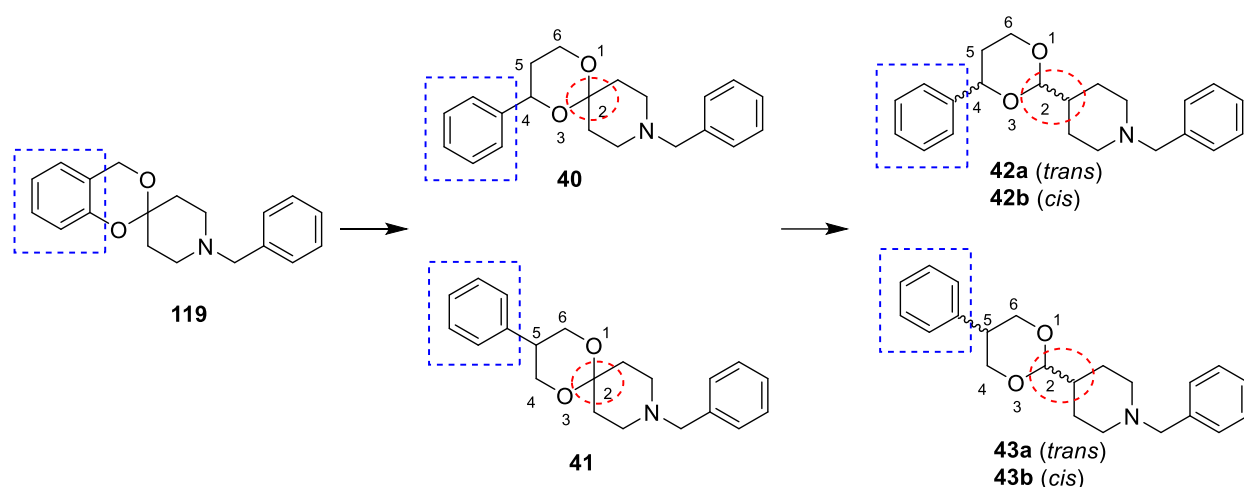


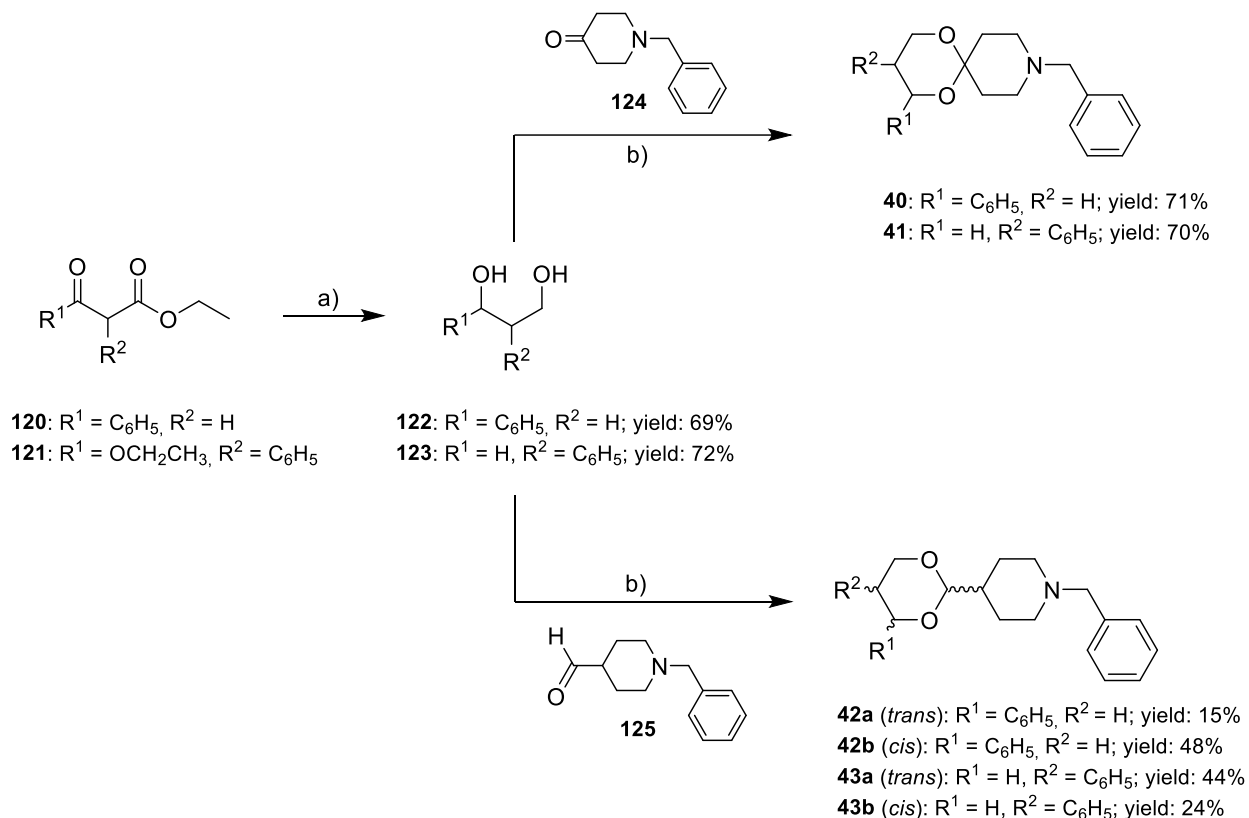
**Figure 33.** Chemical structures of the synthesised compounds **40-43**; analogues of the known potent  $\sigma_1$  receptor ligand **119**.

All the synthesised compounds were subjected to radioligand binding studies at both  $\sigma_1$  and  $\sigma_2$  receptors. Derivatives **40** and **41** were also tested for their affinity at the PCP sites of the NMDA receptor, DAT,  $\mu$ ,  $\kappa$ , and  $\delta$  receptors, which are targets that many  $\sigma_1$  ligands also bind with high affinity and that play a role in binge eating disorders.<sup>161</sup> Additionally, the most promising compound **41** was chosen to be evaluated in a female adult rat model of binge eating.

## 5.3. Results and discussion

### 5.3.1. Synthesis of $\sigma$ 1 ligands

Compounds **40-43** were prepared according to the routes shown in Scheme 8.



**Scheme 8.** Synthetic routes for compounds **40-43**. a)  $LiAlH_4$ , diethyl ether, room temperature for 2 h; b) *p*-toluenesulfonic acid, toluene, under reflux for 5 h.

The commercially available compounds 3-oxo-3-phenylpropionate (**120**) and diethyl 2-phenylmalonate (**121**) were reduced using  $LiAlH_4$ , to obtain intermediates **122** and **123**, respectively. The condensation of **122** and **123** with the suitable *N*-benzylpiperidine carbonyl derivatives **124** and **125** in the presence of *p*-toluenesulfonic acid yielded **40** and



**41**, as well as diastereomer mixtures **42a/42b** and **43a/43b**, respectively. The separation of the diastereomers was performed via flash column chromatography, as reported in the experimental section.

The stereochemical relationship between the *N*-benzylpiperidine moiety in position 2 and the phenyl substituent in positions 4 or 5 of **42a/42b** and **43a/43b**, respectively, was determined by <sup>1</sup>H NMR analysis (NOESY studies). Particularly, an evident NOE was observed between the protons in the positions 2 and 4 (4.48 and 4.65 ppm, respectively) of **42b**, highlighting that both the piperidine and phenyl rings in positions 2 and 4, respectively, are equatorially oriented. Therefore, the stereochemical relationship between the substituents in positions 2 and 4 is *cis* in **42b** and, consequently, *trans* in **42a** (Figure 34). Concerning **43a**, the axial proton in position 4 ( $\delta$  3.78 ppm) showed two large coupling constants ( $J = 10.8$  Hz and  $J = 11.3$  Hz), one with the geminal equatorial proton and the other with the axial proton in the position 5. Consequently, the phenyl ring adopts an equatorial orientation. Moreover, a clear NOE was observed between the axial protons in positions 2 and 4 at 4.36 and 3.78 ppm, respectively, evidencing that the *N*-benzylpiperidine moiety also adopts an equatorial orientation. Therefore, the relative configuration between the substituents in positions 2 and 5 is *trans* in **43a** and, consequently, *cis* in **43b** (Figure 34).

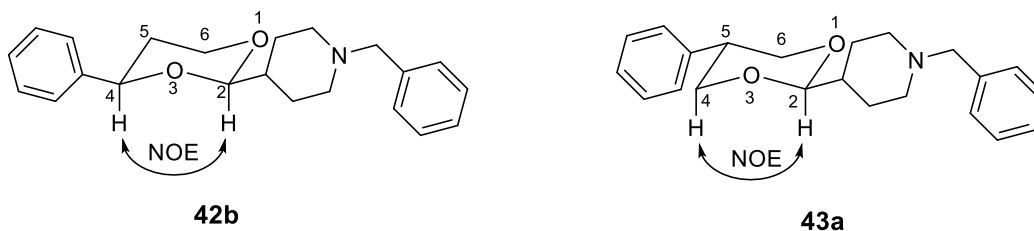


**Figure 34.** Side-view depiction of compounds **42b** and **43a**.

### 5.3.2. Radioligand binding assays

Guinea pig brain and rat liver membranes were used to assess the affinities of **40-43** for  $\sigma_1$  and  $\sigma_2$  receptors, respectively. [ $^3\text{H}$ ]-(+)-pentazocine and [ $^3\text{H}$ ]-di-*o*-tolylguanidine in presence of an excess of (+)-pentazocine were used as radioligands for  $\sigma_1$  and  $\sigma_2$  receptors, respectively.<sup>162</sup> The affinity values of the compounds, expressed as  $\text{pK}_i$  values are shown in Table 11. Lead **119** was included for useful comparison.

**Table 11.** Affinity values, expressed as  $\text{pK}_i$ <sup>a</sup> of compounds **40-43** and **119** at  $\sigma_1$  and  $\sigma_2$  receptors, and of **40** and **41** at DAT, the PCP site of the NMDA receptor;  $\delta$ ,  $\kappa$  and  $\mu$  opioid receptors.

Compound	$\text{pK}_i$						
	$\sigma_1$	$\sigma_2$	DAT	NMDA	$\delta$	$\kappa$	$\mu$
<b>119</b>	10.05 ± 0.08	6.65 ± 0.09	-	-	-	-	-
<b>40</b>	11.00 ± 0.07	6.33 ± 0.11	< 5	< 5	8.60 ± 0.14	< 5	< 5
<b>41</b>	10.89 ± 0.05	6.09 ± 0.07	5.63 ± 0.09	< 5	5.82 ± 0.08	< 5	< 5
<b>42a</b>	8.43 ± 0.07	6.75 ± 0.10	-	-	-	-	-
<b>42b</b>	9.62 ± 0.15	7.42 ± 0.08	-	-	-	-	-
<b>43a</b>	8.44 ± 0.14	7.25 ± 0.02	-	-	-	-	-
<b>43b</b>	8.31 ± 0.06	6.60 ± 0.10	-	-	-	-	-

<sup>a</sup>Equilibrium dissociation constants ( $K_i$ ) were derived from the  $\text{IC}_{50}$  via the Cheng-Prusoff equation.<sup>58</sup>  $\text{pK}_i$  values are expressed as the mean ± S.E.M. of three to five independent experiments, each performed in triplicate.

The data reported in Table 11 revealed that the benzo-cracking approach performed on the 1,3-benzodioxane derivative **119** was favourable for the binding to  $\sigma_1$  receptor, while it caused a slight reduction in  $\sigma_2$  receptor affinity, with a consequent increase in  $\sigma_1/\sigma_2$  selectivity. Indeed, both compounds **40** and **41** displayed very high  $\sigma_1$  affinity and a remarkable  $\sigma_1/\sigma_2$  selectivity. Noteworthy, **41** showed an impressive  $\sigma_1/\sigma_2$  selectivity ratio ( $\sigma_1/\sigma_2 = 63096$ ) and, to our knowledge, is the most selective  $\sigma_1$  ligand reported so far. A significant reduction in affinity for  $\sigma_1$  receptor and an increase in those for  $\sigma_2$  were observed when the benzo-cracking approach is combined with the further increase in the distance between the two lipophilic moieties of **40** and **41**, yielding the diastereomers **42a/42b** and **43a/43b**, respectively. Consequently, the  $\sigma_1/\sigma_2$  affinity ratios displayed by **42a/42b** and **43a/43b** were significantly lower than those of **40** and **41**. Probably, the increase in the conformational freedom and in the distance between the two lipophilic portions was detrimental for the optimal interaction with the  $\sigma_1$  receptor. Stereochemistry appears to play a role in the binding to the  $\sigma_1$  receptor when the phenyl ring is in position 4 of the 1,3-dioxane nucleus, with the *cis* isomer **42b** showing  $\sigma_1$  affinity significantly higher than that of the *trans* diastereomer **42a**. On the contrary, the *trans* and *cis* 5-phenyl diastereomers **43a** and **43b** showed similar affinity values.

The most interesting compounds **40** and **41** were evaluated at DAT (radioligand: [ $^3\text{H}$ ]-WIN35,428; rat striatal cortex), NMDA (radioligand: [ $^3\text{H}$ ]-(+)-MK 801; pig brain cortex),  $\mu$  receptor (radioligand: [ $^3\text{H}$ ]DAMGO; guinea pig brain),  $\kappa$  receptor (radioligand: [ $^3\text{H}$ ]U-69593; guinea pig brain) and  $\delta$  receptor (radioligand: [ $^3\text{H}$ ]DPDPE; rat brain),<sup>26,107,163,164</sup> From the results reported in Table 11 it emerges that ligand **40** showed negligible affinity

for DAT, NMDA,  $\mu$  and  $\kappa$  opioid receptors, and high affinity for  $\delta$  subtype ( $pK_i = 8.60$ ), although it is 251-fold lower than that for  $\sigma_1$ . Interestingly, compound **41**, which also binds  $\delta$  receptor with sub-micromolar affinity, displayed a remarkable selectivity for  $\sigma_1$  receptor over all the evaluated targets ( $\sigma_1/\text{DAT} = 181970$ ,  $\sigma_1/\text{NMDA} > 776247$ ,  $\sigma_1/\mu > 776247$ ,  $\sigma_1/\kappa > 776247$ ,  $\sigma_1/\delta = 117490$ ). The selectivity profile of **41** is noticeable, given that many potent  $\sigma_1$  ligands also bind to DAT, NMDA and/or opioid receptors with high affinity.<sup>129,145,165</sup>

### **5.3.3. Molecular modelling studies**

To rationalize the affinity profiles of the proposed ligands at the  $\sigma_1$  receptor, docking simulations were performed<sup>162</sup> based on the resolved  $\sigma_1$  structure (PDB Id: 5HK1) using the PLANTS software and following the same recently reported computational protocol.<sup>159</sup> As discussed below, the complex stability is evaluated by calculating the APBS score which is focused on the polar interactions.<sup>166</sup> Figure 35 compares the computed putative poses for **119** (Figure 35A) and **40** (Figure 35B) and reveals some differences which can justify the increase of affinity observed for the latter.

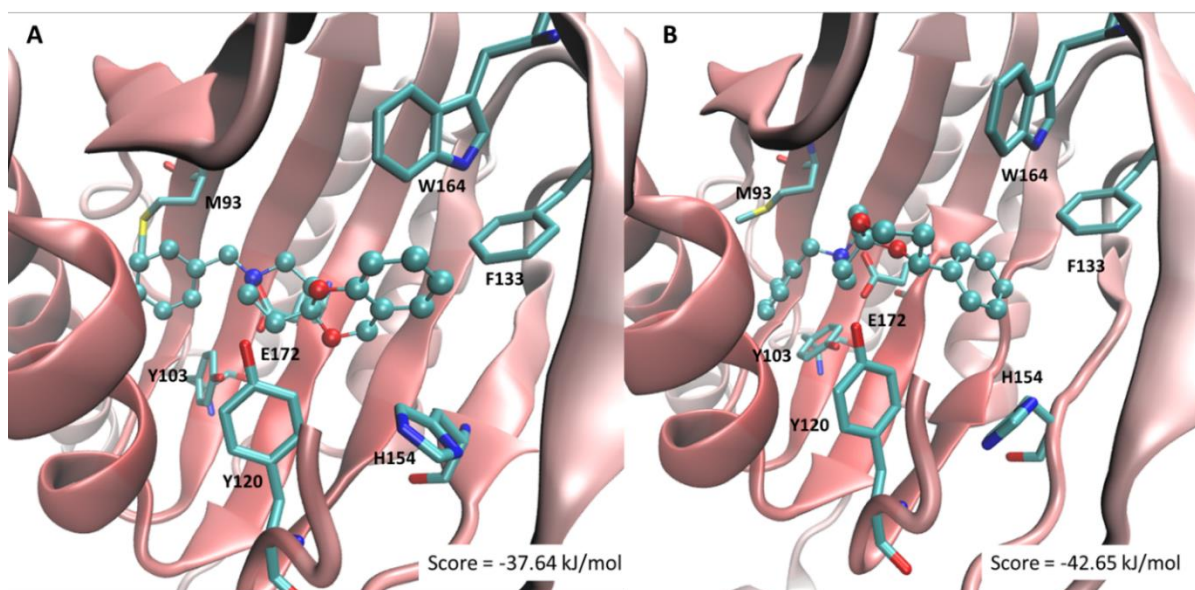


**Figure 35.** Main interactions stabilizing the putative complexes for **119** (A) and (*R*)-**40** (B) as computed using the resolved and reconstructed  $\sigma$ 1 receptor structure. The scores are reported according to the calculations performed employing the APBS method.

In detail, Figure 35A highlights the key interactions stabilized by **119** which can be schematized as follows: (a) the ligand ammonium head stabilizes a clear ion-pair with Glu172 reinforced by an H-bond with Tyr103; (b) the benzyl moiety is inserted within a hydrophobic subpocket where it mostly contacts alkyl side-chains plus  $\pi$ - $\pi$  stacking with Tyr103 and a  $\pi$ -Sulfur contact with Met93; (c) the benzodioxane system is accommodated within a subpocket lined by several aromatic residues while the O1 oxygen atom is engaged by an H-bond with Tyr120. The enantiomers of **40** afford very similar putative complexes and attention is here focused on the complex for (*R*)-**40** since it shows a slightly better APBS score compared to (*S*)-**40** (-42.56 vs. -41.38 kJ/mol). Specifically, Figure 35B emphasizes that (*R*)-**40** elicits an interaction pattern very similar to that already seen in Figure 35A, even though some key interactions appear to be enhanced when compared to those elicited by **119**. This positive effect can be seen in the

contacts stabilized by: (a) the benzyl moiety which elicits an optimized  $\pi$ - $\pi$  stacking with Tyr103; (b) the dioxane oxygen atoms which better approach Tyr120 and (c) the phenyl ring which is engaged by an extended set of  $\pi$ - $\pi$  stacking interactions with Phe107, Phe133, His154 and Trp164. These reinforced contacts are reflected in better complex stability as encoded by the scores displayed in Figure 35A. As also confirmed by the APBS score (-38.91 kJ/mol), compound **41** yields an in-between docking result, with the two aromatic rings being engaged by enhanced contacts, while the dioxane ring is unable to conveniently approach Tyr120, as seen in Figure 35B. Finally, compounds **42** and **43** reveal computed poses rather similar to those observed for the previous ligands, even though the free dioxane ring assumes a rather different arrangement which hampers its interactions with Tyr120. The lack of this contact induces flipped poses of the most hindered ligands by which the dioxane ring approaches Tyr103.

#### **5.3.4. *In vivo* functional assays**

Considering the remarkable  $\sigma_1$  affinity and selectivity profile of compound **41**, it was selected for *in vivo* studies, using a validated preclinical animal model of binge eating, to further investigate the function of the  $\sigma_1$  receptor system on compulsive-like eating disorder.<sup>162</sup> Female rats were used in relation to the higher prevalence of binge eating disorder and bulimia nervosa in women than in men.<sup>167</sup> In the binge-eating model,<sup>168–170</sup> female rats were randomly separated into four groups:

- I) Non-restricted and non-exposed to stress (NR + NS);
- II) Non-restricted and exposed to stress (NR + S);
- III) Restricted and non-exposed to stress (RN + S);

#### IV) Restricted and exposed to stress (R + S).

The association of three consecutive food restriction/refeeding periods and acute stress is able to trigger a strong increase of highly palatable food (HPF) consumption only in R + S rats in a short time (120 min). Stress was induced by placing a coffee cup containing HPF for 15 min, letting the animal see the cup and smell HPF odour, without the possibility to eat it. Thus, on the binge test day, NR + NS and R + NS had immediate access to HPF for 120 min, whereas NR + S and R+S had free access to it only after 15 min of stress. This stressful condition, although mild, has already been shown to enhance the corticosterone blood level in stressed rats.<sup>171-174</sup> In line with previous studies,<sup>175,176</sup> the ANOVA in the vehicle groups revealed a marked interaction among the three factors (food restriction x stress x sessions time) [ $F_{\text{interaction}}(3,72) = 4.8; P < 0.01$ ]. Bonferroni post hoc test revealed a significant ( $P < 0.01$ ) increase in HPF consumption in the first 15 min in the R + S group (binging group), compared to the other three groups. On the other hand, during the time of the other sessions (15-30; 30-60; 60-120 min), no change in HPF intake was observed among all groups (Figure 36, left panel). At the end of the binge eating test (120 min) one-way ANOVA showed a two-way interaction (food restriction x stress) [ $F_{\text{interaction}}(1,24) = 4.3; P < 0.05$ ] and the post hoc analyses ( $P < 0.01$ ) revealed that only R + S rats significantly enhanced HPF eating with respect to the other rats (Figure 36, right panel). Thus, the stress exposure induced binge-like behavior only in previously restricted rats, which consumed a large amount of HPF within 15 min and no compensatory changes during the remaining 15-120 min were detected.

Acute intraperitoneal injection of **41**, 30 min before giving access to HPF, selectively blocked the episode of binge eating in a dose-dependent manner in the R + S group,

without affecting consumption in the other experimental groups during 120 min of observation (Figure 36B-E).

Specifically in R + S rats, ANOVA reported a significant effect of treatment at 0-15 min [ $F(2,20) = 6.7$ ;  $P < 0.05$ ] and in 0-120 min [ $F(2,20) = 10.9$ ;  $P < 0.01$ ]. Post hoc analyses indicated that both used dosages (3 or 7 mg/kg) significantly decreased HPF consumption in R+ S at each time point as indicated in Figure 36E.



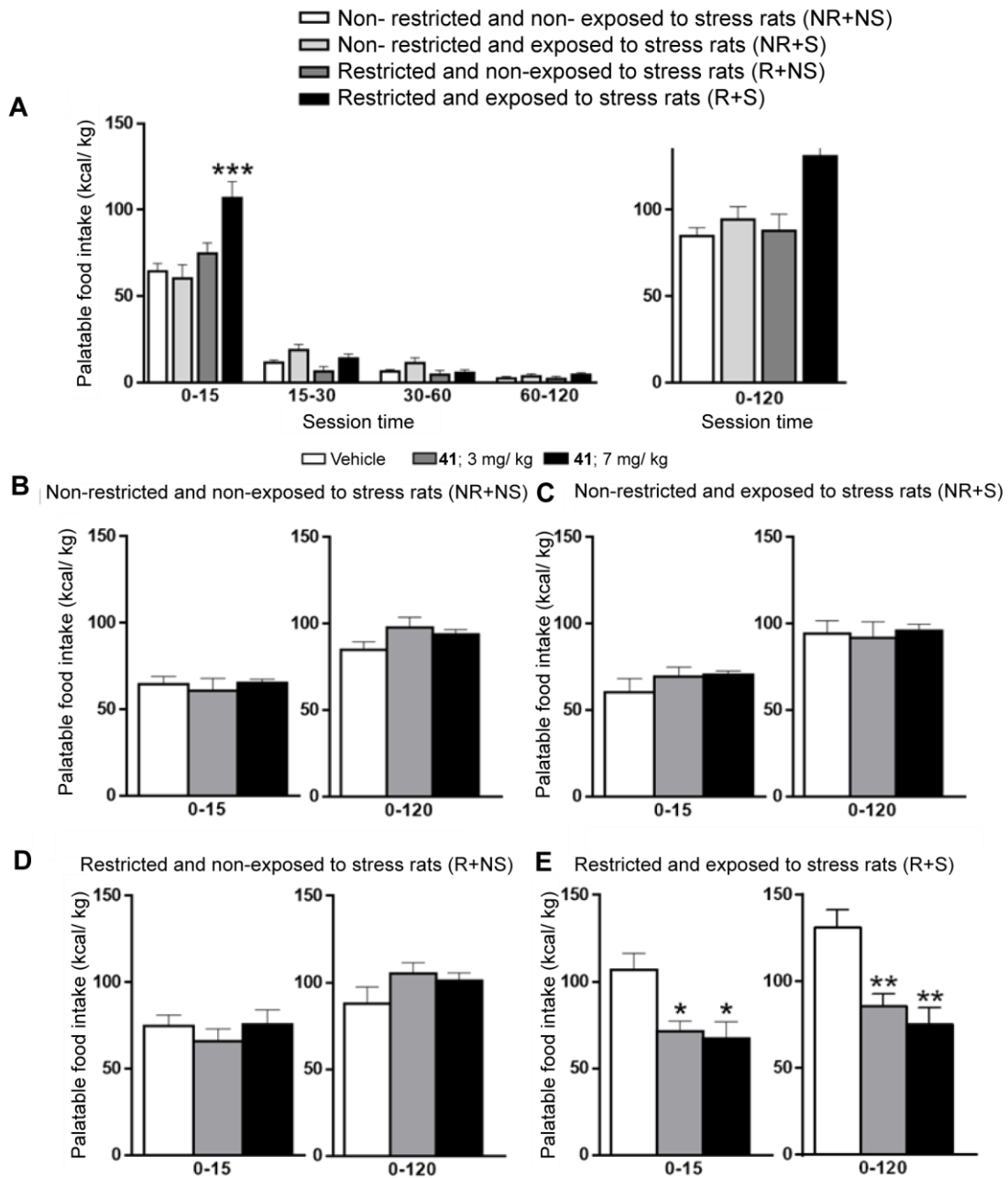


**Figure 36.** Administration of compound **41** prevented the episode of binge eating. (A) HPF intake, expressed as kcal/kg at different time sessions (0-15 minutes, 15-30 minutes, 30-60 minutes, 60-120 minutes; left) and at the end of the experiment (120 minutes; right panel) in the vehicle (veh) injected rats. \*\* $P < 0.01$ ; \*\*\* $P < 0.001$  is different from the other three time periods. (B) HPF consumption, expressed in kcal/kg, after 15 min (left panel) or 120 min (right) of free access to a cup containing chocolate paste in veh. or treated rats: NR + NS (B, Non-Restricted and Non-Stressed), NR + S (C, Non-Restricted and Stressed), R + NS (D, Restricted and Non-Stressed), R + S (E, Restricted and Stressed) groups. \* $P < 0.05$ ; \*\*\* $P < 0.01$  vs R + S veh. Data were expressed as mean  $\pm$  SEM.  $N = 6-8$  animals per group.

In addition, to assess if the systemic injection of **41** may influence different aspects of animal behaviour in the control or binging group, the open field (OF) and forced swimming tests (FST) were performed. The OF test is a validated test, commonly used for evaluating locomotor activity and anxiety-like behaviour in rodents in an unfamiliar environment,<sup>177</sup> while FST is a suitable tool for evaluating a depressed state.<sup>178</sup> The administration of **41** has shown not to affect any measured behavioural parameters in these present tests. In fact, analyzing the locomotor activity in the entire OF arena, ANOVA showed a significant effect of restriction and stress conditions [ $F_{\text{restriction}} (1,48) = 7.9; P < 0.01$ ;  $F_{\text{stress}} (1,48) = 30.9; P < 0.001$ ] and no effect of the treatment with **41** [ $F_{\text{treatment}} (1,48) = 0.6; P > 0.05$ ]. R + S veh and R + S **41** (7 mg/kg) showed the highest distance travelled compared to the other groups (Table 12). Regarding the other parameters, jump and total vertical counts were significantly affected only by stress [ $F_{\text{stress}} (1,48) = 11.9; P < 0.01$ ] and [ $F_{\text{stress}} (1,48) = 86.7; P < 0.001$ ], respectively, but not by restriction or treatment conditions. As shown in Table 12, the stress procedure appeared to increase the general arousal and this effect was confirmed by the significant gain in a vehicle or treated stressed rats (NR + S and R + S) on distance travelled in the central zone [ $F_{\text{stress}} (1,48) = 19.7; P < 0.001$ ] and on zone entries [ $F_{\text{stress}} (1,48) = 39.2; P < 0.001$ ] into the central zone. In particular, the latest finding also suggested that stress does not influence anxiety-like behaviour in stressed rats. Notably, the reduction of distance travelled or low numbers of entries into the central zone of the OF, marked an increased emotionality and anxiety in rats.<sup>179</sup> Finally, no difference in stereotypic counts was found among the groups [ $F_{\text{restriction}} (1,48) = 0.7; P > 0.05$ ;  $F_{\text{stress}} (1,48) = 0.02; P > 0.05$ ;  $F_{\text{treatment}} (1,48) = 1.6; P > 0.05$ ].

**Table 12.** Behavioural parameters in female rats performing the open field (OF) and forced swimming tests (FST)<sup>a</sup>.

OPEN FIELD (OF) TEST								
Parameters	NR + NS		NR + S		R + NS		R + S	
	Vehicle	41 (7 mg/kg)	Vehicle	41 (7 mg/kg)	Vehicle	41 (7 mg/kg)	Vehicle	41 (7 mg/kg)
Total distance travelled/ cm	2305.3 ± 357.3	2492.3 ± 225.3	3602.9 ± 269.3	3467.2 ± 411.8	2626.2 ± 242.5	3132.4 ± 331.6	4335.9 ± 419.3*	4461.5 ± 346.3*
Total vertical counts	99 ± 4	93.7 ± 5	123.9 ± 6.1	125.9 ± 5.4	87 ± 3.3	94.3 ± 6.6	131.7 ± 4.3	126.6 ± 4.5
Jump counts	104.6 ± 4.8	113 ± 17.1	137.1 ± 2.1	152 ± 32.5	97.7 ± 6.3	119.5 ± 9.1	172 ± 20.6	170.4 ± 19
Stereotypical counts	2367.1 ± 116.9	2500.3 ± 89.3	2477.4 ± 161.4	2270.4 ± 137.5	2030.5 ± 280.8	2516.7 ± 79.2	2305.1 ± 79.7	2401 ± 119.6
Distance travelled in the center/ cm	101.2 ± 25.6	112.7 ± 7.1	140.3 ± 30.1	148.1 ± 13.1	84.3 ± 17.1	96.4 ± 6	179.9 ± 24.8	177.5 ± 37.5
Central zone entries	26.4 ± 4.6	28.1 ± 2.7	34.5 ± 4.1	34 ± 6.8	18.7 ± 2.8	22.5 ± 2.1	50.4 ± 2.4	47.2 ± 10
FORCED SWIMMING TEST (FST)								
Parameters	NR + NS		NR + S		R + NS		R + S	
	Vehicle	41 (7 mg/kg)	Vehicle	41 (7 mg/kg)	Vehicle	41 (7 mg/kg)	Vehicle	41 (7 mg/kg)
Immobility time/ s	100.4 ± 12.94	106.7 ± 11.2	92.9 ± 13.5	111.1 ± 11.2	99.6 ± 10.4	94.8 ± 9.2	158.6 ± 10*	163.5 ± 22.5*

<sup>a</sup>The values are given for the entire open field arena as mean values±SEM. \*p < 0.05 vs the other groups. N = 6-8 animals per group.

In addition, using the FST, ANOVA revealed that the immobility time was significantly impacted by restriction [ $F_{\text{restriction}} (1,49) = 8,2; P < 0.01$ ], stress [ $F_{\text{stress}} (1,49) = 11.5; P < 0.01$ ] and by the interaction between these two factors [ $F_{\text{interaction}} (1,49) = 12.7, P < 0.01$ ], while compound **41** [ $F_{\text{treatment}} (1,48) = 1.6; P > 0.05$ ] did not change the swimming/floating behaviour.

Post hoc tests exhibited a significantly longer immobility time in a vehicle or treated R + S rats compared with the other groups, revealing that the cycle of food restriction plus stress may increase depression-like behaviours in female rats.

In summary, the stressed rats, particularly R + S, showed an increase in spontaneous locomotor and exploratory activity, including the central zone of OF test and the vehicle-binging rats revealed the longest immobility time in FST. In this context, **41** pre-treatment did not impact the anxiety and depression-like behaviours in the control groups (NR + NS or NR + S or R + NS) and did not alter the emotional state detected in the binging rats.

## 5.4. Conclusions

The objective of this research activity was to synthesise and analyse ligands with remarkable  $\sigma_1$  receptor affinity and selectivity over the  $\sigma_2$  subtype. To this purpose, the benzo-cracking approach was applied to the potent  $\sigma_1$  receptor antagonist **119**, bearing the conformationally constrained 1,3-benzodioxane, to afford more flexible 1,3-dioxane compounds **40** and **41**. The *cis* and *trans* diastereomers of **42** and **43** were also prepared and studied to evaluate the effect of the increased distance between the two hydrophobic structural elements that flank the basic function. Derivatives **40** and **41** displayed a significantly higher  $\sigma_1$  receptor affinity compared to that of the lead compound **119**.

Particularly, **41** showed unprecedented selectivity over  $\sigma_2$  receptor, opioid receptor subtypes, the PCP site of the NMDA receptor, as well as over DAT. Docking results rationalized the affinity values of the ligands on the  $\sigma_1$  receptor, giving useful information about the binding mode of this series of compounds. Due to its interesting biological profile, derivative **41** was selected for *in vivo* studies, using a validated preclinical animal model of binge eating, to further investigate the role of the  $\sigma_1$  receptor on compulsive-like eating disorder. This compound was able to counteract the overeating of HPF only in bingeing rats, without affecting palatable food intake in the control group, as well as depression-related and anxiety-like behaviours in female rats. These findings strengthened the involvement of the  $\sigma_1$  receptor in compulsive-like eating behaviour, suggesting  $\sigma_1$  receptor antagonists as promising candidates for the treatment of bingeing episodes.

## 5.5. Experimental section

### 5.5.1. Synthesis of $\sigma_1$ ligands

#### 5.5.1.1. *Synthesis of 9-benzyl-2-phenyl-1,5-dioxo-9-azaspiro[5.5]undecane (40).*

A mixture of **122** (11.16 mmol), **124** (11.16 mmol) and p-toluenesulfonic acid (0.85 g, 4.85) in toluene (50 mL) was heated at reflux for 5 h. After the mixture was cooled, water was added. The aqueous phase was basified with 2N NaOH and extracted three times with  $\text{CHCl}_3$ . The organic phase was dried ( $\text{Na}_2\text{SO}_4$ ) and evaporated and the residue was purified by flash chromatography eluting with cyclohexane/EtOAc (7:3) to afford an oil (71% yield).  $^1\text{H}$  NMR ( $\text{CDCl}_3$ ):  $\delta$  7.42-7.21 (m, 10H), 4.98 (dd, 1H), 4.13 (m, 1H), 3.90 (m, 1H), 3.51 (m, 10H), 1.61-2.60 (m, 10H). ESI/MS: m/z 324.2  $[\text{M} + \text{H}]^+$ . The free base was

transformed into the oxalate salt that was crystallized from EtOH: m.p. 202-204 °C. Anal. Calcd for  $C_{21}H_{25}NO_2 \cdot H_2C_2O_4$ : C, 66.81%; H, 6.58%; N, 3.39%. Found: C, 67.05%; H, 6.42%; N, 3.50%.

#### 5.5.1.2. Synthesis of 9-benzyl-3-phenyl-1,5-dioxo-9-azaspiro[5.5]undecane (**41**).

This compound was synthesised from **123** and **124** according to the procedure described for **40**: an oil was obtained (70% yield).  $^1H$  NMR ( $CDCl_3$ ):  $\delta$  7.39-7.21 (m, 10H), 3.99 (m, 4H), 3.53 (s, 2H), 3.18 (m, 1H), 2.50 (m, 4H), 2.18 (m, 2H), 1.82 (m, 2H). ESI/MS: m/z 324.2  $[M + H]^+$ . The free base was transformed into the oxalate salt that was crystallized from EtOH: m.p. 211-212 °C. Anal. Calcd for  $C_{21}H_{25}NO_2 \cdot H_2C_2O_4$ : C, 66.81%; H, 6.58%; N, 3.39%. Found: C, 66.59%; H, 6.40%; N, 3.19%.

#### 5.5.1.3. Synthesis of 1-benzyl-4-(4-phenyl-1,3-dioxan-2-yl)piperidine (**42**).

This compound was synthesised from **122** and **125** according to the procedure described for **40**, to give a mixture of the diastereomers **42a** and **42b**, which were separated by flash chromatography, eluting with cyclohexane/EtOAc (95:5).

The isomer **42a** eluted first as an oil (15% yield).  $^1H$  NMR ( $CDCl_3$ ):  $\delta$  7.42-7.20 (m, 10H), 5.19 (m, 1H), 4.42 (d, 1H,  $J = 6.5$  Hz); 4.16 (m, 1H), 3.92 (m, 1H), 3.49 (s, 2H), 2.94 (m, 2H), 2.42-1.28 (m, 9H). ESI/MS: m/z 338.2  $[M + H]^+$ . The free base was transformed into the oxalate salt that was crystallized from 2-PrOH: m.p. 101-102 °C. Anal. Calcd for  $C_{22}H_{27}NO_2 \cdot H_2C_2O_4$ : C, 67.43%; H, 6.84%; N, 3.28%. Found: C, 67.27%, H, 6.96%; N, 3.50%.

The second fraction was the isomer **42b** (48% yield). <sup>1</sup>H NMR (CDCl<sub>3</sub>): δ 7.42-7.20 (m, 10H), 4.65 (dd, 1H, *J* = 11.3, 2.3 Hz), 4.48 (d, 1H, *J* = 5.6 Hz); 4.20 (m, 1H), 3.89 (m, 1H), 3.50 (s, 2H), 2.92 (m, 2H), 1.94-1.19 (m, 9H). ESI/MS: *m/z* 338.2 [M + H]<sup>+</sup>. The free base was transformed into the oxalate salt that was crystallized from EtOH: m.p. 161-162 °C. Anal. Calcd for C<sub>22</sub>H<sub>27</sub>NO<sub>2</sub>·H<sub>2</sub>C<sub>2</sub>O<sub>4</sub>: C, 67.43%; H, 6.84%; N, 3.28%. Found: C, 67.70%, H, 6.98%; N, 3.05%.

#### 5.5.1.4. Synthesis of 1-benzyl-4-(5-phenyl-1,3-dioxan-2-yl)piperidine (**43**)

This compound was synthesised from **123** and **125** according to the procedure described for **40**, to give a mixture of the diastereomers **43a** and **43b**, that were separated by flash chromatography eluting with cyclohexane/EtOAc (95:5).

The isomer **43a** eluted first as an oil (44% yield). <sup>1</sup>H NMR (CDCl<sub>3</sub>): δ 7.38-7.12 (m, 10H), 4.36 (d, 1H, *J* = 4.9 Hz), 4.17 (dd, 1H, *J* = 11.3, 4.5 Hz), 3.78 (dd, 1H, *J* = 11.3, 10.8 Hz), 3.50 (s, 2H), 3.18 (m, 1H), 2.88 (m, 2H), 1.98- 1.40 (m, 7H). ESI/MS: *m/z* 338.2 [M + H]<sup>+</sup>. The free base was transformed into the oxalate salt that was crystallized from 2-PrOH: m.p. 158-160 °C. Anal. Calcd for C<sub>22</sub>H<sub>27</sub>NO<sub>2</sub>·H<sub>2</sub>C<sub>2</sub>O<sub>4</sub>: C, 67.43%; H, 6.84%; N, 3.28%. Found: C, 67.55%, H, 6.70%; N, 3.48%.

The second fraction was the isomer **43b** (24% yield). <sup>1</sup>H NMR (CDCl<sub>3</sub>): δ 7.59-7.18 (m, 10H), 4.42 (d, 1H, *J* = 5.2 Hz), 4.18 (m, 4H), 3.50 (s, 2H), 2.92 (m, 2H), 2.61 (m, 1H), 1.97-1.42 (m, 7H). ESI/MS: *m/z* 338.2 [M + H]<sup>+</sup>. The free base was transformed into the oxalate salt that was crystallized from 2-PrOH: m.p. 111-112 °C. Anal. Calcd for

$C_{22}H_{27}NO_2 \cdot H_2C_2O_4$ : C, 67.43%; H, 6.84%; N, 3.28%. Found: C, 67.61%, H, 6.97%; N, 3.41%.

#### 5.5.1.5. *Synthesis of 1-phenylpropane-1,3-diol (122).*

A solution of **120** (4.23 mmol) in dry  $Et_2O$  (3 mL) was added dropwise to a suspension of  $LiAlH_4$  (4.5 mmol) in dry  $Et_2O$  (5 mL) at  $0^\circ C$  under a nitrogen atmosphere. The mixture was stirred for 2 h at room temperature, then it was poured onto ice and 2.5 M NaOH (12.65 mL) was added. After the precipitate was filtered off over Celite, the organic phase was dried ( $Na_2SO_4$ ). The evaporation of the solvent afforded a residue that was purified by flash chromatography eluting with cyclohexane/ $EtOAc$  (75:25) to give an oil (69% yield).  $^1H$  NMR ( $CDCl_3$ ):  $\delta$  7.36-7.25 (m, 5H), 4.88 (m, 1H), 3.79 (m, 2H), 3.24 (s, 2H), 1.86 (m, 2H).

#### 5.5.1.6. *Synthesis of 2-phenylpropane-1,3-diol (123).*

This compound was synthesised from **121** according to the procedure described for **122**: a white solid was obtained (72% yield). M.p. 49-50  $^\circ C$ .  $^1H$  NMR ( $CDCl_3$ ):  $\delta$  7.47-7.34 (m, 5H), 4.03-3.96 (m, 4H), 3.08 (m, 1H), 1.95 (s, 2H).

### 5.5.2. Radioligand binding assays

Commercially available rat liver, rat brains and guinea pig brains were used for the  $\sigma_1$ ,  $\sigma_2$ ,  $\mu$ -,  $\kappa$ - and  $\delta$ -opioid receptor binding assays. For the assay of binding to the PCP site of the NMDA receptor, pig brains were used, provided by a slaughterhouse in Germany



(local, as the assays were performed near Coesfeld, Germany). The organs were homogenized using Elvehjem Potter and Soniprep 150 homogenizers. Centrifuges used were a cooling centrifuge model Rotina 35R and a High-speed cooling centrifuge model Sorvall RC-5C plus. Standard 96-well plate multiplates were used. A self-made shaker was used to shake the samples. MicroBeta FilterMate-96 Harvester, Printed Filtermat Typ A and B filters, and Meltilex (Typ A or B) solid-state scintillator were used, and the MicroBeta Trilux scintillation analyzer was used.

A general procedure was applied for the preparation of all membranes. Tissues were cut into small pieces and homogenized in the first buffer. The suspension was then centrifuged for the first time, according to the parameters set for each tissue. The supernatant was removed, and the remaining pellet was resuspended in the same buffer, after which the second centrifugation is performed, under different settings. So obtained pellet was resuspended in the buffer and, in the case of the rat liver sample, incubated as reported. The final pellet was resuspended in the buffer and stored. In Table 13, the specifics for the preparation of membrane homogenates from the obtained tissues were given.

**Table 13.** Parameters for the preparation of membrane homogenates from 4 different tissues used for radioligand binding assays: rat liver, rat brain, guinea pig brain and pig brain cortex.

Parameter	Tissue type			
	Rat liver	Rat brain	Guinea pig brain	Pig brain cortex
<b>Homogenization parameters</b>	Elvehjem Potter homogenizer; 2 rat livers; 500-800 rpm, 10 up-and-down strokes, in 6 volumes of cold 0.32 M sucrose	Elvehjem Potter homogenizer; 5 rat brains (Sprague Dawley); 10 up-and-down strokes, in 6 volumes of cold 0.32 M sucrose	Elvehjem Potter homogenizer; 5 guinea pig brains; 10 up-and-down strokes, in 6 volumes of cold 0.32 M sucrose	Elvehjem Potter homogenizer; fresh pig cortex; 10 up-and-down strokes, in 6 volumes of cold 0.32 M sucrose
<b>First centrifugation settings</b>	1 200x g; 10 minutes at 4°C			
<b>Second centrifugation settings</b>	31 000x g; 20 minutes at 4 °C	23 500x g for 20 minutes at 4 °C	23 500x g for 20 minutes at 4 °C	31 000x g; 20 minutes at 4 °C
<b>Suspension buffer</b>	5-6 volumes of 50 mM TRIS, pH 8.0	5-6 volumes of 50 mM TRIS, pH 7.4	5-6 volumes of 50 mM TRIS, pH 7.4	5-6 volumes of TRIS/EDTA buffer = 5 mM: 1 mM, pH 7.5
<b>Incubation</b>	Room temperature, 30 minutes	/	/	/
<b>Third centrifugation settings</b>	31 000x g; 20 minutes at 4 °C	23 500x g for 20 minutes at 4 °C (repeated twice)	23 500x g for 20 minutes at 4 °C (repeated twice)	31 000x g; 20 minutes at 4 °C
<b>Storage</b>	-80°C, in 1.5 mL portions			
<b>Final protein weight per mL</b>	2 mg protein/mL	1.5 mg protein/mL	1.5 mg protein/mL	0.8 mg protein/mL

*5.5.2.1. Binding assays at  $\sigma_1$ ,  $\sigma_2$  receptors; PCP sites of NMDA receptors;  $\delta$ ,  $\kappa$ , and  $\mu$  opioid receptors*

The binding assays were conducted according to the general procedure as well, after the protein concentration was determined in the samples by measuring UV absorption, according to the Stoscheck-modified<sup>180</sup> Bradford method.<sup>181</sup>

According to the general procedure, 10  $\mu$ mol (2-4 mg) solutions of test compounds were further diluted in DMSO to obtain 10 mM stock. These stock solutions were later diluted

in respected assay buffers to obtain test solutions for the RBA. Filtermats were presoaked for 2 hours at room temperature in a 0.5 % aqueous solution of polyethylenimine. Standard 96-well plates were used as carriers for the experiments that were performed in duplicates. Final concentrations in the assays were noted unchanged. Serial dilutions were prepared according to the procedure under section 3.5.2., in concentrations:  $10^{-5}$ ,  $10^{-6}$ ,  $10^{-7}$ ,  $10^{-8}$ ,  $10^{-9}$  and  $10^{-10}$  mol/L. The preparations of the receptors were always added last to the wells. For the entire duration of the incubation period, the plates were shaken at 500- 600 rpm, at specific temperatures, as mentioned for each test. In most cases, unless reported otherwise, after 120 minutes, the assays were terminated by rapid filtration using the harvester, and the filters were washed five times in total using H<sub>2</sub>O (300  $\mu$ L). The filtermats were subsequently dried at 95 °C, and the scintillators were melted onto the surface of the dry filtermats (at 95 °C, for 5 minutes). After the temperature of such a system returned to room temperature, the remaining radioactivity on the filtermats was measured using a scintillation analyser. Each position on the filtermats corresponded to one well of the 96-well plate and was measured for a total of 5 minutes with [<sup>3</sup>H]-counting protocol (total counting efficiency: 20%). GraphPad Prism software was used for the calculation of IC<sub>50</sub> values by non-linear regression analysis, and these values were then converted into K<sub>i</sub> values via the Cheng-Prusoff equation. K<sub>i</sub> values were expressed as mean values  $\pm$  SEM from three independently-performed experiments. The individual parameters for performing RBA in  $\sigma_1$ ,  $\sigma_2$  receptors; PCP sites of NMDA receptors;  $\delta$ ,  $\kappa$ , and  $\mu$  opioid receptors are shown in Table 14.

**Table 14.** Individual parameters for performing RBA in  $\sigma_1$  and  $\sigma_2$  receptors; PCP sites of NMDA receptors;  $\delta$ ,  $\kappa$ , and  $\mu$  opioid receptors. r.t.-room temperature.

Parameter	Receptor type						
	$\sigma_1$	$\sigma_2$	PCP site of the NMDA receptor	$\delta$	$\kappa$	$\mu$ (guinea pig model)	$\mu$ (human model)
<b>Radioligand</b>	2 nM [ <sup>3</sup> H]-(+)-Pentazocine (22.0 Ci/mmol)	3 nM [ <sup>3</sup> H]DTG (50 Ci/mmol)	2 nM [ <sup>3</sup> H]-(+)-MK-801 (22.0 Ci/mmol)	3 nM [ <sup>3</sup> H]-DPDPE (69 Ci/mmol)	1 nM [ <sup>3</sup> H]-U-69593 (55 Ci/mmol)	3 nM [ <sup>3</sup> H]-DAMGO (51 Ci/mmol)	3 nM [ <sup>3</sup> H]-DAMGO (51 Ci/mmol)
<b>Membrane (thawed)</b>	Guinea pig brain	200,000 RT-4 cells / Rat liver	Pig brain	Rat brain	Guinea pig brain	Guinea pig brain	30 $\mu$ g/ well of HEK293 cells <sup>a</sup>
<b>Total protein used</b>	100 $\mu$ g	150 $\mu$ g (RT-4) / 100 $\mu$ g (rat liver)	100 $\mu$ g	75 $\mu$ g	100 $\mu$ g	100 $\mu$ g	100 $\mu$ g
<b>Buffer</b>	50 mM TRIS buffer, pH 7.4	500 nM (+)-pentazocine in 50 mM TRIS buffer, pH 8.0	TRIS-EDTA buffer (5 mM TRIS, 1 mM EDTA, pH 7.5)	TRIS-MgCl <sub>2</sub> -PMSF buffer (50 mM, 8 mM MgCl <sub>2</sub> , 400 $\mu$ M PMSF, pH 7.4)	50 mM TRIS- 8 mM MgCl <sub>2</sub> , pH 7.4	50 mM TRIS- 8 mM MgCl <sub>2</sub> , pH 7.4	50 mM TRIS- 5 mM MgCl <sub>2</sub> , pH 7.4
<b>Incubation temperature</b>	37 °C	37 °C	r.t.	37 °C	37 °C	37 °C	r.t. (60 minutes)
<b>Unlabelled receptor antagonist used (non-specific binding)</b>	10 $\mu$ M (+)-Pentazocine	10 $\mu$ M DTG	10 $\mu$ M (+)-MK-801	10 $\mu$ M Morphine	10 $\mu$ M U-69593	10 $\mu$ M Naloxon	10 $\mu$ M C-TOP or cold DAMGO
<b>K<sub>d</sub> value of the radioligand</b>	2.9 nM	8.3 nM (RT-4) / 17.9 nM (rat liver)	2.26 nM	0.65 nM	0.69 nM	0.57 nM	2.94 nM

<sup>a</sup> Cells were grown in DMEM medium, supplemented with 10% FBS, 2 mM L-glutamine, 1% penicillin-streptomycin and 50  $\mu$ g/mL of hygromycin B, until 80-90% confluence. Cell solutions were prepared according to the procedure under section 3.5.2.

#### 5.5.2.2. *DAT radioligand binding assays*

From the adult male rat brains (Sprague-Dawley rats) commercially obtained, frozen brain striata was obtained and homogenised in 10-20 volumes (w/ v) of the modified sucrose phosphate buffer (0.32 M sucrose, 7.74 mM Na<sub>2</sub>HPO<sub>4</sub>, 2.26 mM NaH<sub>2</sub>PO<sub>4</sub>; adjusted to pH = 7.4, at 25 °C). Brinkman Polytron was used for homogenisation in two cycles of 10 minutes, at setting 6. The homogenised sample was centrifuged for 10 minutes at 20 000 rpm, at 4 °C, after which the pellet was resuspended in a cold buffer and centrifuged once more. So obtained pellet was resuspended in a cold buffer in a concentration of 15 mg/mL original wet weight.

On the day of the test, the test compounds were dissolved in a 30% aqueous solution of DMSO until reaching a concentration of 1 mM or 100 µM. For stabilisation of the free base compounds, 10 µL of glacial acetic acid was added together with DMSO (in place of the final H<sub>2</sub>O volume of 10 µl). Every test compound was further diluted with a 30% aqueous solution of DMSO into 10 half-long serial dilutions.

Cell solutions for the RBA were prepared as mentioned under section 3.5.2. The aliquots of [<sup>3</sup>H]-WIN35,428 solution were also quantified precisely, to determine the amount of radioactivity added to the samples.

Non-specific binding was evaluated by the use of 10 µL Indatraline, while the total binding was assessed as mentioned under section 3.5.2.

RBA was performed in triplicates and it was initiated by the addition of the tissue. The reaction was incubated for 120 minutes, at 4 °C. After the incubation, the reaction was terminated by filtering, as described under section 3.5.2. The K<sub>d</sub> value for the used

radioligand ( $[^3\text{H}]$ -WIN35,428) was obtained through the homologous competitive binding experiments (performed separately). GraphPad Prism Software was used for the analysis; all  $K_i$  values are reported as mean values of triplicates  $\pm$  SEM.

### **5.5.3. In vivo functional assays**

#### *5.5.3.1. Binge-eating in vivo experiments*

Adult female Sprague Dawley rats were used for the experiment. Their weight was 200-225 g before the experiment was initiated. The rats were housed in a 12-hour light/dark cycle starting from 9:00 AM, Central European Time. The temperature was kept between 20 and 22 °C, the humidity at 45- 55 %, and the animals had unrestricted access to water and food (standard food pellets, 4RF18) during the 7 days preceding the beginning of the experiment. The experiments were conducted according to the European directive 2010/63/UE on animal welfare, as well as with the Italian Ministry of Health guidelines for the care and use of laboratory animals. HPF used for the binge-eating protocol<sup>170</sup> was a paste offered in a china coffee cup, made up of 52% Nutella chocolate cream, 33% of the 4RF18 food pellets and 15% H<sub>2</sub>O.

The animals were divided into 4 groups: NR + NS, NR + S, R + NS, and R + S, as described before. The animals were either exposed or not exposed (depending on the test group) to three 8-day cycles (a total of 24 days) of food restriction/refeeding. This period served to familiarise the animals with the HPF. On the day of the binge intake test, NR+NS and R+NS groups were able to freely access food for 120 minutes, while the NR+S and R+S groups had free access only after applying 15 minutes of stress (the animals could smell and see the food, but not access it). During the stress exposure, rats

would show several signs of stress: repeated movement of front paws, head and trunk in the direction of HPF. When the food was subsequently moved into the cage, the food intake was documented for a total period of 120 minutes. “Binge-eating episode” was considered every significantly higher HSP intake in the RS test group, during the period of the experiment (120 minutes), when compared to the other experimental conditions (NR + NS, NR + S, R + NS). Immediately upon the completion of the test, vaginal smears were taken and analysed to determine the ovarian phase. The conclusion was that the binge-eating episodes in the used animal model<sup>182</sup> were not present during the oestrous phase,<sup>183,184</sup> so all rats in this phase were automatically excluded from the experiments.

#### *5.5.3.2. Behavioural tests*

OF test was performed for all rat test groups, to evaluate their locomotor activity, exploration behaviour, and anxiety-like behaviour.<sup>185</sup> These parameters were analysed over 10 minutes: total distance the animal travelled, total vertical counts; jump counts; stereotypic counts and the number of animal entrances to the central zone. To assess these parameters, commercially available automated locomotor activity boxes were used. These were square plastic boxes with an arena of 43 cm<sup>2</sup>, and a central zone of 25 cm<sup>2</sup>, used to quantify the animals’ spontaneous activity for the duration of the experiment. The locomotor activity of the animals was automatically recorded via software, as the animals would pass and interrupt one of the two orthogonal light beams above the activity box (one was set at 3.5, and the other one at 13 cm). If an increased locomotor activity would be detected, this behaviour was noted as “arousal”, while the decreased activity in the central zone, as well as in other entries, were considered signs of anxiety-like behaviour

(emotionality, anxiety, fear).<sup>182,186</sup> The apparatus was cleaned with 70% EtOH, and dried with a dry cloth between test sessions.

FST is a well-known test<sup>178</sup> used for the analysis of depression-like behaviour in rodents. The test was performed within a transparent cylinder filled with H<sub>2</sub>O at room temperature (23-25 °C), and it was conducted for 5 minutes. The amount of H<sub>2</sub>O in the cylinder had to be high enough so that the rat's tail would not be able to touch the bottom of the cylinder, but high enough for the animal to be unable to climb out of the cylinder.<sup>187</sup> The "depression-like behaviour" would be considered the period of immobility of the animal, floating to keep their head above the water, and the duration of such period/s.<sup>178,188,189</sup> The rats were submitted to two swimming sessions held 24 hours apart. The first session lasted 15 minutes, while the second one lasted 5 minutes. Only the second session was monitored. The water was changed after every trial, and the animals were gently towel-dried after the test.

#### 5.5.3.3. *Statistical analysis*

All data were expressed as the mean of the reported values  $\pm$  SEM. Feeding data shown in Figure 36A (left panel) were statistically analysed by a three-way ANOVA test for repeated measures. The set parameters were: food restriction (no, yes), and stress (no, yes) as the between-subjects factors; with sessions time (0-15, 15-30, 30-60, 60-120 min) as the within-subject factor. The data shown in Figure 36B (right panel) was analysed via a two-way ANOVA test. The set parameters were: food restriction (no, yes) and stress (no, yes). All other panels shown in Figure 36B-E were analysed via one-way ANOVA and were treated as between-subject factors.



OF and FST were analysed via a three-way ANOVA test. The set parameters were: food restriction (no, yes), stress (no, yes) and treatment (no, yes) as the between-subjects factors. Bonferroni's *post hoc* tests were performed to follow up on significant interaction or main effects ( $P < 0.05$ ) from the factorial ANOVA tests. Systat Software was used to perform the statistical analysis.

## 6. REFERENCES

- (1) Ehrlich, P. Über Den Jetzigen Stand Der Chemotherapie. *Berichte der deutschen chemischen Gesellschaft* **1909**, 42 (1), 17–47.
- (2) Gund, P. Three-Dimensional Pharmacophoric Pattern Searching. *Progress in molecular and subcellular biology* **1977**, 5, 117–143.
- (3) Wermuth, C.; Ganellin, C.; Lindberg, P.; Mitscher, L. Glossary of Terms Used in Medicinal Chemistry (IUPAC Recommendations 1998). *Pure and applied Chemistry* **1998**, 70 (5), 1129–1143.
- (4) Jaber, M., Robinson, S. W., Missale, C., Caron, M.G. Dopamine Receptors and Brain Function. *Neuropharmacology* **1996**, 35 (11), 1503–1519.
- (5) Missale, C., Nash, S. R., Robinson, S. W., Jaber, M., Caron, M. G. Dopamine Receptors: From Structure to Function. *Physiological Reviews* **1998**, 78 (1), 189–225. <https://doi.org/10.1152/physrev.1998.78.1.189>.
- (6) Latif, S., Jahangeer, M., Razia, D. M., Ashiq, M., Ghaffar, A., Akram, M., El Allam, A., Bouyahya, A., Garipova, L., Shariati, M. A., Thiruvengadam, M., Ansari, M. A. Dopamine in Parkinson's Disease. *Clinica Chimica Acta* **2021**, 522, 114–126. <https://doi.org/10.1016/j.cca.2021.08.009>.
- (7) Giorgioni, G., Del Bello, F., Pavletić, P., Quaglia, W., Botticelli, L., Cifani, C., Micioni Di Bonaventura, E., Micioni Di Bonaventura, M. V., Piergentili, A. Recent Findings Leading to the Discovery of Selective Dopamine D4 Receptor Ligands for the Treatment of Widespread Diseases. *European Journal of Medicinal Chemistry* **2021**, 212, 113–141. <https://doi.org/10.1016/j.ejmech.2020.113141>.

- (8) Oak, J. N., Oldenhof, J., Van Tol, H. H. M. The Dopamine D4 Receptor: One Decade of Research. *European Journal of Pharmacology* **2000**, *405* (1–3), 303–327. [https://doi.org/10.1016/S0014-2999\(00\)00562-8](https://doi.org/10.1016/S0014-2999(00)00562-8).
- (9) Pavletić, P.; Semeano, A.; Yano, H.; Bonifazi, A.; Giorgioni, G.; Piergentili, A.; Quaglia, W.; Sabbieti, M. G.; Agas, D.; Santoni, G.; Pallini, R.; Ricci-Vitiani, L.; Sabato, E.; Vistoli, G.; Del Bello, F. Highly Potent and Selective Dopamine D4 Receptor Antagonists Potentially Useful for the Treatment of Glioblastoma. *J. Med. Chem.* **2022**, *65* (18), 12124–12139. <https://doi.org/10.1021/acs.jmedchem.2c00840>.
- (10) Bhatia A., Lenchner J. R., Saadabadi A. *Biochemistry, Dopamine Receptors*, Treasure Island (FL); StatPearls Publishing, 2022.
- (11) Martel, J. C.; Gatti McArthur, S. Dopamine Receptor Subtypes, Physiology and Pharmacology: New Ligands and Concepts in Schizophrenia. *Frontiers in Pharmacology* **2020**, *11*.
- (12) Valerio, A.; Belloni, M.; Gorno, M. L.; Tinti, C.; Memo, M.; Spano, P. Dopamine D2, D3, and D4 Receptor mRNA Levels in Rat Brain and Pituitary during Aging. *Neurobiology of Aging* **1994**, *15* (6), 713–719. [https://doi.org/10.1016/0197-4580\(94\)90053-1](https://doi.org/10.1016/0197-4580(94)90053-1).
- (13) Van Tol, H. H. M.; Bunzow, J. R.; Guan, H.-C.; Sunahara, R. K.; Seeman, P.; Niznik, H. B.; Civelli, O. Cloning of the Gene for a Human Dopamine D4 Receptor with High Affinity for the Antipsychotic Clozapine. *Nature* **1991**, *350* (6319), 610–614. <https://doi.org/10.1038/350610a0>.
- (14) Ptáček, R.; Kuželová, H.; Stefano, G. B. Dopamine D4 Receptor Gene DRD4 and Its Association with Psychiatric Disorders. *Medical science monitor: international medical journal of experimental and clinical research* **2011**, *17* (9), RA215.

- (15) Schaber, G.; Stevens, I.; Gaertner, H.; Dietz, K.; Breyer-Pfaff, U. Pharmacokinetics of Clozapine and Its Metabolites in Psychiatric Patients: Plasma Protein Binding and Renal Clearance. *British journal of clinical pharmacology* **1998**, *46* (5), 453.
- (16) Kulkarni, S. K.; Ninan, I. Dopamine D4 Receptors and Development of Newer Antipsychotic Drugs. *Fundamental & Clinical Pharmacology* **2000**, *14* (6), 529–539. <https://doi.org/10.1111/j.1472-8206.2000.tb00437.x>.
- (17) Kramer, M. S.; Last, B.; Getson, A.; Reines, S. A. The Effects of a Selective D4 Dopamine Receptor Antagonist (L-745,870) in Acutely Psychotic Inpatients With Schizophrenia. *Archives of General Psychiatry* **1997**, *54* (6), 567–572. <https://doi.org/10.1001/archpsyc.1997.01830180085011>.
- (18) Smita Patel; Stephen Freedman; Kerry L. Chapman; Frances Emms; Alan E. Fletcher; Mick Knowles; Rosemarie Marwood; George Mcallister; Jan Myers; Shil Patel; Neil Curtis; Jan J. Kulagowski; Paul D. Leeson; Mark Ridgill; Mike Graham; Steve Matheson; Denise Rathbone; Alan P. Watt; Linda J. Bristow; Nadia M. J. Rupniak; Elizabeth Baskin; Joseph J. Lynch; C. Ian Ragan. Biological Profile of L-745,870, a Selective Antagonist with High Affinity for the Dopamine D4 Receptor. *Journal of Pharmacology and Experimental Therapeutics* **1997**, *283* (2), 636.
- (19) Linda J. Bristow; Neil Collinson; Gina P. Cook; Neil Curtis; Stephen B. Freedman; Janusz J. Kulagowski; Paul D. Leeson; Smita Patel; C. Ian Ragan; Mark Ridgill; Kay L. Saywell; Mark D. Tricklebank. L-745,870, a Subtype Selective Dopamine D<sub>4</sub> Receptor Antagonist, Does Not Exhibit a Neuroleptic-Like Profile in Rodent Behavioral Tests. *J Pharmacol Exp Ther* **1997**, *283* (3), 1256.
- (20) Rosas-Cruz, A.; Salinas-Jazmín, N.; Velázquez, M. A. V.-. Dopamine Receptors in Cancer: Are They Valid Therapeutic Targets? *Technology in Cancer Research & Treatment* **2021**, *20*, 1–13. <https://doi.org/10.1177/15330338211027913>.

- (21) Dolma, S.; Selvadurai, H. J.; Lan, X.; Lee, L.; Kushida, M.; Voisin, V.; Whetstone, H.; So, M.; Aviv, T.; Park, N.; Zhu, X.; Xu, C.; Head, R.; Rowland, K. J.; Bernstein, M.; Clarke, I. D.; Bader, G.; Harrington, L.; Brumell, J. H.; Tyers, M.; Dirks, P. B. Inhibition of Dopamine Receptor D4 Impedes Autophagic Flux, Proliferation, and Survival of Glioblastoma Stem Cells. *Cancer Cell* **2016**, *29* (6), 859–873. <https://doi.org/10.1016/j.ccell.2016.05.002>.
- (22) Löber, S.; Hübner, H.; Tschammer, N.; Gmeiner, P. Recent Advances in the Search for D3- and D4-Selective Drugs: Probes, Models and Candidates. *Trends in Pharmacological Sciences* **2011**, *32* (3), 148–157. <https://doi.org/10.1016/j.tips.2010.12.003>.
- (23) Ye, N.; Neumeier, J. L.; Baldessarini, R. J.; Zhen, X.; Zhang, A. Update 1 of: Recent Progress in Development of Dopamine Receptor Subtype-Selective Agents: Potential Therapeutics for Neurological and Psychiatric Disorders. *Chem. Rev* **2013**, *113* (5), 274–302.
- (24) Zhou, Y.; Cao, C.; He, L.; Wang, X.; Zhang, X. C. Crystal Structure of Dopamine Receptor D4 Bound to the Subtype Selective Ligand, L745870. *Elife* **2019**, *8*, e48822. <https://doi.org/10.7554/eLife.48822>.
- (25) Wang, S.; Wacker, D.; Levit, A.; Che, T.; Betz, R. M.; McCorvy, J. D.; Venkatakrishnan, A. J.; Huang, X.-P.; Dror, R. O.; Shoichet, B. K.; Roth, B. L. D4 Dopamine Receptor High-Resolution Structures Enable the Discovery of Selective Agonists. *Science* **2017**, *358* (6361), 381–386. <https://doi.org/10.1126/science.aan5468>.
- (26) Del Bello, F.; Bonifazi, A.; Giorgioni, G.; Cifani, C.; Micioni Di Bonaventura, M. V.; Petrelli, R.; Piergentili, A.; Fontana, S.; Mammoli, V.; Yano, H.; Matucci, R.; Vistoli, G.; Quaglia, W. 1-[3-(4-Butylpiperidin-1-Yl)Propyl]-1,2,3,4-Tetrahydroquinolin-2-One (77-LH-28-1) as a Model for the Rational Design of a Novel Class of Brain Penetrant Ligands with High Affinity and Selectivity for Dopamine D4 Receptor. *Journal of Medicinal Chemistry* **2018**, *61* (8), 3712–3725. <https://doi.org/10.1021/acs.jmedchem.8b00265>.

- (27) Lindsley, C. W.; Hopkins, C. R. Return of D4 Dopamine Receptor Antagonists in Drug Discovery. *J. Med. Chem.* **2017**, *60* (17), 7233–7243. <https://doi.org/10.1021/acs.jmedchem.7b00151>.
- (28) Ertl, P. Craig Plot 2.0: An Interactive Navigation in the Substituent Bioisosteric Space. *Journal of Cheminformatics* **2020**, *12* (1), 8. <https://doi.org/10.1186/s13321-020-0412-1>.
- (29) Yarim, M.; Koksal, M.; Schepmann, D.; Wünsch, B. Synthesis and in Vitro Evaluation of Novel Indole-Based Sigma Receptors Ligands. *Chemical Biology & Drug Design* **2011**, *78* (5), 869–875. <https://doi.org/10.1111/j.1747-0285.2011.01215.x>.
- (30) Zhou, Y.; Zhang, L.; Zhou, J.; Zhou, X. Benzo Five-Membered Nitrogen Heterocyclic Piperidine or Piperazine Derivatives and Preparation Methods and Pharmaceutical Compositions Thereof. US 9,802,929 B2, 2017. <https://patentimages.storage.googleapis.com/03/c4/da/c8cdf55c23dc92/US9802929.pdf>.
- (31) Mokrosz, J. L.; Duszyńska, B.; Paluchowska, M. H. Structure-Activity Relationship Studies of CNS Agents, XV: N-[ $\omega$ -(4-Aryl-1-Piperazinyl)Alkyl]-2-Oxo-1,2,3,4-Tetrahydroquinolines and -4-Oxo-1,2,3,4-Tetrahydropyrazino[1,2-a]Indoles: New, Highly Potent 5-HT<sub>1A</sub> Ligands  $\Omega$ N-[ $\omega$ -(4-Aryl-1-Piperazinyl)Alkyl]-2-Oxo-1,2,3,4-Tetrahydroquinoline Und -4-Oxo-1,2,3,4-Tetrahydropyrazino-[1,2-a]Indole: Neue Starke 5-HT<sub>1A</sub> Liganden. *Archiv der Pharmazie* **1994**, *327* (8), 529–531. <https://doi.org/10.1002/ardp.19943270811>.
- (32) López, L.; Selent, J.; Ortega, R.; Masaguer, C. F.; Domínguez, E.; Areias, F.; Brea, J.; Loza, M. I.; Sanz, F.; Pastor, M. Synthesis, 3D-QSAR, and Structural Modeling of Benzolactam Derivatives with Binding Affinity for the D<sub>2</sub> and D<sub>3</sub> Receptors. *ChemMedChem* **2010**, *5* (8), 1300–1317. <https://doi.org/10.1002/cmdc.201000101>.
- (33) Oshiro, Y.; Sakurai, Y.; Sato, S.; Kurahashi, N.; Tanaka, T.; Kikuchi, T.; Tottori, K.; Uwahodo, Y.; Miwa, T.; Nishi, T. 3,4-Dihydro-2(1H)-Quinolinone as a Novel Antidepressant Drug:

Synthesis and Pharmacology of 1-[3-[4-(3-Chlorophenyl)-1-Piperazinyl]Propyl]-3,4-Dihydro-5-Methoxy-2(1H)-Quinolinone and Its Derivatives. *J. Med. Chem.* **2000**, *43* (2), 177–189. <https://doi.org/10.1021/jm980333v>.

(34) Amélia Santos, M.; Marques, S. M.; Tuccinardi, T.; Carelli, P.; Panelli, L.; Rossello, A. Design, Synthesis and Molecular Modeling Study of Iminodiacetyl Monohydroxamic Acid Derivatives as MMP Inhibitors. *Bioorganic & Medicinal Chemistry* **2006**, *14* (22), 7539–7550. <https://doi.org/10.1016/j.bmc.2006.07.011>.

(35) Na, Y. H.; Hong, S. H.; Lee, J. H.; Park, W.-K.; Baek, D.-J.; Koh, H. Y.; Cho, Y. S.; Choo, H.; Pae, A. N. Novel Quinazolinone Derivatives as 5-HT<sub>7</sub> Receptor Ligands. *Bioorganic & Medicinal Chemistry* **2008**, *16* (5), 2570–2578. <https://doi.org/10.1016/j.bmc.2007.11.049>.

(36) Sampson, D.; Zhu, X. Y.; Eyunni, S. V. K.; Etukala, J. R.; Ofori, E.; Bricker, B.; Lamango, N. S.; Setola, V.; Roth, B. L.; Ablordeppey, S. Y. Identification of a New Selective Dopamine D<sub>4</sub> Receptor Ligand. *Bioorganic & Medicinal Chemistry* **2014**, *22* (12), 3105–3114. <https://doi.org/10.1016/j.bmc.2014.04.026>.

(37) Zhu, X. Y.; Etukala, J. R.; Eyunni, S. V. K.; Setola, V.; Roth, B. L.; Ablordeppey, S. Y. Benzothiazoles as Probes for the 5HT<sub>1A</sub> Receptor and the Serotonin Transporter (SERT): A Search for New Dual-Acting Agents as Potential Antidepressants. *European Journal of Medicinal Chemistry* **2017**, *53*, 124–132. <https://doi.org/10.1016/j.ejmech.2012.03.042>.

(38) Zhou, B.; Hong, K. H.; Ji, M.; Cai, J. Design, Synthesis, and Biological Evaluation of Structurally Constrained Hybrid Analogues Containing Ropinirole Moiety as a Novel Class of Potent and Selective Dopamine D<sub>3</sub> Receptor Ligands. *Chemical Biology & Drug Design* **2018**, *92* (3), 1597–1609. <https://doi.org/10.1111/cbdd.13324>.

(39) Zampieri, D.; Vio, L.; Fermeiglia, M.; Pricl, S.; Wünsch, B.; Schepmann, D.; Romano, M.; Mamolo, M. G.; Laurini, E. Computer-Assisted Design, Synthesis, Binding and Cytotoxicity

Assessments of New 1-(4-(Aryl(Methyl)Amino)Butyl)-Heterocyclic Sigma 1 Ligands. *Therapeutic Approaches of Diseases Related to Misfolded Proteins* **2016**, 121, 712–726. <https://doi.org/10.1016/j.ejmech.2016.06.001>.

(40) Andersen, K.; Bang-Andersen, B.; Felding, J.; Smith, G. Indole Derivatives Useful for the Treatment of Cns Disorders. *WO2001098298 A1* **2001**.

(41) Sams, A. G.; Hentzer, M.; Mikkelsen, G. K.; Larsen, K.; Bundgaard, C.; Plath, N.; Christoffersen, C. T.; Bang-Andersen, B. Discovery of N-{1-[3-(3-Oxo-2,3-Dihydrobenzo[1,4]Oxazin-4-Yl)Propyl]Piperidin-4-Yl}-2-Phenylacetamide (Lu AE51090): An Allosteric Muscarinic M1 Receptor Agonist with Unprecedented Selectivity and Procognitive Potential. *Journal of Medicinal Chemistry* **2010**, 53 (17), 6386–6397. <https://doi.org/10.1021/jm100697g>.

(42) Shaik, A. B.; Boateng, C. A.; Battiti, F. O.; Bonifazi, A.; Cao, J.; Chen, L.; Chitsazi, R.; Ravi, S.; Lee, K. H.; Shi, L.; Newman, A. H. Structure Activity Relationships for a Series of Eticlopride-Based Dopamine D2/D3 Receptor Bitopic Ligands. *J. Med. Chem.* **2021**, 64 (20), 15313–15333. <https://doi.org/10.1021/acs.jmedchem.1c01353>.

(43) Keck, T. M.; Free, R. B.; Day, M. M.; Brown, S. L.; Maddaluna, M. S.; Fountain, G.; Cooper, C.; Fallon, B.; Holmes, M.; Stang, C. T.; Burkhardt, R.; Bonifazi, A.; Ellenberger, M. P.; Newman, A. H.; Sibley, D. R.; Wu, C.; Boateng, C. A. Dopamine D4 Receptor-Selective Compounds Reveal Structure–Activity Relationships That Engender Agonist Efficacy. *J. Med. Chem.* **2019**, 62 (7), 3722–3740. <https://doi.org/10.1021/acs.jmedchem.9b00231>.

(44) Stewart, A. O.; Cowart, M. D.; Moreland, R. B.; Latshaw, S. P.; Matulenko, M. A.; Bhatia, P. A.; Wang, X.; Daanen, J. F.; Nelson, S. L.; Terranova, M. A.; Namovic, M. T.; Donnelly-Roberts, D. L.; Miller, L. N.; Nakane, M.; Sullivan, J. P.; Brioni, J. D. Dopamine D4 Ligands and Models of Receptor Activation: 2-(4-Pyridin-2-Ylpiperazin-1-Ylmethyl)-1H-Benzimidazole and Related



Heteroaryl-methyl-aryl-piperazines Exhibit a Substituent Effect Responsible for Additional Efficacy Tuning. *J. Med. Chem.* **2004**, *47* (9), 2348–2355. <https://doi.org/10.1021/jm0305669>.

(45) Grimme, S. Do Special Noncovalent  $\pi$ – $\pi$  Stacking Interactions Really Exist? *Angewandte Chemie International Edition* **2008**, *47* (18), 3430–3434. <https://doi.org/10.1002/anie.200705157>.

(46) Martinez, C. R.; Iverson, B. L. Rethinking the Term “Pi-Stacking.” *Chemical Science* **2012**, *3* (7), 2191–2201. <https://doi.org/10.1039/c2sc20045g>.

(47) Wang, S.; Che, T.; Levit, A.; Shoichet, B. K.; Wacker, D.; Roth, B. L. Structure of the D2 Dopamine Receptor Bound to the Atypical Antipsychotic Drug Risperidone. *Nature* **2018**, *555* (7695), 269–273. <https://doi.org/10.1038/nature25758>.

(48) Le Guilloux, V.; Schmidtke, P.; Tuffery, P. Fpocket: An Open Source Platform for Ligand Pocket Detection. *BMC Bioinformatics* **2009**, *10* (1), 168. <https://doi.org/10.1186/1471-2105-10-168>.

(49) Pedretti, A.; Mazzolari, A.; Gervasoni, S.; Fumagalli, L.; Vistoli, G. The VEGA Suite of Programs: An Versatile Platform for Cheminformatics and Drug Design Projects. *Bioinformatics* **2021**, *37* (8), 1174–1175. <https://doi.org/10.1093/bioinformatics/btaa774>.

(50) Thomas, T.; Fang, Y.; Yuriev, E.; Chalmers, D. K. Ligand Binding Pathways of Clozapine and Haloperidol in the Dopamine D2 and D3 Receptors. *Journal of Chemical Information and Modeling* **2016**, *56* (2), 308–321.

(51) Bootsma, A. N.; Doney, A. C.; Wheeler, S. E. Predicting the Strength of Stacking Interactions between Heterocycles and Aromatic Amino Acid Side Chains. *Journal of the American Chemical Society* **2019**, *141* (28), 11027–11035. <https://doi.org/10.1021/jacs.9b00936>.

(52) Matsson, P.; Doak, B. C.; Over, B.; Kihlberg, J. Cell Permeability beyond the Rule of 5. *Advanced Drug Delivery Reviews* **2016**, *101*, 42–61. <https://doi.org/10.1016/j.addr.2016.03.013>.

- (53) Daina, A.; Michielin, O.; Zoete, V. SwissADME: A Free Web Tool to Evaluate Pharmacokinetics, Drug-Likeness and Medicinal Chemistry Friendliness of Small Molecules. *Scientific reports* **2017**, *7* (1), 42717.
- (54) Mazzolari, A.; Scaccabarozzi, A.; Vistoli, G.; Pedretti, A. MetaClass, a Comprehensive Classification System for Predicting the Occurrence of Metabolic Reactions Based on the MetaQSAR Database. *Molecules* **2021**, *26* (19), 5857. <https://doi.org/10.3390/molecules26195857>.
- (55) Van Niffterik, K.; Van Den Berg, J.; Van Der Meide, W.; Ameziane, N.; Wedekind, L.; Steenbergen, R.; Leenstra, S.; Lafleur, M.; Slotman, B.; Stalpers, L. Absence of the MGMT Protein as Well as Methylation of the MGMT Promoter Predict the Sensitivity for Temozolomide. *British journal of cancer* **2010**, *103* (1), 29–35. <https://doi.org/10.1038/sj.bjc.6605712>.
- (56) Singh, N.; Miner, A.; Hennis, L.; Mittal, S. Mechanisms of Temozolomide Resistance in Glioblastoma - a Comprehensive Review. *Cancer Drug Resistance* **2021**, *4* (1), 17–43. <https://doi.org/10.20517/cdr.2020.79>.
- (57) Stupp, R.; Brada, M.; Van Den Bent, M.; Tonn, J.-C.; Pentheroudakis, G. High-Grade Glioma: ESMO Clinical Practice Guidelines for Diagnosis, Treatment and Follow-Up. *Annals of oncology* **2014**, *25*, iii93–iii101.
- (58) Yung-Chi, C.; Prusoff, W. H. Relationship between the Inhibition Constant (KI) and the Concentration of Inhibitor Which Causes 50 per Cent Inhibition (I50) of an Enzymatic Reaction. *Biochemical Pharmacology* **1973**, *22* (23), 3099–3108. [https://doi.org/10.1016/0006-2952\(73\)90196-2](https://doi.org/10.1016/0006-2952(73)90196-2).
- (59) Chien, E. Y. T.; Liu, W.; Zhao, Q.; Katritch, V.; Won Han, G.; Hanson, M. A.; Shi, L.; Newman, A. H.; Javitch, J. A.; Cherezov, V.; Stevens, R. C. Structure of the Human Dopamine

D3 Receptor in Complex with a D2/D3 Selective Antagonist. *Science* **2010**, 330 (6007), 1091–1095. <https://doi.org/10.1126/science.1197410>.

(60) Michino, M.; Beuming, T.; Donthamsetti, P.; Newman, A. H.; Javitch, J. A.; Shi, L. What Can Crystal Structures of Aminergic Receptors Tell Us about Designing Subtype-Selective Ligands? *Pharmacological Reviews* **2015**, 67 (1), 198–213. <https://doi.org/10.1124/pr.114.009944>.

(61) Martí-Renom, M. A.; Stuart, A. C.; Fiser, A.; Sánchez, R.; Melo, F.; Šali, A. Comparative Protein Structure Modeling of Genes and Genomes. *Annual Review of Biophysics and Biomolecular Structure* **2000**, 29 (1), 291–325. <https://doi.org/10.1146/annurev.biophys.29.1.291>.

(62) Gordon, J. C.; Myers, J. B.; Folta, T.; Shoja, V.; Heath, L. S.; Onufriev, A. H<sup>++</sup>: A Server for Estimating pK<sub>a</sub>s and Adding Missing Hydrogens to Macromolecules. *Nucleic acids research* **2005**, 33 (suppl\_2), W368–W371. <https://doi.org/10.1093/nar/gki464>.

(63) Stewart, J. J. P. Optimization of Parameters for Semiempirical Methods VI: More Modifications to the NDDO Approximations and Re-Optimization of Parameters. *Journal of Molecular Modeling* **2013**, 19 (1), 1–32. <https://doi.org/10.1007/s00894-012-1667-x>.

(64) Pedretti, A.; Granito, C.; Mazzolari, A.; Vistoli, G. Structural Effects of Some Relevant Missense Mutations on the MECP2-DNA Binding: A MD Study Analyzed by Rescore+, a Versatile Rescoring Tool of the VEGA ZZ Program. *Molecular Informatics* **2016**, 35 (8–9), 424–433. <https://doi.org/10.1002/minf.201501030>.

(65) Santoni, G.; Amantini, C.; Nabissi, M.; Maggi, F.; Arcella, A.; Marinelli, O.; Eleuteri, A. M.; Santoni, M.; Morelli, M. B. Knock-down of Muco1ipin 1 Channel Promotes Tumor Progression and Invasion in Human Glioblastoma Cell Lines. *Frontiers in Oncology* **2021**, 11, 578928. <https://doi.org/10.3389/fonc.2021.578928>.

- (66) Ricci-Vitiani, L.; Pallini, R.; Biffoni, M.; Todaro, M.; Invernici, G.; Cenci, T.; Maira, G.; Parati, E. A.; Stassi, G.; Larocca, L. M.; De Maria, R. Tumour Vascularization via Endothelial Differentiation of Glioblastoma Stem-like Cells. *Nature* **2010**, *468* (7325), 824–828. <https://doi.org/10.1038/nature09557>.
- (67) Agas, D.; Amaroli, A.; Lacava, G.; Yanagawa, T.; Sabbieti, M. G. Loss of P62 Impairs Bone Turnover and Inhibits PTH-Induced Osteogenesis. *Journal of Cellular Physiology* **2020**, *235* (10), 7516–7529. <https://doi.org/10.1002/jcp.29654>.
- (68) Yao, W.-D.; Spealman, R. D.; Zhang, J. Dopaminergic Signaling in Dendritic Spines. *Biochemical Pharmacology* **2008**, *75* (11), 2055–2069. <https://doi.org/10.1016/j.bcp.2008.01.018>.
- (69) Kabbani, N.; Levenson, R. A Proteomic Approach to Receptor Signaling: Molecular Mechanisms and Therapeutic Implications Derived from Discovery of the Dopamine D2 Receptor Signalplex. *European Journal of Pharmacology* **2007**, *572* (2), 83–93. <https://doi.org/10.1016/j.ejphar.2007.06.059>.
- (70) Skieterska, K.; Rondou, P.; Van Craenenbroeck, K. Dopamine D4 Receptor Ubiquitination. *Biochemical Society Transactions* **2016**, *44* (2), 601–605.
- (71) Deshaies, R. J.; Joazeiro, C. A. P. RING Domain E3 Ubiquitin Ligases. *Annual Review of Biochemistry* **2009**, *78* (1), 399–434. <https://doi.org/10.1146/annurev.biochem.78.101807.093809>.
- (72) Rondou, P.; Skieterska, K.; Packeu, A.; Lintermans, B.; Vanhoenacker, P.; Vauquelin, G.; Haegeman, G.; Van Craenenbroeck, K. KLHL12-Mediated Ubiquitination of the Dopamine D4 Receptor Does Not Target the Receptor for Degradation. *Cellular Signalling* **2010**, *22* (6), 900–913. <https://doi.org/10.1016/j.cellsig.2010.01.014>.

- (73) Skieterska, K.; Rondou, P.; Van Craenenbroeck, K. Regulation of G Protein-Coupled Receptors by Ubiquitination. *International Journal of Molecular Sciences* **2017**, *18* (5), 923. <https://doi.org/10.3390/ijms18050923>.
- (74) Han, S.; Xiao, K.; Kim, J.; Wu, J.-H.; Wisler, J. W.; Nakamura, N.; Freedman, N. J.; Shenoy, S. K. MARCH2 Promotes Endocytosis and Lysosomal Sorting of Carvedilol-Bound B2-Adrenergic Receptors. *Journal of Cell Biology* **2012**, *199* (5), 817–830. <https://doi.org/10.1083/jcb.201208192>.
- (75) Komander, D. The Emerging Complexity of Protein Ubiquitination. *Biochemical Society Transactions* **2009**, *37* (5), 937–953. <https://doi.org/10.1042/BST0370937>.
- (76) Shimizu, Y.; Okuda-Shimizu, Y.; Hendershot, L. M. Ubiquitylation of an ERAD Substrate Occurs on Multiple Types of Amino Acids. *Molecular Cell* **2010**, *40* (6), 917–926. <https://doi.org/10.1016/j.molcel.2010.11.033>.
- (77) Wang, X.; Herr, R. A.; Hansen, T. H. Ubiquitination of Substrates by Esterification. *Traffic* **2012**, *13* (1), 19–24. <https://doi.org/10.1111/j.1600-0854.2011.01269.x>.
- (78) Peeler, J. C.; Schedin-Weiss, S.; Soula, M.; Kazmi, M. A.; Sakmar, T. P. Isopeptide and Ester Bond Ubiquitination Both Regulate Degradation of the Human Dopamine Receptor 4. *Journal of Biological Chemistry* **2017**, *292* (52), 21623–21630. <https://doi.org/10.1074/jbc.M116.758961>.
- (79) Li, H.; Dong, J.; Cai, M.; Xu, Z.; Cheng, X.-D.; Qin, J.-J. Protein Degradation Technology: A Strategic Paradigm Shift in Drug Discovery. *Journal of Hematology & Oncology* **2021**, *14* (1), 138. <https://doi.org/10.1186/s13045-021-01146-7>.

- (80) Li, X.; Song, Y. Proteolysis-Targeting Chimera (PROTAC) for Targeted Protein Degradation and Cancer Therapy. *Journal of Hematology & Oncology* **2020**, *13* (1), 50. <https://doi.org/10.1186/s13045-020-00885-3>.
- (81) Gu, S.; Cui, D.; Chen, X.; Xiong, X.; Zhao, Y. PROTACs: An Emerging Targeting Technique for Protein Degradation in Drug Discovery. *BioEssays* **2018**, *40* (4), 1700247. <https://doi.org/10.1002/bies.201700247>.
- (82) Liu, J.; Ma, J.; Liu, Y.; Xia, J.; Li, Y.; Wang, Z. P.; Wei, W. PROTACs: A Novel Strategy for Cancer Therapy. *Seminars in Cancer Biology* **2020**, *67*, 171–179. <https://doi.org/10.1016/j.semcancer.2020.02.006>.
- (83) An, S.; Fu, L. Small-Molecule PROTACs: An Emerging and Promising Approach for the Development of Targeted Therapy Drugs. *EBioMedicine* **2018**, *36*, 553–562. <https://doi.org/10.1016/j.ebiom.2018.09.005>.
- (84) Neklesa, T. K.; Winkler, J. D.; Crews, C. M. Targeted Protein Degradation by PROTACs. *Pharmacology & Therapeutics* **2017**, *174*, 138–144. <https://doi.org/10.1016/j.pharmthera.2017.02.027>.
- (85) Khan, S.; He, Y.; Zhang, X.; Yuan, Y.; Pu, S.; Kong, Q.; Zheng, G.; Zhou, D. PROteolysis TArgeting Chimeras (PROTACs) as Emerging Anticancer Therapeutics. *Oncogene* **2020**, *39* (26), 4909–4924. <https://doi.org/10.1038/s41388-020-1336-y>.
- (86) Kundu, M.; Thompson, C. B. Autophagy: Basic Principles and Relevance to Disease. *Annu. Rev. Pathol. Mech. Dis.* **2008**, *3* (1), 427–455. <https://doi.org/10.1146/annurev.pathmechdis.2.010506.091842>.
- (87) Sakamoto, K. M.; Kim, K. B.; Kumagai, A.; Mercurio, F.; Crews, C. M.; Deshaies, R. J. Protacs: Chimeric Molecules That Target Proteins to the Skp1–Cullin–F Box Complex for

Ubiquitination and Degradation. *Proceedings of the National Academy of Sciences* **2001**, *98* (15), 8554–8559. <https://doi.org/10.1073/pnas.141230798>.

(88) Schneekloth Jr, J. S.; Fonseca, F. N.; Koldobskiy, M.; Mandal, A.; Deshaies, R.; Sakamoto, K.; Crews, C. M. Chemical Genetic Control of Protein Levels: Selective in Vivo Targeted Degradation. *Journal of the American Chemical Society* **2004**, *126* (12), 3748–3754. <https://doi.org/10.1021/ja039025z>.

(89) Ishoey, M.; Chorn, S.; Singh, N.; Jaeger, M. G.; Brand, M.; Paulk, J.; Bauer, S.; Erb, M. A.; Parapatics, K.; Müller, A. C.; Bennett, K. L.; Ecker, G. F.; Bradner, J. E.; Winter, G. E. Translation Termination Factor GSPT1 Is a Phenotypically Relevant Off-Target of Heterobifunctional Phthalimide Degraders. *ACS Chem. Biol.* **2018**, *13* (3), 553–560. <https://doi.org/10.1021/acscchembio.7b00969>.

(90) Savitski, M. M.; Zinn, N.; Faeltsh-Savitski, M.; Poeckel, D.; Gade, S.; Becher, I.; Muelbaier, M.; Wagner, A. J.; Strohmer, K.; Werner, T.; Melchert, S.; Petretich, M.; Rutkowska, A.; Vappiani, J.; Franken, H.; Steidel, M.; Sweetman, G. M.; Gilan, O.; Lam, E. Y. N.; Dawson, M. A.; Prinjha, R. K.; Grandi, P.; Bergamini, G.; Bantscheff, M. Multiplexed Proteome Dynamics Profiling Reveals Mechanisms Controlling Protein Homeostasis. *Cell* **2018**, *173* (1), 260-274.e25. <https://doi.org/10.1016/j.cell.2018.02.030>.

(91) Zhong, Y.; Chi, F.; Wu, H.; Liu, Y.; Xie, Z.; Huang, W.; Shi, W.; Qian, H. Emerging Targeted Protein Degradation Tools for Innovative Drug Discovery: From Classical PROTACs to the Novel and Beyond. *European Journal of Medicinal Chemistry* **2022**, *231*, 114142. <https://doi.org/10.1016/j.ejmech.2022.114142>.

(92) Li, Z.; Lin, Y.; Song, H.; Qin, X.; Yu, Z.; Zhang, Z.; Dong, G.; Li, X.; Shi, X.; Du, L.; Zhao, W.; Li, M. First Small-Molecule PROTACs for G Protein-Coupled Receptors: Inducing A1A-

Adrenergic Receptor Degradation. *Acta Pharmaceutica Sinica B* **2020**, *10* (9), 1669–1679. <https://doi.org/10.1016/j.apsb.2020.01.014>.

(93) Sokoloff, P.; Le Foll, B. The Dopamine D3 Receptor, a Quarter Century Later. *European Journal of Neuroscience* **2017**, *45* (1), 2–19. <https://doi.org/10.1111/ejn.13390>.

(94) Sokoloff, P.; Giros, B.; Martres, M.-P.; Bouthenet, M.-L.; Schwartz, J.-C. Molecular Cloning and Characterization of a Novel Dopamine Receptor (D3) as a Target for Neuroleptics. *Nature* **1990**, *347* (6289), 146–151. <https://doi.org/10.1038/347146a0>.

(95) Sokoloff, P.; Diaz, J.; Foll, B. L.; Guillin, O.; Leriche, L.; Bezard, E.; Gross, C. The Dopamine D3 Receptor: A Therapeutic Target for the Treatment of Neuropsychiatric Disorders. *CNS & Neurological Disorders-Drug Targets (Formerly Current Drug Targets-CNS & Neurological Disorders)* **2006**, *5* (1), 25–43.

(96) Newman, A. H.; Ku, T.; Jordan, C. J.; Bonifazi, A.; Xi, Z.-X. New Drugs, Old Targets: Tweaking the Dopamine System to Treat Psychostimulant Use Disorders. *Annual Review of Pharmacology and Toxicology* **2021**, *61* (1), 609–628. <https://doi.org/10.1146/annurev-pharmtox-030220-124205>.

(97) Das, B.; Modi, G.; Dutta, A. Dopamine D3 Agonists in the Treatment of Parkinson's Disease. *Current Topics in Medicinal Chemistry* **2015**, *15* (10), 908–926.

(98) Heidbreder, C. A.; Gardner, E. L.; Xi, Z.-X.; Thanos, P. K.; Mugnaini, M.; Hagan, J. J.; Ashby, C. R. The Role of Central Dopamine D3 Receptors in Drug Addiction: A Review of Pharmacological Evidence. *Brain Research Reviews* **2005**, *49* (1), 77–105. <https://doi.org/10.1016/j.brainresrev.2004.12.033>.

(99) Michino, M.; Boateng, C. A.; Donthamsetti, P.; Yano, H.; Bakare, O. M.; Bonifazi, A.; Ellenberger, M. P.; Keck, T. M.; Kumar, V.; Zhu, C.; Verma, R.; Deschamps, J. R.; Javitch, J. A.;



Newman, A. H.; Shi, L. Toward Understanding the Structural Basis of Partial Agonism at the Dopamine D3 Receptor. *Journal of Medicinal Chemistry* **2017**, *60* (2), 580–593. <https://doi.org/10.1021/acs.jmedchem.6b01148>.

(100) Shaik, A. B.; Kumar, V.; Bonifazi, A.; Guerrero, A. M.; Cemaj, S. L.; Gadiano, A.; Lam, J.; Xi, Z.-X.; Rais, R.; Slusher, B. S.; Newman, A. H. Investigation of Novel Primary and Secondary Pharmacophores and 3-Substitution in the Linking Chain of a Series of Highly Selective and Bitopic Dopamine D3 Receptor Antagonists and Partial Agonists. *Journal of Medicinal Chemistry* **2019**, *62* (20), 9061–9077. <https://doi.org/10.1021/acs.jmedchem.9b00607>.

(101) Moritz, A. E.; Bonifazi, A.; Guerrero, A. M.; Kumar, V.; Free, R. B.; Lane, J. R.; Verma, R. K.; Shi, L.; Newman, A. H.; Sibley, D. R. Evidence for a Stereoselective Mechanism for Bitopic Activity by Extended-Length Antagonists of the D3 Dopamine Receptor. *ACS Chem. Neurosci.* **2020**, *11* (20), 3309–3320. <https://doi.org/10.1021/acschemneuro.0c00425>.

(102) Newman, A. H.; Battiti, F. O.; Bonifazi, A. 2016 Philip S. Portoghese Medicinal Chemistry Lectureship: Designing Bivalent or Bitopic Molecules for G-Protein Coupled Receptors. The Whole Is Greater Than the Sum of Its Parts. *Journal of Medicinal Chemistry* **2020**, *63* (5), 1779–1797. <https://doi.org/10.1021/acs.jmedchem.9b01105>.

(103) Keck, T. M.; Burzynski, C.; Shi, L.; Newman, A. H. Chapter Seven - Beyond Small-Molecule SAR: Using the Dopamine D3 Receptor Crystal Structure to Guide Drug Design. In *Advances in Pharmacology*; Dwoskin, L. P., Ed.; Academic Press, 2014; Vol. 69, pp 267–300.

(104) Del Bello, F.; Ambrosini, D.; Bonifazi, A.; Newman, A. H.; Keck, T. M.; Giannella, M.; Giorgioni, G.; Piergentili, A.; Cappellacci, L.; Cilia, A.; Franchini, S.; Quaglia, W. Multitarget 1,4-Dioxane Compounds Combining Favorable D2-like and 5-HT1A Receptor Interactions with Potential for the Treatment of Parkinson's Disease or Schizophrenia. *ACS Chem. Neurosci.* **2019**, *10* (5), 2222–2228. <https://doi.org/10.1021/acschemneuro.8b00677>.

(105) Piergentili, A.; Quaglia, W.; Giannella, M.; Bello, F. D.; Bruni, B.; Buccioni, M.; Carrieri, A.; Ciattini, S. Dioxane and Oxathiane Nuclei: Suitable Substructures for Muscarinic Agonists. *Bioorganic & Medicinal Chemistry* **2007**, *15* (2), 886–896. <https://doi.org/10.1016/j.bmc.2006.10.040>.

(106) Quaglia, W.; Piergentili, A.; Del Bello, F.; Farande, Y.; Giannella, M.; Pigni, M.; Rafaiani, G.; Carrieri, A.; Amantini, C.; Lucciarini, R.; Santoni, G.; Poggesi, E.; Leonardi, A. Structure–Activity Relationships in 1,4-Benzodioxan-Related Compounds. 9. From 1,4-Benzodioxane to 1,4-Dioxane Ring as a Promising Template of Novel A1D-Adrenoreceptor Antagonists, 5-HT1A Full Agonists, and Cytotoxic Agents. *Journal of Medicinal Chemistry* **2008**, *51* (20), 6359–6370. <https://doi.org/10.1021/jm800461k>.

(107) Bonifazi, A.; Del Bello, F.; Mammoli, V.; Piergentili, A.; Petrelli, R.; Cimarelli, C.; Pellei, M.; Schepmann, D.; Wunsch, B.; Barocelli, E.; Bertoni, S.; Flammini, L.; Amantini, C.; Nabissi, M.; Santoni, G.; Vistoli, G.; Quaglia, W. Novel Potent N-Methyl-d-Aspartate (NMDA) Receptor Antagonists or  $\Sigma$ 1 Receptor Ligands Based on Properly Substituted 1,4-Dioxane Ring. *Journal of Medicinal Chemistry* **2015**, *58* (21), 8601–8615. <https://doi.org/10.1021/acs.jmedchem.5b01214>.

(108) Del Bello, F.; Bonifazi, A.; Giorgioni, G.; Quaglia, W.; Amantini, C.; Morelli, M. B.; Santoni, G.; Battiti, F. O.; Vistoli, G.; Cilia, A.; Piergentili, A. Chemical Manipulations on the 1,4-Dioxane Ring of 5-HT1A Receptor Agonists Lead to Antagonists Endowed with Antitumor Activity in Prostate Cancer Cells. *European Journal of Medicinal Chemistry* **2019**, *168*, 461–473. <https://doi.org/10.1016/j.ejmech.2019.02.056>.

(109) Del Bello, F.; Bonifazi, A.; Giannella, M.; Giorgioni, G.; Piergentili, A.; Petrelli, R.; Cifani, C.; Micioni Di Bonaventura, M. V.; Keck, T. M.; Mazzolari, A.; Vistoli, G.; Cilia, A.; Poggesi, E.; Matucci, R.; Quaglia, W. The Replacement of the 2-Methoxy Substituent of N-((6,6-Diphenyl-1,4-Dioxan-2-Yl)methyl)-2-(2-Methoxyphenoxy)ethan-1-Amine Improves the Selectivity for 5-HT1A

Receptor over A1-Adrenoceptor and D2-like Receptor Subtypes. *European Journal of Medicinal Chemistry* **2017**, *125*, 233–244. <https://doi.org/10.1016/j.ejmech.2016.09.026>.

(110) Morelli, M. B.; Amantini, C.; Nabissi, M.; Santoni, G.; Wünsch, B.; Schepmann, D.; Cimarelli, C.; Pellei, M.; Santini, C.; Fontana, S.; Mammoli, V.; Quaglia, W.; Bonifazi, A.; Giannella, M.; Giorgioni, G.; Piergentili, A.; Del Bello, F. Role of the NMDA Receptor in the Antitumor Activity of Chiral 1,4-Dioxane Ligands in MCF-7 and SKBR3 Breast Cancer Cells. *ACS Medicinal Chemistry Letters* **2019**, *10* (4), 511–516. <https://doi.org/10.1021/acsmchemlett.8b00536>.

(111) Del Bello, F.; Barocelli, E.; Bertoni, S.; Bonifazi, A.; Camalli, M.; Campi, G.; Giannella, M.; Matucci, R.; Nesi, M.; Pignini, M.; Quaglia, W.; Piergentili, A. 1,4-Dioxane, a Suitable Scaffold for the Development of Novel M3 Muscarinic Receptor Antagonists. *Journal of Medicinal Chemistry* **2012**, *55* (4), 1783–1787. <https://doi.org/10.1021/jm2013216>.

(112) Del Bello, F.; Bonifazi, A.; Giorgioni, G.; Petrelli, R.; Quaglia, W.; Altomare, A.; Falcicchio, A.; Matucci, R.; Vistoli, G.; Piergentili, A. Novel Muscarinic Acetylcholine Receptor Hybrid Ligands Embedding Quinuclidine and 1,4-Dioxane Fragments. *European Journal of Medicinal Chemistry* **2017**, *137*, 327–337. <https://doi.org/10.1016/j.ejmech.2017.06.004>.

(113) Del Bello, F.; Bonifazi, A.; Giorgioni, G.; Piergentili, A.; Sabbieti, M. G.; Agas, D.; Dell'Aera, M.; Matucci, R.; Górecki, M.; Pescitelli, G.; Vistoli, G.; Quaglia, W. Novel Potent Muscarinic Receptor Antagonists: Investigation on the Nature of Lipophilic Substituents in the 5- and/or 6-Positions of the 1,4-Dioxane Nucleus. *J. Med. Chem.* **2020**, *63* (11), 5763–5782. <https://doi.org/10.1021/acs.jmedchem.9b02100>.

(114) Custodio, R. J. P.; Botanas, C. J.; Yoon, S. S.; De La Pena, J. B.; dela Peña, I. J.; Kim, M.; Woo, T.; Seo, J.-W.; Jang, C.-G.; Kwon, Y. H. Evaluation of the Abuse Potential of Novel Amphetamine Derivatives with Modifications on the Amine (NBNA) and Phenyl (EDA, PMEA, 2-

APN) Sites. *Biomolecules & therapeutics* **2017**, *25* (6), 578.  
<https://doi.org/10.4062/biomolther.2017.141>.

(115) Banala, A. K.; Levy, B. A.; Khatri, S. S.; Furman, C. A.; Roof, R. A.; Mishra, Y.; Griffin, S. A.; Sibley, D. R.; Luedtke, R. R.; Newman, A. H. N-(3-Fluoro-4-(4-(2-Methoxy or 2,3-Dichlorophenyl)Piperazine-1-Yl)Butyl)Arylcarboxamides as Selective Dopamine D3 Receptor Ligands: Critical Role of the Carboxamide Linker for D3 Receptor Selectivity. *Journal of Medicinal Chemistry* **2011**, *54* (10), 3581–3594. <https://doi.org/10.1021/jm200288r>.

(116) Grundt, P.; Prevatt, K. M.; Cao, J.; Taylor, M.; Floresca, C. Z.; Choi, J.-K.; Jenkins, B. G.; Luedtke, R. R.; Newman, A. H. Heterocyclic Analogues of N-(4-(4-(2,3-Dichlorophenyl)Piperazin-1-Yl)Butyl)Arylcarboxamides with Functionalized Linking Chains as Novel Dopamine D3 Receptor Ligands: Potential Substance Abuse Therapeutic Agents. *Journal of Medicinal Chemistry* **2007**, *50* (17), 4135–4146. <https://doi.org/10.1021/jm0704200>.

(117) Robarge, M. J.; Husbands, S. M.; Kieltyka, A.; Brodbeck, R.; Thurkauf, A.; Newman, A. H. Design and Synthesis of [(2,3-Dichlorophenyl)Piperazin-1-Yl]Alkylfluorenylcarboxamides as Novel Ligands Selective for the Dopamine D3 Receptor Subtype. *J. Med. Chem.* **2001**, *44* (19), 3175–3186. <https://doi.org/10.1021/jm010146o>.

(118) Bonifazi, A.; Newman, A. H.; Keck, T. M.; Gervasoni, S.; Vistoli, G.; Del Bello, F.; Giorgioni, G.; Pavletić, P.; Quaglia, W.; Piergentili, A. Scaffold Hybridization Strategy Leads to the Discovery of Dopamine D3 Receptor-Selective or Multitarget Bitopic Ligands Potentially Useful for Central Nervous System Disorders. *ACS Chemical Neuroscience* **2021**, *12* (19), 3638–3649. <https://doi.org/10.1021/acscemneuro.1c00368>.

(119) Brindisi, M.; Butini, S.; Franceschini, S.; Brogi, S.; Trotta, F.; Ros, S.; Cagnotto, A.; Salmona, M.; Casagni, A.; Andreassi, M.; Saponara, S.; Gorelli, B.; Weikop, P.; Mikkelsen, J. D.; Scheel-Kruger, J.; Sandager-Nielsen, K.; Novellino, E.; Campiani, G.; Gemma, S. Targeting

Dopamine D3 and Serotonin 5-HT1A and 5-HT2A Receptors for Developing Effective Antipsychotics: Synthesis, Biological Characterization, and Behavioral Studies. *Journal of Medicinal Chemistry* **2014**, 57 (22), 9578–9597. <https://doi.org/10.1021/jm501119j>.

(120) Ye, N.; Song, Z.; Zhang, A. Dual Ligands Targeting Dopamine D2 and Serotonin 5-HT1A Receptors as New Antipsychotical or Anti-Parkinsonian Agents. *Current Medicinal Chemistry* **2014**, 21 (4), 437–457.

(121) Huang, M.; Kwon, S.; He, W.; Meltzer, H. Y. Neurochemical Arguments for the Use of Dopamine D4 Receptor Stimulation to Improve Cognitive Impairment Associated with Schizophrenia. *Pharmacology Biochemistry and Behavior* **2017**, 157, 16–23. <https://doi.org/10.1016/j.pbb.2017.04.010>.

(122) Pogorelov, V. M.; Rodriguiz, R. M.; Cheng, J.; Huang, M.; Schmerberg, C. M.; Meltzer, H. Y.; Roth, B. L.; Kozikowski, A. P.; Wetsel, W. C. 5-HT2C Agonists Modulate Schizophrenia-Like Behaviors in Mice. *Neuropsychopharmacology* **2017**, 42 (11), 2163–2177. <https://doi.org/10.1038/npp.2017.52>.

(123) Ardiana, F.; Lestari, M. L. A. D.; Indrayanto, G. Chapter 3 - Candesartan Cilexetil. In *Profiles of Drug Substances, Excipients and Related Methodology*; Brittain, H. G., Ed.; Academic Press, 2012; Vol. 37, pp 79–112. <https://doi.org/10.1016/B978-0-12-397220-0.00003-9>.

(124) Fjelbye, K.; Marigo, M.; Clausen, R. P.; Jørgensen, E. B.; Christoffersen, C. T.; Juhl, K. Elucidation of Fluorine's Impact on p K a and in Vitro Pgp-Mediated Efflux for a Series of PDE9 Inhibitors. *MedChemComm* **2018**, 9 (5), 893–896.

(125) Stevens, G.; Chen, S.; Huyskens, P.; De Jaegere, S. Influence of the Hydroxyl Groups on the Basicity of Alkanolamines in Water and in Ethanol-Water Mixtures. *Bulletin des Sociétés Chimiques Belges* **1991**, 100 (7), 493–496. <https://doi.org/10.1002/bscb.19911000701>.

- (126) Jo, S.; Kim, T.; Iyer, V. G.; Im, W. CHARMM-GUI: A Web-Based Graphical User Interface for CHARMM. *Journal of Computational Chemistry* **2008**, *29* (11), 1859–1865. <https://doi.org/10.1002/jcc.20945>.
- (127) Lomize, M. A.; Pogozheva, I. D.; Joo, H.; Mosberg, H. I.; Lomize, A. L. OPM Database and PPM Web Server: Resources for Positioning of Proteins in Membranes. *Nucleic Acids Research* **2012**, *40* (D1), D370–D376. <https://doi.org/10.1093/nar/gkr703>.
- (128) W R Martin; C G Eades; J A Thompson; R E Huppler; P E Gilbert. The Effects of Morphine- and Nalorphine- like Drugs in the Nondependent and Morphine-Dependent Chronic Spinal Dog. *Journal of Pharmacology and Experimental Therapeutics* **1976**, *197* (3), 517.
- (129) Smith, S. B. Introduction to Sigma Receptors: Their Role in Disease and as Therapeutic Targets. In *Sigma Receptors: Their Role in Disease and as Therapeutic Targets*; Smith, S. B., Su, T.-P., Eds.; Springer International Publishing, 2017; Vol. 964, pp 1–4. [https://doi.org/10.1007/978-3-319-50174-1\\_1](https://doi.org/10.1007/978-3-319-50174-1_1).
- (130) Schmidt, H. R.; Kruse, A. C. The Molecular Function of  $\sigma$  Receptors: Past, Present, and Future. *Trends in Pharmacological Sciences* **2019**, *40* (9), 636–654. <https://doi.org/10.1016/j.tips.2019.07.006>.
- (131) Yano, H.; Bonifazi, A.; Xu, M.; Guthrie, D. A.; Schneck, S. N.; Abramyan, A. M.; Fant, A. D.; Hong, W. C.; Newman, A. H.; Shi, L. Pharmacological Profiling of Sigma 1 Receptor Ligands by Novel Receptor Homomer Assays. *Neuropharmacology* **2018**, *133*, 264–275. <https://doi.org/10.1016/j.neuropharm.2018.01.042>.
- (132) Hayashi, T.; Su, T.-P. Sigma-1 Receptor Chaperones at the ER- Mitochondrion Interface Regulate Ca<sup>2+</sup> Signaling and Cell Survival. *Cell* **2007**, *131* (3), 596–610. <https://doi.org/10.1016/j.cell.2007.08.036>.

- (133) Hanner, M.; Moebius, F. F.; Flandorfer, A.; Knaus, H. G.; Striessnig, J.; Kempner, E.; Glossmann, H. Purification, Molecular Cloning, and Expression of the Mammalian Sigma1-Binding Site. *Proceedings of the National Academy of Sciences* **1996**, *93* (15), 8072–8077. <https://doi.org/10.1073/pnas.93.15.8072>.
- (134) Rousseaux, C. G.; Greene, S. F. Sigma Receptors [ $\sigma$  Rs]: Biology in Normal and Diseased States. *Journal of Receptors and Signal Transduction* **2016**, *36* (4), 327–388. <https://doi.org/10.3109/10799893.2015.1015737>.
- (135) Albayrak, Y.; Hashimoto, K. Sigma-1 Receptor Agonists and Their Clinical Implications in Neuropsychiatric Disorders. In *Sigma Receptors: Their Role in Disease and as Therapeutic Targets*; Smith, S. B., Su, T.-P., Eds.; Springer International Publishing: Cham, 2017; Vol. 964, pp 153–161. [https://doi.org/10.1007/978-3-319-50174-1\\_11](https://doi.org/10.1007/978-3-319-50174-1_11).
- (136) Behensky, A. A.; Yasny, I. E.; Shuster, A. M.; Seredenin, S. B.; Petrov, A. V.; Cuevas, J. Stimulation of Sigma Receptors with Afobazole Blocks Activation of Microglia and Reduces Toxicity Caused by Amyloid- $\beta_{25-35}$ . *Journal of Pharmacology and Experimental Therapeutics* **2013**, *347* (2), 458. <https://doi.org/10.1124/jpet.113.208348>.
- (137) Francardo, V.; Bez, F.; Wieloch, T.; Nissbrandt, H.; Ruscher, K.; Cenci, M. A. Pharmacological Stimulation of Sigma-1 Receptors Has Neurorestorative Effects in Experimental Parkinsonism. *Brain* **2014**, *137* (7), 1998–2014. <https://doi.org/10.1093/brain/awu107>.
- (138) Merlos, M.; Burgueño, J.; Portillo-Salido, E.; Plata-Salamán, C. R.; Vela, J. M. Pharmacological Modulation of the Sigma 1 Receptor and the Treatment of Pain. In *Sigma Receptors: Their Role in Disease and as Therapeutic Targets*; Smith, S. B., Su, T.-P., Eds.; Springer International Publishing: Cham, 2017; Vol. 964, pp 85–107. [https://doi.org/10.1007/978-3-319-50174-1\\_8](https://doi.org/10.1007/978-3-319-50174-1_8).

- (139) Nguyen, E. C.; McCracken, K. A.; Liu, Y.; Pouw, B.; Matsumoto, R. R. Involvement of Sigma ( $\sigma$ ) Receptors in the Acute Actions of Methamphetamine: Receptor Binding and Behavioral Studies. *Neuropharmacology* **2005**, *49* (5), 638–645. <https://doi.org/10.1016/j.neuropharm.2005.04.016>.
- (140) Hiranita, T.; Soto, P. L.; Tanda, G.; Katz, J. L. Reinforcing Effects of  $\sigma$ -Receptor Agonists in Rats Trained to Self-Administer Cocaine. *Journal of Pharmacology and Experimental Therapeutics* **2010**, *332* (2), 515. <https://doi.org/10.1124/jpet.109.159236>.
- (141) Sabino, V.; Cottone, P.; Zhao, Y.; Iyer, M. R.; Steardo, L.; Steardo, L.; Rice, K. C.; Conti, B.; Koob, G. F.; Zorrilla, E. P. The  $\sigma$ -Receptor Antagonist BD-1063 Decreases Ethanol Intake and Reinforcement in Animal Models of Excessive Drinking. *Neuropsychopharmacology* **2009**, *34* (6), 1482–1493. <https://doi.org/10.1038/npp.2008.192>.
- (142) Blasio, A.; Valenza, M.; Iyer, M. R.; Rice, K. C.; Steardo, L.; Hayashi, T.; Cottone, P.; Sabino, V. Sigma-1 Receptor Mediates Acquisition of Alcohol Drinking and Seeking Behavior in Alcohol-Preferring Rats. *Behavioural Brain Research* **2015**, *287*, 315–322. <https://doi.org/10.1016/j.bbr.2015.03.065>.
- (143) Cottone, P.; Wang, X.; Park, J. W.; Valenza, M.; Blasio, A.; Kwak, J.; Iyer, M. R.; Steardo, L.; Rice, K. C.; Hayashi, T.; Sabino, V. Antagonism of Sigma-1 Receptors Blocks Compulsive-Like Eating. *Neuropsychopharmacology* **2012**, *37* (12), 2593–2604. <https://doi.org/10.1038/npp.2012.89>.
- (144) Tapia, M. A.; Lee, J. R.; Bathe, E. L.; Rivera, L. L.; Mason, K. L.; Cessac, M. E.; Bodeen, J. L.; Miller, D. K.; Will, M. J. Sigma-1 Receptor Antagonist, PD144418, Selectively Reduces Female Motivation for Food during Negative Energy Balance. *Behavioural Brain Research* **2019**, *373*, 112087. <https://doi.org/10.1016/j.bbr.2019.112087>.



- (145) Hiranita, T.; Soto, P. L.; Kohut, S. J.; Kopajtic, T.; Cao, J.; Newman, A. H.; Tanda, G.; Katz, J. L. Decreases in Cocaine Self-Administration with Dual Inhibition of the Dopamine Transporter and  $\sigma$  Receptors. *Journal of Pharmacology and Experimental Therapeutics* **2011**, *339* (2), 662. <https://doi.org/10.1124/jpet.111.185025>.
- (146) Akunne, H. C.; Whetzel, S. Z.; Wiley, J. N.; Corbin, A. E.; Ninteman, F. W.; Teclé, H.; Pei, Y.; Pugsley, T. A.; Heffner, T. G. The Pharmacology of the Novel and Selective Sigma Ligand, PD 144418. *Neuropharmacology* **1997**, *36* (1), 51–62. [https://doi.org/10.1016/S0028-3908\(96\)00161-X](https://doi.org/10.1016/S0028-3908(96)00161-X).
- (147) Pan, Y.-X.; Mei, J.; Xu, J.; Wan, B.-L.; Zuckerman, A.; Pasternak, G. W. Cloning and Characterization of a Mouse  $\Sigma 1$  Receptor. *Journal of Neurochemistry* **1998**, *70* (6), 2279–2285. <https://doi.org/10.1046/j.1471-4159.1998.70062279.x>.
- (148) Kekuda, R.; Prasad, P. D.; Fei, Y.-J.; Leibach, F. H.; Ganapathy, V. Cloning and Functional Expression of the Human Type 1 Sigma Receptor (HSigmaR1). *Biochemical and Biophysical Research Communications* **1996**, *229* (2), 553–558. <https://doi.org/10.1006/bbrc.1996.1842>.
- (149) Schmidt, H. R.; Zheng, S.; Gurpinar, E.; Koehl, A.; Manglik, A.; Kruse, A. C. Crystal Structure of the Human  $\Sigma 1$  Receptor. *Nature* **2016**, *532* (7600), 527–530. <https://doi.org/10.1038/nature17391>.
- (150) Assaf Alon; Jiankun Lyu; Joao M. Braz; Tia A. Tummino; Veronica Craik; Matthew J. O'Meara; Chase M. Webb; Dmytro S. Radchenko; Yurii S. Moroz; Xi-Ping Huang; Yongfeng Liu; Bryan L. Roth; John J. Irwin; Allan I. Basbaum; Brian K. Shoichet; Andrew C. Kruse. Crystal Structures of the  $\Sigma 2$  Receptor Template Large-Library Docking for Selective Chemotypes Active in Vivo. *bioRxiv* **2021**, 2021.04.29.441652. <https://doi.org/10.1101/2021.04.29.441652>.
- (151) Ye, N.; Qin, W.; Tian, S.; Xu, Q.; Wold, E. A.; Zhou, J.; Zhen, X.-C. Small Molecules Selectively Targeting Sigma-1 Receptor for the Treatment of Neurological Diseases. *Journal of*

<https://doi.org/10.1021/acs.jmedchem.0c01192>.

(152) Glennon, R. A.; Ablordeppey, S. Y.; Ismaiel, A. M.; El-Ashmawy, M. B.; Fischer, J. B.; Howie, K. B. Structural Features Important for Sigma-1 Receptor Binding. *Journal of medicinal chemistry* **1994**, 37 (8), 1214–1219.

(153) Laurini, E.; Marson, D.; Dal Col, V.; Fermeiglia, M.; Mamolo, M. G.; Zampieri, D.; Vio, L.; Pricl, S. Another Brick in the Wall. Validation of the  $\Sigma 1$  Receptor 3D Model by Computer-Assisted Design, Synthesis, and Activity of New  $\Sigma 1$  Ligands. *Molecular pharmaceuticals* **2012**, 9 (11), 3107–3126.

(154) Zampieri, D.; Mamolo, M. G.; Laurini, E.; Florio, C.; Zanette, C.; Fermeiglia, M.; Posocco, P.; Paneni, M. S.; Pricl, S.; Vio, L. Synthesis, Biological Evaluation, and Three-Dimensional in Silico Pharmacophore Model for  $\Sigma 1$  Receptor Ligands Based on a Series of Substituted Benzo [d] Oxazol-2 (3 H)-One Derivatives. *Journal of medicinal chemistry* **2009**, 52 (17), 5380–5393.

(155) Glennon, R. Pharmacophore Identification for Sigma-1 (Sigma1) Receptor Binding: Application of the " Deconstruction-Reconstruction-Elaboration" Approach. *Mini reviews in medicinal chemistry* **2005**, 5 (10), 927–940.

(156) Wuensch, B. Pharmacophore Models and Development of Spirocyclic Ligands for  $\Sigma 1$  Receptor. *Curr. Pharm. Des* **2012**, 18, 930–937. <https://doi.org/10.2174/138161212799436548>.

(157) Pascual, R.; Almansa, C.; Plata-Salamán, C.; Vela, J. M. A New Pharmacophore Model for the Design of Sigma-1 Ligands Validated on a Large Experimental Dataset. *Frontiers in Pharmacology* **2019**, 10, 519.

(158) Piergentili, A.; Amantini, C.; Del Bello, F.; Giannella, M.; Mattioli, L.; Palmery, M.; Perfumi, M.; Pignini, M.; Santoni, G.; Tucci, P.; Zotti, M.; Quaglia, W. Novel Highly Potent and Selective  $\Sigma 1$

Receptor Antagonists Related to Spipethiane. *J. Med. Chem.* **2010**, *53* (3), 1261–1269.  
<https://doi.org/10.1021/jm901542q>.

(159) Del Bello, F.; Micioni Di Bonaventura, M. V.; Bonifazi, A.; Wunsch, B.; Schepmann, D.; Giancola, J. B.; Micioni Di Bonaventura, E.; Vistoli, G.; Giorgioni, G.; Quaglia, W.; Piergentili, A.; Cifani, C. Investigation of the Role of Chirality in the Interaction with  $\sigma$  Receptors and Effect on Binge Eating Episode of a Potent  $\Sigma 1$  Antagonist Analogue of Spipethiane. *ACS Chem. Neurosci.* **2019**, *10* (8), 3391–3397. <https://doi.org/10.1021/acschemneuro.9b00261>.

(160) Morice, C.; Wermuth, C. Chapter 9-Ring Transformations. In *The Practice of Medicinal Chemistry*; Academic Press San Diego: San Diego, 2008; pp 243–266.

(161) Hutson, P. H.; Balodis, I. M.; Potenza, M. N. Binge-Eating Disorder: Clinical and Therapeutic Advances. *Pharmacology & Therapeutics* **2018**, *182*, 15–27.  
<https://doi.org/10.1016/j.pharmthera.2017.08.002>.

(162) Cifani, C.; Micioni Di Bonaventura, E.; Botticelli, L.; Del Bello, F.; Giorgioni, G.; Pavletić, P.; Piergentili, A.; Quaglia, W.; Bonifazi, A.; Schepmann, D.; Wunsch, B.; Vistoli, G.; Micioni Di Bonaventura, M. V. Novel Highly Potent and Selective Sigma1 Receptor Antagonists Effectively Block the Binge Eating Episode in Female Rats. *ACS Chemical Neuroscience* **2020**, *11* (19), 3107–3116. <https://doi.org/10.1021/acschemneuro.0c00456>.

(163) Tangherlini, G.; Kalinin, D. V.; Schepmann, D.; Che, T.; Mykicky, N.; Ständer, S.; Loser, K.; Wunsch, B. Development of Novel Quinoxaline-Based  $\kappa$ -Opioid Receptor Agonists for the Treatment of Neuroinflammation. *Journal of Medicinal Chemistry* **2019**, *62* (2), 893–907.  
<https://doi.org/10.1021/acs.jmedchem.8b01609>.

(164) Battiti, F. O.; Newman, A. H.; Bonifazi, A. Exception That Proves the Rule: Investigation of Privileged Stereochemistry in Designing Dopamine D3R Bitopic Agonists. *ACS Medicinal Chemistry Letters* **2020**, *11* (10), 1956–1964. <https://doi.org/10.1021/acsmedchemlett.9b00660>.

- (165) Cao, J.; Kopajtic, T.; Katz, J. L.; Newman, A. H. Dual DAT/ $\Sigma$ 1 Receptor Ligands Based on 3-(4-(3-(Bis(4-Fluorophenyl)Amino)Propyl)Piperazin-1-Yl)-1-Phenylpropan-1-Ol. *Bioorganic & Medicinal Chemistry Letters* **2008**, *18* (19), 5238–5241. <https://doi.org/10.1016/j.bmcl.2008.08.065>.
- (166) Ren, P.; Chun, J.; Thomas, D. G.; Schnieders, M. J.; Marucho, M.; Zhang, J.; Baker, N. A. Biomolecular Electrostatics and Solvation: A Computational Perspective. *Quarterly Reviews of Biophysics* **2012**, *45* (4), 427–491. <https://doi.org/10.1017/S003358351200011X>.
- (167) Hudson, J. I.; Hiripi, E.; Pope, H. G.; Kessler, R. C. The Prevalence and Correlates of Eating Disorders in the National Comorbidity Survey Replication. *Biological Psychiatry* **2007**, *61* (3), 348–358. <https://doi.org/10.1016/j.biopsych.2006.03.040>.
- (168) Micioni Di Bonaventura, M. V.; Pucci, M.; Giusepponi, M. E.; Romano, A.; Lambertucci, C.; Volpini, R.; Micioni Di Bonaventura, E.; Gaetani, S.; Maccarrone, M.; D'Addario, C.; Cifani, C. Regulation of Adenosine A2A Receptor Gene Expression in a Model of Binge Eating in the Amygdaloid Complex of Female Rats. *Journal of Psychopharmacology* **2019**, *33* (12), 1550–1561. <https://doi.org/10.1177/0269881119845798>.
- (169) Romano, A.; Micioni Di Bonaventura, M. V.; Gallelli, C. A.; Koczwara, J. B.; Smeets, D.; Giusepponi, M. E.; De Ceglia, M.; Friuli, M.; Micioni Di Bonaventura, E.; Scuderi, C.; Vitalone, A.; Tramutola, A.; Altieri, F.; Lutz, T. A.; Giudetti, A. M.; Cassano, T.; Cifani, C.; Gaetani, S. Oleoylethanolamide Decreases Frustration Stress-Induced Binge-like Eating in Female Rats: A Novel Potential Treatment for Binge Eating Disorder. *Neuropsychopharmacology* **2020**, *45* (11), 1931–1941. <https://doi.org/10.1038/s41386-020-0686-z>.
- (170) Cifani, C.; Polidori, C.; Melotto, S.; Ciccocioppo, R.; Massi, M. A Preclinical Model of Binge Eating Elicited by Yo-Yo Dieting and Stressful Exposure to Food: Effect of Sibutramine,

Fluoxetine, Topiramate, and Midazolam. *Psychopharmacology* **2009**, *204* (1), 113–125. <https://doi.org/10.1007/s00213-008-1442-y>.

(171) Cifani, C.; Di Bonaventura, M. V. M.; Ciccocioppo, R.; Massi, M. Binge Eating in Female Rats Induced by Yo-Yo Dieting and Stress. In *Animal Models of Eating Disorders*; Avena, N. M., Ed.; Humana Press: Totowa, NJ, 2013; Vol. 74, pp 27–49. [https://doi.org/10.1007/978-1-62703-104-2\\_3](https://doi.org/10.1007/978-1-62703-104-2_3).

(172) Cifani, C.; Micioni Di B., M. V.; Vitale, G.; Ruggieri, V.; Ciccocioppo, R.; Massi, M. Effect of Salidroside, Active Principle of Rhodiola Rosea Extract, on Binge Eating. *Physiology & Behavior* **2010**, *101* (5), 555–562. <https://doi.org/10.1016/j.physbeh.2010.09.006>.

(173) Micioni Di Bonaventura, M. V.; Vitale, G.; Massi, M.; Cifani, C. Effect of Hypericum Perforatum Extract in an Experimental Model of Binge Eating in Female Rats. *Journal of Obesity* **2012**, *2012*, 10. <https://doi.org/10.1155/2012/956137>.

(174) Micioni Di Bonaventura, M. V.; Micioni Di Bonaventura, E.; Polidori, C.; Cifani, C. Preclinical Models of Stress and Environmental Influences on Binge Eating. In *Binge Eating: A Transdiagnostic Psychopathology*; Frank, G. K. W., Berner, L. A., Eds.; Springer International Publishing: Cham, 2020; pp 85–101. [https://doi.org/10.1007/978-3-030-43562-2\\_7](https://doi.org/10.1007/978-3-030-43562-2_7).

(175) Pucci, M.; Micioni Di Bonaventura, M. V.; Giusepponi, M. E.; Romano, A.; Filaferro, M.; Maccarrone, M.; Ciccocioppo, R.; Cifani, C.; D'Addario, C. Epigenetic Regulation of Nociceptin/Orphanin FQ and Corticotropin-Releasing Factor System Genes in Frustration Stress-Induced Binge-like Palatable Food Consumption. *Addiction Biology* **2016**, *21* (6), 1168–1185. <https://doi.org/10.1111/adb.12303>.

(176) Micioni Di Bonaventura, M. V.; Ubaldi, M.; Liberati, S.; Ciccocioppo, R.; Massi, M.; Cifani, C. Caloric Restriction Increases the Sensitivity to the Hyperphagic Effect of Nociceptin/Orphanin

FQ Limiting Its Ability to Reduce Binge Eating in Female Rats. *Psychopharmacology* **2013**, 228 (1), 53–63. <https://doi.org/10.1007/s00213-013-3013-0>.

(177) Ramos, A.; Mormède, P. Stress and Emotionality: A Multidimensional and Genetic Approach. *Neuroscience & Biobehavioral Reviews* **1997**, 22 (1), 33–57. [https://doi.org/10.1016/S0149-7634\(97\)00001-8](https://doi.org/10.1016/S0149-7634(97)00001-8).

(178) Porsolt, R. D.; Anton, G.; Blavet, N.; Jalfre, M. Behavioural Despair in Rats: A New Model Sensitive to Antidepressant Treatments. *European Journal of Pharmacology* **1978**, 47 (4), 379–391. [https://doi.org/10.1016/0014-2999\(78\)90118-8](https://doi.org/10.1016/0014-2999(78)90118-8).

(179) Royce, J. R. On the Construct Validity of Open-Field Measures. *Psychological Bulletin* **1977**, 84, 1098–1106. <https://doi.org/10.1037/0033-2909.84.6.1098>.

(180) Stoscheck, C. M. [6] Quantitation of Protein. In *Methods in Enzymology*; Deutscher, M. P., Ed.; Academic Press, 1990; Vol. 182, pp 50–68. [https://doi.org/10.1016/0076-6879\(90\)82008-P](https://doi.org/10.1016/0076-6879(90)82008-P).

(181) Bradford, M. M. A Rapid and Sensitive Method for the Quantitation of Microgram Quantities of Protein Utilizing the Principle of Protein-Dye Binding. *Analytical Biochemistry* **1976**, 72 (1), 248–254. [https://doi.org/10.1016/0003-2697\(76\)90527-3](https://doi.org/10.1016/0003-2697(76)90527-3).

(182) Bailey, K. R.; Crawley, J. N. Anxiety-Related Behaviors in Mice. In *Methods of behavioral analysis in neuroscience, 2nd ed.*; Frontiers in neuroscience.; CRC Press/Routledge/Taylor & Francis Group: Boca Raton, FL, US, 2009; pp 77–101.

(183) Micioni Di Bonaventura, M. V.; Lutz, T. A.; Romano, A.; Pucci, M.; Geary, N.; Asarian, L.; Cifani, C. Estrogenic Suppression of Binge-like Eating Elicited by Cyclic Food Restriction and Frustrative-Nonreward Stress in Female Rats. *International Journal of Eating Disorders* **2017**, 50 (6), 624–635. <https://doi.org/10.1002/eat.22687>.

- (184) Alboni, S.; Micioni Di Bonaventura, M. V.; Benatti, C.; Giusepponi, M. E.; Brunello, N.; Cifani, C. Hypothalamic Expression of Inflammatory Mediators in an Animal Model of Binge Eating. *Behavioural Brain Research* **2017**, *320*, 420–430. <https://doi.org/10.1016/j.bbr.2016.10.044>.
- (185) Bailey, K.; Buccafusco, J. J.; Rosecrans, J. A. *Methods of Behavioral Analysis in Neuroscience*. CRC Press **2009**.
- (186) Thiel, C. M.; Müller, C. P.; Huston, J. P.; Schwarting, R. K. W. High versus Low Reactivity to a Novel Environment: Behavioural, Pharmacological and Neurochemical Assessments. *Neuroscience* **1999**, *93* (1), 243–251. [https://doi.org/10.1016/S0306-4522\(99\)00158-X](https://doi.org/10.1016/S0306-4522(99)00158-X).
- (187) Gomes, F.; Greidinger, M.; Salviano, M.; Couto, K. C.; Scaperli, G. F.; Alves, S. H. de S.; Cruz, A. P. de M. Antidepressant- and Anxiogenic-like Effects of Acute 5-HT<sub>2C</sub> Receptor Activation in Rats Exposed to the Forced Swim Test and Elevated plus Maze. *Psychology & Neuroscience* **2010**, *3* (2), 245–249. <https://doi.org/10.3922/j.psns.2010.2.014>.
- (188) Porsolt, R. D.; Bertin, A.; Jalfre, M. “Behavioural Despair” in Rats and Mice: Strain Differences and the Effects of Imipramine. *European Journal of Pharmacology* **1978**, *51* (3), 291–294. [https://doi.org/10.1016/0014-2999\(78\)90414-4](https://doi.org/10.1016/0014-2999(78)90414-4).
- (189) Porsolt, R. D.; Le Pichon, M.; Jalfre, M. Depression: A New Animal Model Sensitive to Antidepressant Treatments. *Nature* **1977**, *266* (5604), 730–732. <https://doi.org/10.1038/266730a0>.

## 7. LIST OF CO-AUTHORED PUBLICATIONS

*This doctoral thesis is based on the work presented in the co-authored publications.*

- (1) Carlo Cifani, Emanuela Micioni Di Bonaventura, Luca Botticelli, Fabio Del Bello, Gianfabio Giorgioni, Pegi Pavletić, Alessandro Piergentili, Wilma Quaglia, Alessandro Bonifazi, Dirk Schepmann, Bernhard Wunsch, Giulio Vistoli, Maria Vittoria Micioni Di Bonaventura. Novel Highly Potent and Selective Sigma1 Receptor Antagonists Effectively Block the Binge Eating Episode in Female Rats. *ACS Chem Neurosci.* **2020**, *11* (19), 3107–3116. <https://doi.org/10.1021/acchemneuro.0c00456>.
- (2) Alessandro Bonifazi, Amy H. Newman, Thomas M. Keck, Silvia Gervasoni, Giulio Vistoli, Fabio Del Bello, Gianfabio Giorgioni, Pegi Pavletić, Wilma Quaglia, and Alessandro Piergentili. Scaffold Hybridization Strategy Leads to the Discovery of Dopamine D3 Receptor-Selective or Multitarget Bitopic Ligands Potentially Useful for Central Nervous System Disorders. *ACS Chemical Neuroscience* **2021**, *12* (19), 3638–3649. <https://doi.org/10.1021/acchemneuro.1c00368>.
- (3) Gianfabio Giorgioni, Fabio Del Bello, Pegi Pavletić, Wilma Quaglia, Luca Botticelli, Carlo Cifani, Emanuela Micioni Di Bonaventura, Maria Vittoria Micioni Di Bonaventura, Alessandro Piergentili. Recent Findings Leading to the Discovery of Selective Dopamine D4 Receptor Ligands for the Treatment of Widespread Diseases. *European Journal of Medicinal Chemistry* **2020**, *212* (2021).
- (4) Pavletić, P.; Semeano, A.; Yano, H.; Bonifazi, A.; Giorgioni, G.; Piergentili, A.; Quaglia, W.; Sabbieti, M. G.; Agas, D.; Santoni, G.; Pallini, R.; Ricci-Vitiani, L.; Sabato, E.; Vistoli, G.; Del Bello, F. Highly Potent and Selective Dopamine D4 Receptor Antagonists Potentially Useful for the Treatment of Glioblastoma. *J. Med. Chem.* **2022**, *65* (18), 12124–12139. <https://doi.org/10.1021/acs.jmedchem.2c00840>.



